Detailed analysis of Greendale Fault ground surface rupture displacements and geometries

N. J. Litchfield R. J. Van Dissen S. Hornblow
M. Quigley G. Archibald

GNS Science Report 2013/18
April 2014

GNS SCIENCE
TE PŪ AO

BIBLIOGRAPHIC REFERENCE

Litchfield, N. J.; Van Dissen, R. J.; Hornblow, S.; Quigley, M.; Archibald, G. 2014. Detailed analysis of Greendale Fault ground surface rupture displacements and geometries, *GNS Science Report* 2013/18. 166 p.

N. J. Litchfield, GNS Science, PO Box 30 368, Lower Hutt
R. J. Van Dissen, GNS Science, PO Box 30 368, Lower Hutt
S. Hornblow, Department of Geological Sciences, University of Canterbury, Private Bag 4800, Christchurch
M. Quigley, Department of Geological Sciences, University of Canterbury, Private Bag 4800, Christchurch
G. Archibald, GNS Science, PO Box 30 368, Lower Hutt

ISSN 1177-2425
ISBN 978-1-972192-53-5

CONTENTS

FIGURES

TABLES

APPENDICES

APPENDIX TABLES

LAYMAN'S ABSTRACT

The 4 September 2010 rupture of the Greendale Fault during the Darfield earthquake is one of the best documented in the world and so provides an important opportunity to describe in unprecedented detail a fresh ground surface fault rupture. Such information can be used to estimate deformation of the ground surface (and infrastructure upon it) in future large earthquakes, as well as to understand the uncertainties in these estimates. In this study we make use of multiple datasets to: 1) Compare Greendale Fault ground surface displacement measurements using different datasets and by different geologists; and 2) Describe the deformation across (perpendicular to) the fault. We also present further details and analysis of previously published displacement measurements and a re-survey of selected markers to test for any fault displacement since the Darfield earthquake.

Analysis of ~150 published displacement measurements shows that the distribution of ground surface movement along the Greendale Fault is overall triangular in shape (i.e., increasing from zero at the ends of the fault rupture to a peak in the centre), but in detail has 3 peaks with displacements of ~1.25 m (west and east) and ~4.25 m (centre). None of these peaks, nor virtually any measurements, correspond to the calculated average displacement of ~2.55 m. This highlights the natural variability (up to several metres) in ground surface displacement, which must be taken into account when inferring displacement during future ruptures.

A combined dataset of ~500 published and new displacements measurements (by 1–2 people) shows a surprising amount of variation – up to 4.4 m at a single site with a mean of 1.5 m. The variations appear to mainly be a function of data type, with the variations being smaller for measurements from field-based (ground) datasets than those from remote sensing (aeroplane) datasets. These are measurement uncertainties that need to be taken into account when estimating displacements in future earthquakes. The results also show that multiple measurements at the same site may not reduce uncertainties and that it remains vital to collect field data from a fresh rupture.

Analysis of ~500 measurements made by 9 geologists shows even more variation than those undertaken by 1–2 people – up to 7.62 m at a single site, with a mean 4.44 m. There are no systematic variations between people's measurements and so the variation is considered to mainly be a function of data type. Other factors may include fault zone width and marker orientation, as well as the limited time available and range in people's experience with the software used. This confirms that time and care needs to be taken over each displacement measurement, using the best dataset at each site, followed by review and consensus.

Analysis of 54 profiles across the Greendale Fault rupture confirmed that rupture was wide (~30 to ~300 m) and that much of the displacement is by flexure (warping) rather than discrete rupture (breakage on faults). The Greendale Fault rupture therefore provides an important example of distributed deformation to be considered in land use planning and engineering design. A method is proposed to assist with defining the deformation for engineering design purposes.

A re-survey of 10 sites spread along the fault ~2.5 years after the Darfield earthquake shows that any post-earthquake deformation is less than 0.4 m, which is consistent with other studies.

TECHNICAL ABSTRACT

The 4 September 2010 rupture of the Greendale Fault during the Darfield earthquake is by far the best documented ground surface rupture in New Zealand and one of the best documented in the world. As such it provides an important opportunity to describe the displacement distribution and geometry of an active fault resulting from a single coseismic rupture, which can in turn be used to improve our understanding of fault behaviour during earthquakes and to constrain better single event displacement for fault displacement and seismic hazard studies.

Prior to this study, Greendale Fault surface rupture displacement and geometry had been characterised using selected datasets, but some datasets had not been used at all and others not in any detail. In this study we make use of multiple datasets to:

1. Compare Greendale Fault dextral ground surface displacement measurements using different datasets and by different geologists; and
2. Characterise the width and distribution of across-fault (perpendicular to fault strike) ground surface displacement.

This report also presents a more detailed description and some further analysis of the previously published displacement measurements and a re-survey of selected markers to test for post-seismic displacement approximately 2.5 years after the Darfield earthquake.

The format of the report is a series of mainly stand-alone sections:

Section 2 presents a description of the datasets collected in September 2010. These datasets are: 1) Tape and compass; 2) Real Time Kinematic Global Navigational Satellite System (RTK GNSS); 3) Colour vertical aerial photographs (Orthophotos); 4) Light Detecting and Ranging (Lidar); and 5) Terrestrial laser scans. This section includes a description of the data collection and any post-processing.

Section 3 presents a detailed description of the previously published displacement measurements, including the methods of measurement and calculation of net displacements, and discussion of the average net displacement, the ratio of average to maximum displacement, shape of the net displacement plot and comparison with another Greendale Fault surface rupture displacement dataset. Key findings include that the net displacement plot is best fit by a slightly asymmetric triangle, and that the net displacement is bimodal, with the lower net displacement recorded from two shorter segments and the higher net displacement recorded from the longest, central segment. An important observation is that only 1 displacement measurement corresponds to the calculated average net displacement of 2.55 m for the entire mapped Greendale fault surface trace, which has implications for single event displacement discussed in section 4. There is reasonably good agreement between two previously published displacement datasets.

Section 4 contains 356 new measurements of dextral displacements made by Nicola Litchfield using 11 datasets (Orthophotos, 8 Lidar rasters, and 2 Laser scan datasets) at up to 101 sites. The results show a surprising amount of variation for individual sites, with the ranges (maximum minus minimum) of measurements of displacement of the same marker of up to 4.4 m (±2.2 m about a median measurement of 4.9 m) and a mean of 1.5 m (±0.75 m). Comparison of measurements from different datasets show no systematic variations, but the variations in measurements using the field-based datasets were generally lower than the remote sensing datasets, consistent with the lower uncertainties assigned to them and the

greater number of measurements confidently made using these datasets. There are also no systematic variations in displacement measurements with distance along-strike, displacement, or fault zone width. This suggests the variation is a reflection of measurement uncertainties and leads us to recommend that collection of field-based datasets (e.g., Tape and Compass, RTK, Terrestrial Laser scans) are vital and that measurement uncertainties need to be considered carefully in estimates of single event displacement for past ruptures. Another uncertainty which needs to be taken into account for single event displacement is the natural variability in displacement along-strike, and the preferential preservation of certain markers and parts of a fault.

Section 5 presents the results of two one-day workshops in which 8 geologists measured dextral displacements at 18 sites using 6 datasets (RTK, Orthophoto, and 4 Lidar rasters). These measurements were then combined with those made in section 4 to create a combined dataset of 532 measurements. The combined dataset showed even more variability than the displacement measurements by 1 geologist in section 4. For example the mean range from multiple geologists measurements is 4.44 m (±2.2 m) compared with 1.5 m (±0.75 m) by 1 geologist. As in section 4, most of the variability appears to reflect measurement uncertainties from the different datasets, with the variation from the field-based (RTK) dataset being generally lower than the variation recorded using the remote sensing datasets (Orthophotos and Lidar). No systematic variations were detected between measurements made by different geologists, or with median displacement, but there were some slight positive relationships with fault zone width and marker obliquity. A slight negative relationship with along-site distance may also reflect the increase in experience and potentially accuracy during the workshop (participants worked west to east). The limited time available and the second workshop participants aiming to measure displacements using every dataset (c.f. the first workshop and the measurements in section 4) likely also contributed to the variation. We therefore recommend that for future fault rupture studies, time and care is taken over each displacement measurement, carefully considering uncertainties and the best dataset to use for each site, followed by review and consensus.

Section 6 presents a characterisation of the surface rupture displacement perpendicular to fault strike (i.e., fault distribution and width). Histograms and cumulative displacement plots were constructed from dextral displacement measurements in 5 m increments at 54 selected profiles that cross all or part of the fault. These confirmed that the fault zone width varies from ~30 to ~300 m, much of the displacement is by horizontal flexure, and the width is greatest at step-overs. Grouping of the 30 highest quality profiles according to structural position (single trace, centre or ends of step-overs) confirms that dextral deformation is predominantly distributed (as opposed to concentrated solely on a small number of discrete shears). Thus the Greendale Fault provides an example of the distributed fault complexity parameter in the MfE Active Fault Guidelines. A method is proposed to assist characterisation of strike-slip fault rupture hazard for engineering design, which combines estimated displacement with the likely distribution of rupture according to the three structural groupings to construct displacement distribution curves at a site of interest.

Section 7 describes a RTK re-survey of 10 markers approximately 2.5 years after the Darfield earthquake. Only 1 of these markers showed measureable dextral displacement (4–7 cm), but this is within uncertainty, which we conservatively estimate to be ±20 cm. Thus any post-earthquake deformation is less than 0.4 m, which is consistent with the results from near-fault total station surveys (over 1.5 years) and far-field GPS (1–8 weeks after the Darfield earthquake) and InSAR surveys (up to 6 months after), although the latter noted some post-Darfield earthquake deformation at the major step-over and at the eastern end of the fault. This could be a target of future re-surveys.

KEYWORDS

Greendale Fault, Darfield earthquake, Surface rupture, Dextral displacement, Lidar, Laser scan

1.0 INTRODUCTION

The 4 September 2010 rupture of the Greendale Fault during the Darfield earthquake (e.g., Quigley et al., 2010; Gledhill et al., 2011; Figure 1.1) was the first ground surface rupture in New Zealand in 23 years. The previous ground rupture occurred on multiple faults in the 1987 Edgecumbe earthquake (Beanland et al., 1989, 1990). Prior to 1987, historical ground surface ruptures in New Zealand were not documented in significant detail at the time (e.g., McKay, 1890; Fyfe, 1929; Anderson et al., 1994) or have only been documented retrospectively (e.g., Berryman and Villamor, 2004; Schermer et al., 2004; Rodgers and Little, 2006; Mason and Little, 2006), decades after the event when much of the detail was lost. Rupture of the Greendale Fault across the relatively flat Canterbury Plains crossed by numerous cultural features (e.g., roads, fences), along with its easy access and close proximity to a major city (Christchurch), as well as the availability of relatively new survey techniques such as airborne Lidar (e.g., Hudnut et al., 2002; Oskin et al., 2012) and terrestrial laser scanning (e.g., Gold et al., 2013) means that the rupture is the best documented in New Zealand and one of the best in the world.

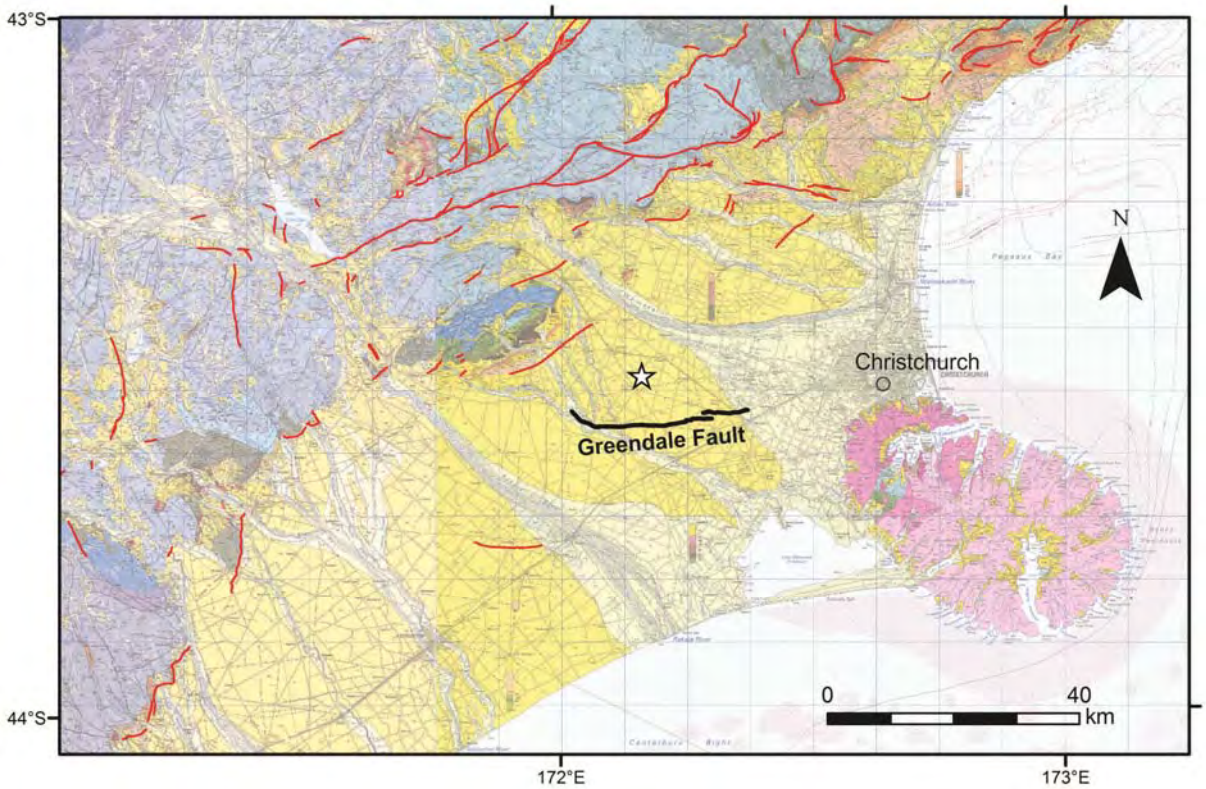

Figure 1.1 Location of the Greendale Fault with respect to Christchurch and major geological features. Red lines are active faults from the GNS Science Active Faults Database of New Zealand (http://data.gns.cri.nz/af/); the white star is the epicentre of the Darfield earthquake (http://www.geonet.org.nz/); and the black circle shows the location of the Christchurch Central Business District. The geological base maps are from Cox and Barrell (2007) and Forsyth et al. (2008).

Within hours of the Darfield earthquake (which occurred at 4.35 am Saturday), a fault rupture reconnaissance team from University of Canterbury and GNS Science had been deployed, locating ground surface rupture within 5 hours, and conducting the first aerial survey within 8 hours (Quigley et al., 2010; Barrell et al., 2011). In the following 3 weeks the fault reconnaissance team collected a large amount of field data, including tape and compass measurements of fault displacement, ground and aerial fault mapping, recording damage to engineered structures on or near the fault, surveying of displaced markers using Real Time Kinematic Global Navigation Satellite System (RTK GNSS), and terrestrial laser scans of selected sites (Quigley et al., 2010, 2012; Barrell et al., 2011; Van Dissen et al., 2011; Villamor et al., 2012). On the 10–11 September (6–7 days after the earthquake) New Zealand Aerial Mapping collected vertical aerial photographs and airborne Lidar covering the central and eastern parts of the fault rupture. In the months and years since, data has continued to be collected along the Greendale Fault, including resurveying some of the displaced markers to test for post-seismic creep (Claridge, 2011; this study), analysis of cadastral and differential Lidar (Duffy et al., 2013), and GPR surveys and paleoseismic trenching (Hornblow et al., 2013; S. Hornblow unpublished data).

Documenting the amount and geometry of ground surface displacement provides important data for understanding fault behaviour during earthquakes (e.g., Sieh et al., 1993; Lin et al., 2001; Barka et al., 2002; Treiman et al., 2002; Haeussler et al., 2004; Klinger et al., 2005; Xu et al., 2009; Oskin et al., 2012) and constraining relationships between (single event) displacement and magnitude for fault displacement and seismic hazard studies (e.g., Wells and Coppersmith, 1994; Wesnousky, 2008; Petersen et al., 2011; Stirling et al., 2013). Documenting Greendale Fault displacement and geometry was undertaken using selected datasets – mainly RTK GNSS and airborne Lidar (Van Dissen et al., 2011; Quigley et al., 2012; Villamor et al., 2012). However, many datasets have not been utilised at all or in any detail prior to this study.

In this study we make use of multiple datasets to:

1. compare Greendale Fault dextral ground surface displacement measurements using different datasets and by different geologists; and
2. characterise the width and distribution of across-fault (perpendicular to fault strike) ground surface displacement.

The comparison of displacement measurements using different datasets and by different geologists (aim 1) provides an opportunity to explore uncertainties in displacement measurements for fresh ground surface ruptures, as well as the measurement uncertainties and natural variabilities of single event displacement on faults that have ruptured in the geological past. It also provides insights into the advantages and disadvantages of collecting different datasets to inform future responses to ground surface fault ruptures.

The characterisation of the distribution of across-fault displacement (aim 2) provides important constraints on the variations in fault avoidance zone widths or set-back distances required to account for local changes in fault trace geometry (e.g., Kerr et al., 2003). Furthermore, comparison of the fault zone geometries with recorded damage to built structures provides an important historical earthquake example for informing engineering design and retrofitting of existing structures across active faults in New Zealand and elsewhere.

This report also presents a more detailed description and some further analysis of the displacement measurements published by Quigley et al. (2012) and a re-survey of selected markers to test for post-seismic displacement approximately 2.5 years after the Darfield earthquake.

The layout of this report is as a series of mainly stand-alone sections containing different aspects of the overall study:

- Section 2 describes each of the datasets used in this study and by Quigley et al. (2012), including data collection and processing.
- Section 3 presents a detailed description of the methods of previous displacement measurements (Quigley et al., 2012). Section 3 also presents some additional analysis of the displacement dataset (Appendix 1), including a comparison with another Greendale Fault surface rupture displacement dataset (Elliott et al., 2012).
- Section 4 presents a comparison of displacement measurements using different datasets, including those previously published by Quigley et al. (2012) and a large number of new measurements (Appendix 2). The analysis is restricted to dextral displacements and was undertaken entirely by the senior author.
- Section 5 presents a comparison of (dextral) displacement measurements undertaken by different geologists (Earthquake Geologists in two 1 day workshops).
- Section 6 presents a characterisation of across-fault displacement, including a method for improved characterisation of strike-slip surface fault rupture hazard, and implications for building on active faults.
- Section 7 contains the re-survey of selected markers (May 2013) to test for post-seismic creep.

Throughout this report we often refer to the Greendale Fault ground surface rupture trace as a fault zone of some width. Figure 1.2 shows our definition of these terms in relation to a cultural feature (fence) deformed by the Greendale Fault surface rupture on 4 September 2010. Thus fault zone width is the width of the entire deformation zone on the ground surface, as measured perpendicular to fault strike, rather than any other definition of fault width, such as down-dip width.

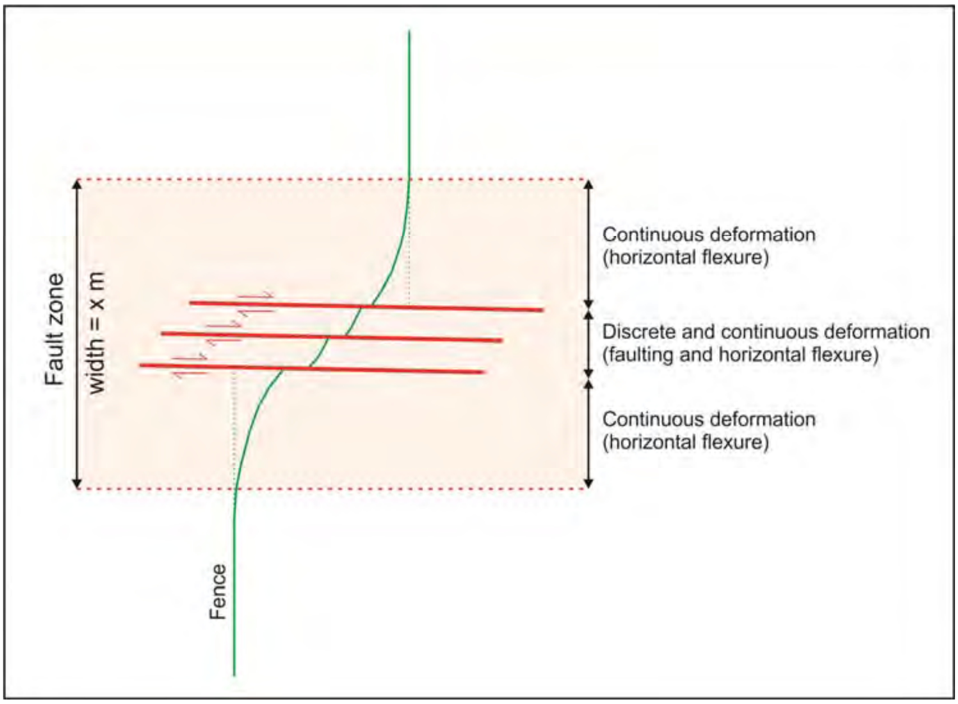

Figure 1.2 Schematic map showing the definitions and components of the Greendale Fault ground surface rupture trace, typically referred to in this report as a fault zone (red shading), in relation to a fence deformed by the rupture (green).

2.0 DATASETS COLLECTED IN SEPTEMBER 2010

2.1 INTRODUCTION

Five datasets were collected along the Greendale Fault rupture in the weeks that followed the 4 September 2010 Darfield earthquake. These include three field-based datasets:

1. Tape and compass;
2. Real Time Kinematic Global Navigation Satellite System (RTK GNSS); and
3. Terrestrial laser scans.

and two remote sensing datasets:

1. Colour vertical aerial photographs (Orthophotos); and
2. Light detecting and ranging (Lidar).

In this section we describe the methods of collection and post-processing to produce the 13 datasets used for the displacement measurements described in the following sections.

2.2 TAPE AND COMPASS

During the first two weeks following the Darfield earthquake a series of field measurements of horizontal and vertical displacements were made using a measuring tape and a standard geological compass (hereafter referred to as "Tape and Compass" measurements). The sites where Tape and Compass measurements have been made are shown in Figure 2.1 with those used in this study shown in yellow.

Figure 2.1 Sites where Tape and Compass displacement measurements were collected during the first two weeks after the Darfield Earthquake (black and yellow dots). Those in yellow and numbered are used in this study – the numbers correspond to the site numbers in Tables A 1.1 and A 2.1 in Appendices 1 and 2. White dots show sites illustrated in figures in this report. The fault trace (red line) is from Villamor et al. (2012).

The Tape and Compass data were collected by Russ Van Dissen, David Barrell, Richard Jongens and Pilar Villamor (GNS Science) and University of Canterbury staff (Mark Quigley, Kate Pedley) and postgraduate students (Eric Bilderback, Timothy Stahl, Brendan Duffy, Duncan Noble, Sharon Hornblow).

The method used was to project a marker (e.g., fence, road edge) across the fault by eye or by extending a line such as a tape measure (Figure 2.2). The displacement was then measured by tape measure in an orientation parallel to the overall strike of the fault at that point, as determined by a compass.

Figure 2.2 Eric Bilderback measuring dextral displacement from a displaced fence at site 50 (see Figure 2.1 for location). Photograph taken by Tim Stahl.

Uncertainties were estimated in the field based on the straightness of the marker, possible ranges in the azimuth at which this marker could be projected into the fault zone, and by trial and error. They range from 10 to 50 cm, with 20 cm being the most common (Appendix 1, Table A 1.1).

2.3 REAL TIME KINEMATIC GLOBAL POSITIONING SYSTEM (RTK GNSS)

RTK GNSS (hereafter referred to as RTK) data were the main field dataset collected during the 3 weeks following the Darfield earthquake. The main purpose was to survey displaced markers for later measurement of displacements, with the first priority for measurement given to those features most at risk of being modified (e.g., roads that needed to be repaired). Some fault features (e.g., cracking) were also surveyed.

The RTK survey data were collected by GNS Science staff (Nicola Litchfield, Pilar Villamor, David Barrell, Dougal Townsend, John Begg) and students from University of Canterbury (e.g., Eric Bilderback, Timothy Stahl).

Two Leica 500 and one 1200 RTK systems were employed in independent, local, surveys and the results were later post-processed. Base stations were set up at a series of convenient locations adjacent to the fault and rover points collected relative to those. Base stations were given a local coordinate, which was later corrected by post-processing (see below). The surveys were not tied together as we were interested in relative positions along individual markers (i.e., not between markers) rather than a very precise (millimetre or centimetre) position of deformation. No local survey marks were surveyed since they had all moved during the Darfield earthquake.

A total of 24,663 rover points were collected (Figure 2.3). Some were collected by walking along road edges or adjacent to fences in automatic mode with a 2–5 m horizontal spacing and the rover pole in a backpack (Figure 2.4A). Others were collected in manual mode using a 2 m pole adjacent to individual fenceposts or telegraph poles (Figure 2.4B); a wooden spacer (stick) was used if a fence was electric.

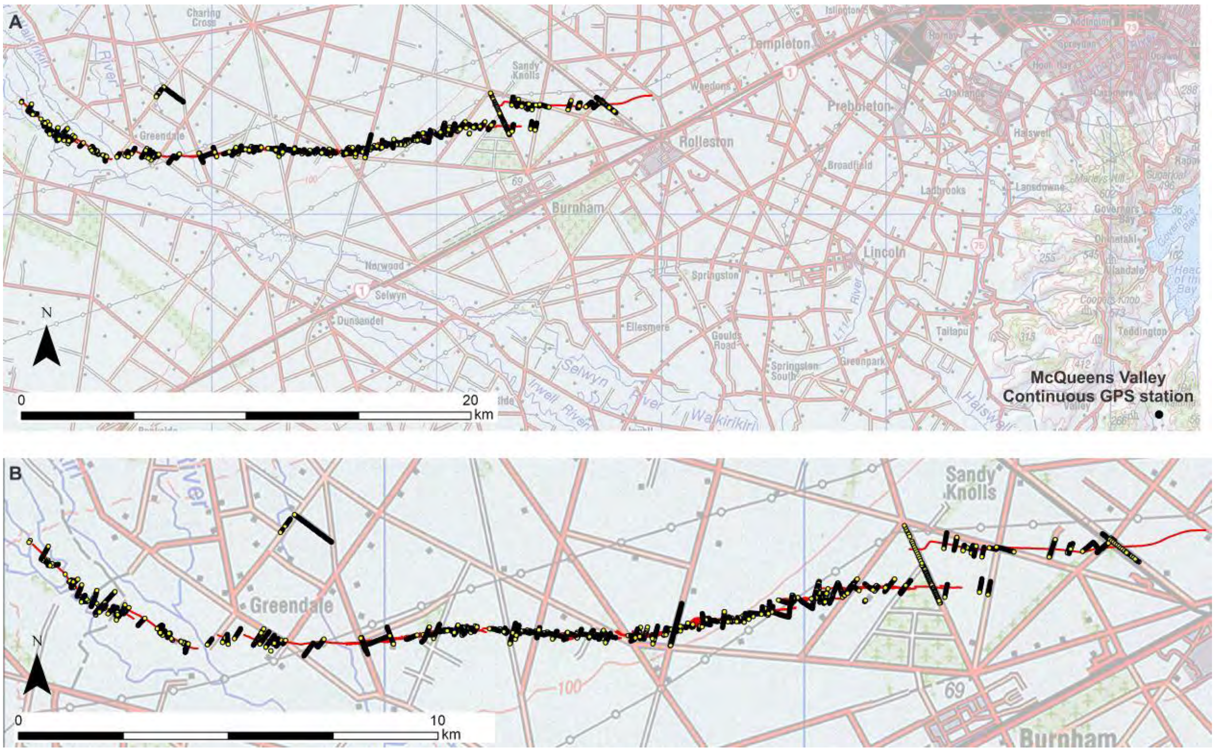

Figure 2.3 RTK rover points collected in the 2 weeks following the Darfield Earthquake. The points to the north of the fault trace were collected in response to a report by a local resident of cracking, but no fault deformation was detected. The fault trace is from Villamor et al. (2012). A) shows the position of the McQueens Valley cGPS station which was used as a reference point for post-processing of the RTK data. B) Shows a closeup of the data in the Greendale Fault area.

Figure 2.4 A) Adam Smith surveying a fenceline with the RTK rover in a backpack at displacement measurement site 36 (see Figure 2.1 for location). Photograph taken by Nicola Litchfield. B) Dougal Townsend surveying fenceposts with the RTK rover on a pole at site 7 (see Figure 2.1 for location). Photograph taken by Pilar Villamor.

Post-processing was undertaken using Leica GeoOffice 8.1. All surveys were post-processed relative to the post-earthquake position of a continuous GPS station situated 27 km southeast of the east end of the fault in McQueens Valley (Figure 2.3A) (N. Palmer, pers. comm. 2010). That is, the position of each base station was corrected relative to the continuous GPS station, which resulted in a shift of all rover points relative to that base station. A minimal amount of clean-up was also undertaken to remove spurious points.

Uncertainties of the locations of datapoints within each survey are inferred to be standard RTK uncertainties of 1–2 cm horizontal and 2–3 cm vertical.

2.4 TERRESTRIAL LASER SCANS

2.4.1 Scan sites and data capture

Terrestrial laser scan (or ground-based Lidar) surveys were collected at 3 sites in the 2–4 weeks following the Darfield earthquake (Figure 2.5; Table 2.1). The sites were selected because they had some interesting, delicate structural features that geologists wished to record.

All sites were farm paddocks although the Highfield Road laser scan also crossed the road. The Melrose site had relatively long (0.15 m) grass whereas the other two sites had short and/or clumpy grass, meaning that the laser scans captured more of the fine fault detail (section 2.4.3). The Highfield Road site had also become degraded by foot traffic, vehicles and the weather prior to the scan. The Yeah Right site is named after the “No fault here – Yeah Right” message cultivated into the paddock by the local farmer after the Darfield earthquake.

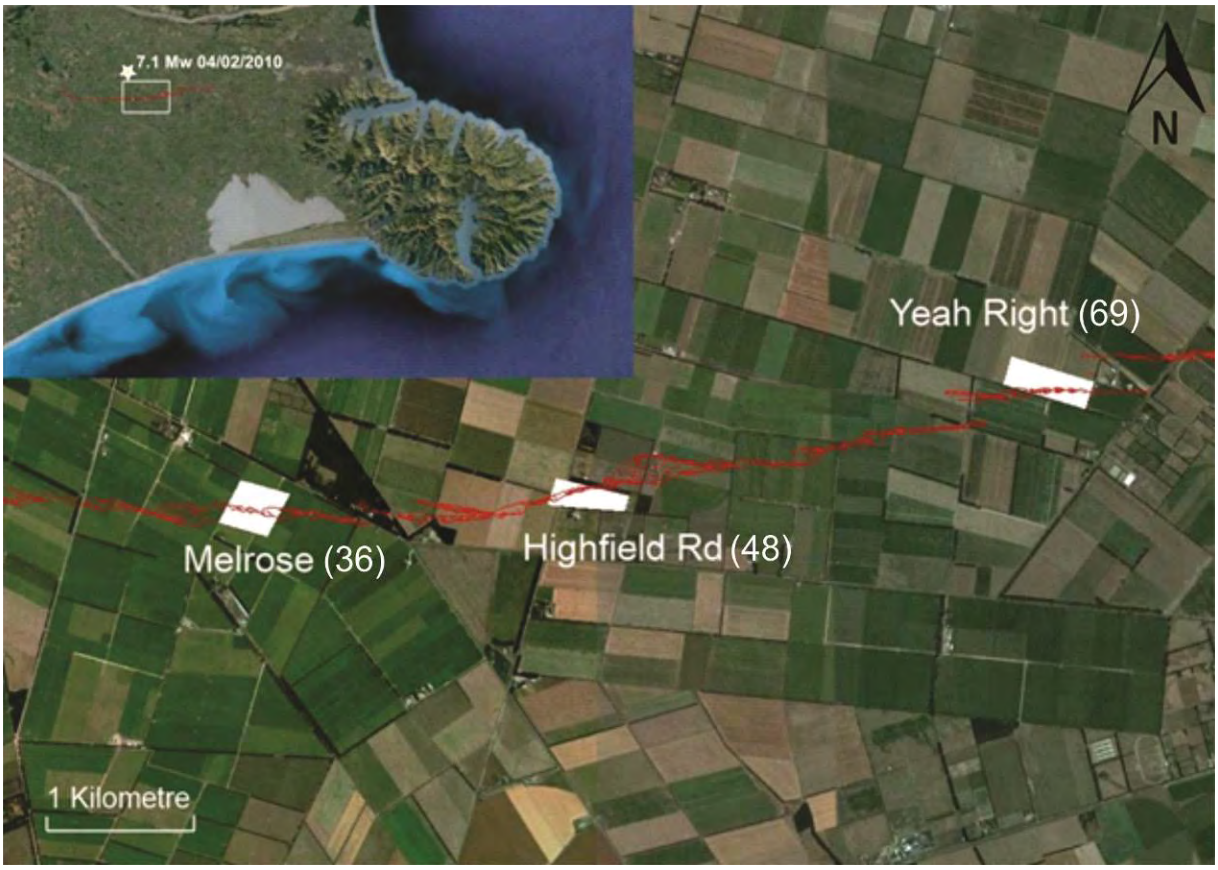

Figure 2.5 The three sites on the central Greendale Fault where terrestrial laser scan data were collected (white polygons) in the 2–4 weeks following the Darfield earthquake. The numbers in brackets are the site numbers in Appendices 1 and 2. The fault trace is from Villamor et al. (2012).

Table 2.1 Summary of the data collected at the three terrestrial laser scan sites (located in Figure 2.5).

Site	Date	Personnel	# of days	# of set ups	# of targets	Length of fault trace surveyed (m)
Melrose	14/09/2010	G. Archibald N. Khajavi	1	6	4	300
Highfield	16–17/09/2010	G. Archibald N. Khajavi	2	18	11	270
Yeah Right	25–27/09/2010	G. Archibald	3	34	7	450

The laser scans were collected using a Riegl LMS z420i terrestrial laser scanner (Figure 2.6) and multiple scans were required at each site (Table 2.2; Figure 2.7). At each set up the scanner was mounted on a heavy duty tripod and its position was captured by a Leica 1200 series RTK GNSS receiver mounted on top of the scanner above the Nikon D200 camera.

Cylindrical targets, mounted on tripods, were placed in the scene and their positions also captured with GNSS RTK. At each set up a 360° scan and associated photographs were captured as well as very high resolution scans of the targets. The scanner was then moved (~30 m) and the process repeated with at least 3 targets in common between successive scans. Scan positions were chosen to view the rupture from both sides and to view into the larger cracks.

Figure 2.6 The Riegl z420i laser scanner and associated gear at the Highfield Rd site (see Figure 2.5 for location). Note the Nikon D200 camera is not mounted in this image.

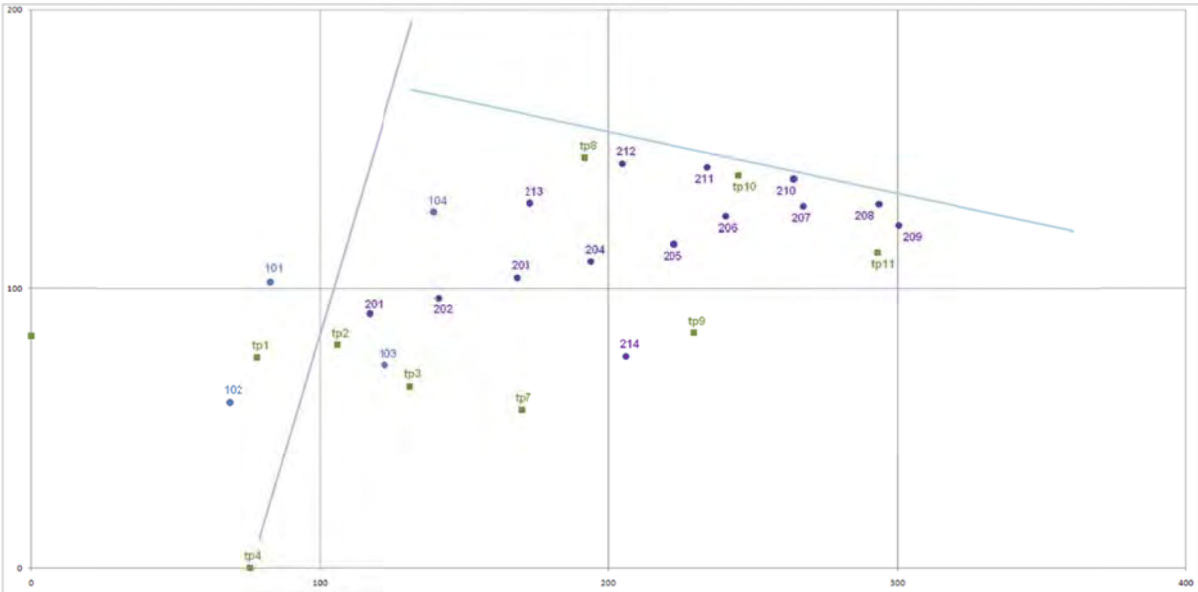

Figure 2.7 Locations of the scanner set ups (101–214) and target positions (tp1-tp11) at the Highfield Road site (see Figure 2.5 for location).

2.4.2 Processing

Terrestrial laser scan point cloud data is captured in a scanner based coordinate system as horizontal and vertical angles associated with range and intensity measurements. In order to combine point clouds from multiple set ups the scanner positions and orientations have to be determined in a geographical Cartesian coordinate system.

As noted above, the scanner set up and target positions were captured by RTK GNSS. The target position relative to the scanner is captured by fine scanning the 100 mm reflective cylindrical targets. Automatic algorithms in the scanner software calculate the centre of the target from the fine scan data. Final scan positions and orientations were calculated using least squares and the GNSS and target scan data. The standard deviation of this adjustment was 0.01 m.

The 360° scan data from each set up extends up to 1 km. In order to limit range errors each scan was range-restricted to 50 m, 42 m or 30 m (Figure 2.8). Scan overlap is necessary to fill the ~2 m diameter, no data, circle directly beneath each set up with data from an adjacent set up.

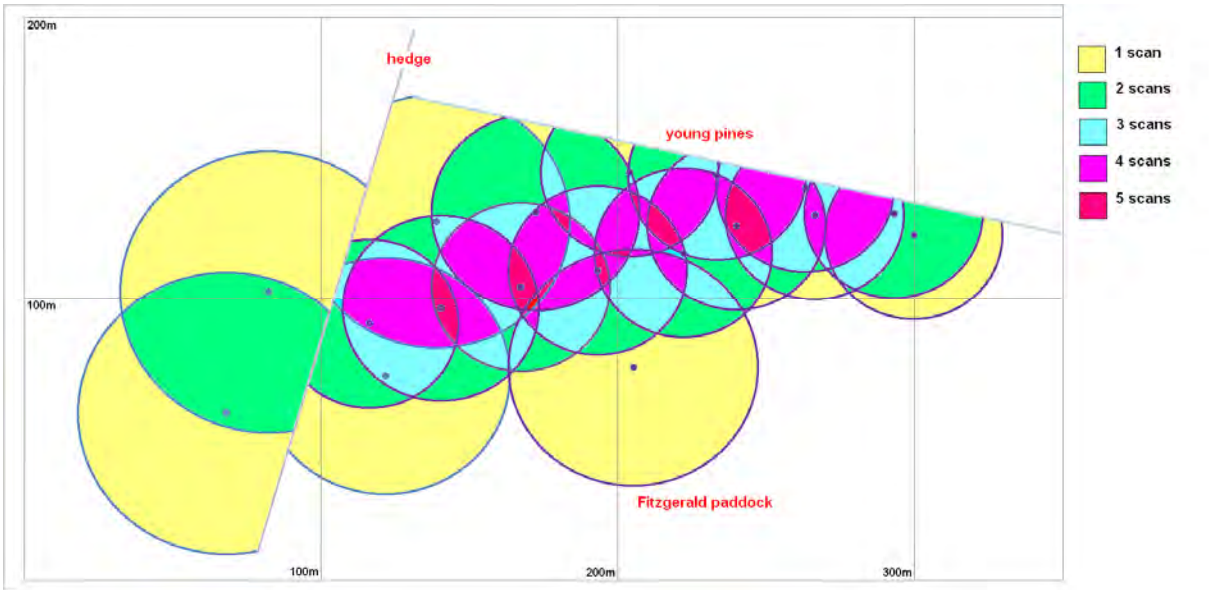

Figure 2.8 The extent of range-restricted scans and scan overlap at the Highfield Road site (see Figure 2.5 for location). The scan positions are represented by the purple dots.

The range-restricted point clouds were then combined together in RiSCAN PRO 1.7.9 and averaged using an octree filter of 0.03 m to obtain an even 3D resolution of points across the fault trace. The combined point cloud was then cleaned by eye to remove non-surface points such as trees, target tripods, people etc. In order to get the ground surface and remove points from grass, as far as possible, a final 2.5D raster filter was used. This filter projects the data onto a 0.03 m horizontal grid and deletes all but the lowest point in each cell. The resulting point cloud was clipped to the area of interest and surfaced using a TIN function which creates triangles between adjacent points. This process created the surface shown in Figure 2.9.

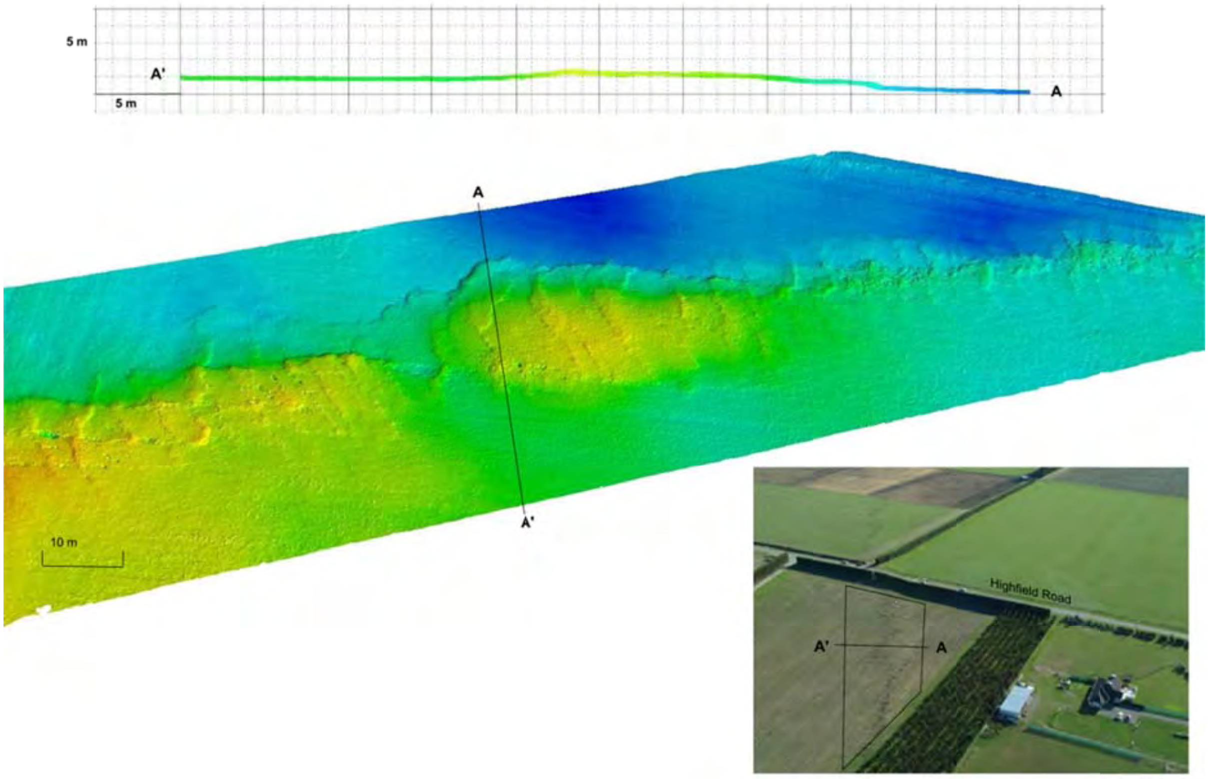

Figure 2.9 An oblique view of a portion of the terrestrial laser scan-derived Highfield Road DEM (located in the below oblique aerial photograph and Figure 2.5), colour-coded by altitude. Also shown is a cross section across the rupture showing elevation changes.

2.4.3 Digital Elevation Models and data selected for displacement measurements

Digital Elevation Models (DEM's) were created from the combined point clouds for the Highfield Road (Figure 2.9) and Yeah Right sites. The point spacing of these models is 3 cm. A DEM was not constructed for the Melrose site since the long grass meant that the ground surface was too difficult to define.

In order to measure dextral displacements, two subsets of the 3D point cloud defining linear markers at high angles to the strike of the Greendale Fault were extracted in RiSCAN PRO at each site. One subset is a linear strip along the marker of interest (e.g., Figure 2.10A). The other subset is points marking the base of one side of individual fenceposts (e.g., Figure 2.10B). These datasets are heareafter referred to as Laser scan – all points, and Laser scan – selected points respectively.

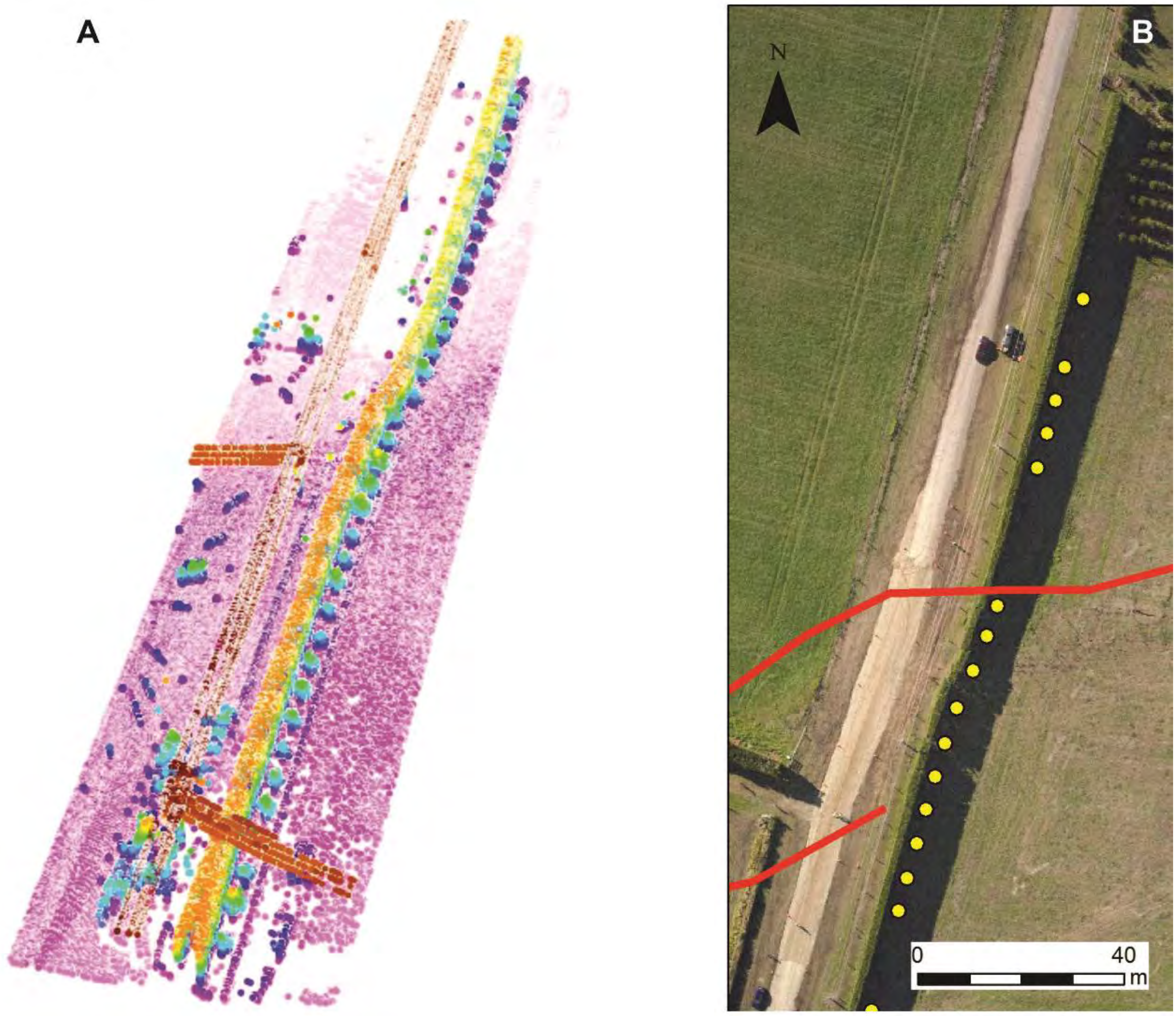

Figure 2.10 A) An oblique view of the point cloud subset along Highfield Road (see Figure 2.8 for location), colour-coded by altitude. Notable features include the power lines (dark orange and brown), hedge (light orange and yellow), trees (purple, blue and green). The fenceposts shown in B) are visible in the lower half of the image to the right of the trees (purple). B) Yellow dots are selected points from the ESE side of individual fenceposts in the paddock adjacent to Highfield Road.

2.5 ORTHOPHOTOS

Colour vertical aerial photographs were collected simultaneously with the collection of airborne Lidar on 10–11 September 2010 (6–7 days after the Darfield earthquake). The Orthophotos and Lidar were collected by New Zealand Aerial Mapping and funded by Environment Canterbury (Canterbury Regional Council).

At the time of collection, field identification and mapping of the western end of the fault had not been completed west of the Selwyn River. Thus, despite the survey being extended west of the known fault at the time, the fault strike is northwest in this area, meaning the western end was unfortunately not captured by this survey (Figure 2.11).

Figure 2.11 Coverage of Orthophotos collected by New Zealand aerial mapping on 10 September 2010. The area of the Lidar coverage is the same as the Orthophotos. The fault trace is from Villamor et al. (2012).

The aerial photographs were collected by a Trimble AIC medium format digital camera flying 600 m above the ground surface and orthorectified using the Lidar point cloud data (Section 2.6) with a ground sample distance of 0.1 m.

The orthorectified aerial photographs (hereafter referred to as Orthophotos) were supplied as a series of tiles in TIFF and ECW formats with a cell size of 0.25 m. The tiles were mosaicked by the Department of Conservation into a single image in ECW format. Adverse weather conditions in the days after the fault rupture meant that the data collection was conducted in less than ideal conditions. Due to low cloud, a lower altitude was used resulting in some mosaic seamlines and some small gaps in the Orthophoto coverage. The effect of the challenging flying conditions is also evident in the quality of the imagery with cloud shadow (e.g., Figure 2.12A) reducing the ability to easily identify the geomorphology of the surface rupture.

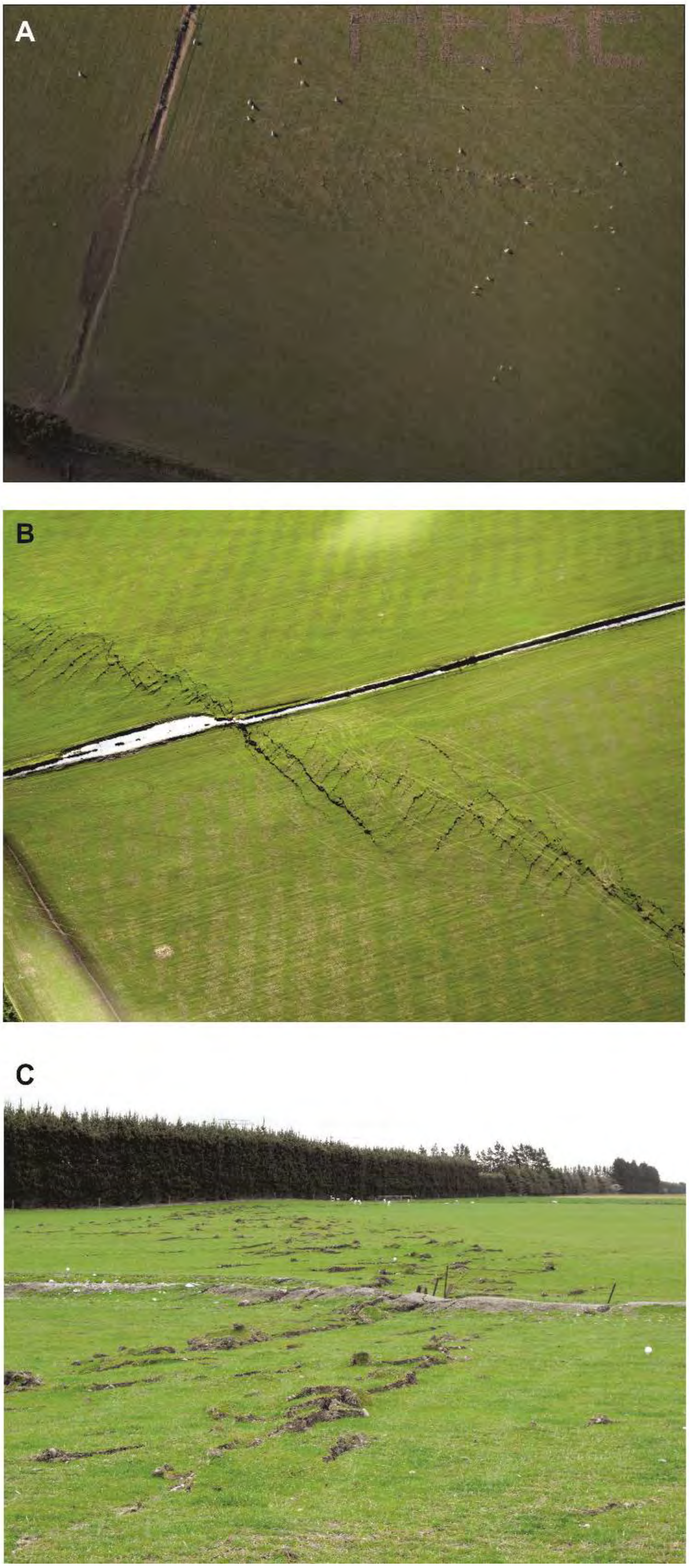

Figure 2.12 Three different photographs of site 69 (see Figure 2.1 for location). A) Orthophoto collected with the Lidar data (photo is oriented with north at the top). B) Oblique aerial photograph taken by Richard Jongens mid-afternoon on a sunny day (Saturday 4 September 2010) (view to the northwest). C) Ground photograph taken by Russ Van Dissen (view to the west).

2.6 LIGHT DETECTING AND RANGING (LIDAR)

An airborne Lidar survey was collected on 10–11 September 2010 by New Zealand Aerial Mapping. As for the Orthophoto survey, the Lidar survey does not cover the west end of the fault − the area is the same as that of the Orthophoto coverage (Figure 2.11).

The survey was collected using an Optech ALTM3100EA instrument at 70 hz, at a flying altitude of 600 m, with a field of view of 38º and a horizontal resolution of less than 1 m.

Lidar point clouds were generated in New Zealand Transverse Mercator (NZTM2000) projection and processing was carried out to identify, as far as possible, the Lidar returns from vegetation and buildings. The height accuracy was checked against control points surveyed by Neville Palmer, GNS Science, and vertical accuracy of ground returns was improved from +/- 0.03 m to 0.00 m. There are some errors associated with swath overlap, which are visible as 0.5 m vertical steps.

A Digital Elevation Model (DEM) was generated using only the ground return points, and a Digital Surface Model (DSM) was generated using all the points including returns from vegetation and buildings. Two resolution models were produced; 0.5 m and 0.25 m cell size (Figure 2.13). The DEM and DSM were produced using the inverse distance weighted interpolation method with a weighting factor of power value 2, a variable search radius using 12 points and a maximum distance of 20 m.

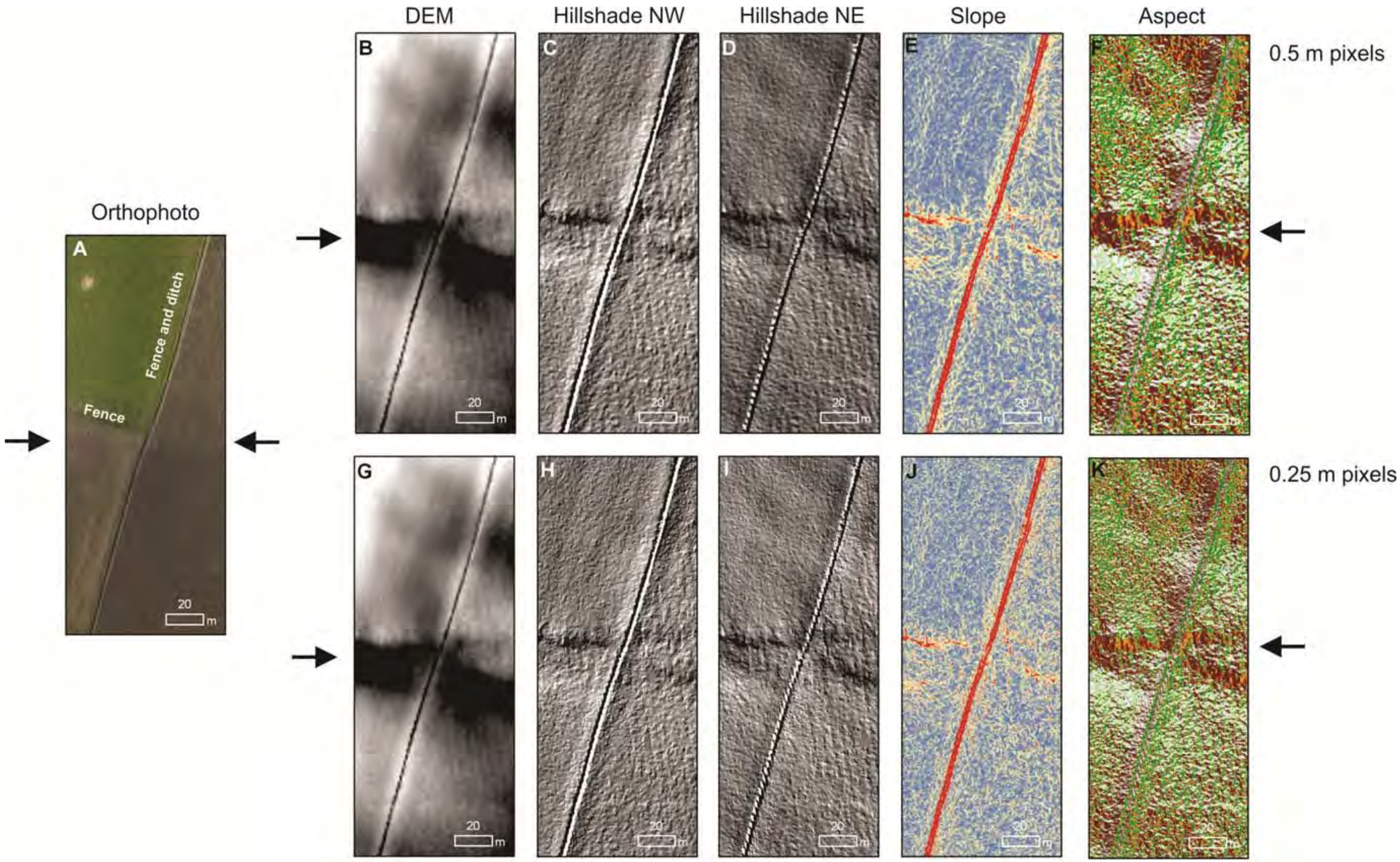

Figure 2.13 Comparison of different remote sensing datasets at site 45 (see Figure 2.1 for location). A) Orthophotos and B-K) Lidar. Arrows point to the Greendale Fault zone. Note that the ENE-trending fence visible in the Orthophoto is so young that there is not yet any visible topography associated with it and so it is not visible on the Lidar rasters.

A series of topographic rasters were developed from the DEM and DSM (Figure 2.13), as summarised in Table 2.2. The 0.5 m cell size model and rasters were developed for, and have been used in, previous studies (Quigley et al., 2010, 2012; Villamor et al., 2011, 2012; Duffy et al., 2013). The 0.25 m cell size model and rasters were developed for this study.

Table 2.2 Topographic rasters developed from the Lidar Digital Elevation Model (DEM) and Digital Surface Model (DSM) and used in this study.

Source model	Cell size (m)	Topographic raster type	Details	Name used in this study
DEM	0.5	Hillshade	Azimuth – 335º Viewing angle – 30º	Lidar 0.5 m HSNW
DSM	0.5	Hillshade	Azimuth – 45º Viewing angle – 30º	Lidar 0.5 m HSNE
DEM	0.5	Slope		Lidar 0.5 m Slope
DEM	0.5	Aspect		Lidar 0.5 m Aspect
DEM	0.25	Hillshade	Azimuth – 335º Viewing angle – 30º	Lidar 0.25 m HSNW
DEM	0.25	Hillshade	Azimuth – 45º Viewing angle – 30º	Lidar 0.25 m HSNE
DEM	0.25	Slope		Lidar 0.25 m Slope
DEM	0.25	Aspect		Lidar 0.25 m Aspect

3.0 PREVIOUSLY PUBLISHED DISPLACEMENT MEASUREMENTS

3.1 INTRODUCTION

In the months following the Darfield earthquake, Greendale Fault ground surface rupture displacement measurements were made by Nicola Litchfield and Russ Van Dissen and published by Quigley et al. (2012) (Figure 3.1). The aim was to provide the best estimates of ground surface displacement on the Greendale Fault during the Darfield earthquake, and as such focused on obtaining maximum coverage along the fault (Figure 3.2) using the highest resolution datasets available (generally RTK).

In this section we provide more details of the methods of measurement and construction of the displacement plots in Figure 3.1 than published by Quigley et al. (2012), as well as some more analysis of the results. The full dataset is contained in Appendix 1.

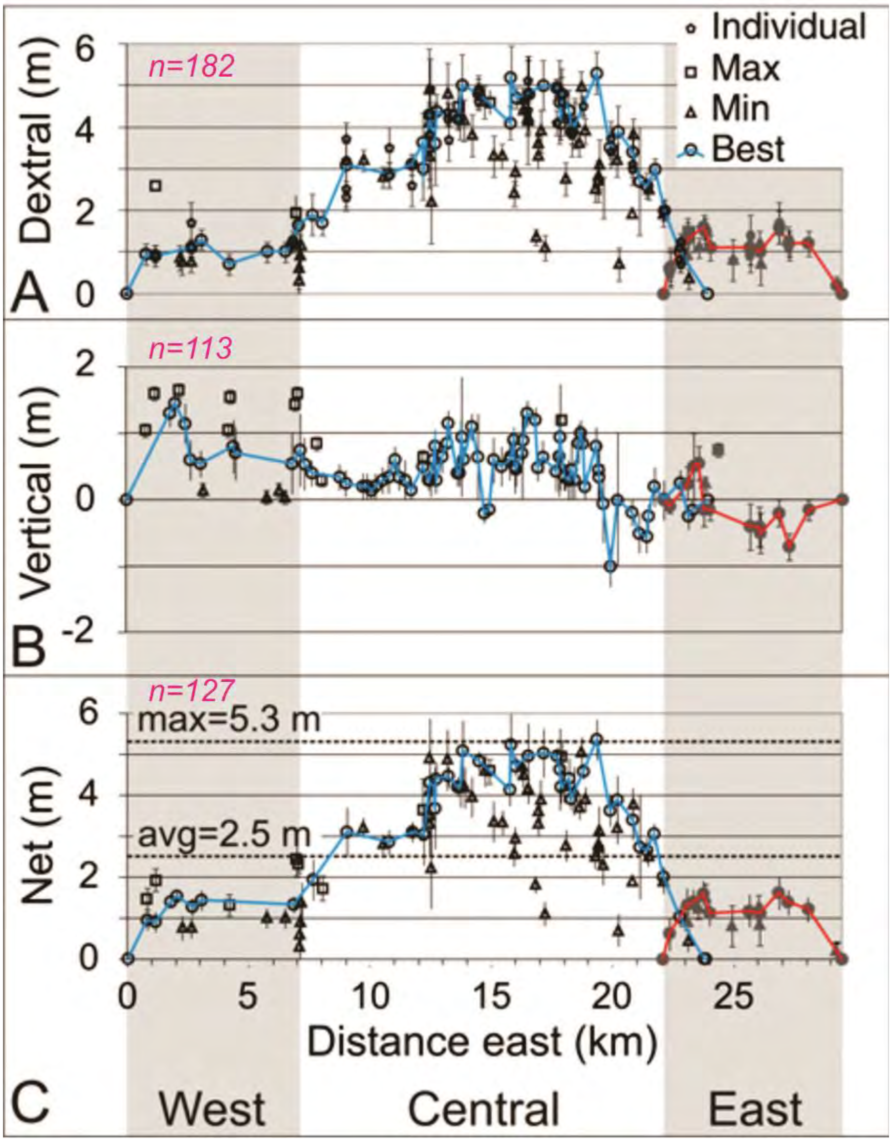

Figure 3.1 Along-strike (west-east) displacement plots published by Quigley et al. (2012). A) Dextral, B) Vertical (positive values are south-side up, negative are south-side down), and C) Net displacements including maximum and average values. Open symbols and blue line – west/central segments, filled grey circles and red line – eastern segment.

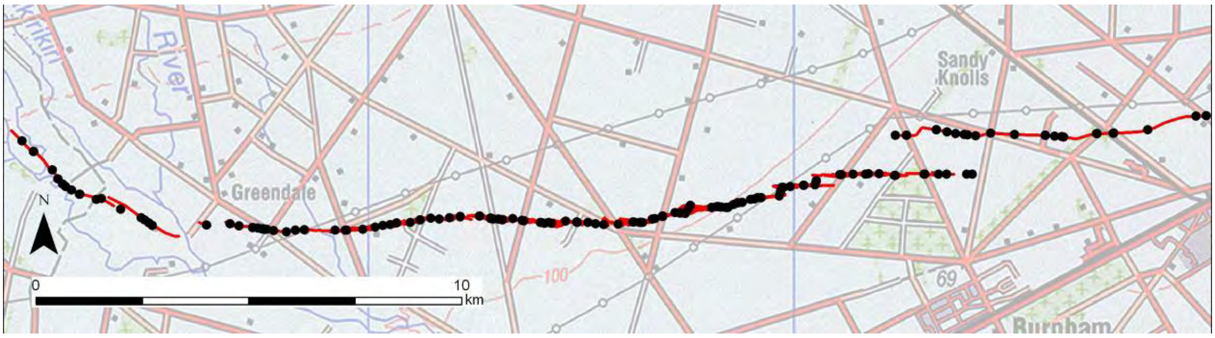

Figure 3.2 Sites (black dots) where the dextral and vertical displacements in Figure 3.1 (Quigley et al., 2012) were measured. The results and grid references for each site are contained in Appendices 1 and 2.

3.2 METHODS OF MEASUREMENT

3.2.1 Dextral displacements

The dextral displacements published by Quigley et al. (2012) were predominantly measured from RTK survey data, but where this was absent or insufficient (e.g., RTK surveys didn't span all the deformation) some supplementary measurements were undertaken using Orthophoto and Lidar data (Appendix 1, Table A 1.1).

The displacements were measured using standard techniques (e.g., Rockwell et al., 2002; Rockwell and Klinger 2013) of reconstructing straight features and measuring their displacement (offset) along the strike of the fault. Specifically, the measurements were undertaken manually in ArcGIS using the following steps (illustrated in Figure 3.3):

1. Where RTK data was used, marker profile lines (black lines in Figure 3.3) were constructed joining the survey points (yellow dots).
2. Straight lines were then fitted to (manually drawn along) the profile line (or directly along the marker on Orthophotos, Lidar rasters or Laser scan point cloud maps) on one side of the fault, beyond the deformation zone (light blue lines). This straight line was then extended to the simplified fault trace (red lines) or an average fault strike line between multiple traces (orange lines).
3. A copy of the straight line (light blue line) was then manually moved to overlay the originally continuous, and straight, feature on the opposite side of the fault (dark blue lines). Copying assured that the strike of the straight lines remained identical. The new straight line was then extended or trimmed at the fault or average fault strike line, as required.
4. The displacement was measured using the ArcGIS measuring tool, between the straight lines along the fault trace or average fault strike line (inset B).
5. Dextral displacement uncertainties were estimated based on data quality (e.g., straightness of the marker or irregularity of the auto RTK survey points) and measurement uncertainties derived by trial and error. Uncertainties were accompanied by subjective quality rankings (High, Medium, or Low, or some combinations of these) and comments (Appendix 1, Table A 1.1). The quality rankings reflect the original straightness of the marker and if the marker could be fit by a line of the same strike on both sides of the fault. That is, a relatively sinuous marker (and/or RTK survey points) which had a different strike on either side of the fault received a Low ranking and vice versa.

Each measurement was also classified as either a Total, Minimum, or Maximum displacement, depending on whether the marker was considered to entirely cross the deformation zone, or in some cases, where the marker appeared to not be originally straight (Appendix 1, Table A 1.1).

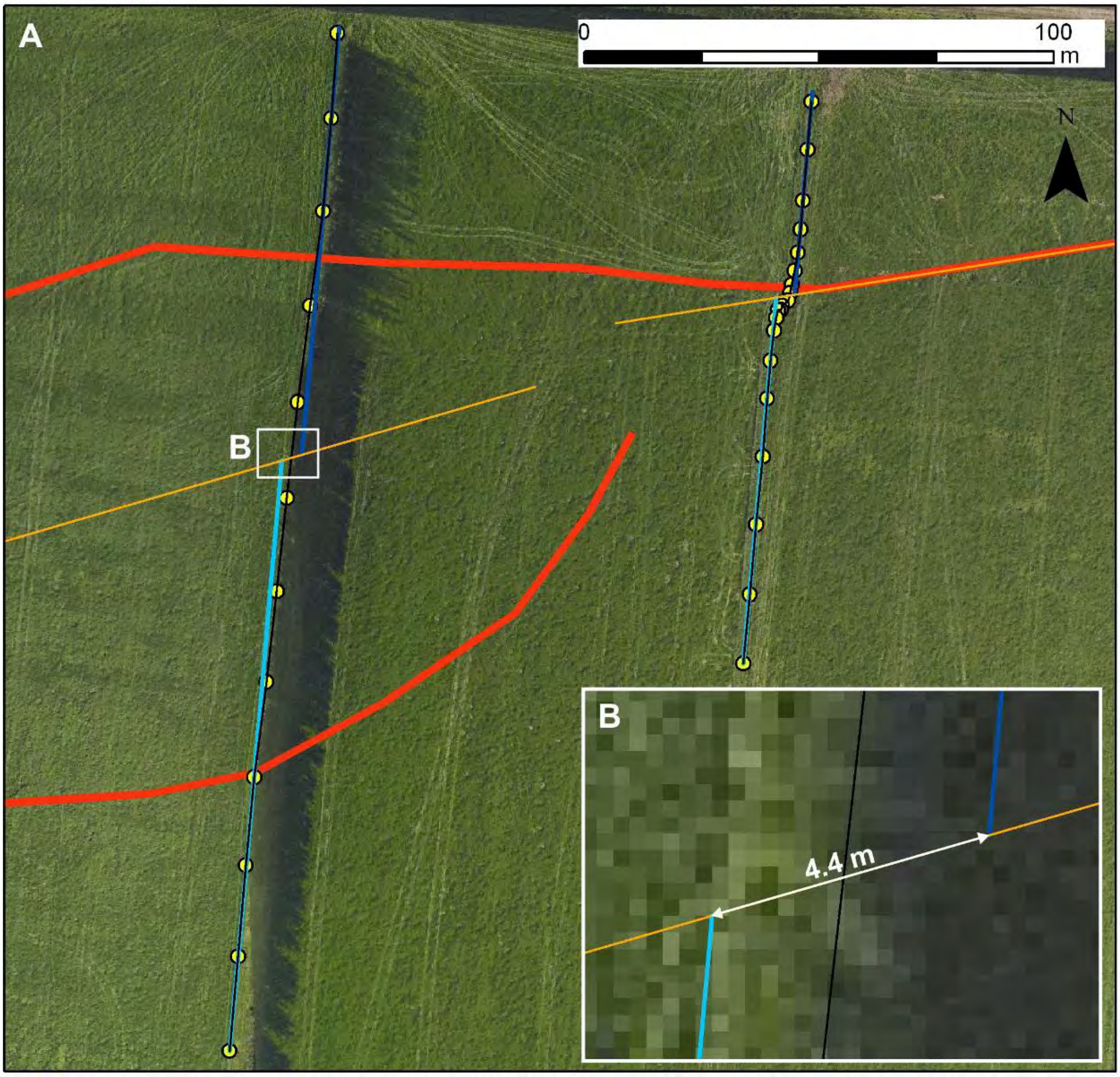

Figure 3.3 Examples of the manual measurement of dextral displacements in ArcGIS (sites 58 – left, and 59 – right; see Figure 2.1 for location). In order of construction the features are: Red lines – simplified fault traces; Orange lines – average fault strike lines; Yellow points – RTK survey points of fenceposts and fault detail; Black lines – profile lines joining the RTK survey points; Light blue lines – straight lines fitted through the portion of the profile lines located outside of the zone of ground surface fault rupture deformation; Dark blue lines – straight lines copied and pasted from the light blue line and fit through the profile lines on the opposite side of the fault. See text for more details.

3.2.2 Vertical displacements

The vertical displacements were generally measured using cross sections extracted from the 0.5 m Lidar DEM. The exceptions are at the west end, where Lidar coverage is absent and so RTK survey data was used instead. The reason for preferring Lidar data over RTK data for the majority of the fault is that, although the fault ruptured across a relatively flat alluvial fan surface (e.g., Forsyth et al., 2008), in detail the surface has a gradient and more importantly, is cut by multiple braided channels (e.g., Figure 3.4). The presence of this topography meant that the measurement of vertical displacements required relatively long cross sections to reliably fit a straight line to the ground surface, and the RTK profiles were invariably too short (e.g., Figure 3.4A, Figure 3.5).

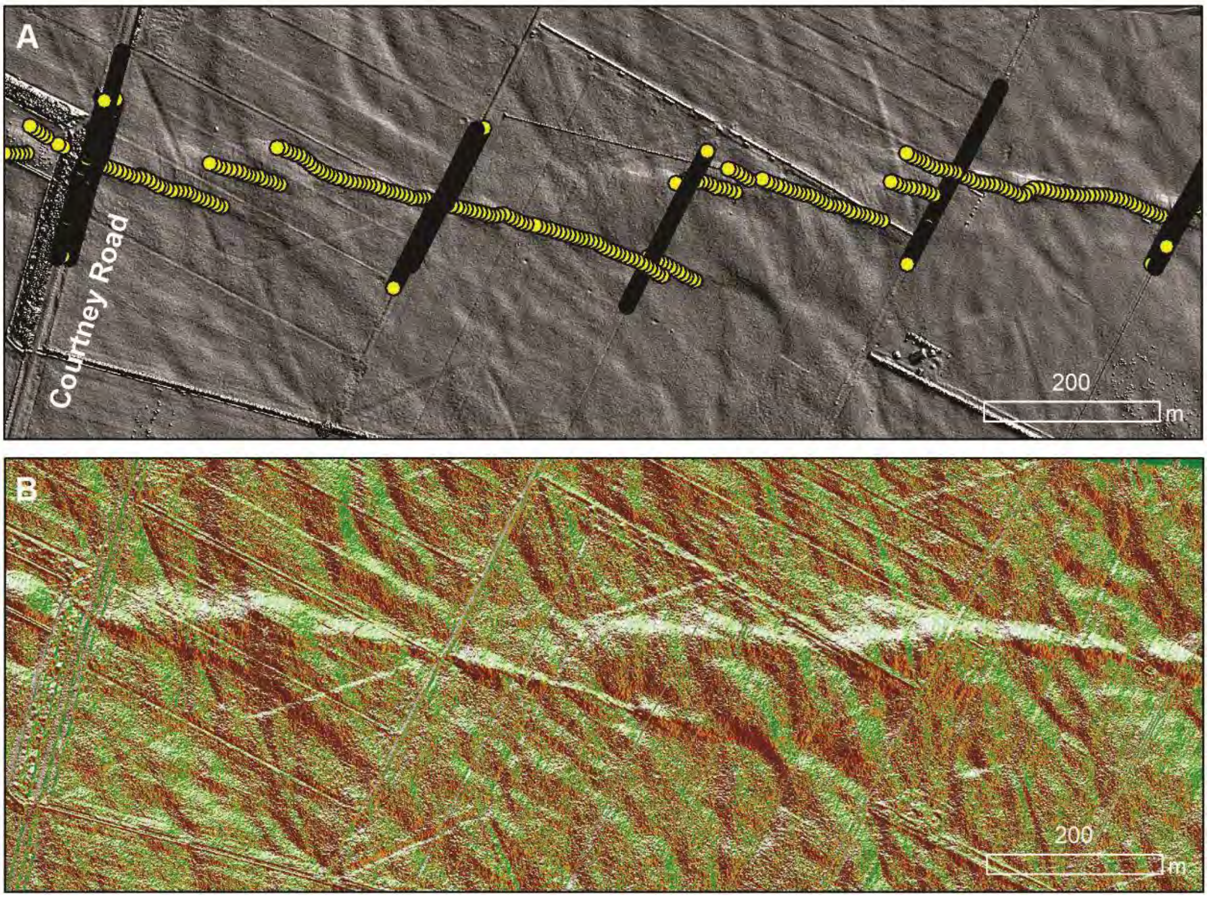

Figure 3.4 NNW-trending alluvial channels are barely visible in the field but are particularly obvious in the Lidar A) Hillshade NE (illuminated from the northeast) and B) Aspect maps. The area shown is in the centre of the fault; channels are even more developed at the east end of the fault (e.g., Villamor et al., 2011). Yellow dots in A) are RTK survey points.

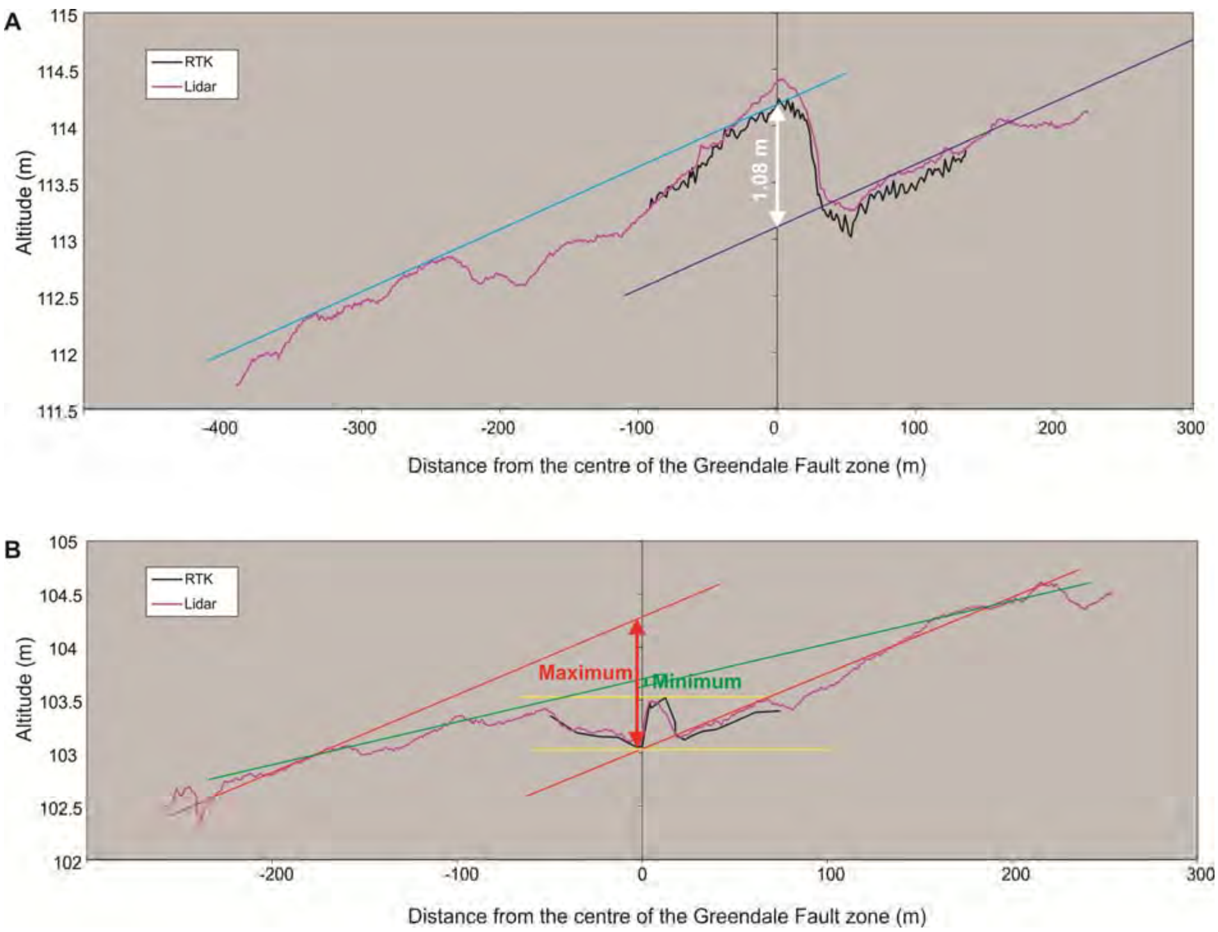

Figure 3.5 Examples of the manual measurement of vertical displacement from cross sections extracted from the 0.5 m Lidar DEM. A) site 35, B) site 53 (see Figure 2.1 for locations). These examples also show how the RTK profiles (black) were typically too short to capture the true topographic gradient.

Cross sections were extracted from the 0.5 m Lidar DEM along, or immediately adjacent to (e.g., to avoid cultural features), selected dextral displacement profiles in ArcGIS. The Lidar cross section and corresponding RTK profile were then plotted, and displacements measured, in Excel.

The measurement process was very similar to the dextral displacement measurements, and is illustrated in Figure 3.5A:

1. A straight line was fitted to the ground surface beyond the deformation zone (light blue line), making sure it crossed the fault.
2. The straight line was then “copied and pasted” to fit the corresponding ground surface on the opposite side of the fault (dark blue line) and crossing the fault.
3. The vertical displacement was measured from the y-axis of the plots (generally manually measured with a ruler on hardcopies).
4. For many sites however, the ground surface topography was so significant that no single value could be measured. In these cases, a mean value was calculated between minimum and maximum displacements (Figure 3.5B).
5. Vertical displacement uncertainties were estimated based on the visually-defined best fit line to the topography and measurement uncertainties derived by trial and error.

At some sites the heights of the pop-ups were also measured (yellow lines in Figure 3.5B; bulge amplitudes in Appendix 1, Table A 1.2). Like the dextral displacements, values were then classified as either: Total; Minimum; or Maximum (Appendix 1, Table A 1.2).

3.3 CONSTRUCTION OF DISPLACEMENT DISTRIBUTIONS (FIGURE 3.1)

3.3.1 Dextral displacement distribution (Figure 3.1A)

The along-strike (west-east) displacement plot shown in Figure 3.1A contains 154 dextral displacements measured from the data sources listed in Table 3.1.

Table 3.1 Data sources of the dextral displacements shown in Figure 3.1A (published by Quigley et al., 2012).

Dataset	Number of dextral displacements
RTK	111
Tape and Compass	21
Orthophoto	16
Lidar 0.5 m – Hillshade NW	6
SUBTOTAL	*154*
0 m displacements	4
Preferred or best displacements	24
TOTAL	*182*

There are also two other types of datapoints shown on Figure 3.1A:

- 0 m displacements at the ends of the two major traces. These were situated mid-way between the last deformed marker and the first undeformed marker.
- Preferred or best displacements made from combining measurements of markers situated within a few metres of each other (e.g., either side of a road, or a road edge and the adjacent fenceline) (Type “p” in Appendix 1, Table A 1.1). The combined values were derived from the individual measurements using judgement (rather than calculating an average), taking into account the relative uncertainties and quality ranking of each measurement, as well as Tape and Compass measurements.

These bring the total number of datapoints on Figure 3.1A to 182.

A "best” line was constructed connecting the preferred or best values as well as displacements from individual sites classified as Medium, Medium-High, or High quality (Type “pt” in the table in Appendix 1, Table A 1.1). No Tape and Compass measurements were included in the best fit line.

3.3.2 Vertical displacement distribution (Figure 3.1B)

A total of 113 vertical displacement datapoints are shown on Figure 3.1B, from the data sources listed in Table 3.2. Like the dextral displacements, the 0 m displacements at the ends of the traces are situated mid-way between the last deformed marker and the first undeformed marker. No cross sections were situated within a few metres of each other, so there was no need to combine values to obtain preferred displacements.

Table 3.2 Data sources of the vertical displacements shown in Figure 3.1B (published by Quigley et al., 2012).

Dataset		Number of vertical displacements
Lidar 0.5 m DEM		108
Tape and Compass		1
	SUBTOTAL	*109*
0 m displacements		4
	TOTAL	*113*

A "best" line was constructed through all the values classified as measuring the total displacement (i.e., not minimum or maximum measurements).

3.3.3 Net displacement distribution and calculation of average displacement (Figure 3.1C)

Net displacements were calculated for 127 sites where both dextral and vertical displacements had been measured. They were calculated from the square root of the sum of the dextral and dip-slip displacements squared. Dip-slip displacements were calculated from the vertical displacements and an average fault dip of 80º ± 10º to the south for the central Greendale Fault, as inferred by geodetic modelling (Beavan et al., 2012).

The average net displacement (2.55 m) was calculated from integration of the area under the net slip displacement curve, for which a single curve combining both strands was constructed (Figure 3.6). Combining the two curves was achieved by manual addition of displacements in the overlap zone, using sites as close to each other in distance east along the fault as possible. The area under the curve (74,934 m^2) was calculated in ArcGIS, and the average displacement was calculated from the area divided by the fault length (29,441 m).

The average net displacement uncertainty was calculated by two methods. The first method (by Russ Van Dissen) was a manual trial and error using different curve fits. The second method (by David Rhoades and described in the supplementary material of Quigley et al., 2012) was to run 1000 monte carlo samples between the individual error bars. These resulted in minimum and maximum average values of 2.4 and 2.8 m respectively.

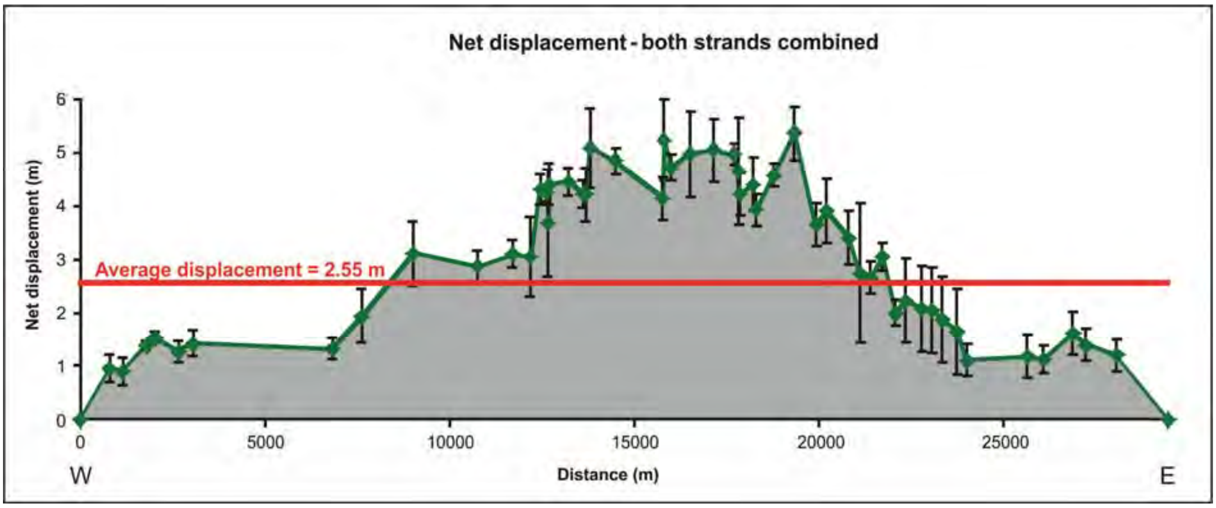

Figure 3.6 Calculation of the average displacement (red) from the integration of the area (shaded) under the net surface rupture displacement profile (both strands combined), divided by the fault length.

3.4 DISCUSSION

3.4.1 Average net displacement

There are several ways to calculate the average net displacement. The integration of the area under the displacement curve method used by Quigley et al. (2012) has the advantage that it takes account of the shape of the curve and hence is not biased by the distribution of individual datapoints along the fault. For example, if you simply calculate the average by adding the 120 “best” measurements (not including 0 m displacement) and dividing by the total number (120), the result is 2.93 m. That this value is higher than the 2.55 m calculated from the displacement curve integration method is simply a function of there being a greater number of high values in the centre of the fault than low ones towards the fault tips (the median value is 3.08 m).

The displacement curve integration method is dependent upon the reliability of the shape of the curve however, which is subject to error if there are data gaps. Quigley et al. (2012) also briefly explore fitting different curves and note that fitting a smoother curve results in an average displacement of 2.8 m. The method is also dependent upon the length of the fault/rupture. In the case of the Greendale Fault, we were confident that we had sufficient along-strike coverage (average distance between measurements is 230 m) to determine the shape of the curve and that we had reliably identified the fault endpoints (to within ±100 m at the east end and ±450 m at the west end). This may not always be the case for fault surface ruptures in areas of difficult access, significant vegetation, or covered by earthquake-triggered landslides (e.g., Fyfe, 1929; Klinger et al., 2005; Kaneda et al., 2008; Liu-Zeng et al., 2010).

One issue with the Greendale Fault however, is that only 1 net displacement of 2.55 m was calculated (Figure 3.6), and in fact only 16 (out of 127) were between 2 and 3 m. Plotting the net displacements as a histogram in Figure 3.7 shows that there is a bimodal distribution, with two peaks centred at ~1.25 m and ~4.25 m. This bimodality is also apparent in the shape of the net displacement plot (Figures 3.1C and 3.6), which has three distinct segments, west (0-7600 m), central (7600-22,000 m), and east (22,000-29,500 m); the shape of the plot is discussed further in section 3.4.3. Calculation of the average net displacement values for each of those segments by simply adding each of the values and dividing by the total, results in net displacements of 1.34, 4.11, and 1.26 m for the west, central, and east segments respectively (Figure 3.8). These three segments are consistent with seismological and geodetic evidence for the Darfield earthquake consisting of multiple rupture planes (Holden et al., 2011; Beavan et al. 2012) that relate to the three delineated surface rupture segments (Figure 3.1; Quigley et al., 2012; Duffy et al., 2013). Many other historical fault ruptures also have multi-peaked displacement plots indicative of multiple rupture segments (e.g., Beanland et al., 1990; Sieh et al., 1993; Barka et al., 2002; Haessler et al., 2004; Wesnousky, 2008).

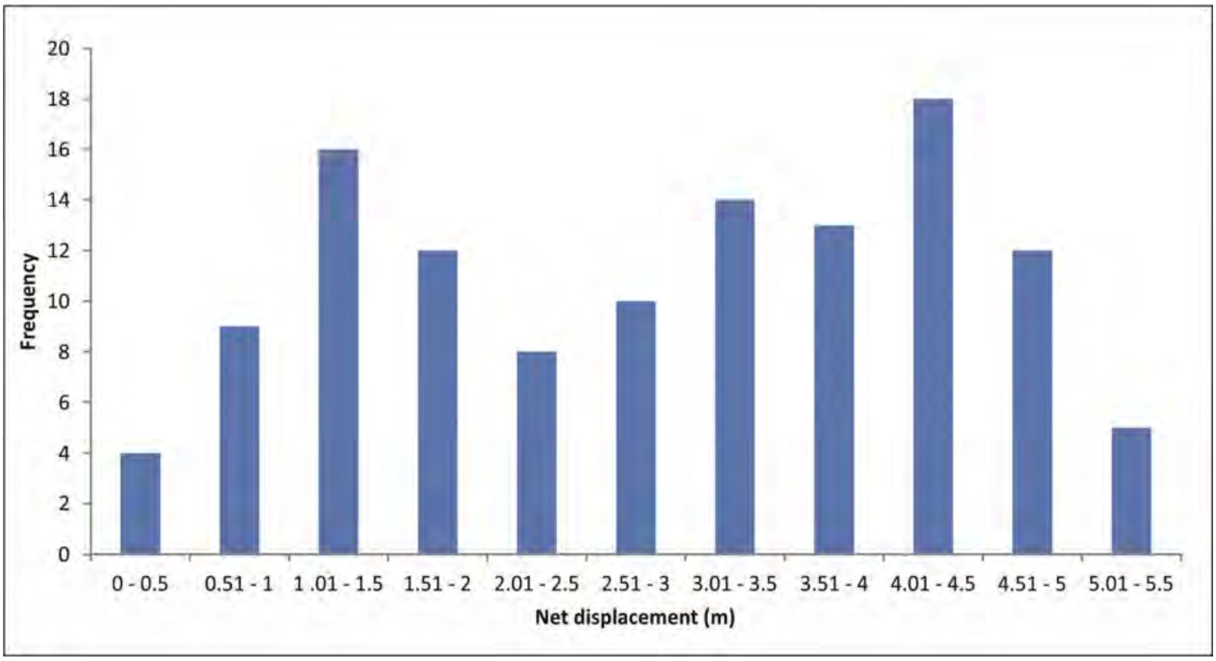

Figure 3.7 Net displacement (best) values showing a bimodal distribution.

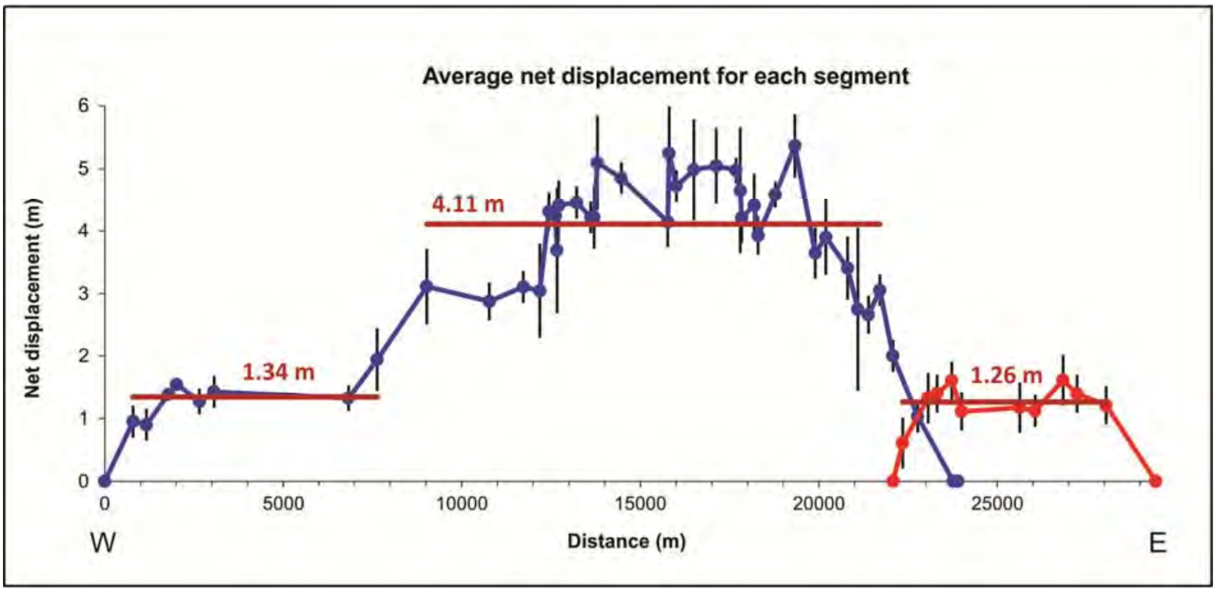

Figure 3.8 Average net surface rupture displacements calculated for three segments of the Greendale Fault.

3.4.2 Ratio of average to maximum displacement

Setting aside the uncertainties associated with the average net displacement, one interesting feature to note is that the ratio of the average (2.55 m) to maximum (5.36 m) displacement is 0.45, which falls entirely within the average ratio of 0.4 ± 0.14 derived from 37 global historical ruptures (Wesnousky, 2008) (Figure 3.9). Furthermore, it is similar to the average ratio of 0.44 ± 0.14 for 21 strike-slip ruptures (Wesnousky, 2008) (Figure 3.9).

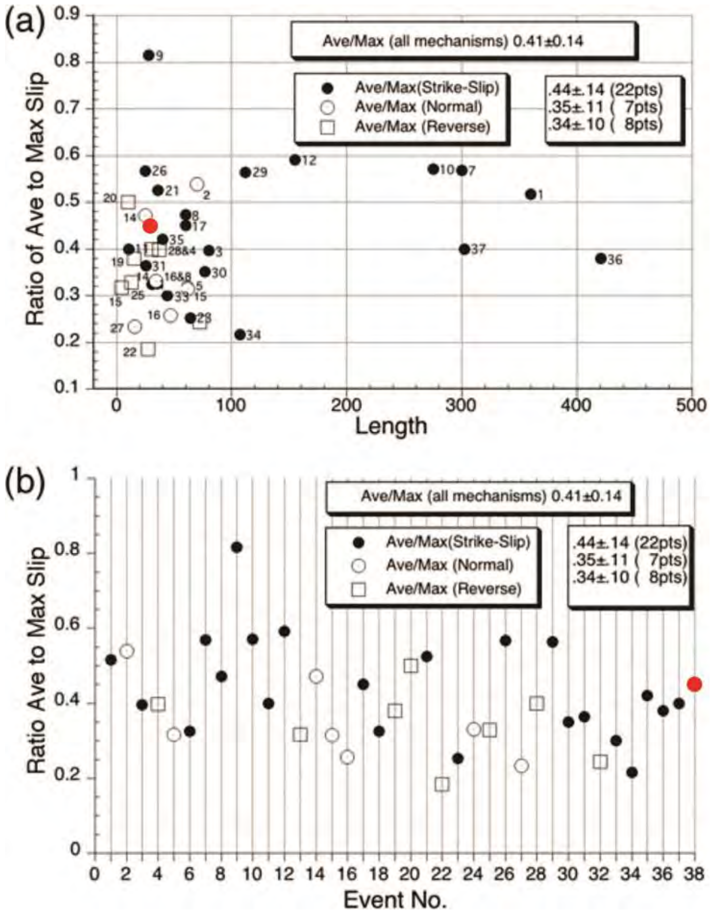

Figure 3.9 Comparison of the Greendale Fault (red dots) with a global ground surface rupture dataset (Wesnousky, 2008) of the ratio of average to maximum ground surface displacement as a function of a) rupture length and b) event number.

The consistency in the ratio of average to maximum displacement with global examples confirms that the ratio appears to be independent of length. For example, it is intriguing to note that the average and maximum ground surface rupture displacements during the 1999 M_w 7.1 Hector Mine Earthquake were exactly the same as the Greendale Fault, despite the Hector Mine Earthquake ground rupture being considerably longer (48 km; Treiman et al., 2002). This consistency may therefore instead be a function of the profile shape, which may in turn be a function of fault interactions, which happen on all scales.

3.4.3 Shape of the net displacement plot

Defining the shape of the historical fault rupture displacement plots is useful because if a simple curve can be fitted to the datapoints, then such curves could be used to model future ground surface rupture displacements in fault displacement hazard studies. Figure 3.10 shows different types of simple curves fitted to the net displacement distribution, after Weskousky (2008). The flat line in Figure 3.10 is the average net displacement (2.55 m) as described in Section 3.3.3. The remaining curves were fitted by visual trial and error (altering the position of the maximum point on the curve), ensuring that the area under each curve was kept the same.

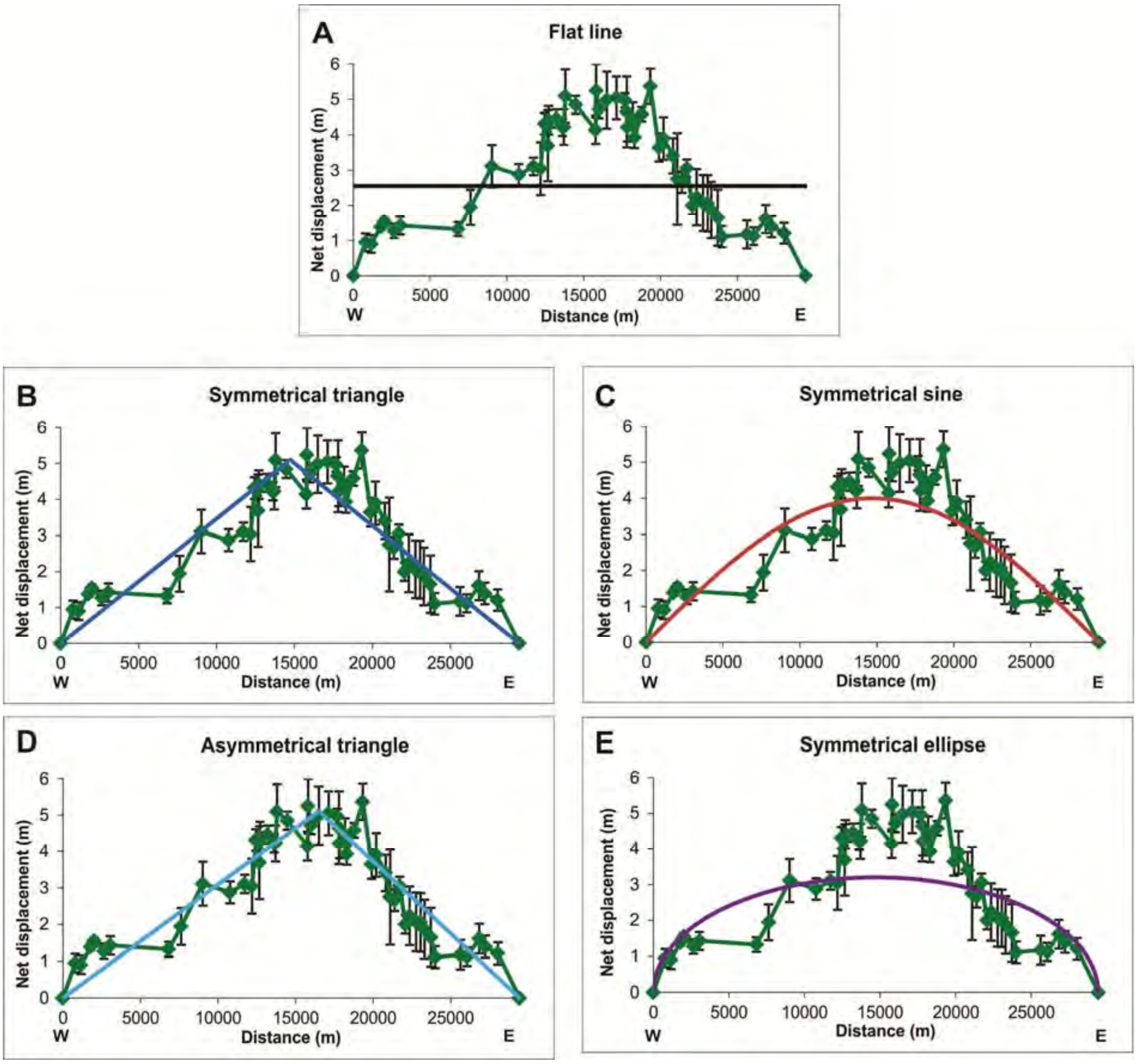

Figure 3.10 Different types of simple curves fitted to the Greendale Fault net displacement distribution (both strands combined).

Visual comparison of the curves in Figure 3.10 shows that the Greendale Fault net displacement distribution is best fit by a triangle, particularly the asymmetric triangle, followed by the symmetrical sine curve. We were unable to generate an asymmetrical sine curve, but suspect it fits just as well as the asymmetrical triangle. The flat line is the least well fit. This is consistent with Wesnousky (2008), who found that an asymmetrical curve fit was the best fit to most distributions. The better fit of a triangle than a curve reflects the three segments described in section 3.4.1 and the fact that the central segment is the longest, and so dominates the overall shape (i.e., if the west and east segments were longer the distribution would have an overall flatter shape).

3.4.4 Comparison with the displacement measurements of Elliott et al. (2012)

A detailed comparison of the Greendale Fault surface rupture displacements with displacements from other datasets such as seismology, geodesy and InSAR (e.g., Barnhart et al. 2011; Beavan et al., 2011; Holden et al., 2011) are beyond the scope of this study. However, in Figure 3.11 we show a comparison with the only other Greendale Fault ground surface rupture displacement dataset that we are aware of. These are from Elliot et al.

(2012), who measured dextral displacements along the central and east segments using 3 datasets:

1. field (technique not stated, but assumed to be a tape measure);
2. orthophoto (0.25 m resolution; presumably the same as used in this study); and
3. satellite (Worldview imagery; 0.5 m resolution).

Elliott et al.'s measurement technique does differ somewhat from ours however, in that dextral displacements were initially measured perpendicular to the azimuth of the marker and then converted to strike-slip (horizontal) displacements onto a west-east striking trace. Vertical displacements were measured using a Lidar DEM (2 m resolution; presumably the same as used in this study). Uncertainties were estimated to be 10 cm for the vertical displacements (Figure 3.11B), but none were estimated for the dextral displacements, and so none are shown on Figure 3.11A.

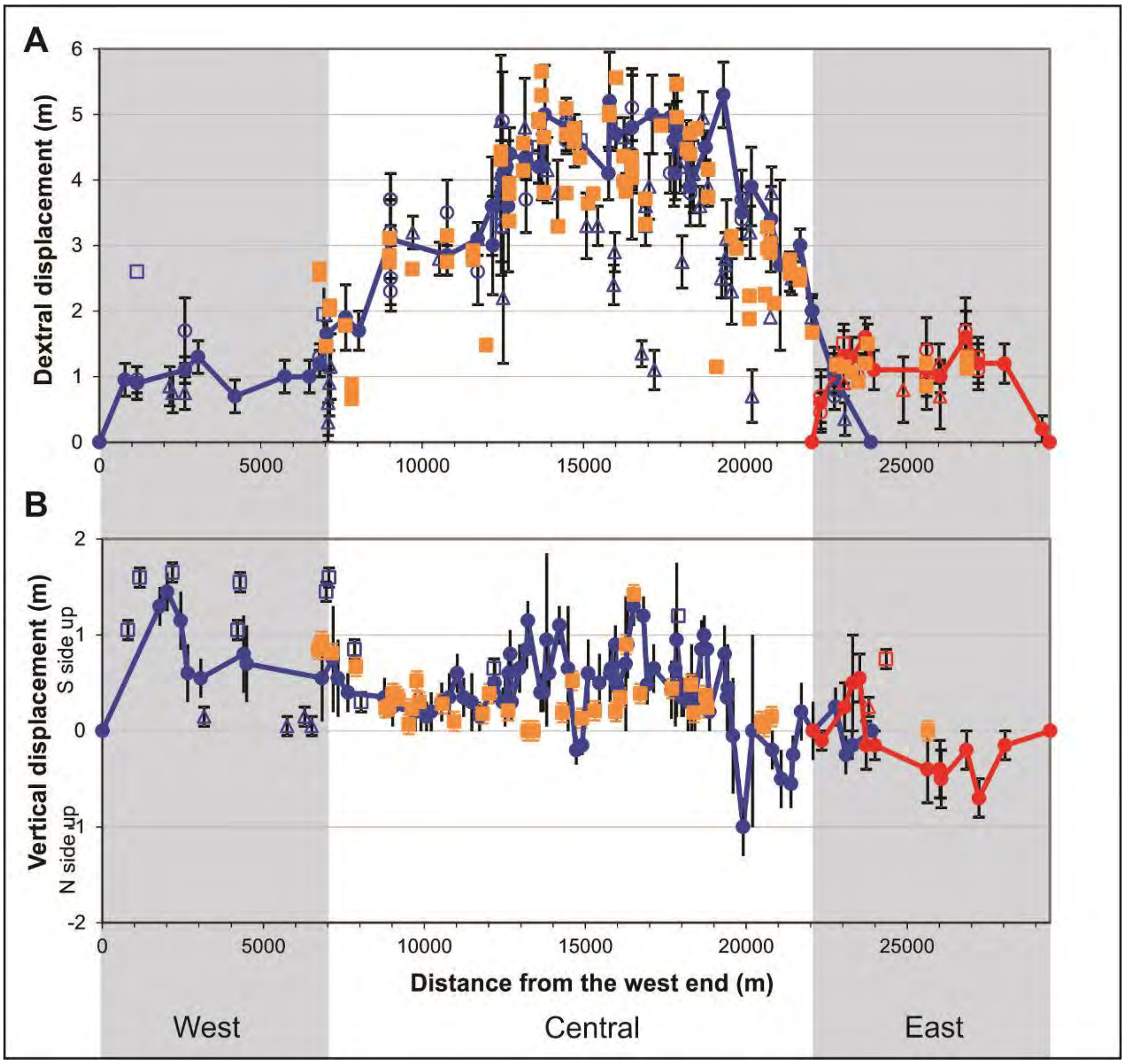

Figure 3.11 Dextral (A) and Vertical (B) Greendale Fault displacement measurements of Elliott et al. (2012) (orange) and Quigley et al. (2012) (blue and red – refer to Figure 3.1 for explanation of these symbols). The Elliott et al. (2012) data are from their Table 1 but note that the locations may not match exactly between datasets, for reasons described in the text. Note the reasonable correlation for dextral displacement, but Elliott et al. (2012) generally have lower measurements of the vertical displacement in the central segment of the fault.

Visual comparison of the two datasets in Figure 3.11 shows that there is reasonably good agreement between the two. The main exception is that many of Elliott et al.’s vertical displacements in the centre of the fault are lower than that of Quigley et al. (2012), for which we have no clear explanation. We note that their maximum vertical displacement measurement (1.4 m at ~16,500 m; Highfield Road) matched ours. They also have slightly higher maximum dextral displacement measurements in the centre of the fault; their maximum is 5.65 m, whereas ours is 5.3 m. It is not documented if the low dextral displacement measurements in the centre of the fault of Elliot et al. (2012) are minimum, as compared to total, measurements, as for Quigley et al. (2012) who do make the distinction between minimum, maximum and best (i.e. total).

More detailed comparison (e.g., at individual sites) is not warranted for a number of reasons including: 1) differences in measurement technique (e.g., the conversion of Elliott et al.’s dextral measurements to W-E traces); 2) uncertainty in matching sites between datasets (e.g., Elliott et al.’s locations were published as latitudes and longitudes to 4 decimal places and don’t plot exactly on markers and some different sites have the same latitudes and longitudes); and 3) differences in ways of combining measurements (e.g., Quigley et al.’s use of judgement to derive “best” measurements). However, some further comparison is undertaken between measurements from different datasets in Section 4.4.2.

4.0 NEW DEXTRAL DISPLACEMENTS USING MULTIPLE DATASETS

4.1 INTRODUCTION

The previous measurements of Greendale Fault ground surface rupture displacements published by Quigley et al. (2012) were primarily undertaken using two datasets – RTK and Tape and Compass (Table 4.1 and section 3). In this section we present new measurements of dextral displacements using 11 other datasets (Table 4.1). The purpose is to explore uncertainties in displacement measurements using different datasets and then to use these to inform single event displacement uncertainties for faults that have ruptured in the geological past.

Table 4.1 Numbers of previous (Quigley et al., 2012) and new (this study) dextral displacement measurements.

Number	Dataset	Previous	New	Combined
1	RTK	111	0	111
2	Tape and Compass	21	0	21
3	Orthophoto	16	71	87
4	Lidar 0.5 m – Hillshade NW	6	45	51
5	Lidar 0.5 m – Hillshade NE	0	36	36
6	Lidar 0.5 m – Slope	0	27	27
7	Lidar 0.5 m – Aspect	0	28	28
8	Lidar 0.25 m – Hillshade NW	0	40	40
9	Lidar 0.25 m – Hillshade NE	0	28	28
10	Lidar 0.25 m – Slope	0	37	37
11	Lidar 0.25 m – Aspect	0	31	31
12	Laser scan – All points	0	8	8
13	Laser scan – Selected points	0	5	5
	TOTAL	**154**	**356**	**508**

The new displacement measurements were undertaken by one person (Nicola Litchfield) at the same sites as measured previously. Only dextral displacements were measured because of the unsuitability of the RTK data for vertical displacement measurements (section 3.2.2). To emphasise that the new measurements are additional measurements at the same sites, we hereafter refer to the new displacements as “displacement measurements”.

4.2 METHODS OF MEASUREMENT

The methods used to obtain the new dextral displacement measurements were the same as used for the previously published measurements (section 3.2.1), involving copying and pasting straight lines fitted along markers on one side of the fault to the equivalent marker on the other side, and then measuring the displacement along the fault or an average strike line, in ArcGIS.

Because the aim of this study is to compare measurements using different datasets, rather than to obtain the best surface displacements, notes, including whether the measurement was considered a maximum or minimum displacement, were not taken for each measurement.

Dextral displacement uncertainties were assigned based on a combination of the data quality and measurement uncertainties. The latter were derived by trial and error. The uncertainties do not take into account the registering of the remote sensing data (Orthophotos and Lidar) to GPS datapoints, as these were considered to be insignificant compared with the measurement uncertainties. The resolution of the Orthophoto and Lidar datasets (0.5 and 0.25 m) were also not explicitly included in a calculation of uncertainties in that they were also considered smaller than the measurement uncertainties (discussed further in sections 4.3.2 and 4.4).

All available datasets were examined at each of the 101 previously measured sites (Figure 3.2), but it was not always possible to measure a displacement using each dataset at each site, mainly due to poor resolution of markers in some datasets. For example, relatively new fencelines are often not visible in the Lidar rasters because there was no ground surface expression in the 0.25 and 0.5 m pixel rasters (i.e., a ridge left by ploughing paddocks either side) (e.g., Figure 2.7). Road edges and centrelines were also generally not visible in the Lidar rasters. A lack of a measurement at a site therefore provides a further expression of uncertainty, as discussed in sections 4.3.2 and 4.4.

4.3 RESULTS

A total of 356 new dextral displacements measurements were obtained from 11 datasets. The full table of displacement measurements is included in Appendix 2 and the number of measurements per dataset are summarised in Table 4.1.

Figure 4.1 shows an along-strike (west-east) plot with the new dextral displacement measurements plotted against the previous measurements. This shows that there is considerable variability in the new displacement measurements, many of which are outside the uncertainties of the previous measurements. Note that because the focus of this study is on comparing measurements using different datasets, in this and subsequent plots, measurements are not distinguished as total, minimum or maximum measurements as was shown by Quigley et al. (2012) in Figure 3.1.

Figures 4.2 and 4.3 show all the measurements (new and previous) colour-coded by dataset. These figures suggest that some of the variability does appear to be a function of the dataset, with the Lidar measurements appearing to show the most variation. It is however, difficult to assess differences at individual sites due to the large number of data on these along-strike plots. We therefore examine the differences in some detail in the following sections.

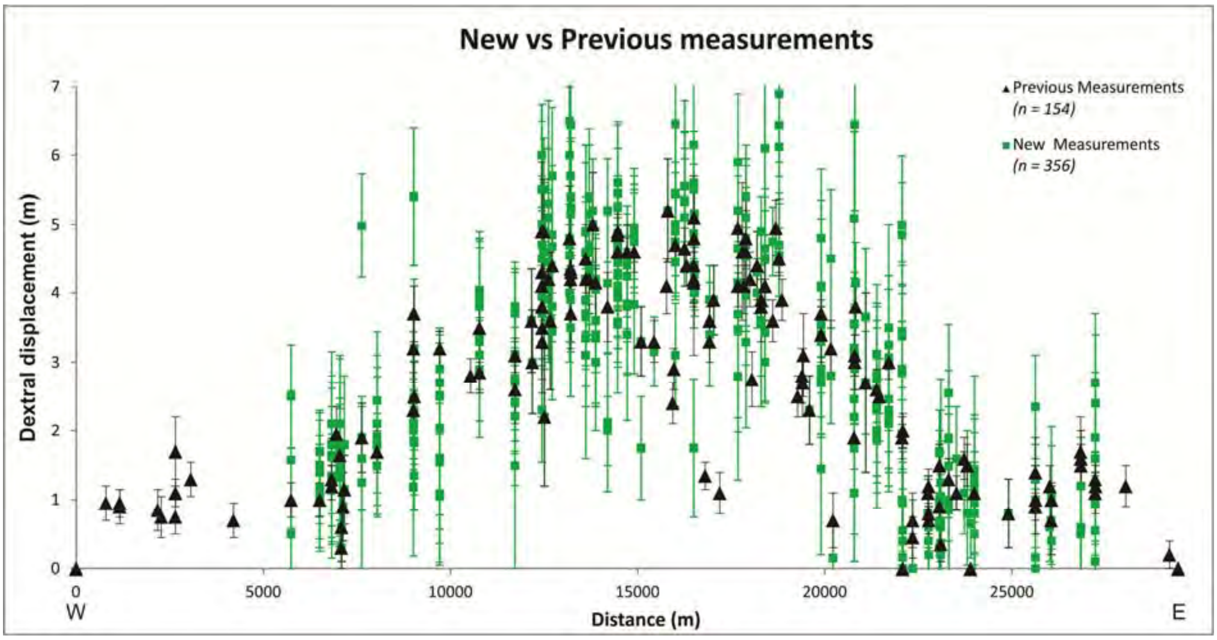

Figure 4.1 Along-strike (West-East) plots showing new (this study – by Nicola Litchfield) compared with previous (Quigley et al., 2012) dextral displacement measurements.

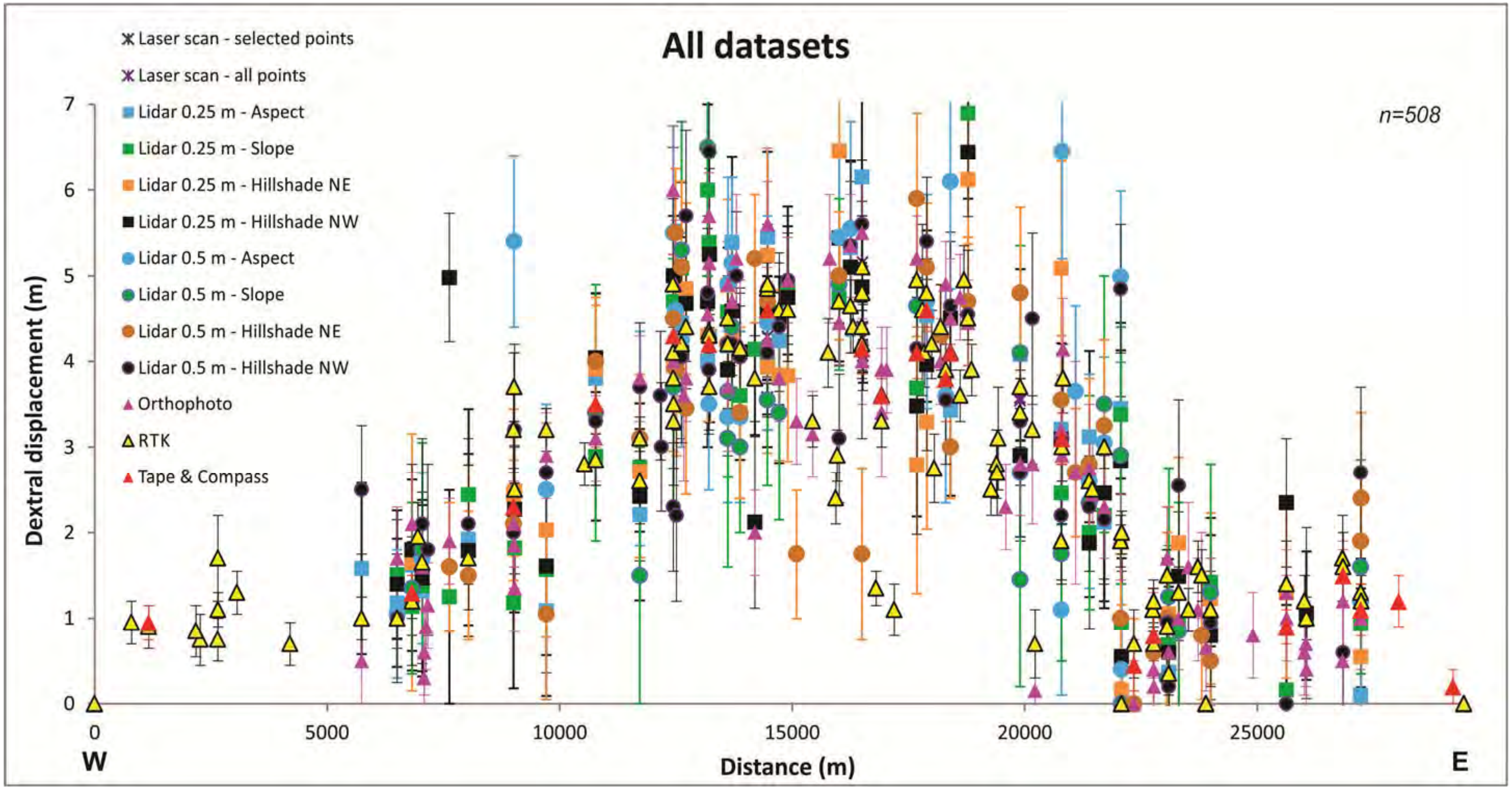

Figure 4.2 All (new and previous) dextral displacement measurements, colour-coded by dataset.

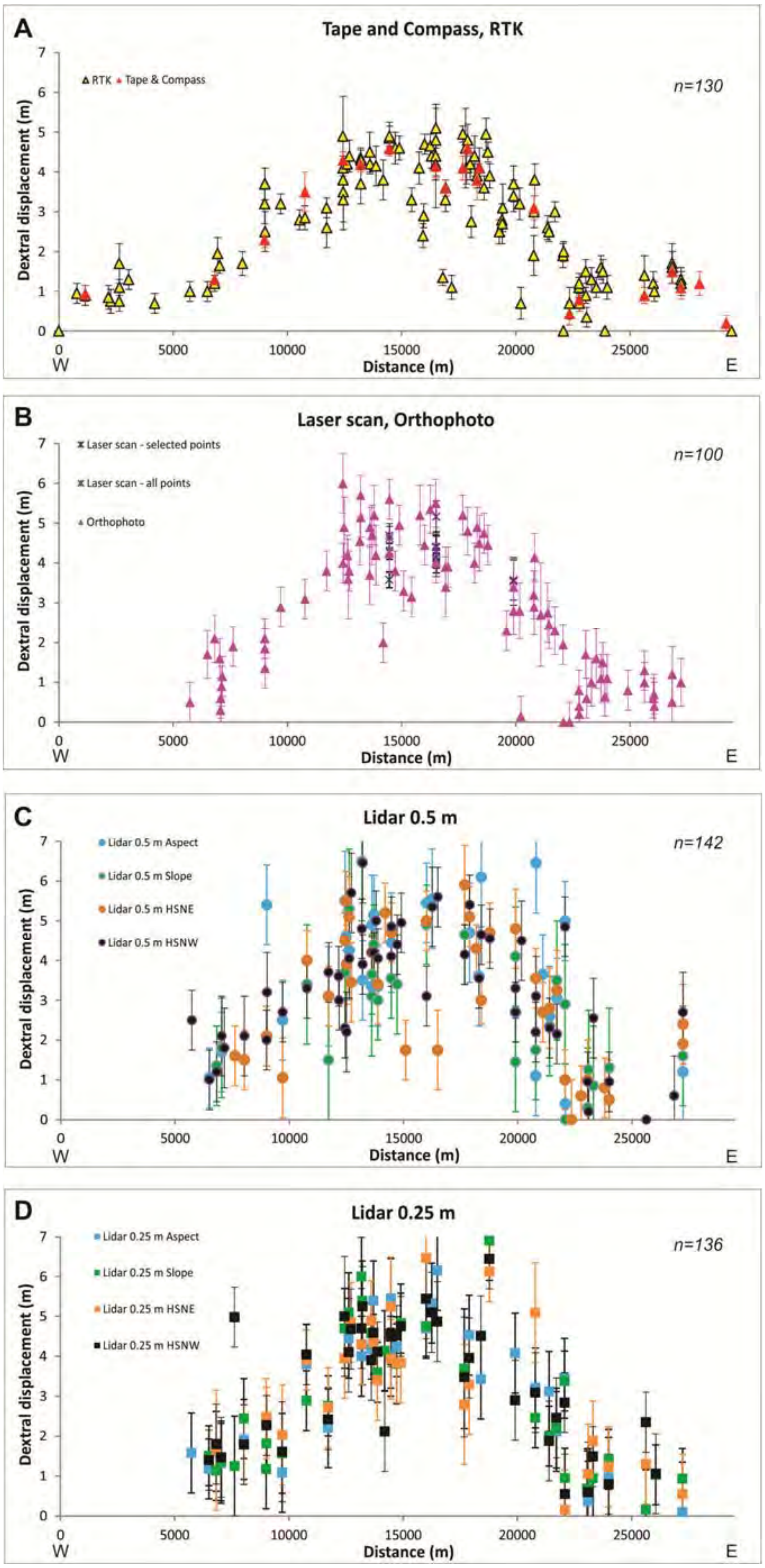

Figure 4.3 All (previous and new) dextral displacement measurements, colour-coded by dataset and separated onto four along-strike plots with roughly similar numbers of datapoints on each.

4.3.1 Range of measurements at individual sites

Figure 4.4 summarises the ranges of measurements at individual sites, by plotting the maximum minus minimum measurement (not taking into account uncertainties) at sites with 2 or more measurements. The maximum range is 4.4 m (±2.2 m about a median measurement of 4.9 m), and the mean is 1.5 m (±0.75 m). If the assigned uncertainties are taken into account (i.e., maximum + uncertainty minus minimum – uncertainty), the maximum range of measurements at an individual site (which is still the same site, 48a, Highfield Road) increases to 6.4 m (±3.2 m about a median of 4.9 m).

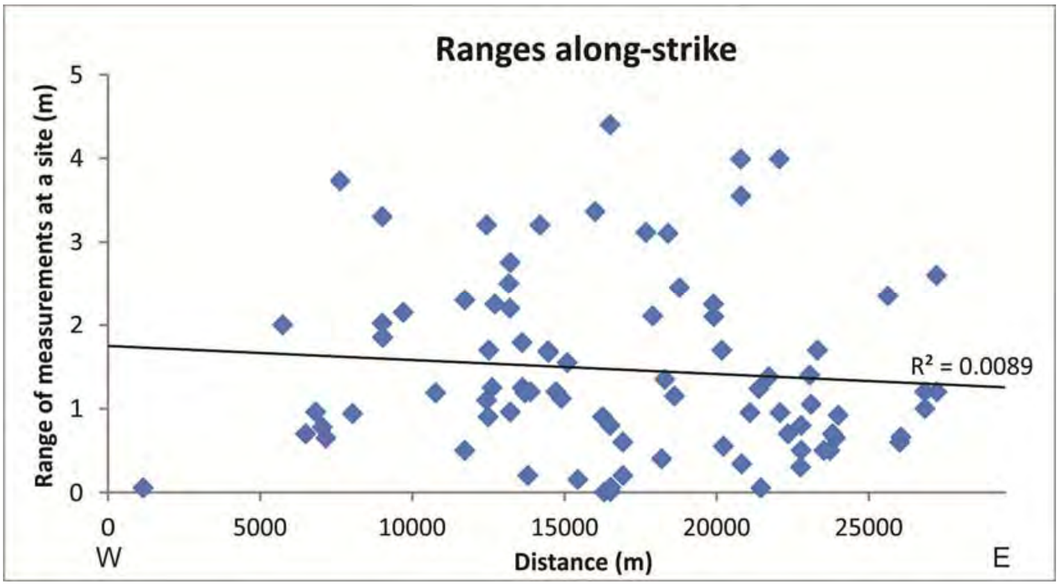

Figure 4.4 Ranges (maximum measured value minus minimum measured value) of measurements at individual sites. These ranges do not include uncertainties.

Figure 4.4 also doesn't appear to show any correlation between the range of measurements and distance along-strike. For example, the range of measurements is not necessarily larger in the centre of the fault, where displacement is greater. This is further confirmed by Figure 4.5, which shows no correlation between the range of measurements and the median displacement measured at each site.

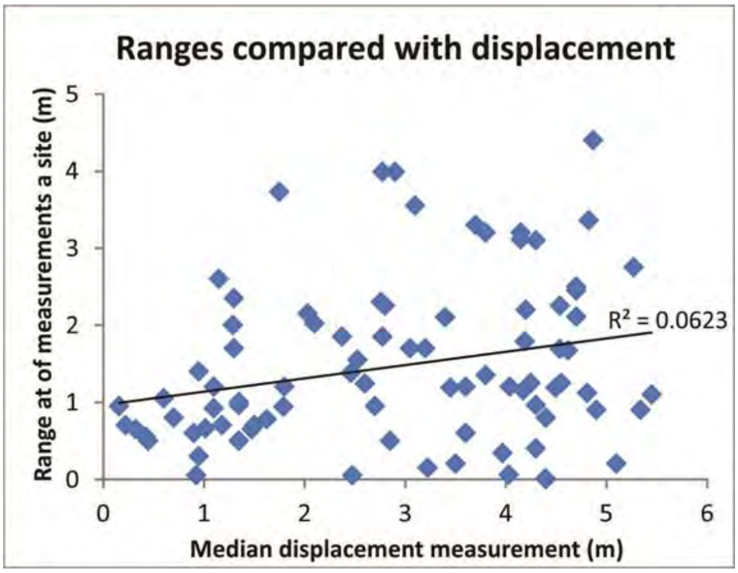

Figure 4.5 Ranges of measurements at each site compared with the median displacement measured at that site. These ranges do not include uncertainties.

Figure 4.6 shows the ranges plotted against fault zone width (Appendix 1, Table A 1.1; see also Figure 2.1 for definition of fault zone width). This plot also shows no correlation. For example, the ranges are not necessarily larger where the fault zone is widest and where there may be more error in projecting the markers to the fault.

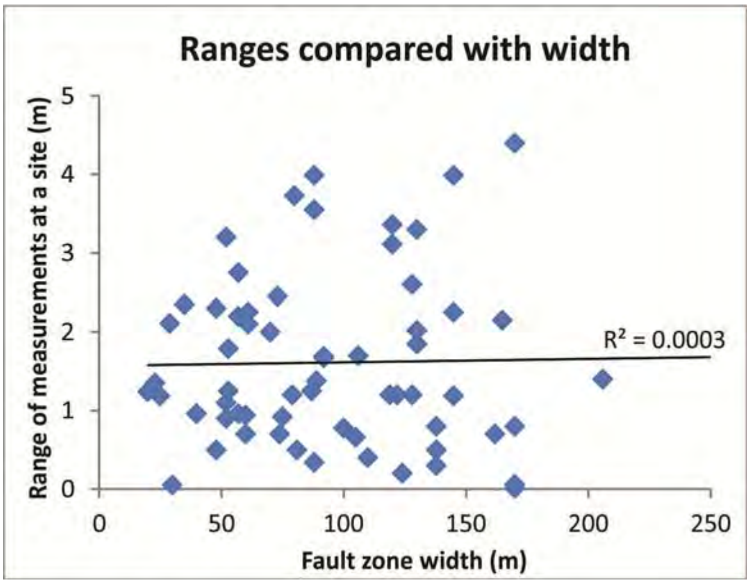

Figure 4.6 Ranges of measurements at each site compared with Greendale Fault zone width. The widths are contained in Appendix 1 (Table A 1.1) and are discussed in Section 6. See Figure 2.1 for the definition of fault zone width.

4.3.2 Comparison of measurements between datasets

To compare measurements made using different datasets, three types of plots showing two datasets at a time have been constructed. An example of these plots is shown in Figure 4.7 and the full set of plots are contained in Appendices 3 (A), 4 (B), and 5 (C). These are briefly described below.

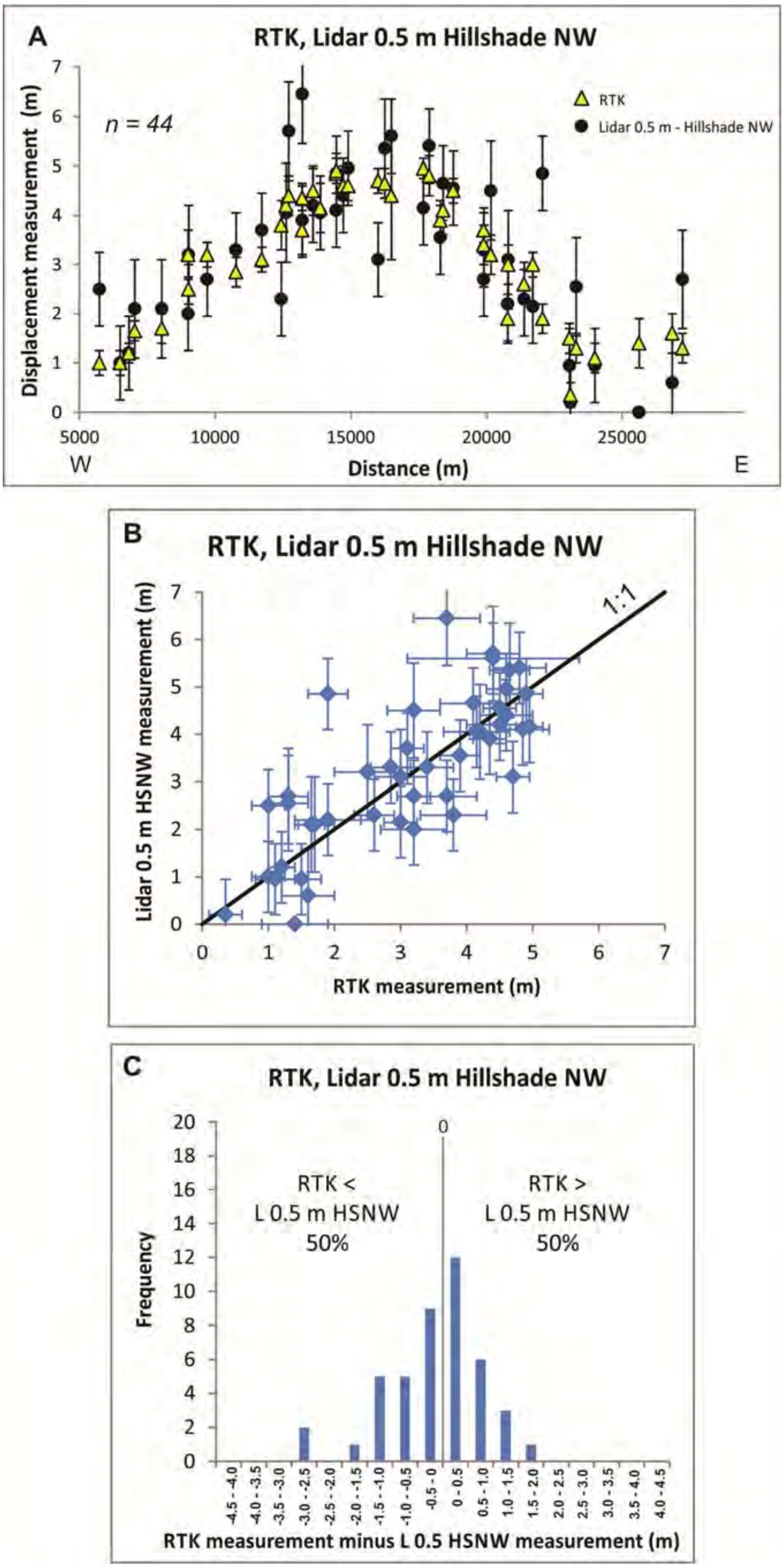

Figure 4.7 Example of the three types of plots comparing measurements from two datasets at a time. In this case, RTK compared with Lidar 0.5 m HSNW. The full set of plots are in Appendices 3, 4 and 5. A) Along-strike plot. B) X-Y plot comparing two measurements at a site. C) Histogram of the difference between the mean displacement measurements at each site.

Plot type A in Figure 4.7 (Appendix 3) are along-strike plots as shown throughout this report, but only showing measurements at sites where measurements have been made using both datasets. These should highlight any systematic differences in measurements along-strike.

Type B (Appendix 4) are X-Y plots plotting measurements from 1 dataset against another. These should highlight any systematic differences between datasets (e.g., most datapoints falling on one side of the 1:1 line) and with displacement (e.g., an overall divergence away from the 1:1 line).

Type C (Appendix 5) are histograms of the difference between measurements from each dataset, not taking into account uncertainties (i.e., subtracting mean measurements of 1 dataset from the other). Type C plots show the spread and distribution of measurement differences and so should highlight any systematic differences (e.g., most datapoints falling on one side of the zero line) as well as the difference ranges (i.e., the spread of values on the x-axis).

In the following sections we make semi-quantitative comparisons between two datasets and the others using these plots, but particularly plot type B. The comparisons are semi-quantitative in that the differences at individual sites are quantified, but an overall assessment of the differences between two datasets is qualitative. The basis for these qualitative assessments is explained in the footnote to Table 4.2, which summarises all the comparisons between two datasets described in the following sections.

Table 4.2 Summary of semi-quantitative comparisons of dextral displacement measurements between two datasets.

Dataset	Tape and Compass	RTK	Laser scan – all	Laser scan – selected	Orthophoto	L 0.5 m HSNW	L 0.5 m HSNE	L 0.5 m Slope	L 0.5 m Aspect	L 0.25 m HSNW	L 0.25 m HSNE	L 0.25 m Slope	L 0.25 m Aspect
Tape and Compass		G	B	B	B	B	B	C	B	G	G	G	B
RTK	G		B	V	B	B	B	B	B	B	B	B	B
Laser scan – All	B	B		B	V	V	V	V	B	C	C	C	V
Laser scan – selected	B	V	B		V	V	V	C	C	G	V	V	V
Orthophoto	B	B	V	V		B	B	B	V	B	B	B	B
L 0.5 m HSNW	B	B	V	V	B		V	B	B	B	B	B	B
L 0.5 m HSNE	B	B	V	V	B	V		B	V	V	B	B	B
L 0.5 m Slope	C	B	V	C	B	B	B		B	G	V	G	B
L 0.5 m Aspect	B	B	B	C	V	B	V	B		B	B	G	B
L 0.25 m HSNW	G	B	C	G	B	B	V	G	B		G	B	G
L 0.25 m HSNE	G	B	C	V	B	B	B	V	B	G		B	B
L 0.25 m Slope	G	B	C	V	B	B	B	G	G	B	B		B
L 0.25 m Aspect	B	B	V	V	B	B	B	B	B	G	B	B	

	Semi-quantitative assessment	**General definition**	**Specific definition with respect to plot type B (Appendix 4)**
C	Consistent (within uncertainties)	Small differences between measurements	Uncertainties of all measurements overlap the 1:1 line
G	Generally consistent (within uncertainties)	Relatively small differences between measurements	Uncertainties of most measurements overlap the 1:1 line
B	Broadly consistent (with a few exceptions)	Moderate differences between measurements	Trend along the 1:1 line, but considerable scatter
V	Variable consistency	Range of small to large differences between measurements	No real trend along the 1:1 line

Tape and Compass (Figures A3.1, 4.1, 5.1)

The Tape and Compass measurements are consistent (within uncertainties) with the Lidar 0.5 m Slope measurements, and are generally consistent (within uncertainties) with the RTK, Lidar 0.25 m HSNW, Lidar 0.25 m HSNE, and Lidar 0.25 m Slope measurements. They are broadly consistent (with a few exceptions) with the Laser scan – all, Laser scan – selected, Orthophoto, Lidar 0.5 m HSNW, Lidar 0.5 m HSNE, Lidar 0.5 m Aspect, and Lidar 0.25 m Aspect measurements.

There doesn't seem to be any systematic difference between the Tape and Compass measurements and other datasets, but the relatively low total number of Tape and Compass measurements means that this is not very statistically robust. There doesn't appear to be any systematic differences with position along the fault or with displacement.

RTK (Figures A3.2, 4.2, 5.2)

The RTK measurements are generally consistent (within uncertainties) with the Tape and Compass measurements and are broadly consistent (with a few exceptions) with the Laser scan – all, Orthophoto, Lidar 0.5 m HSNW, Lidar 0.5 m HSNE, Lidar 0.5 m Slope, Lidar 0.5 m Aspect, Lidar 0.25 m HSNW, Lidar 0.25 m HSNE, Lidar 0.25 m Slope, and Lidar 0.25 m Aspect measurements.

The RTK measurements are consistently higher than the Laser scan – selected measurements, but otherwise there are no systematic differences with other measurements. The higher RTK measurements may reflect the fact that the RTK profiles are longer than the laser scan profiles, and therefore it is possible that the laser scan profiles don't span the entire deformation. There does not appear to be any systematic variability along the fault or with displacement.

Laser scan – all points (Figures A3.3, 4.3, 5.3)

The Laser scan – all measurements are consistent (within uncertainties) with the Lidar 0.25 m HSNW, Lidar 0.25 m HSNE, and Lidar 0.25 m Slope measurements, but these datasets have only a few points, so the comparisons may not be statistically robust. They are broadly consistent (with a few exceptions) with the Tape and Compass, RTK, Laser scan – selected and Lidar 0.5 m Aspect measurements, but the comparison is more variable with the remainder (Orthophoto, Lidar 0.5 m HSNW, Lidar 0.5 m HSNE, Lidar 0.25 m HSNE, Lidar 0.25 m Slope and Lidar 0.25 m Aspect).

The relatively small number of measurements means that it is difficult to reliably assess systematic differences, but at face value there don't appear to be any, either along-strike, or with displacement. It also should be noted that some of these measurements, although generally at the same site as the other measurements, were not always on the exact same marker (fenceline or row of trees), which could account for some of the variability.

Laser scan – selected points (Figures A3.4, 4.4, 5.4)

The Laser scan – selected measurements are consistent (within uncertainties) with the Lidar 0.5 m Slope and Lidar 0.5 m Aspect measurements, but both datasets only contain a single datapoint, so the comparisons may not be meaningful. The measurements are generally consistent (within uncertainties) with the Lidar 0.25 m HSNW measurements, and are broadly consistent (with a few exceptions) with the Tape and Compass and Laser scan – all measurements. The comparison is more variable with the remaining datasets (RTK, Orthophoto, Lidar 0.5 m HSNW, Lidar 0.5 m HSNE, Lidar 0.25 m HSNE, Lidar 0.25 m Slope, and Lidar 0.25 m Aspect).

The Laser scan – selected measurements are consistently lower than the RTK, Orthophoto and Lidar 0.25 m Aspect measurements, and are more scattered (higher and lower) than the other datasets. Some of the reason for the lower measurements may be that the laser scan profiles were shorter than the profiles for the other datasets, but as for the Laser scan – all measurements, the relatively small number of measurements means that these differences may not be statistically robust. Some of these measurements were also not always on exactly the same marker as the other dataset measurements.

Orthophotos (Figures A3.5, 4.5, 5.5)

The Orthophotos measurements are broadly consistent (with a few exceptions) with the Tape and Compass, RTK, Lidar 0.5 m HSNW, Lidar 0.5 m HSNE, Lidar 0.5 m Slope, Lidar 0.25 m HSNW, Lidar 0.25 m HSNE, Lidar 0.25 m Slope, and Lidar 0.25 m Aspect measurements, but the comparison is more variable with the Laser scan – all, Laser scan – selected, and Lidar 0.5 m Aspect measurements.

The Orthophoto measurements are consistently larger than the Laser scan – selected points measurements, but otherwise there are no systematic variability with other measurements. The systematic difference with the Laser scan – selected measurements is, as discussed previously, probably a combination of the shorter profile length, the few datapoints and the difference in the actual marker measured. There doesn't appear to be any systematic differences with position along the fault or with displacement.

Lidar 0.5 m Hillshade NW (Figures A3.6, 4.6, 5.6)

The Lidar 0.5 m Hillshade NW measurements are broadly consistent (with a few exceptions) with the Tape and Compass, RTK, Orthophoto, Lidar 0.5 m Slope, Lidar 0.5 m Aspect, Lidar 0.25 m HSNW, Lidar 0.25 m HSNE, Lidar 0.25 m Slope, and Lidar 0.25 m Aspect measurements, but the comparison with the Laser scan – all, Laser scan – selected and Lidar 0.5 m HSNE measurements is more variable.

The Lidar 0.5 m HSNW measurements are higher than the Laser scan – selected measurements, although there are only a few datapoints. None of the variability appears to be systematic and there doesn't appear to be any systematic differences with position along the fault or with displacement.

Lidar 0.5 m Hillshade NE (Figures A3.7, 4.7, 5.7)

The Lidar 0.5 m Hillshade NE measurements are broadly consistent (with a few exceptions) with the Tape and Compass, RTK, Orthophoto, Lidar 0.5 m Slope, Lidar 0.25 m HSNE, Lidar 0.25 m Slope and Lidar 0.25 m Aspect measurements, but the comparison with the other datasets (Laser scan – all, Laser scan – selected, Lidar 0.5 m HSNW, Lidar 0.5 m Aspect and Lidar 0.25 m HSNW) is more variable.

None of the variability appears to be systematic and there doesn't appear to be any systematic differences with position along the fault or with displacement.

Lidar 0.5 m Slope (Figures A3.8, 4.8, 5.8)

The Lidar 0.5 m Slope measurements are consistent (within uncertainties) with the Tape and Compass and Laser scan – selected measurements, although the latter has only 1 datapoint and so may not be meaningful. They are generally consistent (within uncertainties) with the Lidar 0.25 m HSNW and Lidar 0.25 m Slope measurements and are broadly consistent with the RTK, Orthophoto, Lidar 0.5 m HSNW, Lidar 0.5 m HSNE, Lidar 0.5 m Aspect, and Lidar 0.25 m Aspect measurements. The comparisons with the Laser scan – all and Lidar 0.25 m HSNE are more variable.

There is a slight systematic difference with the Lidar 0.5 m HSNE, which are generally higher than the Lidar 0.5 m Slope measurements. There doesn't appear to be any systematic differences with position along the fault or with displacement.

Lidar 0.5 m Aspect (Figures A3.9, 4.9, 5.9)

The Lidar 0.5 m Aspect measurement is consistent with the Laser scan – selected measurement, but there is only 1 datapoint, so the comparison may not be meaningful. The measurements are generally consistent (within uncertainties) with the Lidar 0.25 m Slope measurements and are broadly consistent with the Tape and Compass, RTK, Laser scan – all, Lidar 0.5 m HSNW, Lidar 0.5 m Slope, Lidar 0.25 m HSNW, Lidar 0.25 m HSNE and Lidar 0.25 m Aspect measurements. The comparison is more variable with the Orthophoto and Lidar 0.5 m HSNE measurements.

Some of the measurements (RTK, Orthophoto, and Lidar 0.5 m HSNW) are slightly lower than the Lidar 0.5 m Aspect measurements at larger displacements. There doesn't appear to be any systematic differences with position along the fault.

Lidar 0.25 m Hillshade NW (Figures A3.10, 4.10, 5.10)

The Lidar 0.25 m Hillshade NW measurements are consistent with the Laser scan – all measurements, and are generally consistent (within uncertainties) with the Tape and Compass, Laser scan – selected, Lidar 0.5 m Slope, Lidar 0.25 m HSNE and Lidar 0.25 m Aspect measurements. They are broadly consistent (with a few exceptions) with the RTK, Orthophoto, Lidar 0.5 m HSNW, Lidar 0.5 m Aspect and Lidar 0.25 m Slope measurements, but the comparison with the Lidar 0.5 m HSNE measurements is more variable.

The Lidar 0.25 m HSNW measurements are almost all higher than the Laser scan – selected measurements, but are generally within uncertainty. Otherwise, there doesn't appear to be any systematic differences with position along the fault or with displacement.

Lidar 0.25 m Hillshade NE (Figures A3.11, 4.11, 5.11)

The Lidar 0.25 m Hillshade NE measurements are consistent (within uncertainties) with the Laser scan – all measurements, although there are only 2 datapoints, so the comparison may not be meaningful. They are generally consistent (within uncertainties) with the Tape and Compass and Lidar 0.25 m HSNW measurements and are broadly consistent (with a few exceptions) with the RTK, Orthophoto, Lidar 0.5 m HSNW, Lidar 0.5 m HSNE, Lidar 0.5 m Aspect, Lidar 0.25 m Slope and Lidar 0.25 m Aspect measurements. The comparison with the Laser scan – selected and Lidar 0.5 m Slope measurements is more variable.

There doesn't appear to be any systematic differences between datasets, with position along the fault, or with displacement.

Lidar 0.25 m Slope (Figures A3.12, 4.12, 5.12)

The Lidar 0.25 m Slope measurements are consistent with the Laser scan – all measurements, although there are only 2 datapoints, so the comparison may not be meaningful. They are generally consistent with the Tape and Compass, Lidar 0.5 m Slope and Lidar 0.5 m Aspect measurements, and are broadly consistent with the RTK, Orthophoto, Lidar 0.5 m HSNW, Lidar 0.5 m HSNE, Lidar 0.25 m HSNW, Lidar 0.25 m HSNE and Lidar 0.25 m Aspect measurements. The comparison with the Laser scan – selected is more variable, although the dataset only consists of 2 datapoints.

There doesn't appear to be any systematic differences between datasets, with position along the fault or with displacement.

Lidar 0.25 m Aspect (Figures A3.13, 4.13, 5.13)

The Lidar 0.25 m Aspect measurements are generally consistent (within uncertainties) with the Lidar 0.25 m HSNW measurement and are broadly consistent (with a few exceptions) with the Tape and Compass, RTK, Orthophoto, Lidar 0.5 m HSNW, Lidar 0.5 m HSNE, Lidar 0.5 m Slope, Lidar 0.5 m Aspect, Lidar 0.25 m HSNE and Lidar 0.25 m Slope measurements. The comparisons with the Laser scan – all and Laser scan – selected measurements are more variable.

There doesn't appear to be any systematic differences between datasets, with position along the fault or with displacement.

4.3.3 Assigned uncertainties

The mean and range of uncertainties assigned to measurements from each dataset are summarised in Table 4.3 and Figures 4.8 and 4.9. For the remote sensing datasets (Orthophotos and Lidar), the total number of measurements (N in Table 4.3) is also a reflection of uncertainties, as measurements weren't made for markers which were not easily visible in the Orthophotos or Lidar rasters. For example, only 26 measurements were made using the Lidar 0.5 m Slope raster, out of a total number of 101 markers, meaning that the uncertainties were considered too large for the remaining 75 markers. Thus if measurements were made using all datasets at all sites, the variability would most likely be even larger.

Table 4.3 Minimum, mean and maximum uncertainties assigned to each dataset. N is the total number of measurements to which uncertainties were assigned for each dataset. These are plotted in Figures 4.8 and 4.9.

Dataset	Minimum (m)	Mean (m)	Maximum (m)	N[1]
Tape and Compass	0.1	0.26	0.5	21
RTK	0.15	0.37	1.3	105
Laser scan – all	0.3	0.41	0.6	8
Laser scan – sel.	0.2	0.24	0.3	5
Orthophoto	0.3	0.58	1.3	86
Lidar 0.5 m HSNW	0.5	0.82	1	50
Lidar 0.5 m HSNE	0.6	0.84	1	36
Lidar 0.5 m Slope	1	1.31	1.5	26
Lidar 0.5 m Aspect	0.75	1.09	1.25	28
Lidar 0.25 m HSNW	0.75	0.94	1.5	40
Lidar 0.25 m HSNE	0.75	1.05	1.5	28
Lidar 0.25 m Slope	0.75	0.89	1.5	37
Lidar 0.25 m Aspect	0.75	0.98	1.25	31

[1] Note the number is slightly lower than the number of measurements for some datasets (Table 4.1) because uncertainties were not assigned to some measurements (accidentally or deliberately – e.g., none were assigned for a displacement of 0 m).

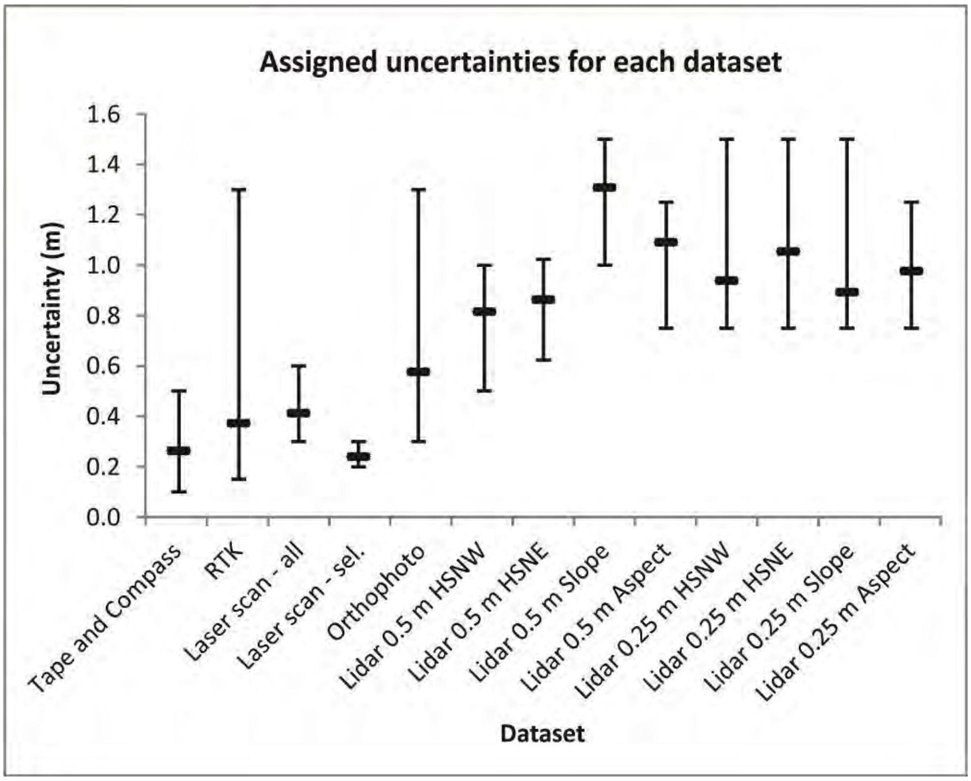

Figure 4.8 Mean and ranges of uncertainties assigned to measurements from each dataset.

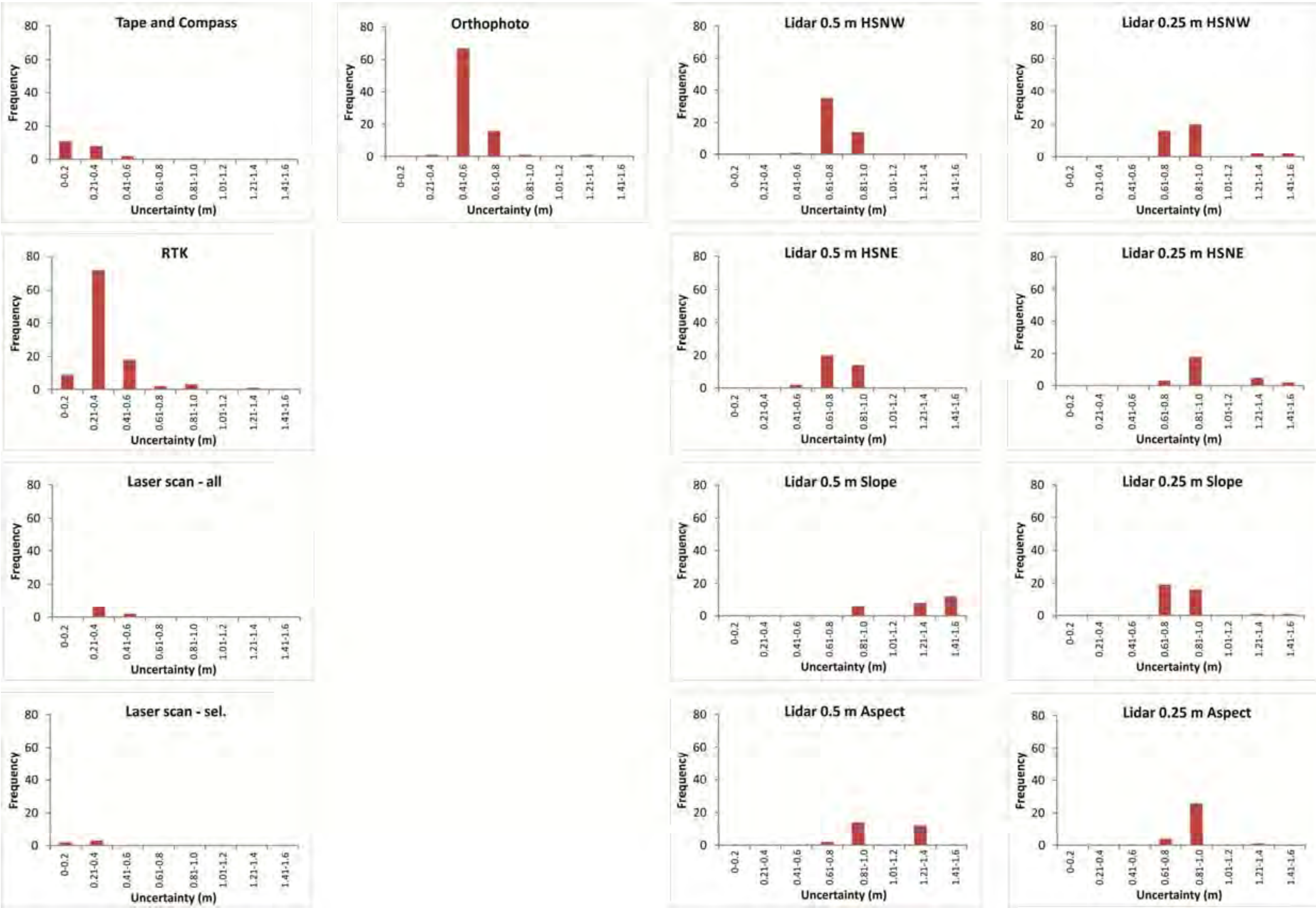

Figure 4.9 Histograms of uncertainties assigned to measurements from each dataset. These show the same ranges as Figure 4.8, but also the number and distribution of values making up each range.

Table 4.3, Figure 4.8 and Figure 4.9 show that the uncertainties assigned to the primarily field-based (Tape and Compass, RTK, Laser scan – all, Laser scan – selected) dataset measurements are generally lower than the uncertainties assigned to the remote sensing (Orthophoto and Lidar) dataset measurements. The mean uncertainties assigned to the field-based measurements are all less than 0.5 m, whereas the mean uncertainties assigned to the Lidar measurements are between 0.8 and 1.3 m. There is some overlap in that the upper uncertainties assigned to the RTK measurements overlap with the uncertainties of the Orthophoto and Lidar datasets, but the histograms in Figure 4.9 show that this upper tail for the RTK measurements consists of only a few datapoints (there are only 4 assigned uncertainties greater than 0.8 m).

The uncertainties assigned to the Orthophoto measurements are generally in between those assigned to the field-based dataset (Tape and Compass, RTK, and Laser scan) measurements and the Lidar measurements. Like the RTK measurements, there is an upper tail, but this only consists of 2 datapoints above 0.8 m (Figure 4.9).

The uncertainties assigned to the Lidar measurements are all between 0.5 and 1.5 m. Somewhat unexpectedly, the uncertainties assigned to the Lidar 0.25 m measurements are not always lower than the Lidar 0.5 m measurement uncertainties.

4.4 DISCUSSION

4.4.1 Comparison of measurements between datasets

The comparison of measurements from two different datasets (section 4.3.2) confirmed the inference from examining the along-strike plots of all measurements (Figures 4.1 – 4.3) that although there are quite a lot of broad consistencies between measurements from different datasets, there is also a surprising amount of variability. The variability would probably have been even larger if measurements had been made using all datasets at each site.

At first glance, the large variability seems alarming, especially when considering that the displacement of any individual marker during the Darfield earthquake was by a unique amount, not by a range of values. Some along-strike variability in displacement is to be expected, as has been noted for almost all other historical ground surface ruptures (e.g., Wesnousky 2008; Xu et al., 2009: Rockwell and Klinger, 2013) and considering the complexity of the Darfield earthquake (e.g., Gledhill et al., 2011; Holden et al., 2011; Beavan et al., 2012) and the complexity and variation in width of the Greendale Fault zone (Villamor et al., 2012; section 6). However, the variability at an individual site (i.e., for a single marker) must reflect measurement uncertainties, most likely from using different datasets.

Another important observation from the comparisons between different datasets (section 4.3.2) is that generally there are no systematic differences between measurements from different datasets. We were particularly surprised that there is no systematic difference between the Tape and Compass measurements and those from other datasets. The reason is that our perception during mapping of the Greendale Fault using the Lidar data (e.g., Villamor et al., 2012) and the previous measurements (Quigley et al., 2012) was that the Tape and Compass measurements may have not captured the complete deformation. That is, that the very subtle outer edges of the fault zone (discussed further in section 6) may not have been visible in the field, and hence the Tape and Compass measurements may have systematically underestimated the true value. While a consistency with other datasets may not on its own be proof that all of the deformation was captured in the Tape and Compass measurements, there is conversely no evidence from our results that measuring displacements from the remote sensing datasets (Orthophoto and Lidar), which covered a wider region across the fault zone, always captured all the deformation. For similar reasons (i.e., short survey lengths), we also thought there may be systematic differences between the other field-based datasets (RTK and Laser scan) and the remote sensing datasets, but this does not appear to be the case.

We consider there are two main reasons for the lack of systematic difference between measurements from the field-based and remote sensing datasets:

- Although the field-based datasets may not have spanned the entire width of the fault zone, the amount of deformation at the outer edges is only a very small percentage of the entire deformation (section 6), probably much less than ~10%. Therefore, the difference in displacement measurements from these datasets and the remote sensing datasets are most likely so small that they are within uncertainties.
- There is so much variability in the remote sensing datasets measurements that any systematic variations are masked. That is, the measurements from any one remote sensing dataset are so variable (for reasons described in Section 4.4.2) that it is difficult to determine if there are any overall systematic differences with any other dataset. Perhaps a more rigorous statistical comparison on a site-by site basis may identify any systematic differences, but that is beyond the scope of this study.

There also does not appear to be any systematic differences in measurements from different datasets along-strike (Figure 4.4) or with displacement (Figure 4.5). The former is perhaps not surprising, in that there is no particular reason why measurements should differ according to position along the fault, apart from the fact that the displacement varies along-strike, with the highest in the centre and tapering to zero at the ends. The lack of difference with displacement is however, more surprising, as it seems intuitive that the larger the displacement the more likely any systematic differences would be observed. We suspect that this lack of difference is again because there is so much variability in the remote sensing data measurements that any systematic variations are masked.

4.4.2 Assigned uncertainties

The greater variability in the remote sensing datasets measurements than the field-based datasets measurements is also reflected in the assignment of generally larger uncertainties to the former (section 4.3.3; Figure 4.8). One key reason for the larger remote sensing measurement uncertainties is simply the resolution (cell size) of the Orthophoto and Lidar rasters – 0.5 and 0.25 m. Although these were not explicitly included in a calculation of the uncertainties, our trial and error experiments to define the uncertainties showed clearly that straight marker lines were not able to be defined as accurately in the Orthophotos and Lidar rasters, as they were from profiles constructed from individual RTK and Laser scan survey points.

Another related point is that, because the remote sensing datasets generally covered a wider area (e.g., Figure 3.4), the projection lines for the remote sensing datasets were fitted to a longer marker and thus were generally projected to the fault from a greater distance. This means that even very small changes in the orientation of the projection line can result in significant differences in displacement.

Furthermore, some of the markers proved to not be straight over distances of several hundred meters. Particular examples are Courtney Road (site 30) and Highfield Road (site 48). There is therefore a trade-off between the length of the profile line covering the entire deformation and the uncertainties associated with fitting a projection line to a longer, potentially non-straight, non-parallel, marker, as well as projecting to the fault from a greater distance.

Another perhaps surprising result from the comparison of the uncertainties assigned to each dataset is that the uncertainties assigned to the 0.25 m Lidar raster measurements are not always smaller than those assigned to the 0.5 m Lidar raster measurements (Table 4.3 and Figure 4.9). This probably reflects the observation made during undertaking the measurements that, although some markers were sharper in the 0.25 m Lidar rasters, many others were less sharp in the 0.25 m Lidar rasters compared with the 0.5 m Lidars. This was generally for two main reasons: 1) the marker is a relatively broad topographic feature (e.g., a ditch) and so a smaller cell size simply results in a more gradational representation in the raster; or 2) the marker has considerable roughness (e.g., a hedge) and so a smaller cell size simply results in a more complex representation in the raster.

The importance of the sharpness of the marker in making measurements and assigning uncertainties is also highlighted by the Orthophoto measurements and uncertainties. Although the resolution of the Orthophotos was too poor to map many of the detailed geometries of the Greendale Fault trace (Villamor et al., 2012), many markers were nevertheless much sharper on the Orthophotos than on the Lidar rasters. Not surprisingly, this was particularly the case for those markers that do not have much topographic expression, such as road centrelines, road edges, and relatively new fences (e.g., Figure 2.7). This difference in resolution is reflected in the generally smaller uncertainties assigned to the Orthophoto measurements (Figure 4.8) and also in the greater number of Orthophoto measurements than Lidar measurements (Table 4.3 and Figure 4.9).

There are many other factors which control marker resolution on the Lidar rasters, which probably account for much of the variability and generally larger uncertainties of these measurements. For example, the predominantly NNE orientation of many of the markers means that they are generally much sharper in the Lidar HSNW than in the HSNE rasters. Sudden contrasts in roughness (e.g., between a hedge and bare ground) results in better definition of makers in the Lidar Aspect rasters and sudden changes in topography (e.g., the edge of a steep ditch) results in better definition of markers in the Lidar Slope rasters.

4.4.3 Comparison with the displacement measurements of Elliott et al. (2012)

Elliott et al. (2012) measured Greendale Fault dextral displacements using 3 datasets (field, orthophotos, and satellite images). Figure 4.10 shows their measurements plotted against all our measurements (previous and this study), as well as our measurements using the same datasets – Tape and Compass and Orthophoto’s. Note that these plots do not necessarily show measurements at the same sites (as is shown in plot type A in Figure 4.7 and Appendix 3) as we cannot be certain that the markers measured are exactly the same, since we only have their locations as latitudes and longitudes, not detailed descriptions of the markers measured (e.g., the side or the centreline of the road). There could also be some differences in the along-strike distances since the distances for each dataset were calculated independently, without attempting to match the distances for individual sites. Therefore these plots should only be used to examine general comparisons along-strike, rather than actual differences at individual sites.

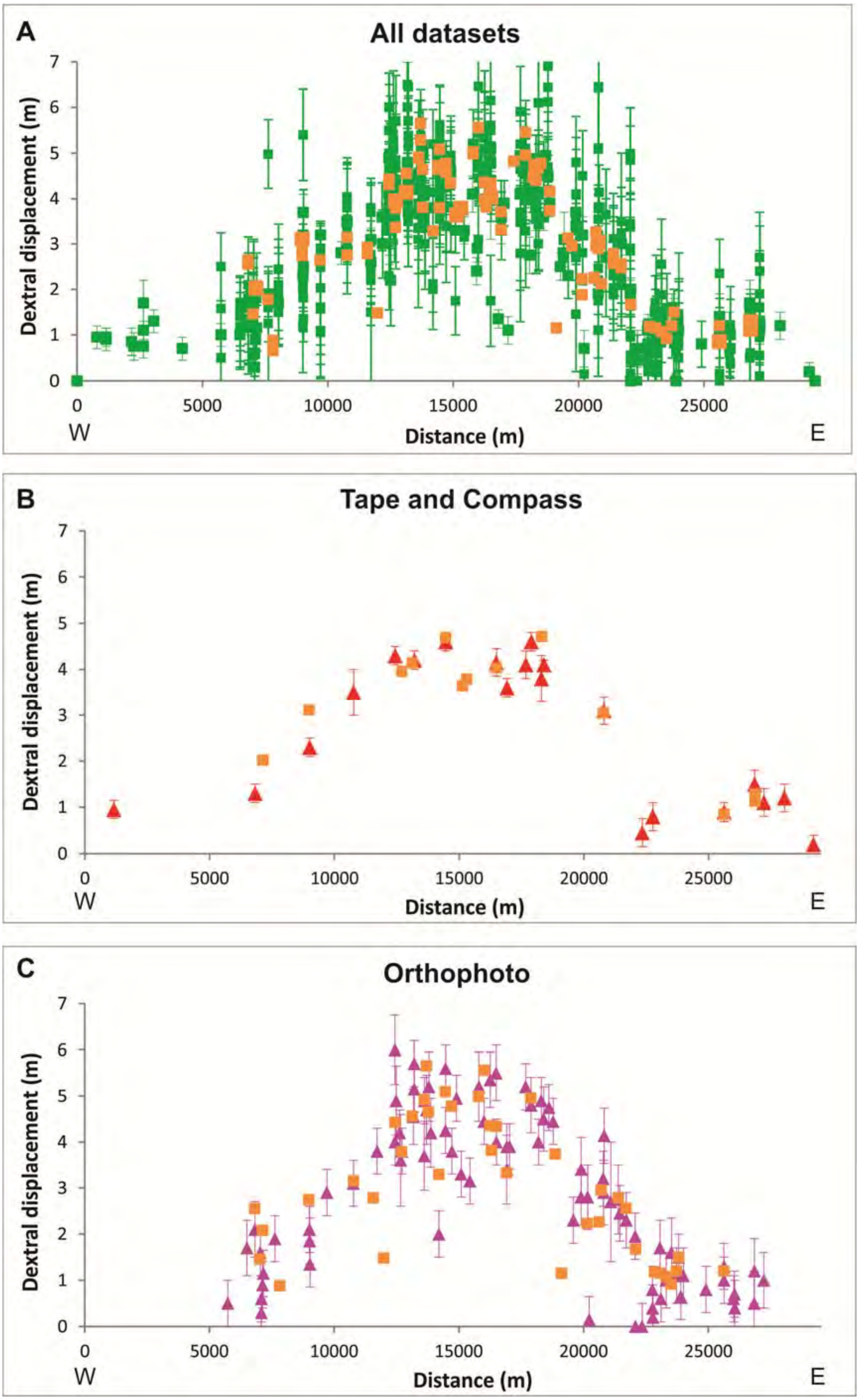

Figure 4.10 Dextral displacement measurements of Elliott et al. (2012) (orange) and A) all (previous and this study), B) Tape and Compass, and C) Orthophoto displacement measurements.

Comparison of Elliott et al.'s dextral displacement measurements with all of our dextral displacement measurements (Figure 4.10A) shows reasonably good agreement, with almost all of their measurements lying within the uncertainties of ours. In particular, they show a similar overall shape and a bimodal distribution defining the three segments. Elliott et al. (2012) didn't document if the low dextral displacement measurements in the centre of the fault are minimum measurements.

Both the Tape and Compass (Figure 3.1B) and the Orthophoto (Figure 3.1C) measurements also show reasonably good agreement. Some of the Tape and Compass measurements are exactly the same, which may suggest they did measure the same markers. There is more variability in the Orthophoto measurements between the two studies, which is consistent with the findings of this study that there are greater uncertainties associated with measuring displacements using remote sensing datasets.

4.4.4 Implications for measuring future fault rupture displacements

The results of this study can be used to assess the relative merits of collection of different datasets immediately following a fault ground surface rupture. In particular, with the availability of many remote sensing datasets today, there could be a temptation not to collect high-quality field measurements, or any field measurements at all, particularly in remote areas.

The results of this study show that the field-based datasets measurements, and most notably the Tape and Compass measurements, were overall consistent with those from other datasets. Furthermore, the field-based dataset measurements almost always had lower assigned uncertainties than those from the remote sensing datasets.

One of the reasons the Tape and Compass measurements were so consistent with other datasets and had low assigned uncertainties is that the markers surveyed were relatively straight, which greatly aided sighting and visual projection across the fault. This, along with the availability of people to make the measurements and the relative ease of access along the fault, meant that they were relatively quick to collect. Tape and Compass measurements of vertical displacements were not collected however, because of the difficulty in projecting horizontally and the need for long profiles crossing the surface channelisation barely visible in the field. The favourable comparison with other datasets suggests that the Tape and Compass adequately spanned the Greendale Fault deformation, which includes subtle folding. Although not specifically documented in this study, manual field measurements, such as Tape and Compass measurements, also provide an opportunity to record additional data, such as whether the displacement was on a single or multiple strands, notes on the origin and reliability of the marker, or whether the displacement was by discrete rupture or by flexure. We therefore suggest that, where possible and particularly where markers are relatively straight, Tape and Compass dextral displacement measurements remain a most useful dataset to collect immediately following a ground surface rupture.

The Laser scan data was very useful for recording a detailed 3-dimensional representation of the fault rupture and displaced features, but is much more time consuming to collect, and as a result the areas captured in this study didn't always span the entire width of the fault zone. The definition of the fault rupture features and the displaced markers are also dependent on the nature of the surfaces – delicate fault rupture features were only captured in paddocks with short grass (Yeah Right and Highfield Road) and fenceposts were found to be more accurate than hedges for delineating displaced markers. The large amount of datapoints collected by the Laser scan surveys also required considerable post-processing and subsampling before these data were readily usable in GIS.

The RTK survey data was considered in our previous study (Quigley et al., 2012) to be the most reliable for characterising dextral displacement, which is confirmed by the results of this study. RTK survey data are relatively quick to collect (marker surveys take on average 10-20 minutes) although some post-processing is required and profile lines need to be digitised in GIS. We recommend that RTK survey measurements are made using a survey pole on fence posts, as some made by walking with the antenna in a backpack were more irregular, and hence more difficult to fit a straight line, leading to greater uncertainties. The RTK survey data was found to generally not be useful for Greendale Fault vertical displacement measurements because of the intensive channelisation however. This could be overcome by collecting longer profiles specifically for this purpose.

The remote sensing datasets (e.g., Orthophotos and Lidar) were especially useful for mapping the Greendale Fault rupture (Quigley et al., 2012; Villamor et al., 2012; this study) and displacement measurements were relatively quick and easy to make. We are aware of at least one automated procedure for measuring displacements (Zielke and Arrowsmith, 2012), but this was not employed because: 1) it involves matching of fault-parallel profiles of topographic features (e.g., channels), but many markers along the Greendale Fault had little topographic expression; 2) the procedure was developed for relatively narrow deformation zones (a few metres) which is clearly not the case for the Greendale Fault; and 3) many of the Greendale Fault markers were not perpendicular to the fault. The results of this study show that remote sensing dataset measurements showed considerable variation, which is consistent with the larger assigned uncertainties, but may not necessarily be captured by them. We therefore recommend the remote sensing datasets are mainly used for obtaining additional displacement measurements in places where field-based data are not, or cannot be, obtained and that careful consideration is given to the assigned uncertainties. Remote sensing datasets can be useful for displaying markers in different ways (e.g., hillshades versus slope rasters), and so another recommendation is to assess the markers in different rasters to select the sharpest characterisation of individual markers possible.

4.4.5 Implications for characterising single event displacement

The outcomes of this study regarding the uncertainties in displacement measurements for a fresh ground surface rupture also have implications for measuring single event displacement for past fault ruptures.

As noted in several places, because the displacement of individual markers in the Greendale Fault rupture was by a finite amount, the sometimes surprisingly large ranges of measurements obtained mainly reflect measurement uncertainties. These measurement uncertainties are additional to the uncertainties for past ruptures from issues such as the preservation of the marker and the reliability of matching markers across the fault. The fact that the variability was found to be up to ±2.2 m (mean ±0.75 m) for straight, well defined, markers on a fresh rupture suggests that the measurement uncertainties for displacement in past ruptures should be considered carefully and in some cases may need to be increased.

It is unclear whether the uncertainties assigned to measurements from some of the datasets for this fresh rupture can simply be transferred to the measurement uncertainties for single event displacement of past ruptures. This is because the Greendale Fault displacements were measured using long, straight, well-defined features and therefore much of the uncertainty is from dataset resolution. However, for past ruptures there is an additional uncertainty from the preservation and matching of markers across the fault. As a result, remote sensing datasets are often favoured for past ruptures in that they are considered to provide an objective map of the features and an opportunity to robustly define how uncertainties are calculated (e.g., Rodgers and Little, 2006; Mason and Little, 2006; Little et al., 2010; Berryman et al., 2012; Gold et al., 2013). This is particularly the case where the markers are not linear. We therefore recommend caution in applying the conclusion from this study that displacement measurements from remote sensing datasets have higher uncertainties than field-based measurements, to past ruptures.

This study also highlights the natural variability in ground surface displacements along the strike of the fault, which has been identified in many previous surface rupture displacement studies (e.g., Sieh et al., 1993; Lin et al., 2001; Barka et al., 2002; Haeussler et al., 2004; Klinger et al., 2005). The calculated average net displacement for the Greendale Fault rupture of 2.55 m was only measured at one site and net displacement plot has a bimodal distribution with peaks at ~1.25 and ~4.25 m. Added to this, much of the Greendale Fault deformation was by subtle folding (about both vertical and horizontal axes), leading Quigley et al. (2012) to note that "large stretches of the Greendale Fault rupture will be challenging to recognise in as little as 10^1-10^3 years". It is therefore easy to envisage a scenario where future estimates of single event displacement for the Greendale Fault are likely to be higher than the true average displacement across the entire rupture, because only the highest displacement central segment is preserved. Furthermore, given the natural along-strike variability, measured displacements could be anything from about 3 to 6 m, depending upon which markers are preserved. Thus, when estimating an average single event displacement for a paleo-fault rupture, for example for the purposes of seismic or fault rupture hazard studies, careful consideration needs to be given to make sure the uncertainties take into account both the measurement uncertainties and natural variability in surface rupture displacement along-strike.

5.0 NEW DEXTRAL MEASUREMENTS BY MULTIPLE GEOLOGISTS

5.1 INTRODUCTION

In this section we present new measurements of Greendale Fault dextral displacements made by multiple geologists. The purpose is to test the repeatability of measurements by different people, which is another potential measurement uncertainty. The use of multiple datasets also provides additional measurements to compare with those made by one person using multiple datasets (section 4). As far as we are aware, a comparison and analysis of measurements of multiple deformed cultural features by multiple geologists have not been undertaken previously.

5.2 METHODS

Displacement measurements by 8 geologists (Mark Quigley, Russ Van Dissen, Sharon Hornblow, Robert Langridge, William Ries, Andy Nicol, Dougal Townsend, Pilar Villamor) were made during two 1 day workshops. All have paleoseismology expertise, but only Russ Van Dissen had been involved in the previous (Quigley et al., 2012) Greendale Fault displacement measurements. Henceforth, the geologists are referred to as geologists 1-8. The new measurements presented in section 4 are also included in the dataset (geologist 9), bringing the total number of geologists to 9. However, it should be noted that the measurements by Nicola Litchfield (geologist 9) were undertaken over a longer period than a single 1 day workshop.

The measurements in the workshops were undertaken in a GIS using the methods described in section 3.2.1. Each geologist was given a series of template GIS shapefiles for making the measurements and a demonstration of the method at the start of the workshop. The geologists had a range of GIS skills, which in part contributed to the different total numbers of measurements made within the time available (about 8 hours for each workshop). Those more proficient in GNS made a greater number of measurements and vice versa.

Each geologist was asked to measure displacements at 18 sites spread along the fault (Figure 5.1). These are sites where Tape and Compass displacement measurements were available and those measurements were provided at the start of the workshop. These were provided to simulate the conditions of the previous (Quigley et al., 2012) and new measurements (section 4) in this study, and were in the form of a displacement and an uncertainty. In the interests of time, geologists were not asked to assign uncertainties.

Figure 5.1 Sites where displacement measurements were made by multiple people. The numbers are the site numbers used previously (Appendices 1 and 2).

Each geologist was asked to measure the displacements at the 18 sites using as many datasets as possible during the time available. The datasets supplied were RTK, Orthophoto, Lidar 0.5 m HSNW, Lidar 0.5 m HSNE, Lidar 0.5 m Slope, Lidar 0.5 m Aspect.

Those who participated in the first workshop chose to select the best Lidar raster to make measurements; whereas, those in the second workshop made measurements using all the Lidar rasters.

5.3 RESULTS

A total of 532 measurements were made and the full set of results is contained in Appendix 6 and is shown on Figure 5.2. The previous measurements (red dots on Figure 5.2) are the RTK measurements published by Quigley et al (2012) – the Tape and Compass measurements are not shown.

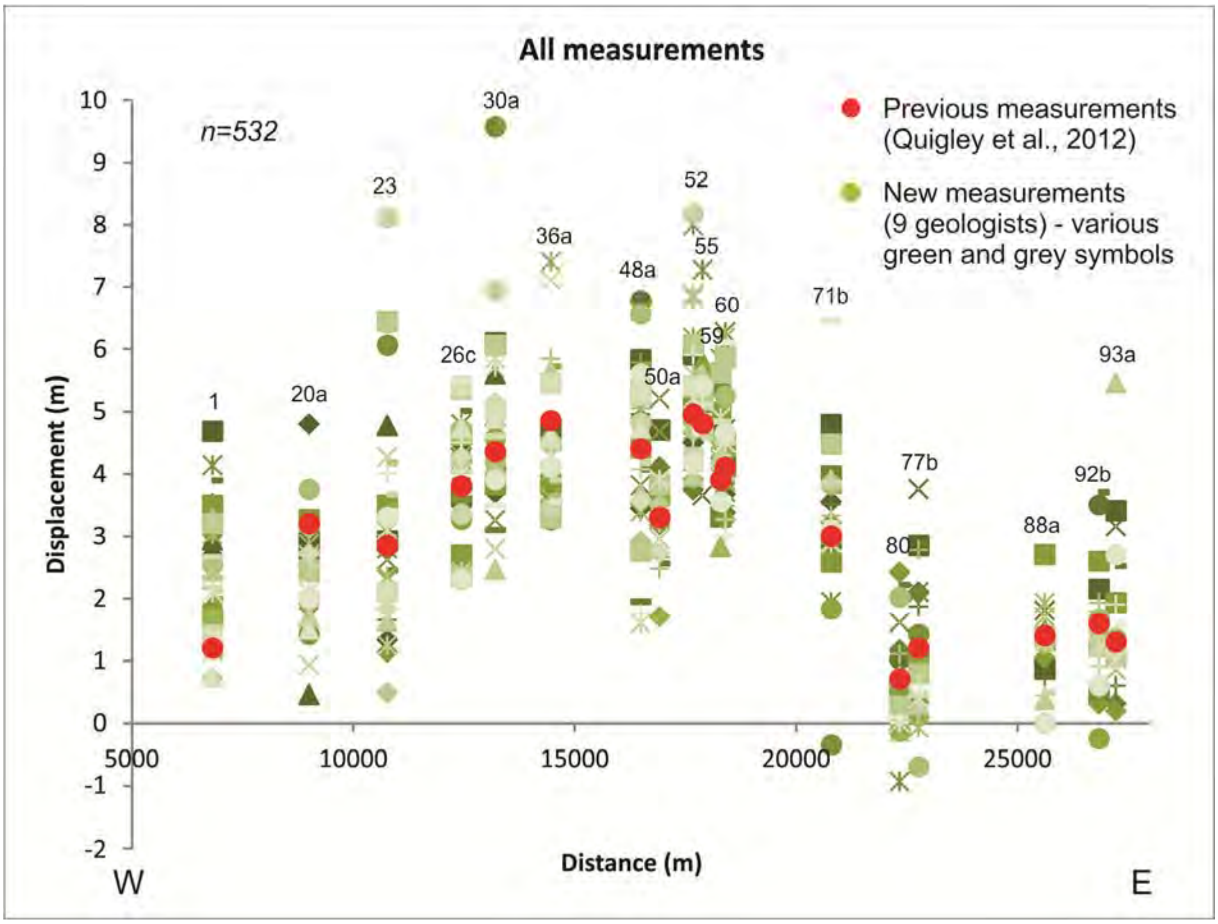

Figure 5.2 Along-strike plot of all the displacement measurements made by eight geologists during two one day workshops and the new measurements made in this study (Section 4). The numbers above each set of measurements correspond to the sites located in Figure 5.1 and are the same as used previously (Appendices 1 and 2).

5.3.1 Ranges from all datasets

Figure 5.2 shows considerable ranges of measurements at any given site, and the ranges (maximum minus minimum measurement) are summarised in Table 5.1. The maximum range at a single site from all datasets is 7.62 m (±3.8 m about a median of 3.0 m) and the mean range is 4.44 m (±2.2 m). If the highest measurements for sites 23, 30a, 71b and 93a and the lowest (sinistral) measurement for site 71b are considered outliers and removed, then the maximum range reduces to 5.96 m (±3.0 m about a median of 2.9 m) and the mean to 3.87 m (±1.9 m).

The measurements from all the datasets span the previously published measurements (red dots on Figure 5.2), but are not always symmetrical about them – notable exceptions are site 1, where the majority of measurements are higher than the previous ones, and site 20a, where the majority of measurements are lower than the previous ones.

Table 5.1 Ranges of displacements measured for each site using all datasets (column 2) and different datasets (columns 3-8). The values in brackets are calculated from the removal of 5 potential outliers as discussed in the text.

Site	All	RTK	Orthophoto	L 0.5 m HSNW	L 0.5 m HSNE	L 0.5 m Slope	L 0.5 m Aspect
	Range (m)	Range (m)	Range (m)	Range (m)	Range (m)	Range (m)	Range (m)
1	3.96	2.81	2.69	2.07	0.29	0.69	1.59
20a	4.34	2.5	1.55	3.3	2.23	0.06	1.23
23	7.62	2.37	4.09	4.79	2.44	2.94	5.95
26c	3.2	0.71	2.66	3.05	1.11	2.97	2.23
30a	7.11	1.53	2.27	7.11	2.35	1.84	3.44
36a	4.14	1.24	2.43	2.38	2.59	3.97	1.13
48a	5.18	3.69	3.06	4.61	3.58	3.72	2.26
50a	3.5	2.02	2.14		2.97		
52	4.43	*0.54*	3.65	0.89	3.07	1.53	
55	3.62	0.72	2.69	0.96	1.88		
59	3.01	1.18	1.4	1.82	1.55		1.79
60	3.26	0.84	2.14	1.86	1.71		2.04
71b	6.8	0.96	2.85	4.25			4.62
77b	4.45	1.96	2.96	2.12	3.15		
80	3.36	2.38	3.16	1.28	1.17		1.15
88a	2.7	1.26	2.21	1.49	0.37		
92b	3.95	1.35	2.5	1.07			3.75
93a	5.26	1.11	2.41	4.35	2.84	0.4	
Mean	4.44 (3.87)	1.62	2.60	2.79 (2.2)	2.08	2.01	2.60 (1.8)
Min	2.7	0.54	1.4	0.89	0.29	0.06	1.13
Max	7.62 (5.96)	3.69	4.09	7.11 (4.79)	3.58	3.97	5.95 (3.75)

5.3.2 Ranges for different datasets

Table 5.1 and Figure 5.3 show that the maximum ranges of measurements at a given site using a single dataset vary between 3.58 m (±1.79 m) and 7.11 m (±3.55 m) and the mean ranges vary between 1.62 m (±0.81) and 2.79 m (±1.4 m).

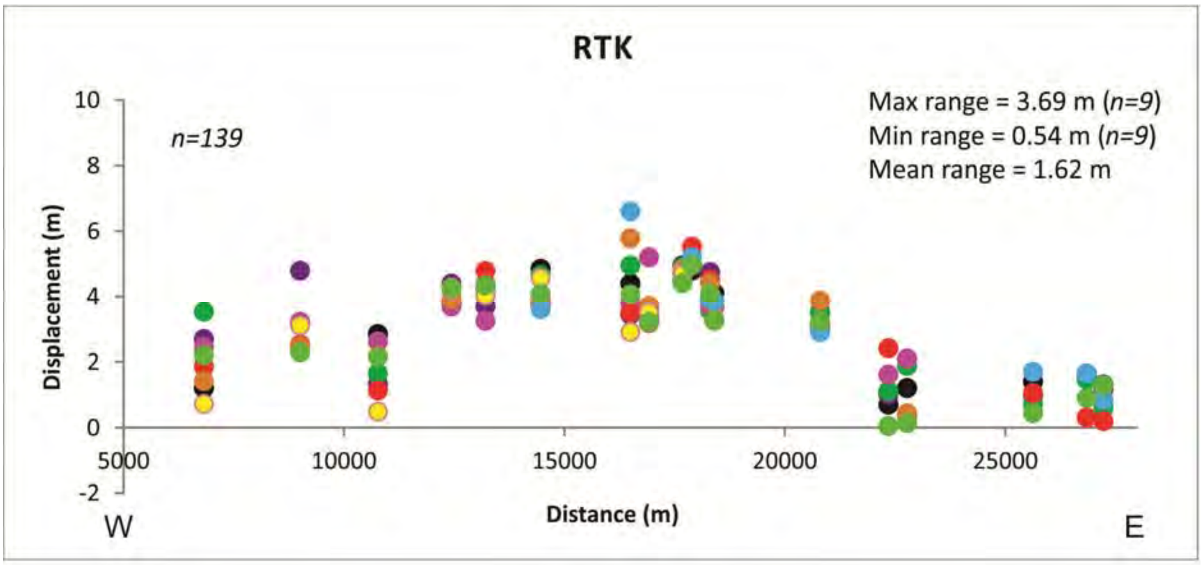

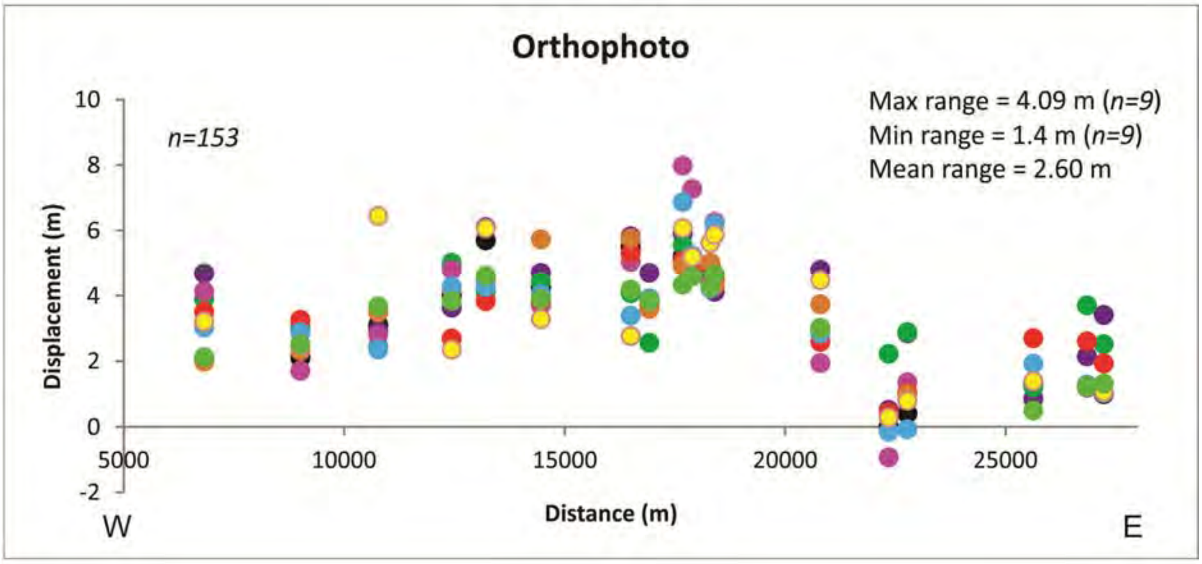

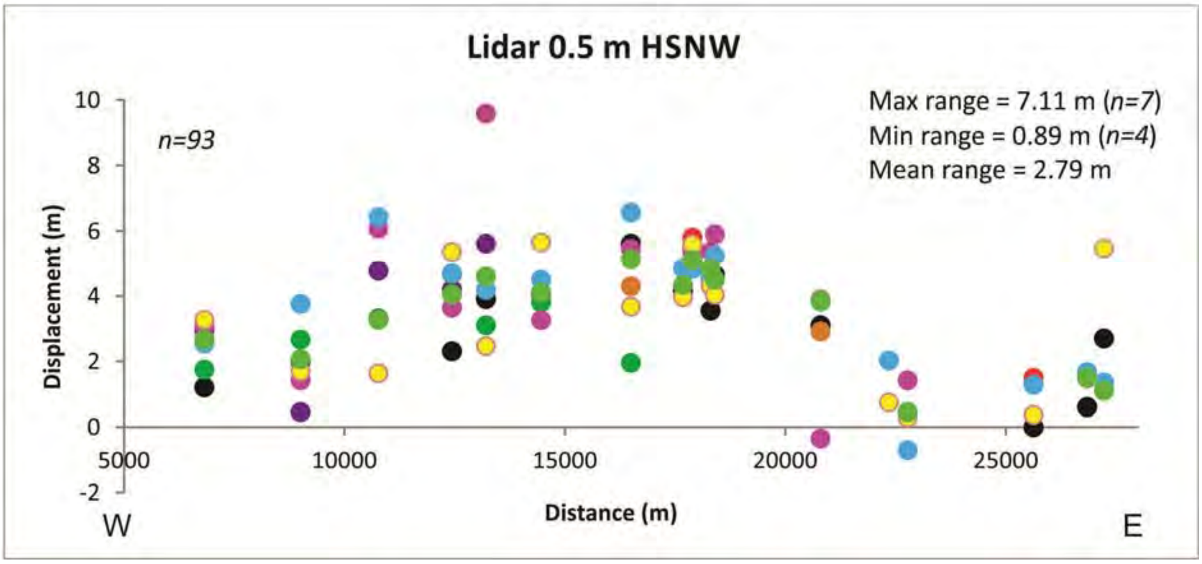

Figure 5.3 Along-strike plots of displacement measurements made by multiple geologists for different datasets. The colours are individuals measurements and the same colour is used in each plot.

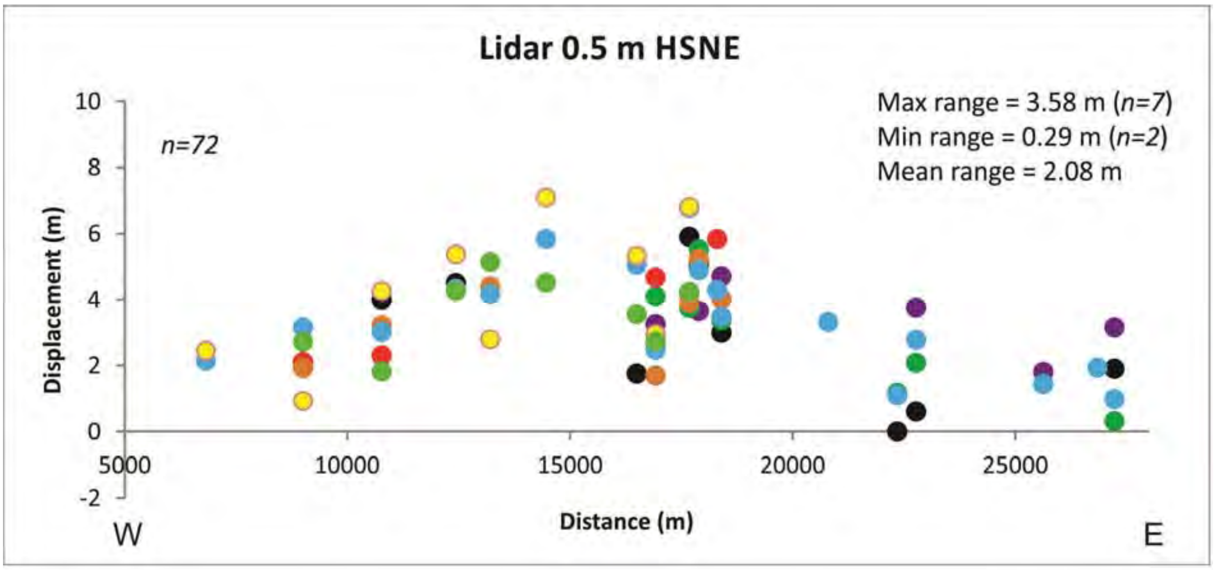

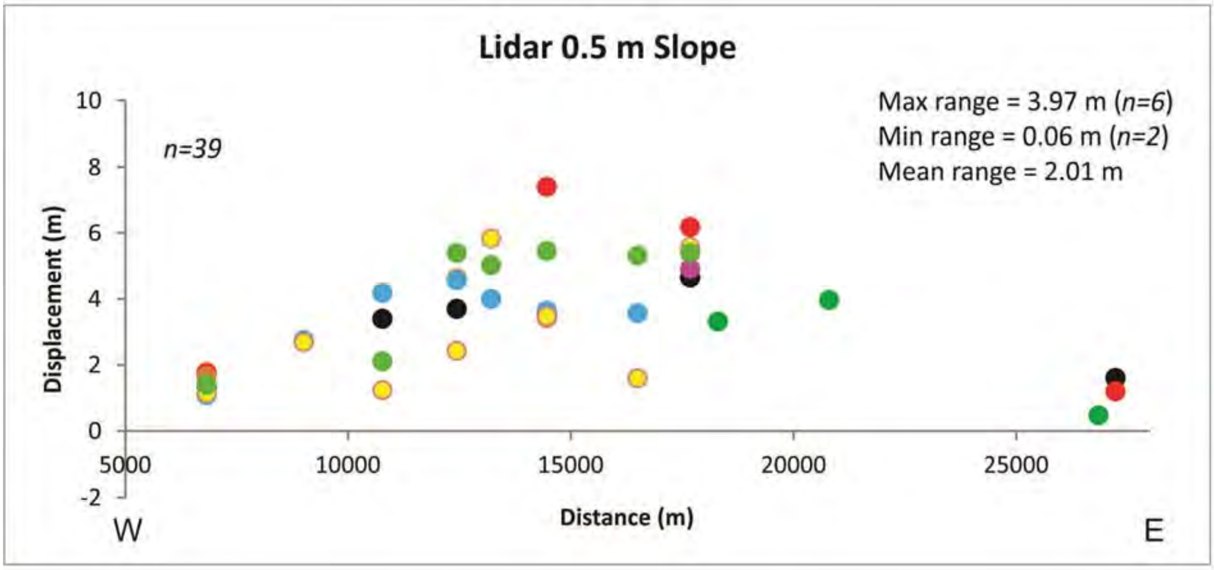

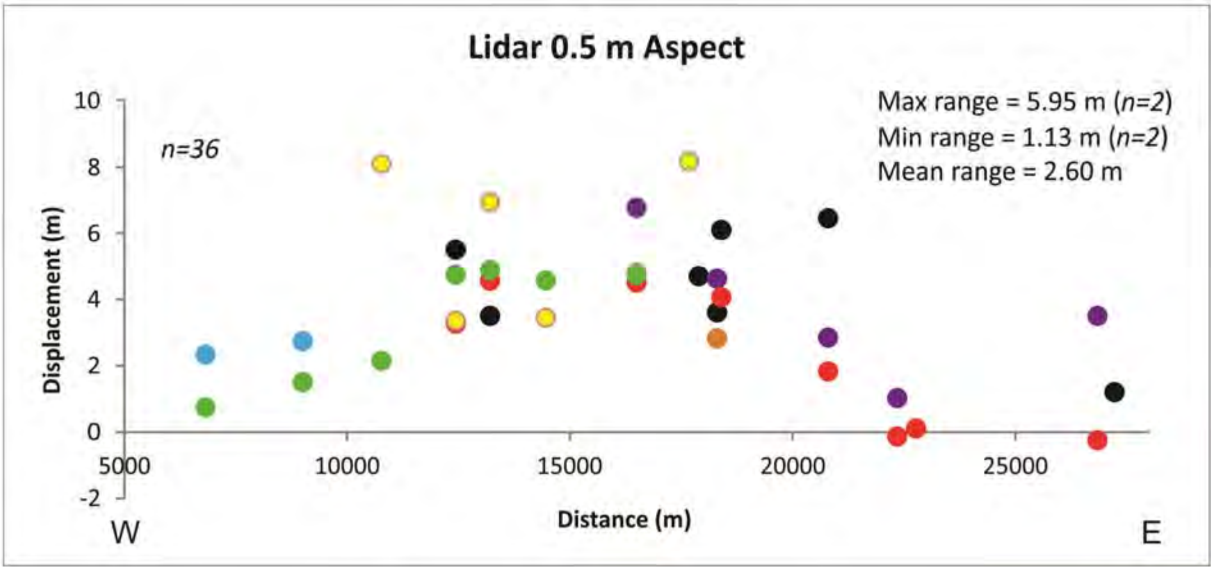

Figure 5.4 continued Along-strike plots of displacement measurements made by multiple geologists for different datasets. The colours are individuals measurements and the same colour is used in each plot.

If outliers (the highest measurements for sites 23, 30a, 71b and 93a and the lowest measurement for site 71b) are removed, then the maximum and mean ranges for the Lidar 0.5 m HSNW and Lidar 0.5 m Aspect datasets reduce by several metres as shown in Table 5.1.

The datasets ranked from smallest to largest ranges of measurements are:

- RTK (mean 1.62 m)
- Lidar 0.5 m Aspect with outliers removed (mean 1.8 m)
- Lidar 0.5 m Slope (mean 2.01 m)
- Lidar 0.5 m HSNE (mean 2.08 m)
- Orthophoto (mean 2.60 m)
- Lidar 0.5 m HSNW (mean 2.79 m)

5.3.3 Ranges compared with distance along-strike and median displacement

Examination of the ranges for each dataset on the along-strike plots in Figures 5.2 and 5.3 suggests there is no systematic variation in the ranges of measurements by multiple geologists with along-strike distance. This is supported by Figure 5.4, which summarises the ranges (maximum minus minimum measurement) at each site. Some of the best fit lines have a negative slope (especially all datasets and the RTK dataset), but the low R^2 values means this may not be statistically significant. This suggests there is no systematic variation with displacement (i.e., the ranges are not larger in the centre of the fault where displacement is largest). This is confirmed in Figure 5.5 which shows the ranges for each site plotted against median displacement obtained for that site. The only plot with a notable positive correlation is the Lidar 0.5 m Slope dataset, but this plot only has 9 datapoints, which contributes to the relatively low R^2 value (0.44).

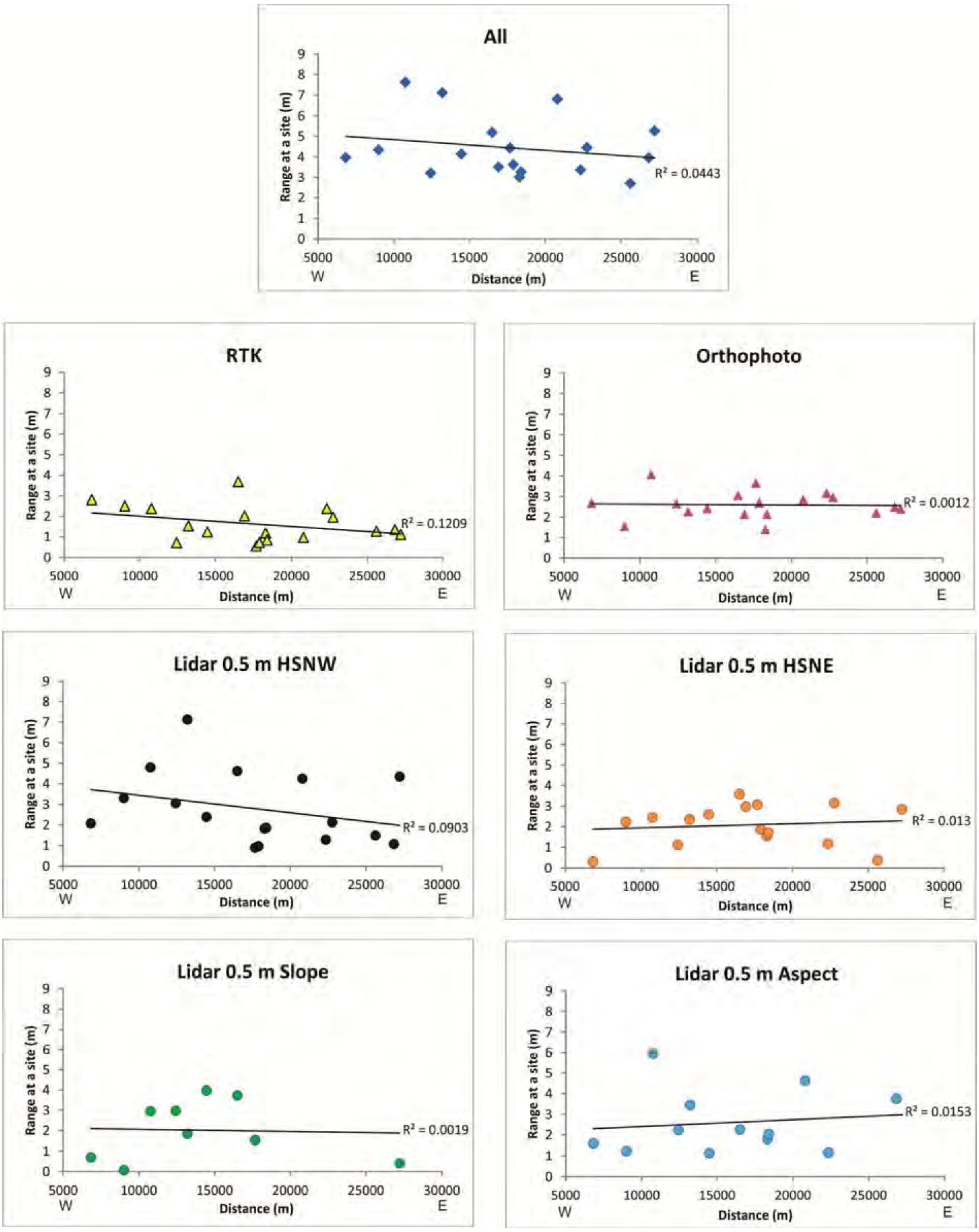

Figure 5.5 Ranges of displacements measured by multiple geologists at each site, compared with the along-strike distance.

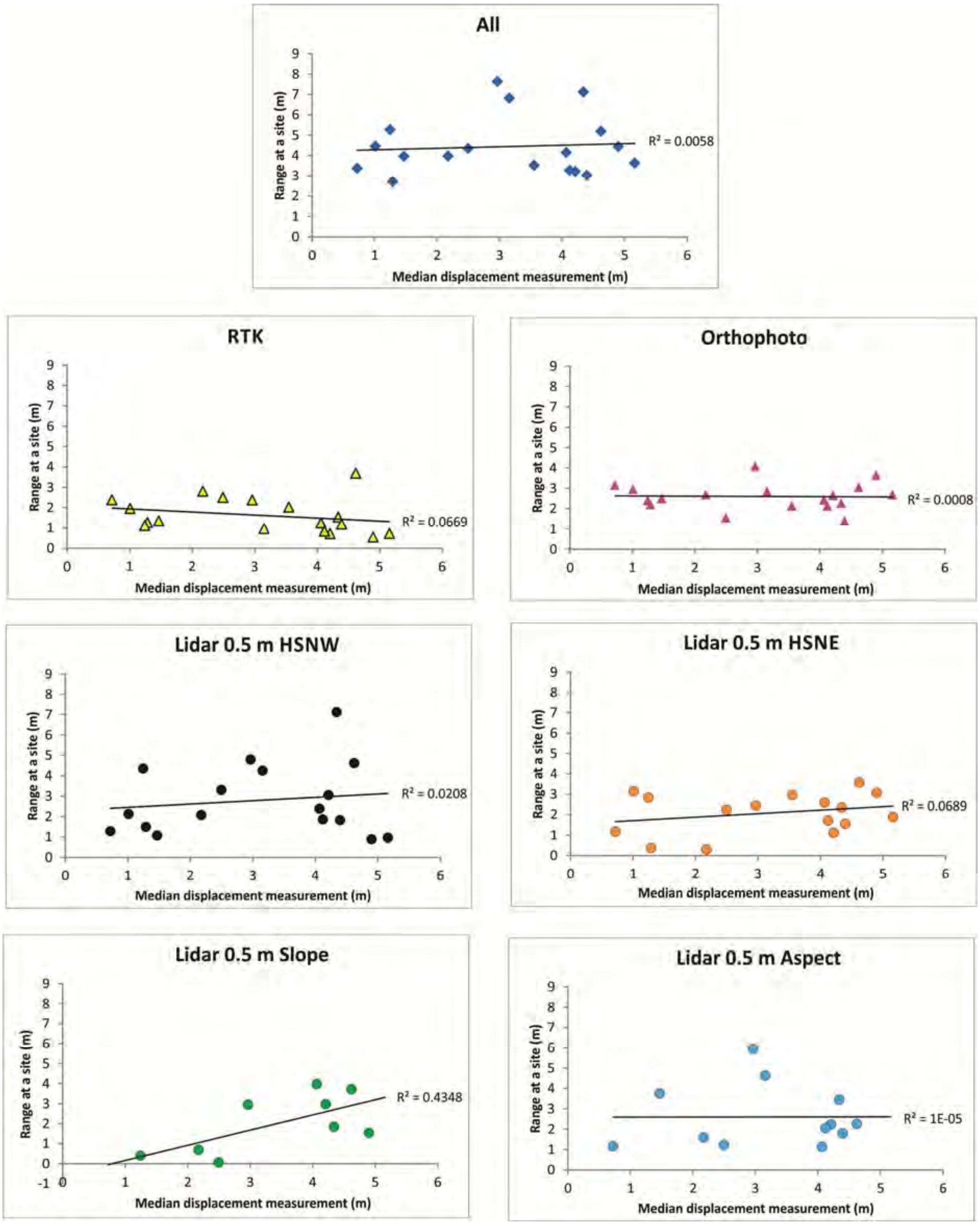

Figure 5.6 Ranges of displacements measured by multiple geologists at each site, compared with the median displacement measured at that site.

5.3.4 Ranges compared with fault zone width

To test if there are increased uncertainties associated with projecting to the fault over greater fault zone widths, we plot the ranges of measurements obtained by multiple geologists at each site plotted against the fault zone width at that site (Figure 5.6; see Figure 2.1 for definition of fault zone width). The width at each site is from Appendix 1 (Table A 1.1), although for some sites the width was not explicitly measured and so the width from the nearest marker is used.

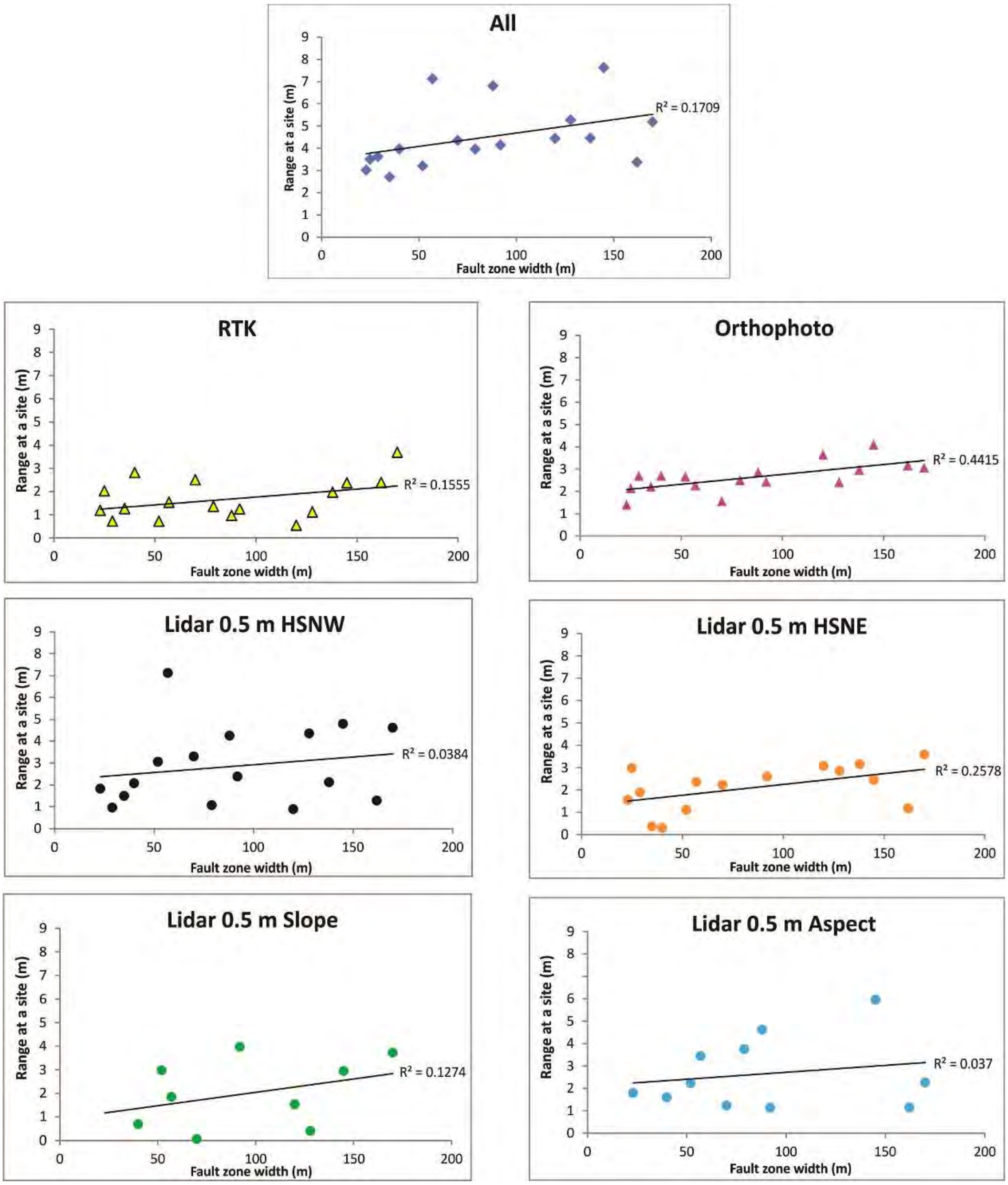

Figure 5.7 Ranges of displacements measured by multiple geologists at each site, compared with width of the Greendale Fault. The widths are derived from Appendix 1 (Table A 1.1).

All of the plots in Figure 5.7 show a small positive correlation suggesting that wide fault zones produce greater measurement uncertainty, but all the R^2 values are relatively low (≤0.44), so the relationship may not be statistically significant.

5.3.5 Ranges compared with marker obliquity

Figure 5.7 shows the range of measurements for each site plotted against the angle between the marker and a line drawn normal to the Greendale Fault. The purpose of this is to test if some of the variability in measurements are a function the obliquity of the marker, such that the greater the obliquity the more uncertainty in projecting to the Greendale Fault, and hence the greater uncertainty and range in values. With the exception of the Lidar 0.5 m Slope dataset, all plots show a small positive correlation suggesting that greater marker obliquity results in greater uncertainty, although R^2 values are again low.

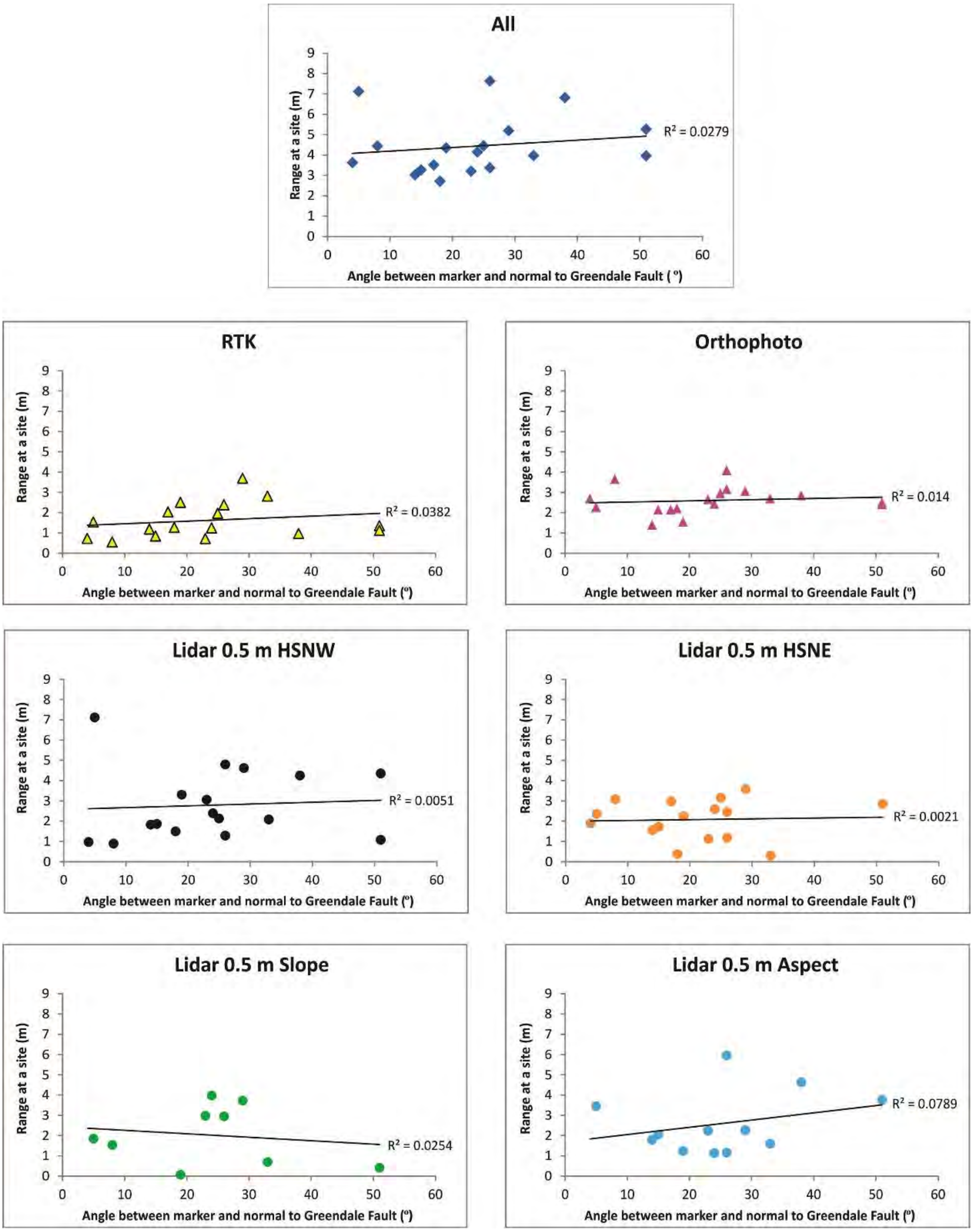

Figure 5.8 Ranges of displacements measured by multiple geologists at each site, compared with the angle between the marker at each site and a line drawn normal to the Greendale Fault.

5.3.6 Individual’s measurements

Examination of the along-strike plots colour-coded by geologist (Figure 5.3) suggests that there is no systematic bias between any individual’s measurements and others measurements at the same site (i.e., no individual consistently over- or under-estimates the displacement compared with their peers). To further test this, histograms have been plotted showing the difference between an individual’s measurements at each site and the median measurement for that site, for the different datasets. If there is a complete systematic bias, then an individual’s measurements should all sit on one side of the zero (median) line. Figure 5.8 shows histograms for the datasets with the greatest number of measurements (RTK and Orthophotos), but for completeness, histograms for all the datasets are contained in Appendix 7.

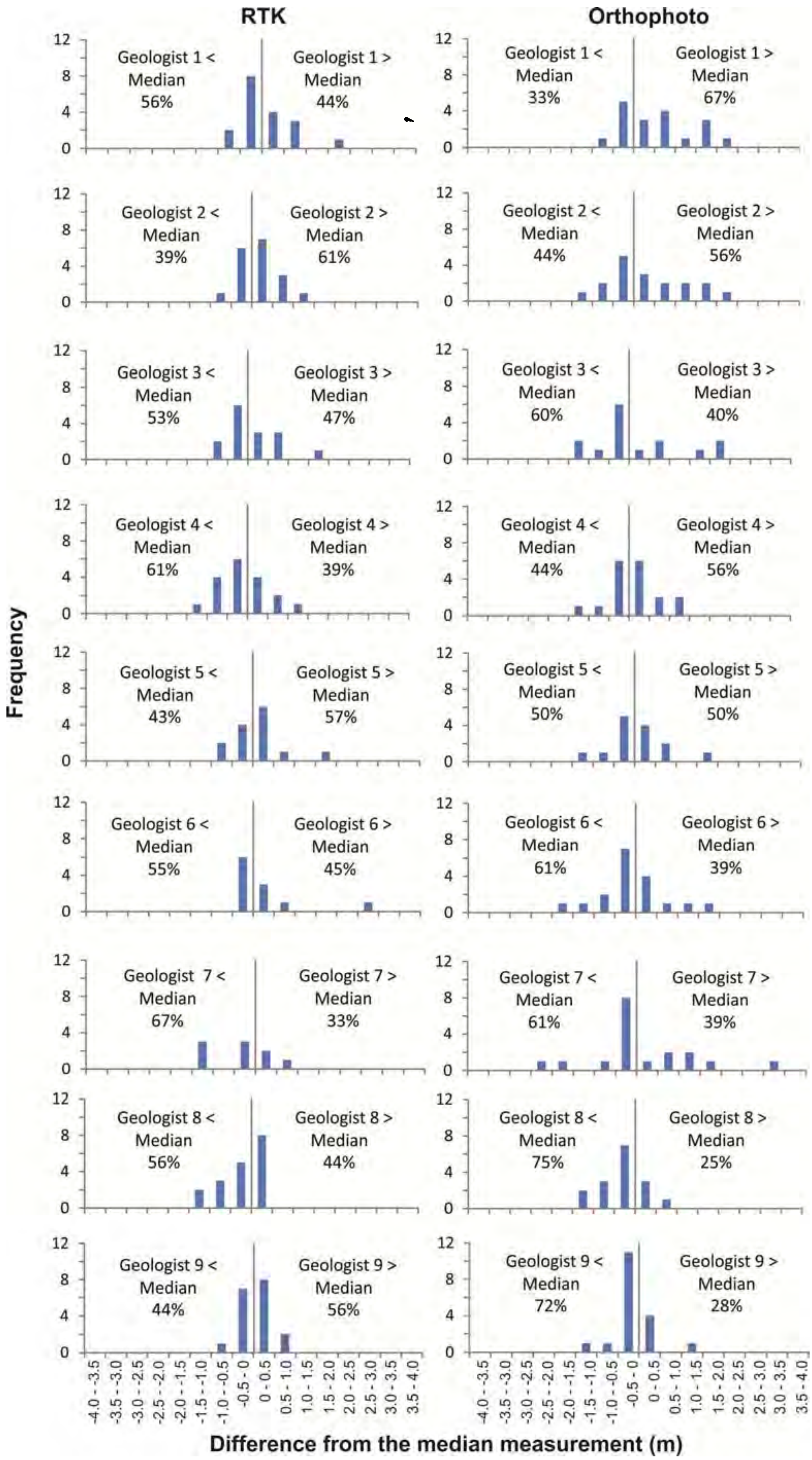

Figure 5.9 The difference between an individual's displacement measurement at each site and the median displacement measurement (from everyone's measurements) at that site.

Figure 5.8 and Appendix 6 show that there is no clear systematic difference in measurements between individuals. There are some slight tendencies, e.g., many of Geologist 1's Orthophoto measurements are higher than others and many of Geologist 8 and 9's Orthophoto measurements are lower than others. However, when all measurements made by an individual are examined (Appendix 7), there are no overall consistent patterns.

Another use of the histograms is to look at the spread of measurements for each geologist, since the histograms effectively normalise all the measurements. Examination of the full set of histograms in Appendix 7 shows that there is some variability in the spread of individual's measurements. For example, Geologists 4, 5 and 8's measurements were generally within a narrower range (<4 m) than the others (≤7 m).

5.4 DISCUSSION

The dextral displacement measurements made by 9 geologists at 18 sites show a surprisingly large amount of variability, especially considering that uncertainties were not assigned. The variability is even larger than that from the measurements by 1 geologist (Nicola Litchfield) using multiple datasets (section 4). For example, the mean range of measurements using multiple datasets by one geologist (section 4) is 1.5 m (±0.75 m), whereas the mean range by multiple geologists using multiple datasets (this section) is 4.44 m (±2.2 m), or 3.87 m (±1.9 m) if 5 potential outliers are removed.

Separating the multiple geologist measurements into different datasets shows that, as was demonstrated in section 4, much of this variability is likely a result of using different datasets. The mean ranges for each dataset (1.62 to 2.79 m) are roughly half the mean range for all datasets (4.44 m). As was also found in section 4, the range from the field-based RTK dataset (mean 1.62 m) is generally smaller than ranges for the remote sensing (Orthophoto and Lidar) datasets (mean 2.10 to 2.6 m, or with potential outliers removed mean 1.8 to 2.6 m).

There are some slight trends between the ranges of displacement measured for each site and along-site distance (negative), fault zone width (positive) and marker obliquity (positive), but not with the median measurement. The slight positive trends with fault zone width and marker obliquity are what you would intuitively expect – that measurements are more variable where they are projected across greater fault zone widths and where markers are not fault-perpendicular. The slight negative trend with distance along-strike may reflect the fact that workshop participants all started their measurements at the west end, and so became more experienced and potentially more accurate, as they progressed eastwards. Therefore a better test for variations with along-strike distance would be to measure displacements in a random order. There do not appear to be any systematic variations between individual's measurements and the measurements of others. This supports the above conclusion that much of the variability is a result of using different datasets, and the potential factors (e.g., marker resolution in different Lidar rasters as discussed in section 4.4.2).

Another possible reason for the larger ranges of measurements by multiple geologists than those made by 1 geologist in section 4 are differences in the time spent on each measurement. For financial and logistical reasons, the multiple geologist measurements were made during one of two 1 day workshops, with the aim of completing as many measurements as possible to develop a statistically useful dataset. By contrast, the measurements in section 4 were made over several months, by someone with more experience at making these measurements, included assigning uncertainties, and as a result more time and/or care was probably taken over each measurement. This is even more true for the previously published displacements (Quigley et al., 2012), since the aim of those measurements were to obtain the actual ground surface displacement of the Greendale Fault with robust uncertainties. Thus we speculate that the variability in the multiple geologist measurements would be lower if they had been given more time and/or more training to make the measurements.

Another potential factor relating to the time available in the workshops was the decision by the geologists in the first workshop to select the best Lidar raster to make measurements, whereas those in the second workshop attempted to make measurements using all the datasets. Although this has not been explored in detail, we speculate that the Lidar dataset measurements from the second workshop may show greater variability than those in the first workshop.

Given all of the above we would recommend that for future ground surface ruptures, time and care needs to be taken over each displacement measurement, carefully considering uncertainties and selecting the best dataset to use for each site. Ideally, each measurement should be scrutinised by a working party or in peer review, and consensus reached over the measurement.

6.0 DISTRIBUTION OF DISPLACEMENT ACROSS THE FAULT

6.1 INTRODUCTION

Ground surface rupture of the Greendale Fault extended for ~30 km across the gravel-dominated alluvial plains west of Christchurch, and comprised a distinctive series of en echelon, east-west striking, left-stepping traces (Figure 6.1a) (Quigley et al. 2010a, 2010b). As discussed in previous sections of this report, many linear cultural features such as fences, roads and crop-rows were displaced by the fault rupture. Over 100 of these were accurately surveyed, and they provide ideal markers for documenting – in unprecedented detail – the amounts and patterns of coseismic surface rupture deformation.

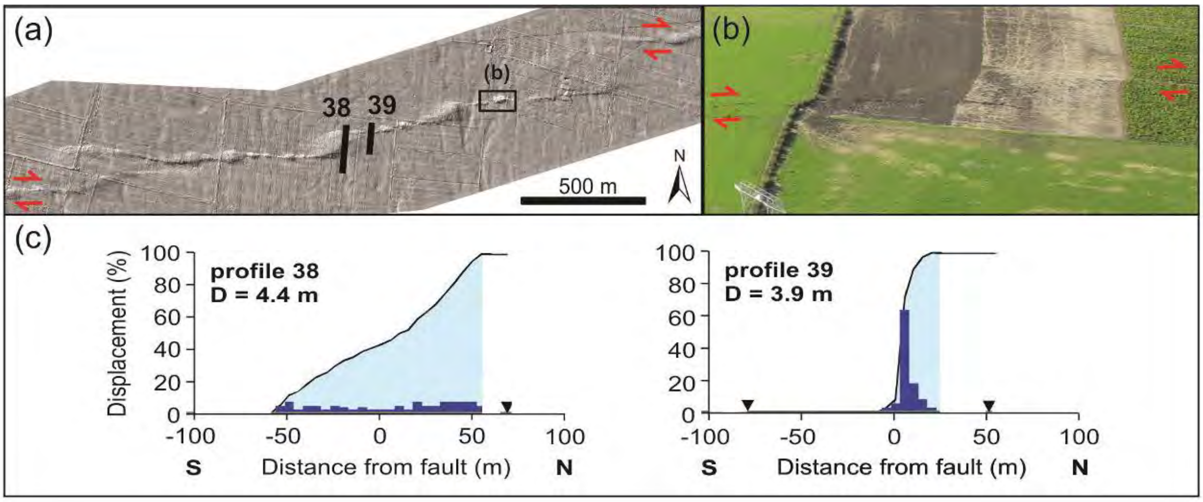

Figure 6.1 a) Lidar hillshade digital elevation model, illuminated from the NW, of a section of the Greendale Fault's ground surface rupture. b) Photo showing along-strike variation of surface rupture deformation zone width. For scale, the two bare fields are each ~40 m wide, and total dextral displacement is ~4.5 m (after Barrell et al. 2011). c) Plots of cumulative strike-slip surface rupture displacement and histograms of displacement distribution at two representative sites across the Greendale Fault, located in Figures 6.1a & 6.3. Surface rupture deformation is widest, and more evenly distributed, at step-overs (profile 38), and narrowest and more spiked where rupture comprises a single trace (profile 39). In these profiles, deformation is projected perpendicular to fault strike, and binned in 5 m increments (see text and Figure 6.2 for more detail). D = dextral displacement across the length of the profile. (After Figure 2 of Van Dissen et al. 2013).

The amounts of surface rupture displacement at the 101 survey sites are tabulated in Appendix 1. The survey data have also enabled us to characterise the distribution, and variability, of coseismic slip across the fault rupture deformation zone (e.g., Figure 6.1c). This type of characterisation is of particular value with regards to, for example, the design of resilient lifeline fault crossings (e.g., Bray and Kelson 2006), or set-back distances required to account for local changes in fault trace geometry (e.g., Kerr et al., 2003).

Figure 6.2 presents a schematic illustration of how the distribution of dextral surface rupture displacement was documented at 54 selected profile sites that cross all, or part, of the Greendale Fault's surface rupture deformation zone. At the selected profile sites, the survey points were connected via straight lines in a GIS environment, and parallel projection lines were established for the survey points outside of the surface rupture deformation zone on either side of the fault. Then, incremental dextral displacements were measured parallel to fault strike, every 5 m perpendicular to fault strike. The 5 m distance between incremental displacement measurements was chosen because this is the nominal distance between fence posts throughout the study area (though, in places, fence post spacing did range up to 15 m), and because fence posts were commonly utilised survey points in our investigations.

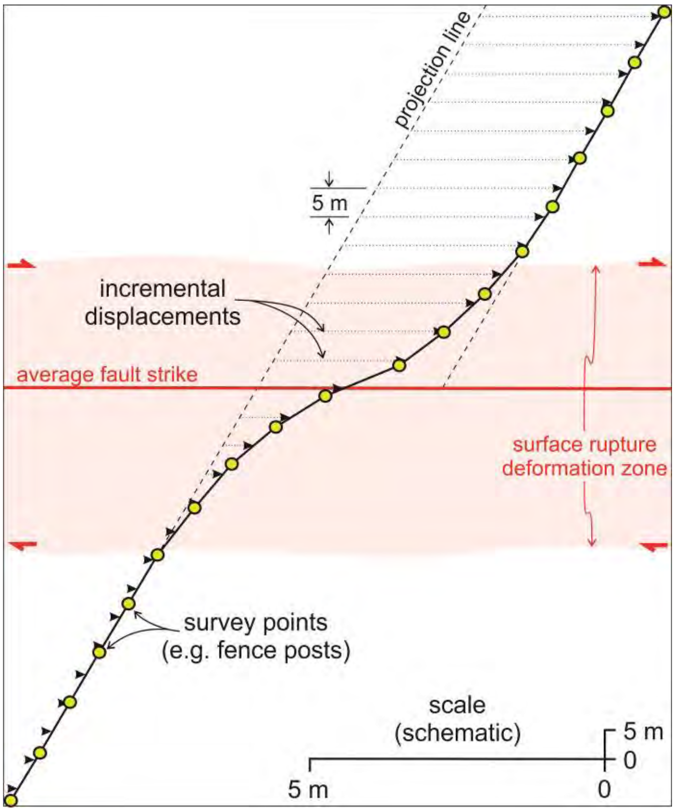

Figure 6.2 Schematic diagram showing how the distribution of dextral surface rupture displacement was measured at selected profile sites across the Greendale Fault's surface rupture deformation zone.

The locations of the 54 selected dextral deformation profile sites are shown in Figure 6.3 (sequentially numbered from west to east), and their corresponding plots of cumulative dextral surface rupture displacement and histograms of displacement distribution are depicted in Figure 6.4. Note, there are more survey sites (Figure 3.2) than there are deformation profile sites (Figure 6.3) because at sites where there are multiple profiles in close proximity (e.g., at Hollands Road there are 5 profiles within ~20 m of each other), we chose the one that provided the most accurate evaluation of dextral displacement for further deformation profile appraisal. Appendix 1 (Table A 1.1) lists which deformation profile site corresponds to which survey site.

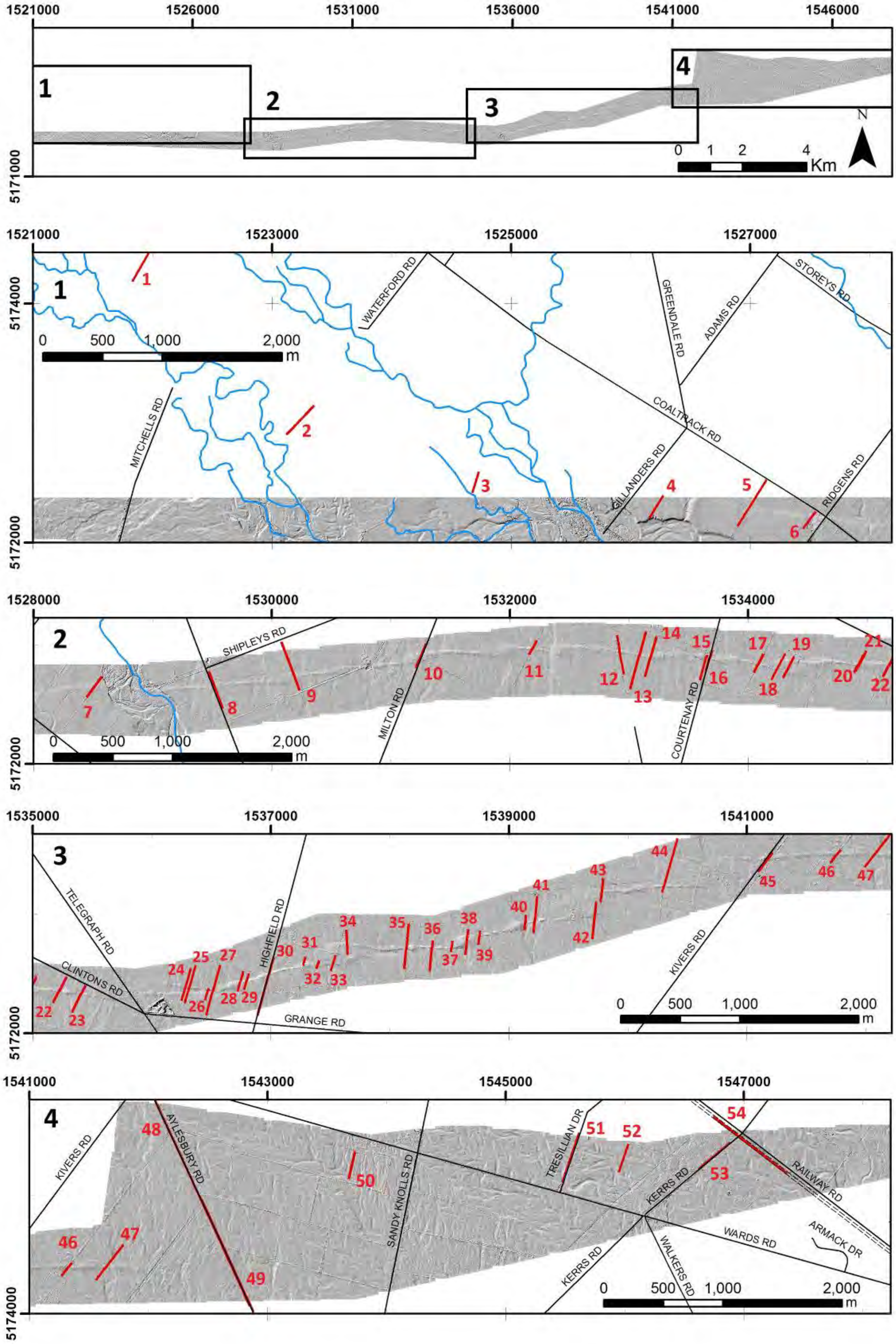

Figure 6.3 Locations of dextral deformation profile sites across the Greendale Fault's surface rupture deformation zone. Figure 6.4 presents the plots of cumulative strike-slip surface rupture displacement and histograms of displacement distribution for these profile sites.

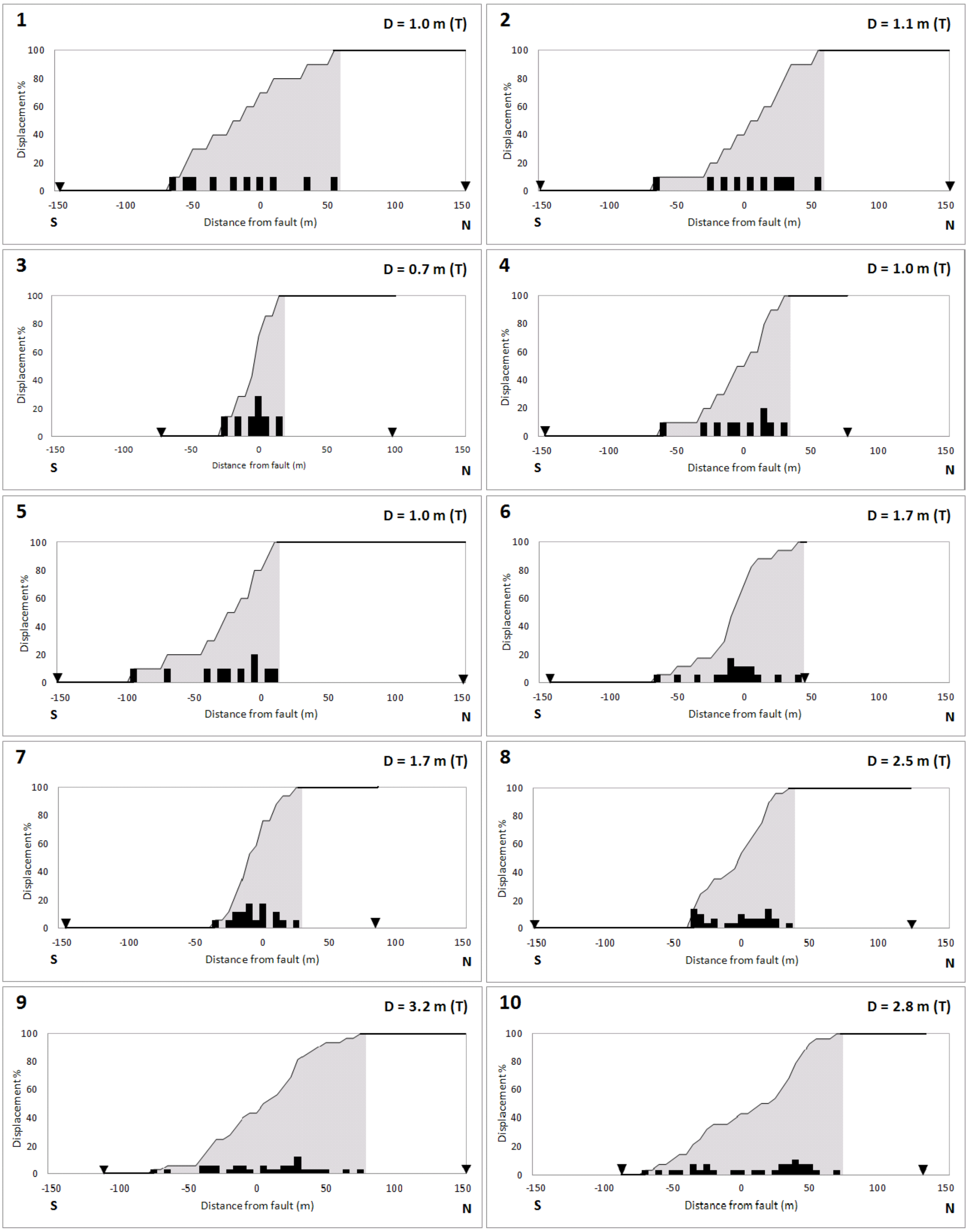

Figure 6.4 Cumulative strike-slip surface rupture displacement and histograms of displacement distribution for deformation profile sites 1–10 (see Figure 6.3 for profile locations). D = dextral displacement across the length of the profile; T = total dextral displacement (i.e. the profile spans the entire width of the surface rupture deformation zone).

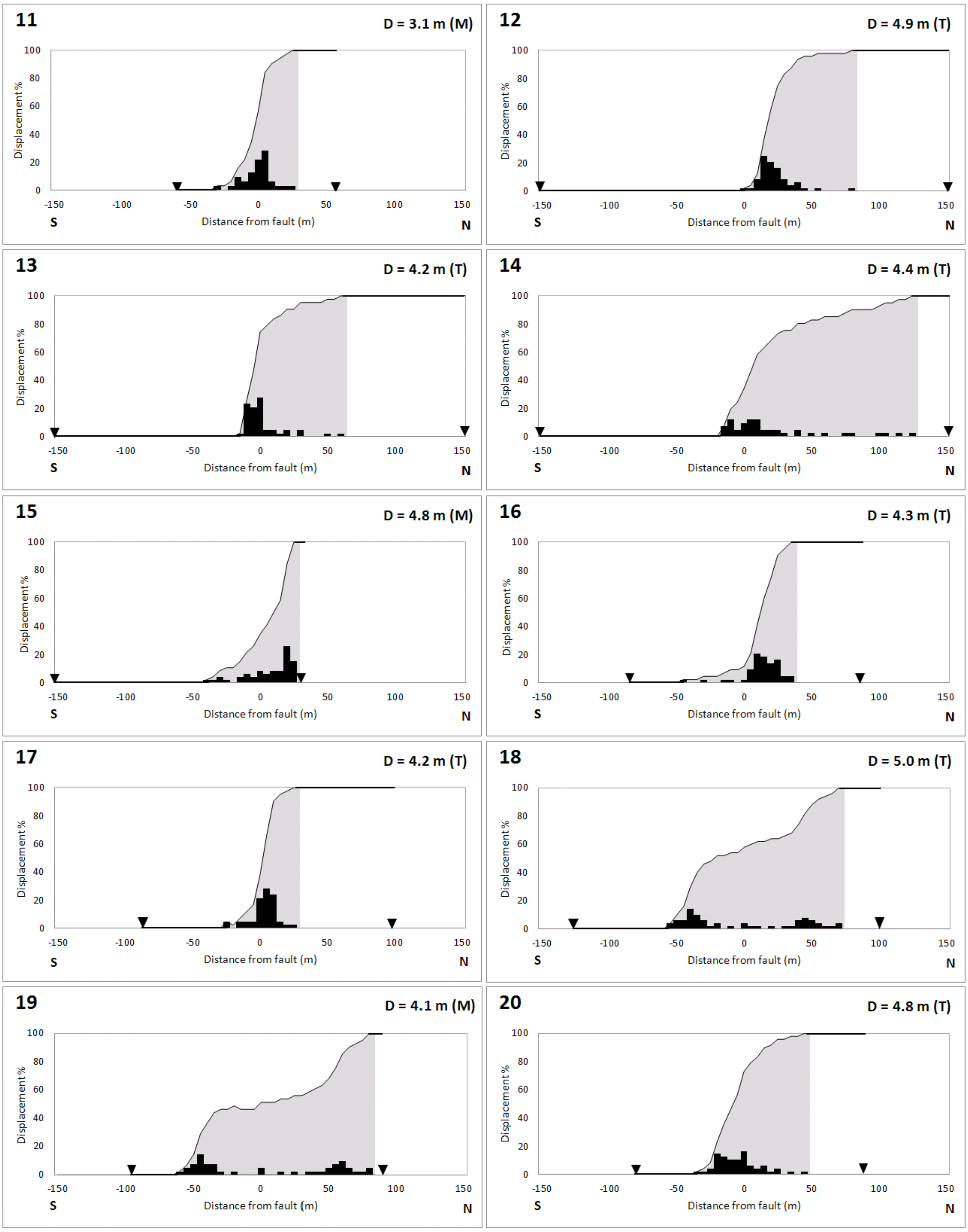

Figure 6.4 continued Cumulative strike-slip surface rupture displacement and histograms of displacement distribution for deformation profile sites 11–20 (see Figure 6.3 for profile locations). D = dextral displacement across the length of the profile; T = total dextral displacement (i.e. the profile spans the entire width of the surface rupture deformation zone); M = minimum dextral displacement (i.e. the profile does not quite span the entire width of the surface rupture deformation zone).

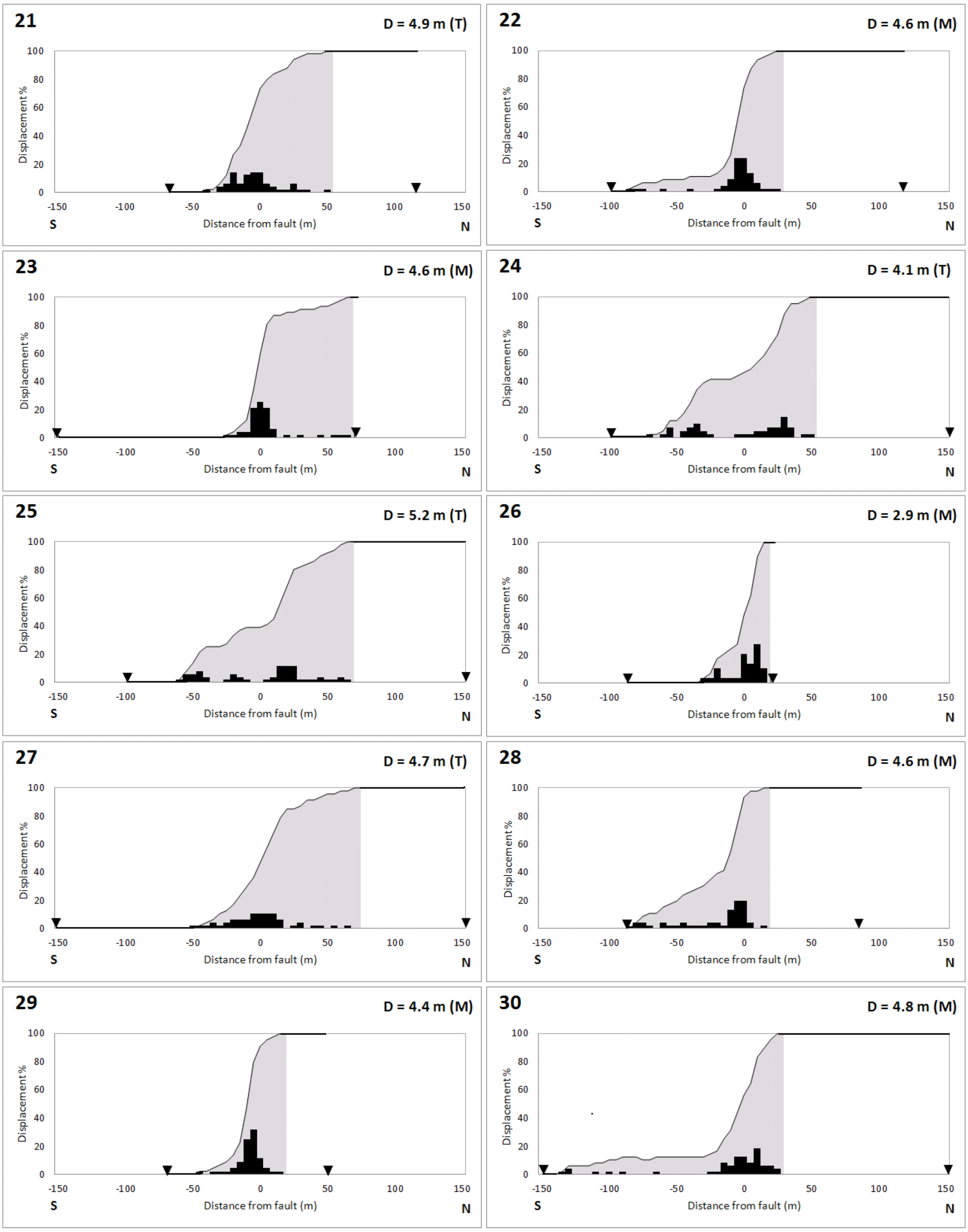

Figure 6.4 continued Cumulative strike-slip surface rupture displacement and histograms of displacement distribution for deformation profile sites 21–30 (see Figure 6.3 for profile locations). D = dextral displacement across the length of the profile; T = total dextral displacement (i.e. the profile spans the entire width of the surface rupture deformation zone); M = minimum dextral displacement (i.e. the profile does not quite span the entire width of the surface rupture deformation zone).

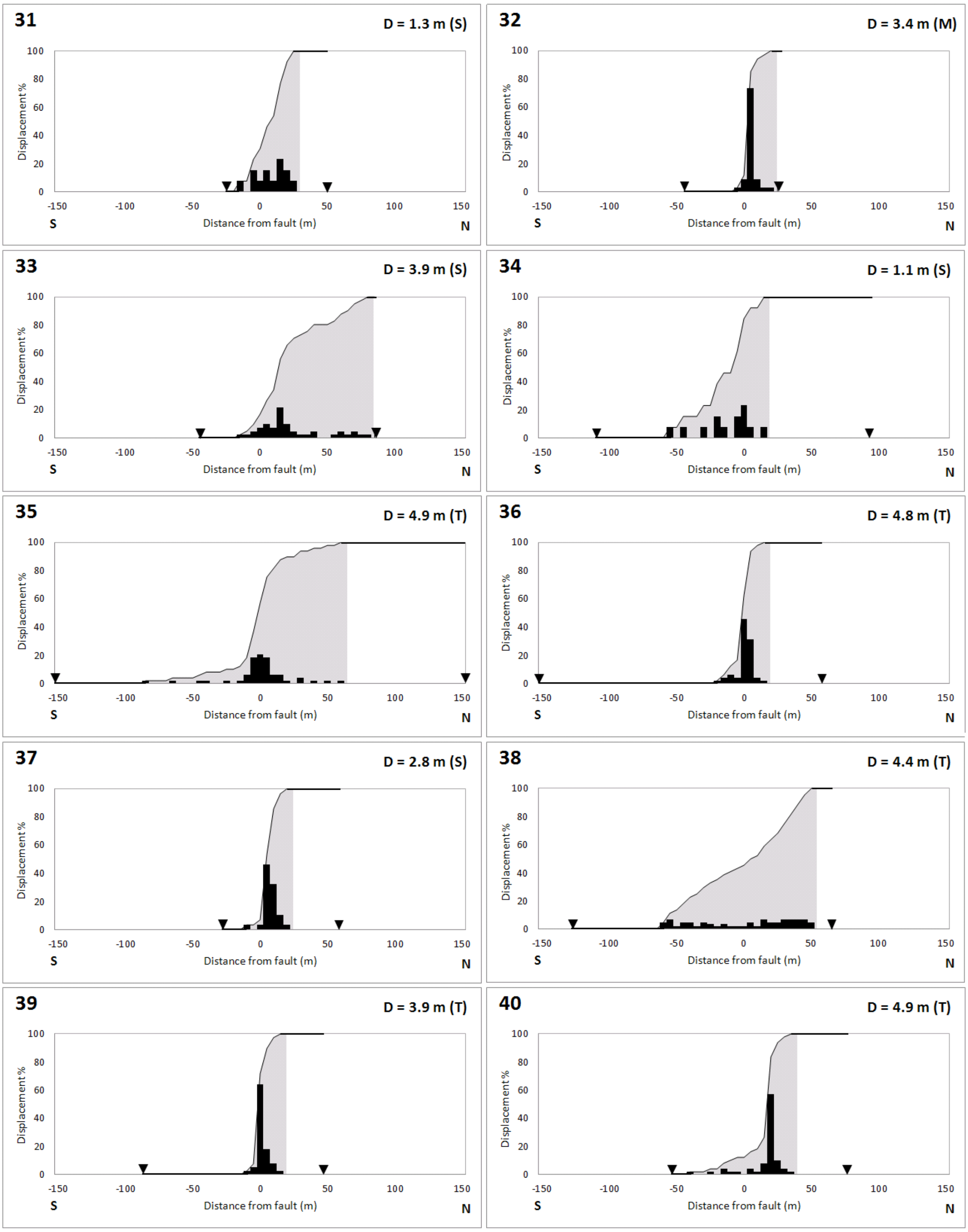

Figure 6.4 continued Cumulative strike-slip surface rupture displacement and histograms of displacement distribution for deformation profile sites 31–40 (see Figure 6.3 for profile locations). D = dextral displacement across the length of the profile; T = total dextral displacement (i.e. the profile spans the entire width of the surface rupture deformation zone); M = minimum dextral displacement (i.e. the profile does not quite span the entire width of the surface rupture deformation zone); S = single trace of two (i.e. profile crosses only one side of a fault trace step-over).

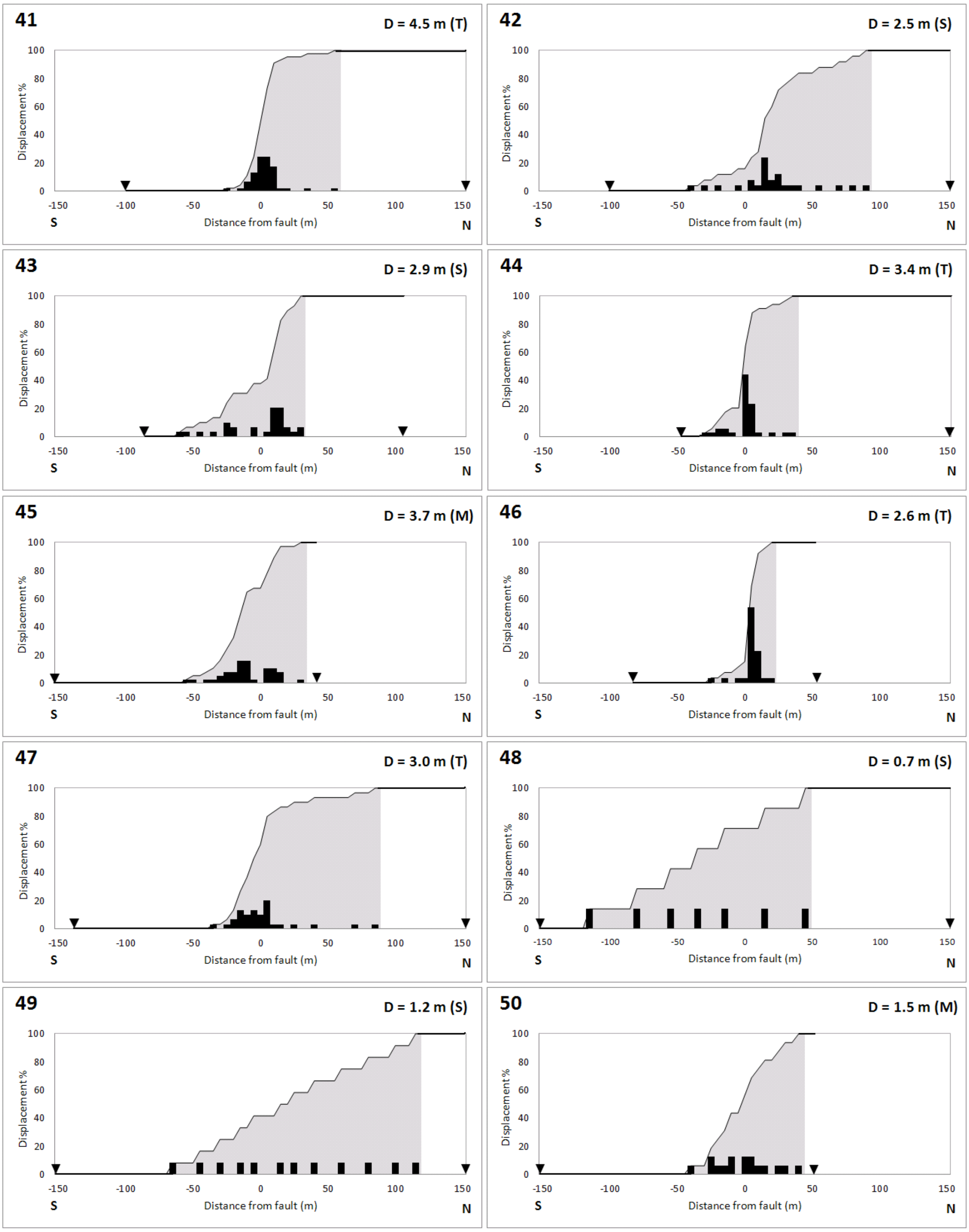

Figure 6.4 continued Cumulative strike-slip surface rupture displacement and histograms of displacement distribution for deformation profile sites 41–50 (see Figure 6.3 for profile locations). D = dextral displacement across the length of the profile; T = total dextral displacement (i.e. the profile spans the entire width of the surface rupture deformation zone); M = minimum dextral displacement (i.e. the profile does not quite span the entire width of the surface rupture deformation zone); S = single trace of two (i.e. profile crosses only one side of a fault trace step-over).

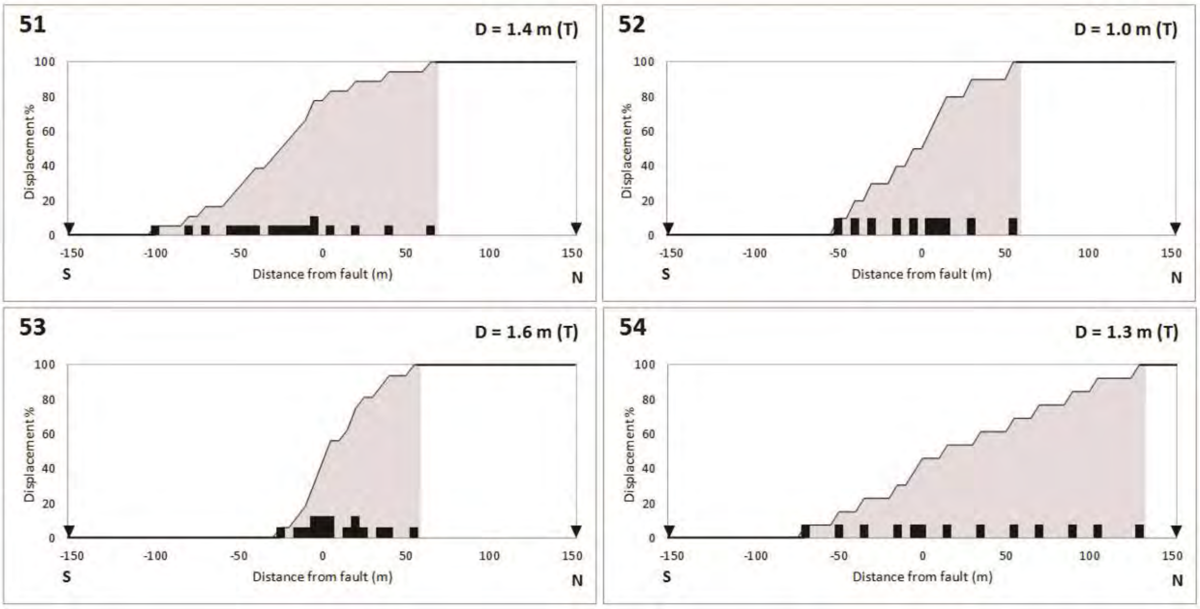

Figure 6.4 continued Cumulative strike-slip surface rupture displacement and histograms of displacement distribution for deformation profile sites 51–54 (see Figure 6.3 for profile locations). D = dextral displacement across the length of the profile; T = total dextral displacement (i.e. the profile spans the entire width of the surface rupture deformation zone).

In the sections below, and using the data tabulated in Appendix 1 (Table A 1.1) and the deformation profiles presented in Figures 6.3 and 6.4, we further assess and characterise the width of the Greendale Fault's surface rupture deformation zone (see Figure 2.1 for definition of fault zone width), and the distribution of dextral displacement across the surface rupture deformation zone.

6.2 WIDTH OF SURFACE RUPTURE DEFORMATION ZONE

Perpendicular to fault strike, surface rupture displacement was distributed across a ~30 to 300 m wide deformation zone, largely as horizontal flexure (i.e. non-elastic folding about a vertical axis) (Van Dissen et al., 2011; Quigley et al., 2012; Villamor et al. 2012; Figure 2.1). The average width of the Greendale Fault's surface rupture deformation zone is about 80 to 90 m (Figure 6.5; Appendix 1, Table A 1.1), excluding the largest step-overs. The width of the deformation zone is greatest at step-overs, and damaging ground strains developed within these. The largest step-over is ~1 km wide, and there is a multitude of smaller ones. Push-up "bulges" formed at most of these restraining left-steps (Figures 3.4, 6.1 and 6.6a), with amplitudes up to ~1 m, but typically less than 0.5 m.

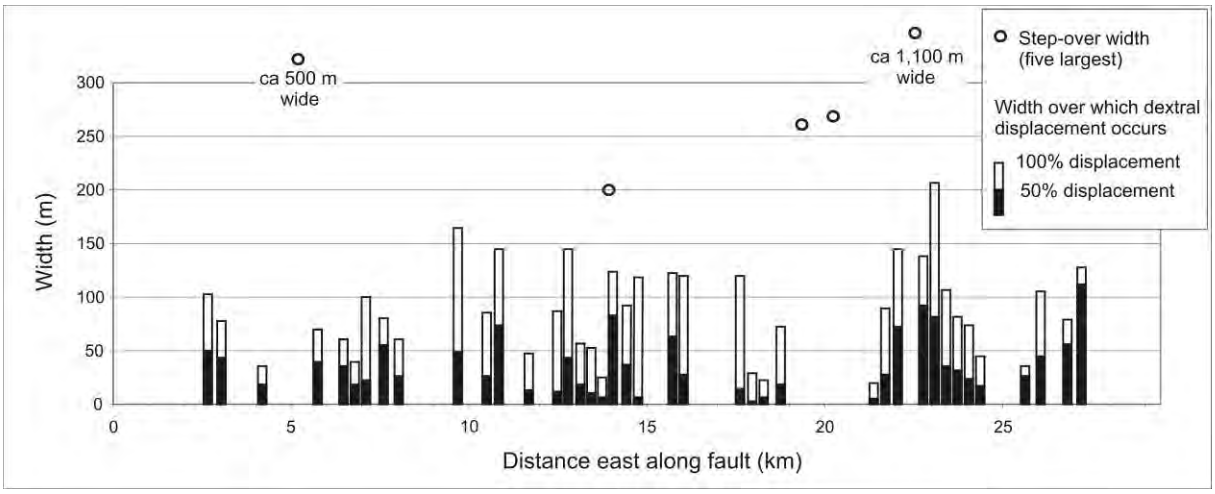

Figure 6.5 Width (horizontal distance) measured perpendicular to fault strike over which it takes to accumulate 50% and 100% of the total dextral surface rupture displacement at 40 sites along the Greendale Fault. 50% widths are centred over the portion of the deformation zone that exhibits the greatest amount of displacement. (After Figure 3 of Van Dissen et al., 2011).

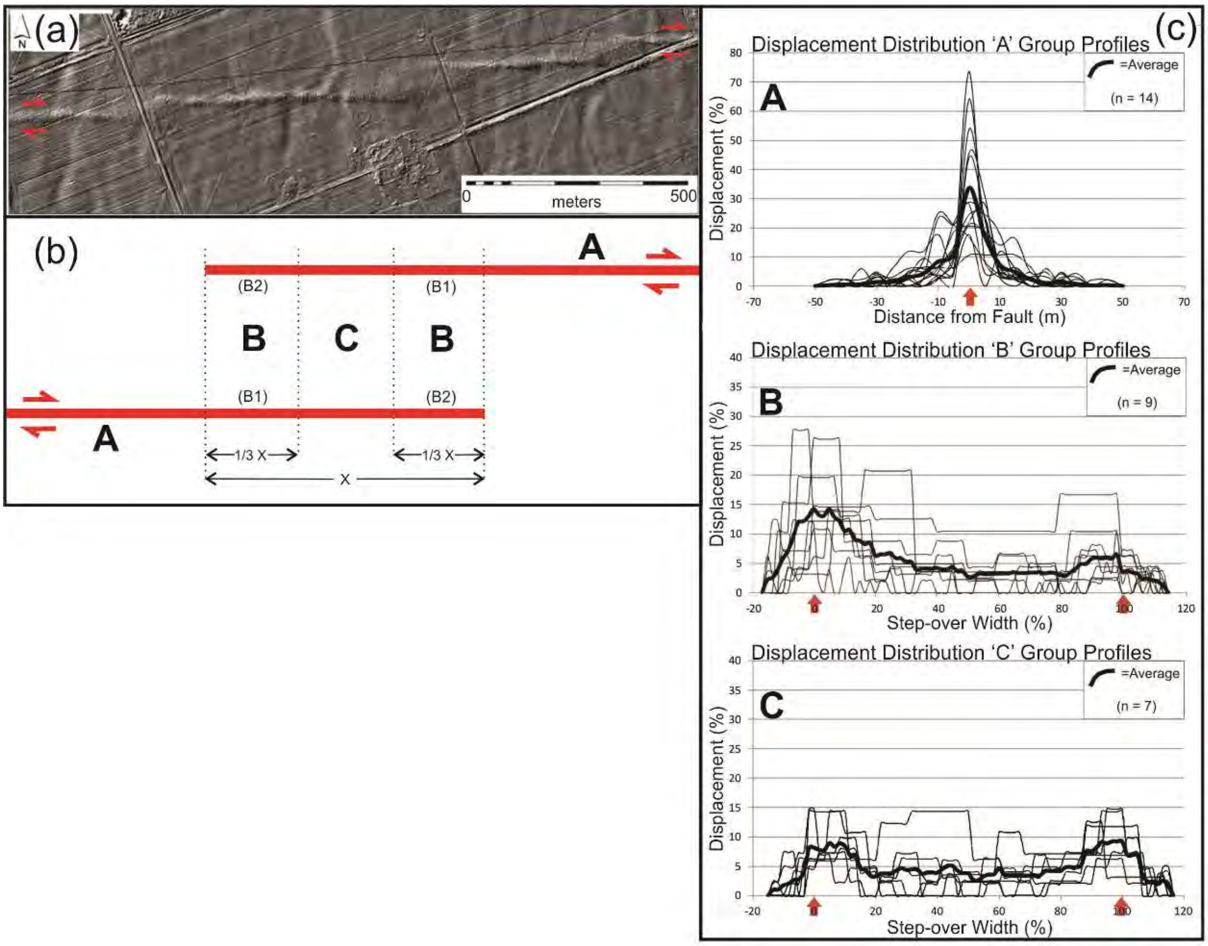

Figure 6.6 a) LiDAR hillshade image showing distinctive pattern of side-stepping traces along a 1.5 km-long portion of Greendale Fault surface rupture. b) Idealised fault step-over illustrating how structural positions A, B & C are defined. c) Displacement distribution plots, and their averages, of dextral deformation profiles across the Greendale Fault grouped according to the fault trace structural positions, A, B & C, defined in Figure 6.b. (After Figure 3 of Van Dissen et al. 2013).The fourteen A Group profiles are 7, 11, 12, 13, 16, 17, 27, 32, 35, 36, 39, 41, 44 & 46; the nine B Group profiles are 9, 10, 14, 15, 18, 20, 26, 28 & 42; and the seven C Group profiles are 8, 9, 19, 21, 24, 25, and 38.

On average, 50% of the dextral displacement occurred over 40% of the total width of the deformation zone (Figure 6.5; Appendix 1, Table A 1.1) with offset on observable discrete shears, where present, typically accounting for less than about a third of the total displacement (e.g., Quigley et al. 2012; Van Dissen et al. 2013). Across the paddocks deformed by fault rupture, there is a threshold of surface rupture displacement of ~1 to 1.5 m; greater than this discrete ground cracks and shears occur and form part of the surface rupture deformation zone, and less than this they are rarely present. The distributed nature of Greendale Fault ground surface rupture displacement is undoubtedly, in part, a consequence of the considerable thickness (exceeding 0.5 km in places; Jongens et al., 2012) of Quaternary gravel deposits that underlie the Canterbury Plains in the vicinity of the fault rupture, and that are loose near the ground surface.

It is relevant to note that the true width of deformation, as documented in the field through detailed surveys of deformed fences and the like, is usually several tens of metres wider than the width of deformation evident in the Lidar hillshade rasters as processed and depicted in Figures 3.4, 6.1 and 6.6a, and can be over 100 m wider. For example, the eastern ~7 km of surface rupture, across which there is as much as ~1.5 m of dextral and ~0.5 m of vertical distributed deformation, is not visible in Lidar hillshade rasters similar to those depicted in Figures 3.4, 6.1 and 6.6a (Van Dissen et al. 2011; Villamor et al. 2012).

6.3 DISTRIBUTION OF DEXTRAL DISPLACEMENT

As noted above, the width of the ground surface rupture deformation zone is greatest at step-overs. To further evaluate this, and its potential influence on the distribution of surface rupture deformation, the 30 highest quality dextral deformation profiles that cross the entire fault zone were grouped, and plotted, according to their structural position on the fault trace (Figure 6.6). The 30 selected profile sites were chosen based on the following criteria:

1. the profile, or combination of approximately in-line profiles, crosses all of the surface rupture deformation zone;
2. the profile crosses the fault at a relatively high angle (typically within ~30° of being perpendicular to fault strike); and
3. at sites where there are multiple profiles, we chose the one that we considered best exemplified the displacement at that site.

In the plots shown in Figure 6.6c, all deformation profiles are normalised to total displacement, and for those profiles crossing a step-over, they are also normalized to step-over width. Step-over width is defined, in most cases, as the width perpendicular to fault strike between the southern-most and northern-most discrete Riedel shears (denoted as red arrows in the lower two panels of Figure 6.6c) encompassed by the surface rupture deformation zone at the specific site.

All three structural groupings (A, B and C of Figure 6.6c) show that dextral deformation is predominantly distributed (as opposed to concentrated solely on a small number of discrete shears). Even when the surface rupture deformation zone comprises a single trace (group A of Figure 6.6) significant deformation occurs over a width of ~40 m. Across the central part of a step-over (group C), dextral deformation is distributed and equally shared across both sides of the step-over. At the beginnings/endings of a step-over (group B) deformation is, again, distributed, with the dominant side of the step-over (B1 of Figure 6.6b) carrying about three times more displacement than the subordinate side (B2 of Figure 6.6b).

Figure 6.7a plots the Greendale Fault's average displacement distributions for the three structural groupings (A, B and C) defined in Figure 6.6, along with their corresponding cumulative displacement curves. Figure 6.7b shows analogous plots for a hypothetical strike-slip case where deformation is entirely discrete. Figure 6.7c combines the plots shown in Figures 6.7a and 6.7b onto a single diagram. Comparable displacement plots are available for two sites along the 1906 rupture of the San Andreas Fault (Bray and Kelson, 2006) and 11 sites along the 1999 ruptures of the North Anatolian Fault (Rockwell et al., 2002). Invariably, these strike-slip displacements are less distributed than the Greendale case, more distributed than the hypothetical discrete case, and would fall between the two "bounding" curves of Figure 6.7c.

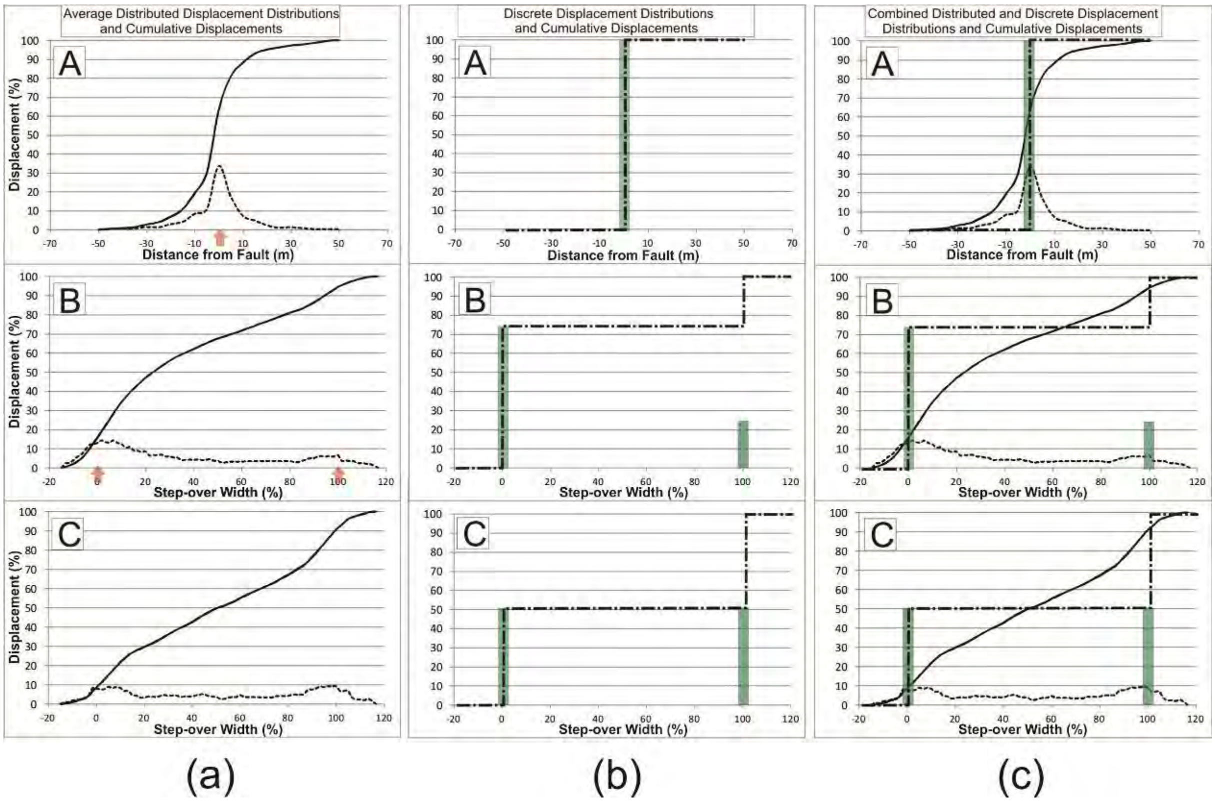

Figure 6.7 a) Average displacement distributions (dotted lines) and cumulative displacement curves (solid lines) for the Greendale Fault for the three fault trace structural groupings – A, B & C – defined in Figure 6.6. b) Displacement distributions (green shaded bars) and cumulative displacement curves (dot-dash lines) for a hypothetical case where strike-slip deformation is entirely discrete. Fault trace structural groupings – A, B & C – are as defined in Figure 6.6. c) Figures 6.7a & 6.7b combined, highlighting the differences in slip distribution between the hypothetical end-member discrete displacement example, and the near end-member distributed displacement (Greendale) example. (After Figure 4 of Van Dissen et al., 2013).

6.4 IMPROVING THE CHARACTERISATION, AND MITIGATION, OF SURFACE FAULT RUPTURE HAZARD THROUGH THE USE OF DISPLACEMENT DISTRIBUTION AND CUMULATIVE DISPLACEMENT CURVES

The Canterbury earthquake sequence is the most costly natural hazard event to impact New Zealand. Estimated losses are upwards of $40 billion (equivalent to ~30% real GDP). This level of loss is debilitatingly large and illustrates a clear economic and societal need in New Zealand to improve earthquake resilience. For this to be achieved, progress on a number of related fronts is needed; the most important being improved levels of damage limitation and post-event functionality in the built environment, and greater sustainability in land-use. Related to this is the realisation that as performance expectations increase for a structure (e.g., building /lifeline), then increased characterisations of the hazards that may impact that structure are also required so that the risks posed by those hazards can be more fully accommodated /mitigated in the design, construction and siting of the structure.

Ground deformation can contribute significantly to losses in major earthquakes. Compared with areas that experience only strong ground shaking during an earthquake, those areas that also suffer permanent ground deformation (e.g., liquefaction, slope failure, surface fault rupture), sustain greater levels of damage and loss. This relationship was clearly demonstrated during the 2010-2011 Canterbury earthquakes (e.g., NZSEE 2010, Kaiser et al. 2012; SRL 2011; NZSEE 2012). Ultimately, the mitigation of the risks these hazards pose depends on the integrated application of appropriate engineering design and risk-based land-use policy (e.g., Mileti 1999; Bray 2001; Kerr et al. 2003; Saunders and Beban 2012). For such approaches to be successful, however, there is a critical requirement to accurately characterise the ground deformation hazards. In this section, we develop a framework for doing this for strike-slip surface fault rupture.

We consider that the displacement distribution curves presented in Figure 6.7c can be used, following the indicative steps outlined below, to assist improved characterisation of strike-slip surface fault rupture hazard. In general terms, this approach is similar to that described in Kelson et al. (2004).

1. Determine the amount of surface rupture displacement at the site of interest using, for example, a combination of site specific investigations and empirical ground surface displacement regressions such as Well and Coppersmith (1994) and Wesnousky (2008).
2. Establish the location of the site in relation to fault trace structural position (i.e., is the site on, or across, the middle of a step-over, the beginning/end of a step-over, or a single trace). If the site is on, or across, a step-over, determine the width of the step-over.
3. Determine if the site is likely to experience distributed (Greendale-like) displacement, discrete displacement, or something in between. This is potentially the most subjective step. Settings that would tend to favour discrete displacement include, but are not limited to, those where bedrock is at or very near the ground surface, and the fault has a short recurrence interval and large total offset. Conversely, settings favouring distributed deformation would include those where there is a thick sequence of weak/loose material above bedrock (e.g., Bray et al., 1994), and the fault has a long recurrence interval and small total offset (i.e., is geologically immature).
4. Use Figure 6.7c and the determinations of items 1–3 above to construct displacement distribution and cumulative displacement curves for the site of interest. Note that Figure 6.7c applies only to strike-slip ruptures, and is based on data where the step-overs are exclusively restraining/contractional. The curves are untested in releasing/extensional step-over settings. Also, these curves do not account for vertical displacement nor, in a distributed displacement setting, do they explicitly constrain the location and amount of any discrete displacement that may occur. To the extent that these aspects may be of relevance to the engineering / planning project at hand, they will need to be assessed separately.

Improved parameterisation of surface fault rupture hazard - especially when combined with the rupture resilient design concepts presented in Bray (2001) and Bray and Kelson (2006), and the land-use planning guidance provided in Kerr et al. (2003) – will facilitate development of mitigation strategies aimed at reducing the damage caused by surface fault rupture, and improving the post-event functionality of structures that may be impacted by fault rupture.

6.5 DISTRIBUTED SURFACE FAULT RUPTURE AND APPLICATION OF THE MINISTRY FOR THE ENVIRONMENT'S ACTIVE FAULT GUIDELINES

The Darfield earthquake (including Greendale Fault rupture) was the first ground surface fault rupture earthquake to impact New Zealand since the 1987 M_w 6.3 Edgecumbe Earthquake, Bay of Plenty, North Island. Over a dozen buildings, typically timber-framed houses and farm sheds with light-weight roofs, lay either wholly, or partially, within the Greendale Fault's surface rupture deformation zone (Van Dissen et al. 2011). None of these buildings collapsed, even the two with 0.5 to 1 m of discrete shear extending through/under them, but all were more damaged than comparable structures immediately outside the zone of surface rupture deformation. Some of the dwellings worst damaged by fault rupture have since been demolished.

From a life safety standpoint, all these buildings performed satisfactorily (i.e., they did not collapse). There were, however, notable differences in the respective performances of the buildings. Houses with only lightly-reinforced concrete slab foundations suffered moderate to severe structural and non-structural damage. Three other types of buildings performed more favourably and far exceeded life-safety objectives: one had a robust concrete slab foundation that was stronger than the surrounding soil, another had a shallow-seated pile foundation that isolated ground deformation from the superstructure, and the third had a structural system that enabled the building to tilt and rotate as a rigid body. This third building suffered very little internal deformation, was straightforward to re-level, and demonstrated, the potential for a high degree of post-event functionality for certain types of buildings in relation to, in this case, distributed surface fault rupture (Van Dissen et al. 2011).

In 2003, the Ministry for the Environment (MfE), New Zealand, published best practice guidelines for mitigating surface fault rupture hazard (Kerr et al. 2003; hereafter referred to as the MfE Active Fault Guidelines; also see Van Dissen et al. (2006). Key rupture hazard parameters in the MfE Active Fault Guidelines are Fault Complexity along with Building Importance and surface fault rupture recurrence interval. Fault Complexity is an important hazard parameter because for a given displacement, the amount of deformation at a specific locality is less within a distributed rupture zone where displacement is spread out, than it is within a narrow zone where rupture is concentrated. The relative fault rupture hazard is therefore less within a zone of distributed deformation than it is within a narrow concentrated zone.

As discussed above, surface rupture displacement on the Greendale Fault was typically distributed across a relatively wide zone of deformation. Buildings located within this distributed zone of deformation were subjected to only a portion of the fault's total surface rupture displacement, and no building within this zone collapsed. This provides a clear example of the appropriateness of the MfE's *Distributed Fault Complexity* parameter, at least for Building Importance Category 2a buildings (i.e. residential structures), and with respect to life-safety. Villamor et al. (2012) have subsequently mapped the Greendale Fault in accordance with the MfE Active Fault Guidelines, including the definition Fault Avoidance Zones based on *Distributed Fault Complexity.*

7.0 2013 RTK SURVEY TO TEST FOR POST-SEISMIC DISPLACEMENT

7.1 INTRODUCTION

In this section we present the results of re-surveying selected markers along the Greendale Fault approximately 2.5 years after the Darfield earthquake. The purpose was to test if there has been any post-seismic displacement (creep), as has been documented from other fault ruptures (e.g., Massonnet et al., 1994; Pollitz et al., 2001; Burgmann et al., 2002; Pollitz, 2005; Ryder et al., 2007; Hsu et al., 2007; Jouanne et al., 2011). We then briefly compare our results with those from other Greendale Fault studies.

7.2 METHODS

On 7 March 2013 10 markers (mostly fences beside roads) displaced by the Greendale Fault on 4 September 2010 were re-surveyed using RTK. Some of the markers had been repaired where they crossed the rupture, so the details of displacements in the centre of the fault zone were lost, but all still preserved the overall dextral displacement.

The sites re-surveyed are shown in Figure 7.1 and are listed in Table 7.1. The sites are broadly spread along the Greendale Fault, although several markers were surveyed near the centre, adjacent to a paleoseismic trench that was being analysed at the time (Hornblow et al., 2013). Unfortunately 3 of the markers (site numbers in brackets in Figure 7.1 and Table 7.1) turned out to not have been surveyed by RTK in 2010, although one (48d) was surveyed by laser scanning. However, since each are within a few metres of markers that were surveyed in 2010, the 2013 data are compared with the nearest marker surveyed in 2010 and the results are given a lower confidence ranking.

Figure 7.1 Sites re-surveyed by RTK on 7 March 2013. Numbers in brackets refer to sites where the exact same marker was not surveyed in both 2010 and 2013 and so the comparison is with the nearest marker (see text for details).

Table 7.1 Sites re-surveyed by RTK on 7th March 2013 (from west to east)

2010 Site number[1]	Marker description	Surveyed in 2010
20a	Wire fenceposts on the west side of Hollands Road.	Yes
(26b)	Power poles on the west side of Stranges Road.	No – compared with adjacent wire fence.
30b	East side of Courtney Road (gravel road edge)	Yes
36b	Wire fenceposts on the east side of the drive to Melrose.	Yes
37	Wire fenceposts 1 paddock east of the drive to Melrose.	Yes
38	Wire fenceposts 2 paddocks east of the drive to Melrose.	Yes
(48d)	Wire fenceposts on the east side of Highfield Road.	No – compared with adjacent wire fence.
(71a)	Wire fenceposts on the west side of Kivers Road	No – compared with adjacent crop mark.
88a	Wire fenceposts on the west side of Tresilian Road.	Yes
92a	Wire fenceposts on the west side of Kerrs Road.	Yes

[1] Site numbers are the displacement measurement sites in 2010 contained in Appendix 1 (Table A 1.1). Numbers in brackets are sites where the exact same marker was not surveyed in 2010, but the 2013 resurvey results are compared with the nearest marker.

As in 2010, the RTK surveys were local surveys, with base stations set up at several convenient locations along the fault. Unlike the 2010 surveys, however, the 2013 RTK surveys were not post-processed. This is because of the considerable deformation since the Darfield earthquake, most notably the 22 February 2011 Christchurch earthquake, which affected the McQueens Valley continuous GPS station used to post-process the 2010 survey (Section 2.3). This means that although each RTK survey is internally consistent, the absolute position of the survey points are not accurately fixed in space. As a result, the relative positions of markers cannot be directly compared by simply overlaying the 2013 positions on the 2010 positions in a GIS. Instead, the 2013 profiles were manually shifted to overlie the 2010 profiles and any deviations were noted. Specifically, the method involved the following steps in a GIS, as illustrated in Figure 7.2:

1. Drawing a 2013 profile line joining the RTK survey points (Figure 7.2A).
2. Manually shifting a copy of the 2013 profile line to overlay the correlative 2010 profile line (Figure 7.2B) on one side of the fault outside the fault zone.
3. Checking if there is any difference in position of the 2013 profile line with the 2010 profile line on the other side of the fault; any differences in position should reflect post-seismic deformation.
4. Repeating the process two more times and where possible, on both sides of the fault, to test for consistency.
5. Assign a relative confidence ranking*, from low to high.

These analyses were undertaken by the Nicola Litchfield, with one analysis for each site in consultation with Russ Van Dissen.

* The confidence rankings take into account:

- the straightness of either or both the 2010 and 2013 profiles, which in turn is a function of both the marker itself and the surveying (e.g., surveying posts or by walking);
- if the profile spans all the deformation; and
- if the same exact marker is compared in both surveys.

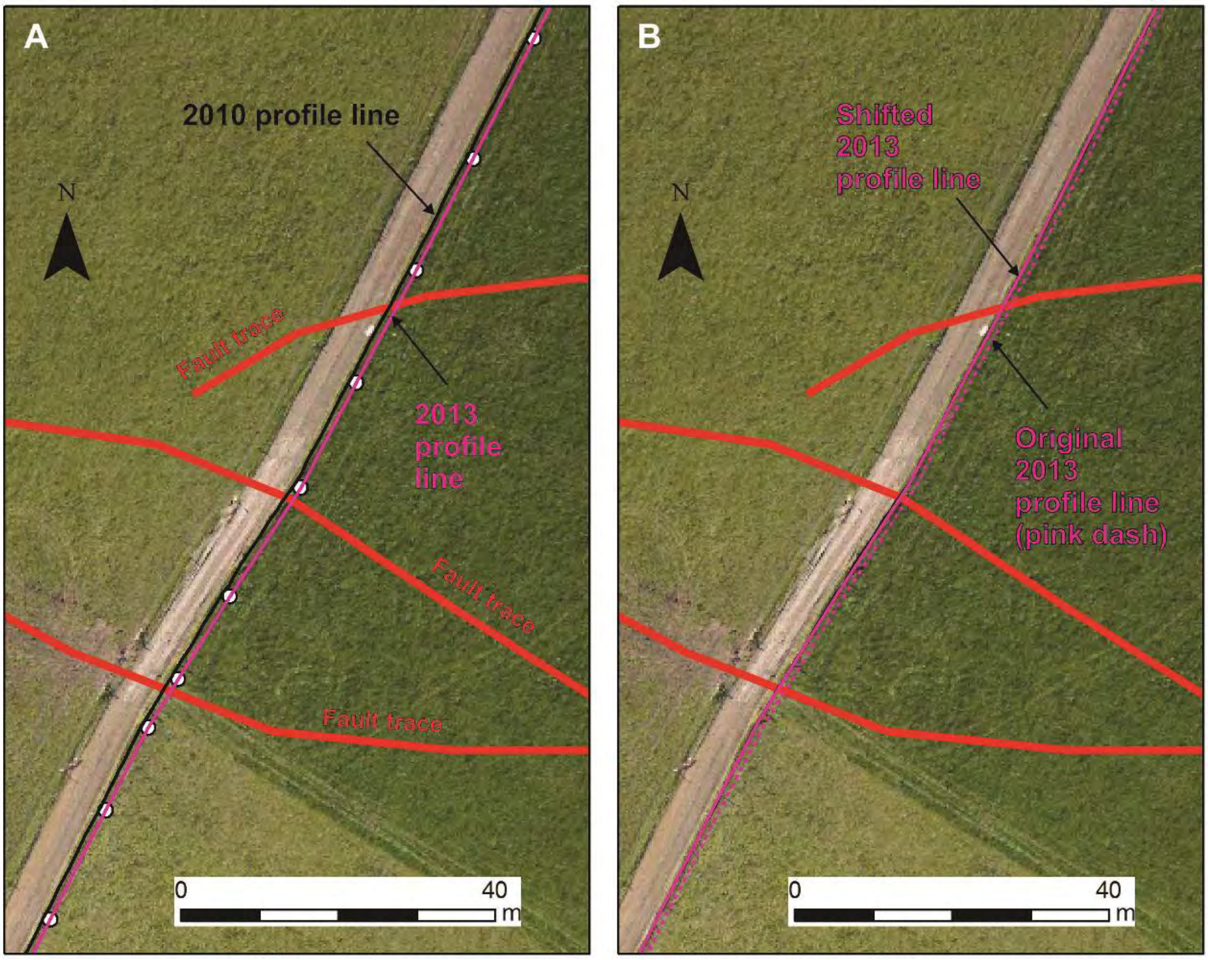

Figure 7.2 Example of the method used to assess if there was any post-seismic dextral displacement between the original, September 2010 survey and the March 2013 re-survey at site 36b (see Figure 7.1 for location). A) shows the 2013 profile line (pink) constructed from joining the 2013 RTK survey points (white dots), which doesn't lie exactly upon the 2010 profile line (black) because the 2013 RTK surveys were not post-processed. B) shows the manually shifted 2013 profile line to overlie the 2010 profile line (black, barely visible). The manual shift was undertaken on one side of the fault far away from the fault and any divergence on the other side of the fault is interpreted to reflect post-seismic dextral displacement.

7.3 Results

The results are summarised in Table 7.2 and are shown in Figure 7.3.

Table 7.2 Results of the comparison of re-surveying of selected profiles along the Greendale Fault ~2.5 years after the Darfield earthquake.

Site	First survey date	Second survey date	Displacement (m)	Side of the fault profile shifted	Confidence	Comments
20a	5 Sept 2010	7 March 2013	0.00	South	Medium	2010 profile irregular.
(26b)	5 Sept 2010	7 March 2013	0.00	South and North	Low	2010 profile too short and irregular to measure accurately. 2013 profile may record less displacement than 2010 profile.
30b	6 Sept 2010	7 March 2013	0.00	South and North	Low	2010 profile irregular. Marker (road edge) has greater uncertainty than other profiles (e.g., fenceposts). Road may not be parallel on both sides of the fault. 2013 profile may record less displacement than 2010 profile.
36b	7 Sept 2010	7 March 2013	0.00	North	Medium/High	2010 profile more irregular than 2013 profile.
37	7 Sept 2010	7 March 2013	0.00	North	Medium/High	2010 profile more irregular than 2013 profile.
38	7 Sept 2010	7 March 2013	0.00	South	Medium/High	2010 profile more irregular than 2013 profile.
(48d)	6 Sept 2010	7 March 2013	0.00	South and North	Low/Medium	2010 profile more irregular than 2013 profile. 2013 profile may record less displacement than 2010 profile.
(71a)	11 Sept 2010	7 March 2013	0.00	South	Low/Medium	2010 profile more irregular than 2013 profile.
88a	8 Sept 2010	7 March 2013	0.04-0.07	South and North	High	2010 profile straight and longer than 2013. Multiple measurements consistently results in a very small displacement. Possible displacement is consistent across the main fault zone.
92a	17 Sept 2010	7 March 2013	0.00	South and North	High	2010 profile relatively straight.

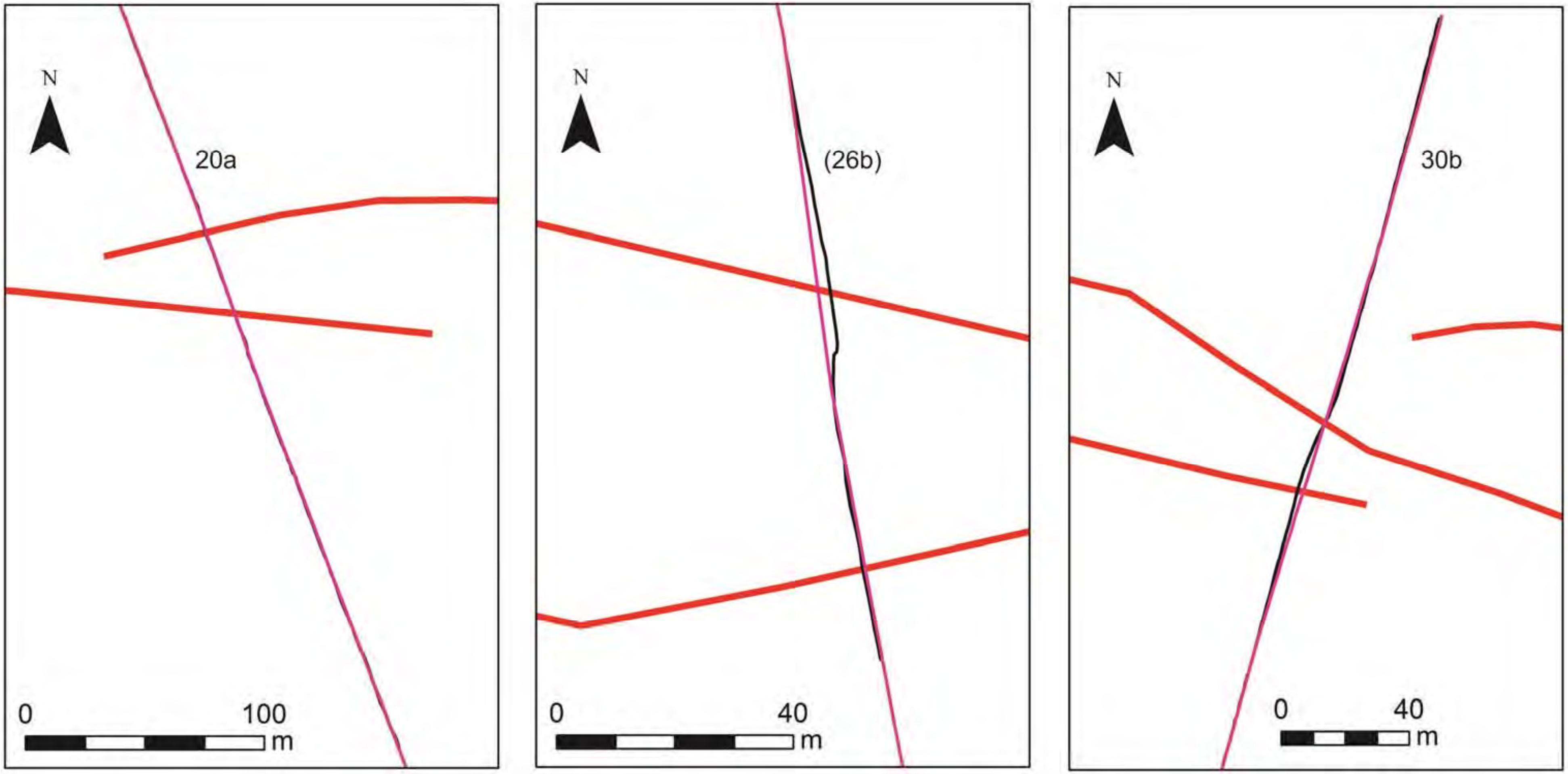

Figure 7.3 Maps showing the 2010 profile line (black) overlain by the shifted 2013 line (pink) for each of the re-survey sites. Note the scale is different for each map. The sites (numbers on the profiles) are shown from west to east. See Figure 7.1 for locations.

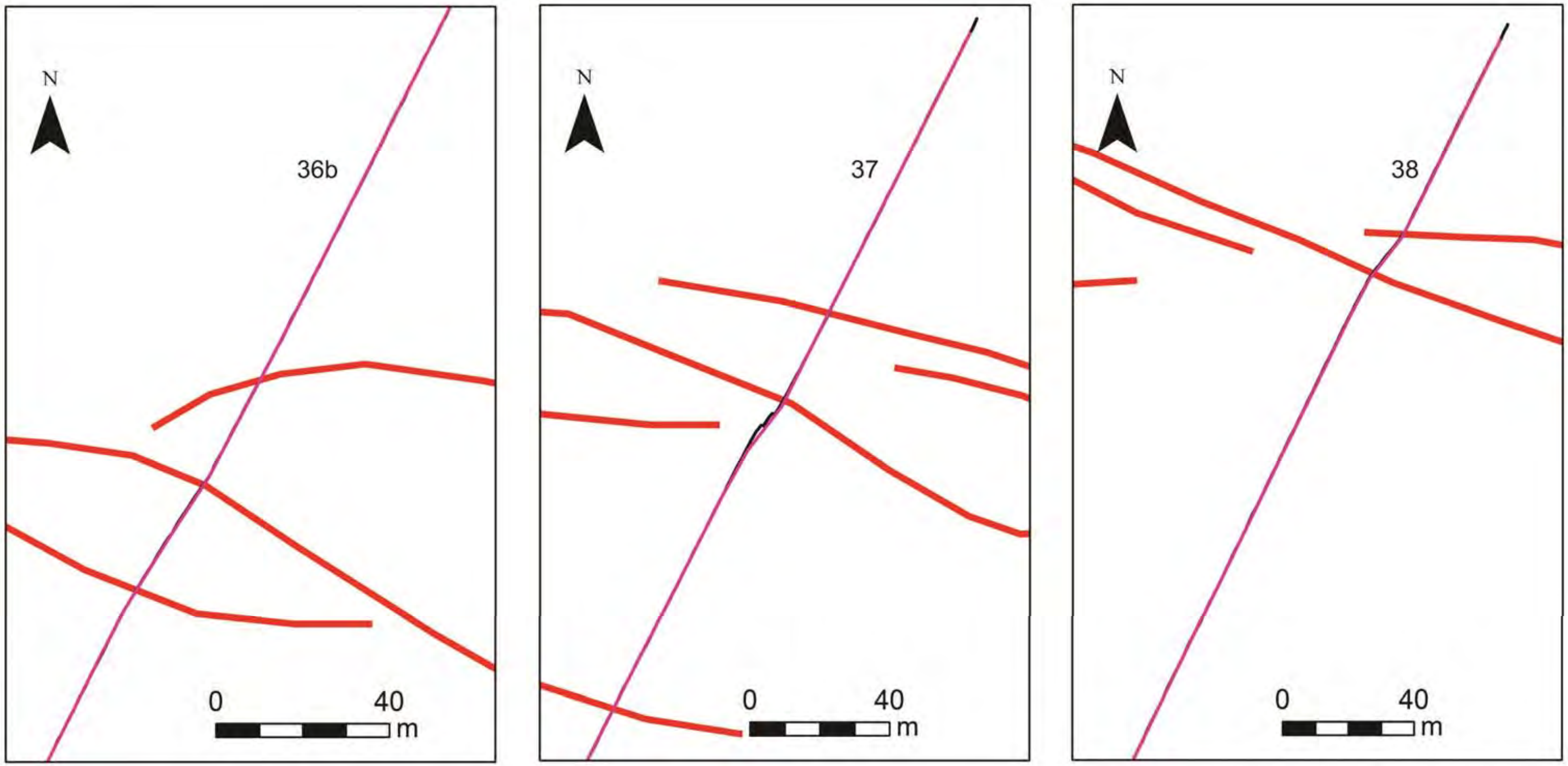

Figure **7.3 continued** Maps showing the 2010 profile line (black) overlain by the shifted 2013 line (pink) for each of the re-survey sites. Note the scale is different for each map. The sites (numbers on the profiles) are shown from west to east. See Figure 7.1 for locations.

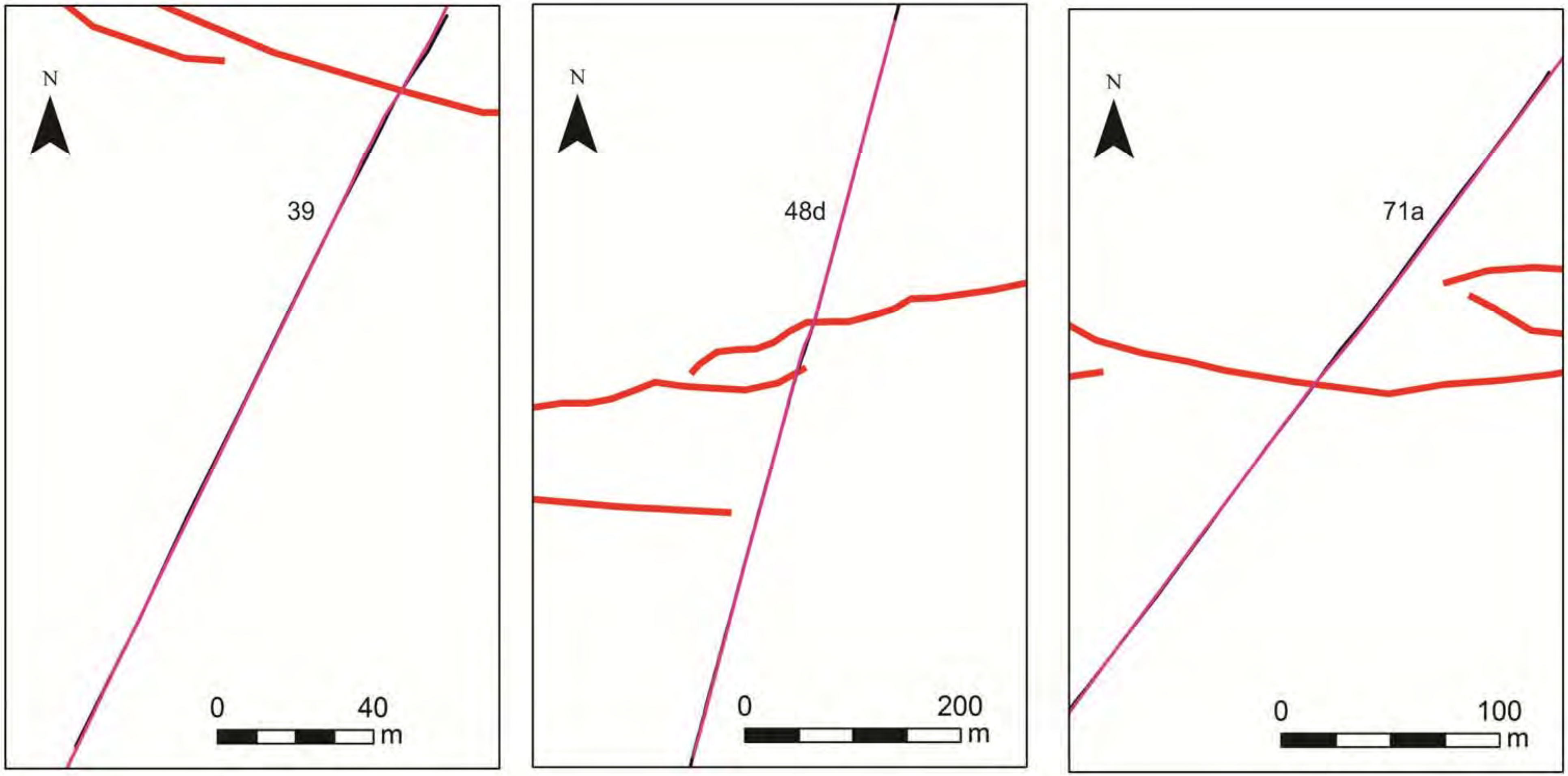

Figure 7.3 continued Maps showing the 2010 profile line (black) overlain by the shifted 2013 line (pink) for each of the re-survey sites. Note the scale is different for each map. The sites (numbers on the profiles) are shown from west to east. See Figure 7.1 for locations.

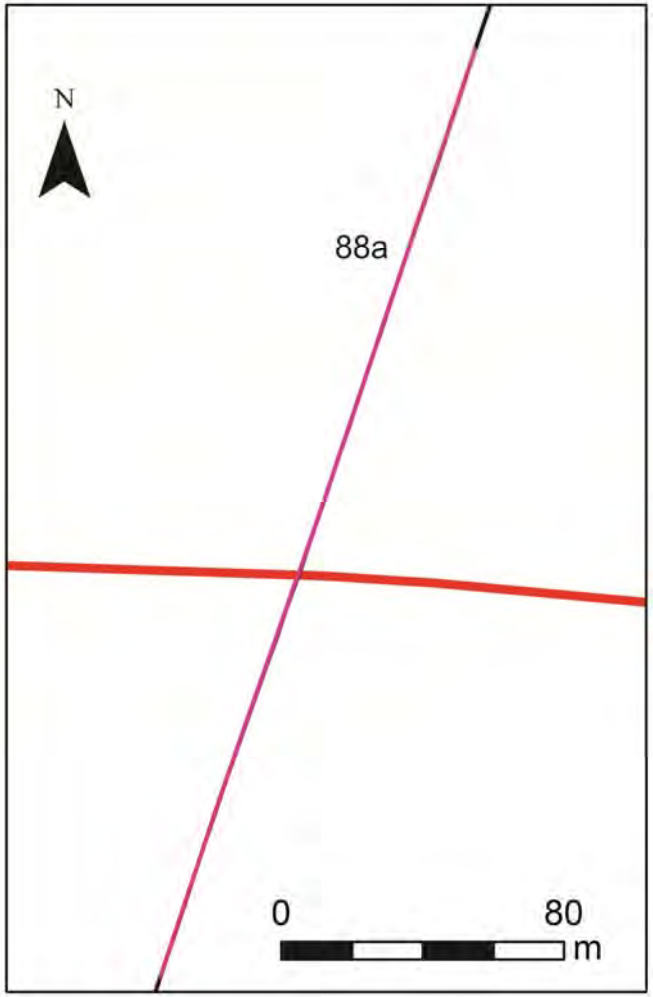

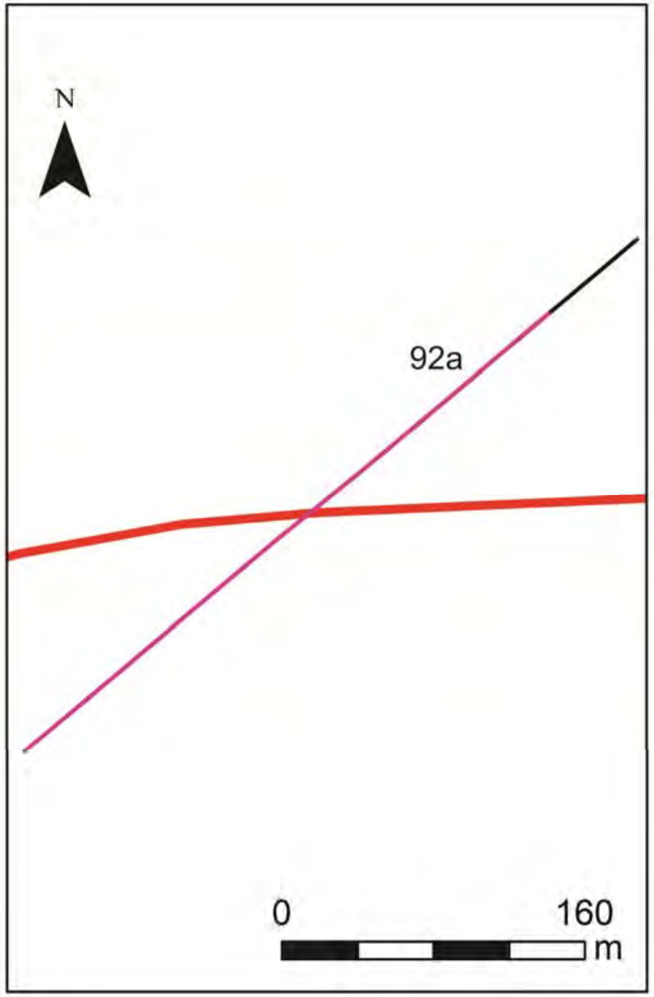

Figure 7.3 continued Maps showing the 2010 profile line (black) overlain by the shifted 2013 line (pink) for each of the re-survey sites. Note the scale is different for each map. The sites (numbers on the profiles) are shown from west to east. See Figure 7.1 for locations.

Table 7.2 shows that only 1 site possibly records post-seismic dextral displacement. This is site 88a, which has apparent dextral post-seismic displacement of 0.04 to 0.07 m, with relatively high confidence. The range of values is the result of multiple measurements and the high confidence is because of the straightness of the profile and length of the marker (Figure 7.3).

The remainder of the sites showed no measurable post-seismic displacement, and in fact several of the 2013 profiles appeared to record less displacement than the 2010 profiles (Figure 7.3). We estimate the uncertainty on these to be ±0.05 m to ±0.1 m, based on the variability in straightness of the profile lines and markers.

The other uncertainties that need to be taken into account are the uncertainty in the RTK survey location (±0.02 m) and the manual shifting of the profiles. We conservatively estimate the latter to be ±0.1 m.

The possible displacement of 0.04-0.07 m is therefore most likely within measurement uncertainties. That is, if we conservatively estimate our uncertainties to be ±0.2 m, which is at the low end of the uncertainties assigned to the 2010 displacement measurements, then we can say that any post-seismic deformation over 2.5 years was less than 0.4 m.

7.4 DISCUSSION

The conclusion that there has been no significant (>0.4 m) post-seismic displacement on the Greendale Fault in the ~2.5 years since the Darfield earthquake is consistent with other datasets (Beavan et al., 2010; Claridge, 2011; Motagh et al., 2013), which are briefly discussed below.

7.4.1 Near-fault total station surveys

Claridge (2011) used a total station survey of 120-300 m lines of marker pins (nails) set along roads across the Greendale Fault on 9 September 2010 (i.e., 5 days after the Darfield earthquake) and re-surveyed 13 September 2010, 18 September 2010, 13 October 2010 and 1 July 2011 to investigate whether any post-Darfield mainshock displacement could be identified. The total time is therefore approximately 10 months after the Darfield earthquake. Three of the sites (Highfield Road = 48d, Kivers Road = 71a; Kerrs Road = 92a) are ones we re-surveyed on 7 March 2013.

The total station surveys showed no evidence for post-seismic slip across the Greendale Fault surface rupture trace. However, evidence for a few (3–10) centimetres of relative displacement was detected at all sites except one (Kivers Road). Interestingly, the postseismic displacements field seems to be characterised by counterclockwise (sinistral) relative relocations of points with respect to a ‘fixed’ reference point (either at the fault, or at the survey tips). Claridge (2011) interpreted this displacement field to reflect post-seismic movement along unidentified Riedel shear zones or other unidentified and/or buried structures (e.g. Charing Cross Fault). Further analysis in combination with other datasets is required to further test this hypothesis; however, it is clear that none of this postseismic creep can be directly attributed to slip on the Greendale Fault. Although we didn’t detect any displacement outside of uncertainties at any of our sites, it is potentially of interest that we noted that four of our 2013 profiles appeared to show less displacement than the 2010 profiles (Table 7.2). It is possible that this could reflect a very small component of sinistral motion as documented by Claridge (2011).

7.4.2 Far-field GPS surveys

As far as we are aware, there have been no focused studies on post-seismic deformation on the Greendale Fault. However, Beavan et al. (2010) notes that post-seismic deformation from campaign-style GPS measurements 7–13 September 2010 (80 sites), 27–30 September 2010 (45 sites) (i.e., 1–8 weeks after the Darfield earthquake) was 10 mm or less.

7.4.3 Far-field InSAR surveys

Barnhart et al. (2011) undertook InSAR analysis of pairs of images collected 11 September–11 October 2010 (1 month after the Darfield earthquake), 11 September–14 March 2011 (6 months after), 27 October–14 March 2011 (1 to 6 months after). They attributed misfits near the centre and easternmost end of the rupture to significant postseismic deformation, but provided no further details.

Motagh et al. (2014) analysed pairs of images collected 6 September–9 October 2010 (~1 month after the Darfield earthquake), 11 September–27 October 2010 (~2 months after), 6 September–22 September 2010 (~3 weeks after) and 13 September–29 September 2010 (~1–4 weeks after). They found three areas of post-seismic deformation, two of which are associated with the Greendale Fault.

The first is an area of subsidence in the step-over region between the two main Greendale Fault traces (central and eastern segments). Analysis of other images showed that this subsidence continued during the first 6 months after the event, with >4 cm occurring between October 2010 and February 2011. The second area is at the eastern end of the Greendale Fault, where they observe a 15 km wide zone of dextral shear parallel to the Greendale Fault. It is difficult to compare the position of this precisely with the locations of our survey markers, but it could be east of our farthest east site, Kerrs Road (92a).

Motagh et al. (2014) don’t note any other areas of post-seismic displacement along the Greendale Fault (although note they didn’t appear to have data at the western end), so we conclude their results are consistent with our lack of displacement >0.4 m. It may suggest that future re-surveys focus on markers at the far eastern end of the Greendale Fault, such as Railway Road.

8.0 KEY CONCULSIONS AND RECOMMENDATIONS

- Greendale Fault net displacements have a bimodal distribution centred on peaks of ~1.25 and ~4.25 m (section 3). These peaks don't correspond to the calculated average net displacement of 2.55 m and there was only 1 individual calculated net displacement or 2.55 m. This, combined with the likely preferential preservation of certain markers or portions of a fault, demonstrates that natural variability (e.g., resulting from the involvement of multiple fault segments in the rupture process) should be taken into account when estimating an average single event displacement for an active fault in seismic or fault rupture hazard studies.
- The comparison of displacement measurements using multiple datasets (section 4) shows that multiple measurements of a single marker may not reduce uncertainty, but due to different measurement uncertainties, may instead increase the variability. We therefore recommend that measurements are made using the best available dataset at each site. The best dataset may vary from site to site depending on the type of marker present, and how it is captured by a particular dataset.
- The variations in measurements for the field-based datasets (Tape and Compass, RTK, and Laser scans) were found to generally be lower than the remote sensing datasets (Orthophotos and Lidar rasters), consistent with the lower assigned uncertainties and the lower number of measurements made using the remote sensing datasets (section 4). One of the reasons for relatively low uncertainties for the field-based datasets is that the markers crossing the Greendale Fault were very straight and continuous. Nevertheless, we consider the results of our study to show that:
    - Field-based measurements remain vital;
    - RTK surveys are currently the best dataset for measuring displacements; and
    - Remote sensing datasets are useful for adding additional measurements in places unable to be surveyed in the field, as well as for other purposes such as fault rupture mapping and digital capture of the fresh rupture.
- Displacement measurements made by 9 geologists (section 5) show that measurements made by different people provide an additional measurement uncertainty. The uncertainty is again mostly a result of using multiple datasets, but there were also some slight relationships with fault zone width and marker obliquity. The time constraints in the two 1 day workshops probably added further uncertainty. We therefore recommend that time and care is taken over each displacement measurement, carefully considering uncertainties and the best dataset to use for each site, followed by review and consensus.
- Measurements of dextral displacement perpendicular to fault strike (section 6) confirm that the Greendale Fault zone width is highly variable (~30 to ~300 m) and largely occurred as horizontal flexure. This makes the Greendale Fault a useful example of the distributed fault complexity in the MfE Active Fault Guidelines and as the basis of developing a method for assessing fault rupture hazard on strike-slip faults.
- A re-survey of 10 markers approximately 2.5 years after the Darfield earthquake shows that any post-earthquake deformation is less than 0.4 m. This is consistent with other post-earthquake surveys (using total station, GPS and InSAR).

9.0 ACKNOWLEDGEMENTS

We would like to thank Pilar Villamor, David Barrell, Dougal Townsend, John Begg, Rob Langridge (GNS Science) and Timothy Stahl, Brendan Duffy, Eric Bilderback, Duncan Noble, Narges Khajavi, Kate Pedley (University of Canterbury) for assistance with collection of the field data (RTK and Laser scans). Neville Palmer is thanked for his assistance with post-processing the RTK survey data and William Ries for developing the Lidar datasets and assisting with the data descriptions.

Pilar Villamor, Rob Langridge, Andy Nicol, William Ries, and Dougal Townsend are thanked for their participation in the “multiple geologist measurement workshops”.

We thank Andy Nicol and Kate Clark for their helpful reviews of this report.

We would also like to thank the landowners for their ongoing unlimited access to the Greendale Fault rupture.

This work was primarily funded by an Earthquake Commission Biennial Grant (12/622), with additional financial support from the Ministry for the Business, Innovation, and Employment Core Funding (Natural Hazards Research Platform) and GNS Science internal funding.

10.0 REFERENCES

Anderson, H.; Beanland, S.; Blick, G.; Darby, D.; Downes, G.; Haines, J.; Jackson, J.; Robinson, J.; Robinson, R.; Webb, T. 1994. The 1968 Inangahua, New Zealand, earthquake: an integrated geological, geodetic, and seismological source model. New Zealand Journal of Geology and Geophysics 37: 59-86.

Barka, A., Akyuz, H.S., Altunel, E., Sunal, G., Cakir, S.Z., Dikbas, A., Yerli, B., Armijo, R., Meyer, B., de Chabalier, J.B., Rockwell, T., Dolan, J.R., Hartleb, R., Dawson, T., Christofferson, W., Tucker, A., Fumal, T., Langridge, R., Stenner, H., Lettis, W., Bachhuber, J., Page, W. 2002. The surface rupture and slip distribution of the 17 August 1999 Izmut Earthquake (M 7.4), North Anatolian Fault. Bulletin of the Seismological Society of America 92: 43-60.

Barnhart, W.D., Willis, M.J., Lohman, R.B., Melkonian, A.K. 2011. InSAR and optical constraints on fault slip during the 2010-2011 New Zealand earthquake sequence. Seismological Research Letters 82: 815-823.

Barrell, D.J.A., Litchfield, N.J., Townsend, D.B., Quigley, M., Van Dissen, R.J., Cosgrove, R., Cox, S.C., Furlong, K., Villamor, P., Begg, J.G., Hemmings-Sykes, S., Jongens, R., Mackenzie, H., Noble, D., Stahl, T., Bilderback, E., Duffy, B., Henham, H., Klahn, A., Lang, E.M.W., Moody, L., Nicol, R., Pedley, K. and Smith, A. 2011. Strike-slip ground-surface rupture (Greendale Fault) associated with the 4 September 2010 Darfield earthquake, Canterbury, New Zealand. Quarterly Journal of Engineering Geology and Hydrogeology 44: 283-291, doi:10.1144/1470-9236/11-034.

Beanland, S., Berryman, K.R., Blick, G.H. 1989. Geological investigations of the 1987 Edgecumbe earthquake, New Zealand. New Zealand Journal of Geology and Geophysics 32: 73-91.

Beanland, S., Blick, G.H., Darby, D.J. 1990. Normal faulting in a back arc basin: geological and geodetic characteristics of the 1987 Edgecumbe Earthquake, New Zealand. Journal of Geophysical Research 95(B4): 4693-4707.

Beavan, J., Samsonov, S., Motagh, M., Wallace, L., Ellis, S., Palmer, N. 2010. The Darfield (Canterbury) Earthquake: geodetic observations and prelminary source model. Bulletin of the New Zealand Society for Earthquake Engineering 43: 228-235.

Beavan, J., Fielding, E., Motagh, M., Samsanov, S., Donnelly, N. 2011. Fault location and slip distribution of the 22 February 2011 Mw 6.2 Christchurch, New Zealand, Earthquake from geodetic data. Seismological Research Letters 82: 789-799.

Beavan, J., Motagh, M., Fielding, E.J., Donnelly, N., Collett, D. 2012. Fault slip models of the 2010-2011 Canterbury, New Zealand, earthquakes from geodetic data and observations of postseismic ground deformation. New Zealand Journal of Geology and Geophysics 55: 207-221.

Berryman, K.; Villamor, P. 2004. Surface rupture of the Poulter Fault in the 1929 March 9 Arthur's Pass earthquake, and redefinition of the Kakapo Fault, New Zealand. New Zealand Journal of Geology and Geophysics 47: 341-351.

Berryman, K., Cooper, A., Norris, R., Villamor, P., Sutherland, R., Wright, T., Schermer, E., Langridge, R., Biasi, G. 2012. Late Holocene rupture history of the Alpine Fault in South Westland, New Zealand. Bulletin of the Seismological Society of America 102: 620-638.

Bray, J.D. 2001. Developing mitigation measures for the hazards associated with earthquake surface fault rupture. *Proceedings, A Workshop on Seismic Fault-Induced Failures – Possible Remedies for Damage to Urban Facilities*, Japan Society for the Promotion of Science, Tokyo, Japan: 55-79.

Bray, J.D., Kelson, K.I. 2006. Observations of surface fault rupture from the 1906 earthquake in the context of current practice. Earthquake Spectra 22: S69-S89.

Bray, J.D., Seed, R.B., Cluff, L.S., Seed, H.B. 1994, Earthquake fault rupture propagation through soil**.** Journal of Geotechnical Engineering - ASCE 120 (3): 543-561.

Burgmann, R., Ergintav, S., Segall, P., Hearn, E.H., McClusky, S., Reilinger, R.E., Woith, H., Zschau, J. 2002. Time-dependent distributed afterslip on and deep below the Izmit Earthquake rupture. Bulletin of the Seismological Society of America 92: 126-137.

Claridge, J. 2011, Patterns of Crustal Deformation Resulting from the 2010 Earthquake Sequence in Christchurch, New Zealand, unpublished M.Sc. Thesis, University of Canterbury, 217 p.

Cox, S.C., Barrell, D.J.A. 2007. Geology of the Aoraki area. Institute of Geological and Nuclear Sciences 1:250,000 geological map 15. 1 sheet + 71 p. GNS Science, Lower Hutt.

Duffy, B., Quigley, M., Barrell, D.J.A., Van Dissen, R., Stahl, T., Leprince, S., McInnes, C. and Bilderback, E. 2013. Fault kinematics and surface deformation across a releasing bend during the 2010 Mw 7.1 Darfield, New Zealand, earthquake revealed by differential Lidar and cadastral surveying. Geological Society of American Bulletin 125: 420-431.

Elliott, J.R., Nissen, E.K., England, P.C., Jackson, J.A., Lamb, S., Li, Z., Oehlers, M., Parsons, B. 2012. Slip in the 2010-2011 Canterbury earthquakes, New Zealand. Journal of Geophysical Research 117, B03401, doi:10.1029/2011JB008868.

Forsyth, P.J., Barrell, D.J.A., Jongens, R. 2008. Geology of the Christchurch area. Institute of Geological and Nuclear Sciences 1:250,000 geological map 16. 1 sheet + 67 p. GNS Science, Lower Hutt.

Fyffe, H.E. 1929. Movement on White Creek Fault, New Zealand, during the Murchison Earthquake of 17 June 1929. The New Zealand Journal of Science and Technology 11: 192-197.

Gledhill, K., Ristau, J., Reyners, M., Fry, B., Holden, C. 2011. The Darfield (Canterbury, New Zealand) Mw 7.1 Earthquake of September 2010: A preliminary seismological report. Seismological Research Letters 82: 378-386.

Gold, P.O., Oskin, M.E., Elliott, A.J., Hinojosa-Corona, A., Taylor, M.H., Kreylos, O., Cowgill, E. 2013. Coseismic slip variation assessed from terrestrial lidar scans of the El Mayor-Cucapah surface rupture. Earth and Planetary Science Letters 366: 151-162.

Haeussler, P.J., Schwartz, D.P., Dawson, T.E., Stenner, H.D., Lienkaemper, J.J., Sherrod, B., Cinti, F.R., Montone, P., Craw, P.A., Crone, A.J., Personius, S.F. 2004. Surface rupture and slip distribution of the Denali and Totschunda Faults in the 3 November 2002 M 7.9 Earthquake, Alaska. Bulletin of the Seismological Society of America 94: S23-S52.

Holden, C., Beavan, J., Fry, B., Reyners, M., Ristau, J., Van Dissen, R., Villamor, P. 2011. Preliminary source model of the Mw 7.1 Darfield earthquake from geological, geodetic and seismic data. Proceedings of the Ninth Pacific Conference on Earthquake Engineering, 14-16 April 2011, Auckland, New Zealand. Paper number 164.

Hudnut, K.W., Borsa, A., Glennie, C., Minster, J.-B. 2002. High-resolution topography along surface rupture of the 16 October 1999 Hector Mine, California, Earthquake (Mw 7.1) from Airborne Laser Swath Mapping. Bulletin of the Seismological Society of America 92: 1570-1576.

Hornblow, S., Quigley, M., Nicol, A., Van Dissen, R. 2013. Paleoseismology of the 2010 M_W 7.1 Darfield (Canterbury) earthquake source, Greendale Fault. In: Reid, C.M and Wandres, A. (eds). Abstracts, Geosciences 2013 Conference, Christchurch, New Zealand. Geoscience Society of New Zealand Miscellaneous Publication 136A: 47.

Hsu, Y-J., Segall, P., Yu, W-B., Kuo, L-C., Williams, C.A. 2007. Temporal and spatial variations of post-seismic deformation following the 1999 Chi-Chi, Taiwan earthquake. Geophysical Journal International 169: 367-379.

Jongens, R., Barrell, D.J.A., Campbell, J.K., Pettinga, J. 2012. Faulting and folding beneath the Canterbury Plains identified prior to the 2010 emergence of the Greendale Fault. New Zealand Journal of Geology and Geophysics 55: 169-176.

Jouanne, F., Awan, A., Madji, A., Pecher, A., Latif, M., Kausar, A., Mugnier, J.L., Khan, I., Khan, N.A. 2011. Postseismic deformation in Pakistan after the 8 October 2005 earthquake: evidence of afterslip along a flat north of the Balakot-Bagh thrust. Journal of Geophysical Research 116, B07401, doi:10.1029/2010JB007903.

Kaiser, A., Holden, C., Beavan, J., Beetham, D., Benites, R., Celentano, A., Collett, D., Cousins, J., Cubrinovski, M., Dellow, G., Denys, P., Fielding, E., Fry, B., Gerstenberger, M., Langridge, R., Massey, C., Motagh, M., Pondard, N., McVerry, G., Ristau, J., Stirling, M., Thomas, J., Uma, S.R., and Zhao, J. 2012. The M_w 6.2 Christchurch earthquake of February 2011: preliminary report. New Zealand Journal of Geology and Geophysics 55: 67-90.

Kelson, K.I., Hitchcock, C.S., Baldwin, J.N., Hart, J.D., Gamble, J.C., Lee, C-H., Dauby, F. 2004. Fault rupture assessment for high-pressure pipelines in the southern San Francisco Bay area, California. *Proceedings, International Pipe Conference*, Calgary, Canada. Paper IPC2004-212: 8 p.

Kerr J., Nathan S., Van Dissen R., Webb P., Brunsdon D., King A. 2003. Planning for development of land on or close to active faults. Institute of Geological & Nuclear Sciences Client Report 2002/124. Published by the Ministry for the Environment, *ME numbers 483 & 565*.

Klinger, Y., Xu, X., Tapponnier, P., Van der Woerd, J., Lasserre, C., King, G. 2005. High-resolution sattelite imagery mapping of the surface rupture and slip distribution of the Mw ~7.8 November 2001 Kakoxili Earthquake, Kunlun Fault, Northern Tibet, China. Bulletin of the Seismological Society of America 95: 1970-1987.

Lin, A., Ouchi, T., Chen, A., Maruyama, T. 2001. Co-seismic displacements, folding and shortening structures along the Chelungpu surface rupture zone occurred during the 1999 Chi-Chi (Taiwan) earthquake. Tectonophysics 330: 225-244.

Little, T.A., Van Dissen, R., Rieser, U., Smith, E.G.C., Langridge, R.M. 2010. Coseismic strike slip at a point during the last four earthquakes on the Wellington fault near Wellington, New Zealand. Journal of Geophysical Research 115, B05403, doi:10.1029/2009JB006589.

Liu-Zeng, J., Zhang, Z., Wen, L., Tapponier, P., Sun, J., Xing, X., Xu, Q., Zeng, L., Ding, L., Ji, C., Hudnut, K.W., van der Woerd, J. 2009. Co-seismic ruptures of the 12 May 2008, Mw 8.0 Wenchuan earthquake, Sichuan: east-west crustal shortening on oblique, parallel thrusts along the eastern edge of Tibet. Earth and Planetary Science Letters 286: 355-370.

McKay, A. 1890. On the earthquakes of September 1888, in the Amuri and Marlborough districts of the South Island. New Zealand Geological Survey Report on geological explorations 20: 1-16.

Mason, D.P.M., Little, T.A. 2006. Refined slip distribution and moment magnitude of the 1848 Marlborough earthquake, Awatere Fault, New Zealand. New Zealand Journal of Geology and Geophysics 49: 375-382.

Massonnet, D., Feigl, K., Rossi, M., Adragna, F. 1994. Radar interferometric mapping of deformation in the year after the Landers earthquake. Nature 369: 227-230.

Mileti, D.S. 1999. Disasters by design: a reassessment of natural hazards in the United States. Joseph Henry Press, Washington, D.C.: 351 p.

Motagh, M., Beavan, J., Fielding, E.J., Haghsehnas, M. 2014. Postseismic ground deformation following the September 2010 Darfield, New Zealand, earthquake from TerraSAR-X, COSMO-SkyMed, and ALOS InSAR. IEE Geoscience and Remote Sensing Letters 11: 186-190.

NZSEE 2010. Special Issue: Preliminary observations of the September 2010 Darfield (Canterbury) earthquake sequence. Bulletin of the New Zealand Society for Earthquake Engineering 43: 215-439.

NZSEE 2011. Special Issue: Effects of the 22 February 2011 Christchurch earthquake and its aftershocks. Bulletin of the New Zealand Society for Earthquake Engineering 44: 181-430.

Oskin, M.E., Arrosmith, J.R., Hinojosa Corona, A., Elliott, A.J., Fletcher, J.M., Fielding, E.J., Gold, P.O., Gonzalez Garcia, J.J., Hudnut, K.W., Lio-Seng, J., Teran, O.J. 2012. Near-field deformation from the El Mayor-Cucapah Earthquake revealed by differential Lidar. Science 335: 702-705.

Petersen, M.D., Dawson, T.E., Chen, R., Cao, T., Wills, C.J., Schwartz, D.P., Frankel, A.D. 2011. Fault displacement hazard for strike-slip faults. Bulletin of the Seismological Society of America 101: 805-825.

Quigley, M., Villamor, P., Furlong, K., Beavan, J., Van Dissen, R., Litchfield, N., Stahl, T., Duffy, B., Bilderback, E., Noble, D., Barrell, D., Jongens, R., Cox, S. 2010a. Previously unknown fault shakes New Zealand's South Island. Eos, 91 (49): 469-470.

Quigley, M., Van Dissen, R., Villamor, P., Litchfield, N., Barrell, D., Furlong, K., Stahl, T., Duffy, B., Bilderback, E., Noble, D., Townsend, D., Begg, J., Jongens, R., Ries, W., Claridge, J., Klahn, A., Mackenzie, H., Smith, A., Hornblow, S., Nicol, R., Cox, S., Langridge, R., Pedley, K. 2010b. Surface rupture of the Greendale Fault during the M_w 7.1 Darfield (Canterbury) Earthquake, New Zealand: initial findings. Bulletin of the New Zealand Society for Earthquake Engineering 43: 236-242.

Quigley, M., Van Dissen, R., Litchfield, N., Villamor, P., Duffy, B., Barrell, D., Furlong, K., Beavan, J., Stahl, T., Bilderback, E. and Noble, D. 2012. Surface rupture during the 2010 Mw 7.1 Darfield (Canterbury) earthquake: implications for fault rupture dynamics and seismic-hazard analysis. Geology 40: 55-58.

Pollitz, F.F. 2005. Transient rheology of the upper mantle beneath central Alaska inferred from the crustal velocity field following the 2002 Denali earthquake. Journal of Geophysical Research 110, B08407, doi:10.1029/2005JB003672.

Pollitz, F.F., Wicks, C., Thatcher, W. 2001. Mantle flow beneath a continental strike-slip fault: Postseismic deformation after the 1999 Hector Mine Earthquake. Science 293: 1814-1818.

Rockwell, T.K., Lindvall, S., Dawson, T., Langridge, R., Lettis, W., Klinger, Y. 2002. Lateral offsets on surveyed cultural features resulting from the 1999 Izmit and Duzce Earthquakes, Turkey. Bulletin of the Seismological Society of America 92: 79-94.

Rockwell, T.K., Klinger, Y. 2013. Surface rupture and slip distribution of the 1940 Imperial Valley Earthquake, Imperial Fault, Southern California: implications for rupture segmentation and dynamics. Bulletin of the Seismological Society of America 103: 629-640.

Rodgers, D.W.; Little, T.A. 2006. World's largest coseismic strike-slip offset: The 1855 rupture of the Wairarapa Fault, New Zealand, and implications for displacement/length scaling of continental earthquakes. Journal of Geophysical Research 111: B12408, doi:10.1029/2005JB004065.

Ryder, I., Parsons, B., Wright, T.J., Funning, G.J. 2007. Post-seismic motion following the 1997 Manyi (Tibet) earthquake: InSAR observations and modelling. Geophysical Journal International 169: 1009-1027.

Saunders, W.S.A., Beban, J.S. 2012. Putting R(isk) in the RMA: technical Advisory Group recommendations on the Resource Management Act 1991 and implications for natural hazards planning. GNS Miscellaneous Series 48: 57 p.

Schermer, E.R.; Van Dissen, R.; Berryman, K.; Kelsey, H.M.; Cashman, S.M. 2004. Active faults, paleoseismology, and historical fault rupture in northern Wairarapa, North Island, New Zealand. New Zealand Journal of Geology and Geophysics 47: 101-122.

Sieh, K., Jones, L., Haukkson, E., Hudnut, K., Eberhart-Phillips, D., Heaton, T., Hough, S., Hutton, K., Kanamori, H., Lilje, A., Lindvall, S., McGill, S.F., Mori, J., Rubin, C., Spotila, J.A., Stock, J., Thio, H.K., Treiman, J., Wernicke, B., Zachariasen, J. 1993. Near-field investigations of the Landers Earthquake sequence, April to July 1992. Science 260: 171-176.

SRL 2011. Special Issue: The 22 February 2011 magnitude 6.2 Christchurch earthquake. Seismological Research Letters, 82: 765-964.

Stirling, M., Goded, T., Berryman, K., Litchfield, N. 2013. Selection of Magnitude Scaling Relationships for Seismic Hazard Analysis. Bulletin of the Seismological Society of America 103: 2993-3011.

Treiman, J.A., Kendrick, K.J., Bryant, W.A., Rockwell, T.K., McGill, S.F. 2002. Primary surface rupture associated with the Mw 7.1 16 October 1999 Hector Mine Earthquake, San Bernadino County, California. Bulletin of the Seismological Society of America 92: 1171-1191.

Van Dissen, R., Heron, D., Becker, J., King, A., Kerr, J. 2006. Mitigating active fault surface rupture hazard in New Zealand: development of national guidelines, and assessment of their implementation. *in proceedings*, 8th U.S. National Conference on Earthquake Engineering, San Francisco, California, 18-22 April, 2006. Paper No. 633, 10 p.

Van Dissen, R.J., Barrell, D.J.A., Litchfield, N.J., Villamor, P., Quigley, M., King, A.B., Furlong, K., Begg, J.G., Townsend, D.B., Mackenzie, H., Stahl, T., Noble, D., Duffy, B., Bilderback, E., Claridge, J., Klahn, A., Jongens, R., Cox, S.C., Langridge, R.M., Ries, W., Dhakal, R., Smith, A., Hornblow, S., Nicol, R., Pedley, K., Henham, H., Hunter, R., Zajac, A. and Mote, T. 2011. Surface rupture displacement on the Greendale Fault during the Mw 7.1 Darfield (Canterbury) Earthquake, New Zealand, and its impact on man-made structures. paper 186 In: Ninth Pacific Conference on Earthquake Engineering: building an earthquake resilient society, April 14-16, 2011, University of Auckland, Auckland, New Zealand. Auckland, NZ: 9PCEE.

Van Dissen, R., Hornblow, S., Quigley, M., Litchfield, N., Villamor, P., Nicol, A., Barrell, D.J.A., Sasnett, P., Newton, K. 2013. Towards the development of design curves for characterising distributed strike-slip surface fault rupture displacement: an example from the 4 September, 2010, Greendale Fault rupture, New Zealand. In: Chin, C.Y. (ed.). Proceedings, 19th NZGS Geotechnical Symposium, Queenstown, New Zealand, 20-23, November, 2013.

Villamor, P., Litchfield, N., Barrell, D., Van Dissen, R., Hornblow, S., Quigley, M., Levick, S., Ries, W., Duffy, B., Begg, J., Townsend, D., Stahl, T., Bilderback, E., Noble, D., Furlong, K. and Grant, H. 2012. Map of the 2010 Greendale Fault surface rupture, Canterbury, New Zealand: application to land use planning. New Zealand Journal of Geology and Geophysics 55: 223-230.

Wells, D.L., Coppersmith, K.J. 1994. New empirical relationships among magnitude, rupture length, rupture width, rupture area, and surface displacement. Bulletin of the Seismological Society of America 84: 974-1002.

Wesnousky, S.G. 2008. Displacement and geometrical characteristics of earthquake surface ruptures: issues and implications for seismic-hazard analysis and the process of earthquake rupture. Bulletin of the Seismological Society of America 98: 1609-1632.

Xu, X., Wen, X., Yu, G., Chen, G., Klinger, Y., Hubbard, J., Shaw, J. 2009. Coseismic reverse- and oblique-slip surface faulting generated by the 2008 Mw 7.9 Wenchuan Earthquake, China. Geology 37: 515-518.

Zielke, O., Arrowsmith, R.J. 2012. LaDiCaoz and LiDARimager – MATLAB GUIs for Lidar data handling and lateral displacement measurement. Geosphere 8: 206-221.

APPENDICES

APPENDIX 1: PREVIOUSLY PUBLISHED DISPLACEMENT MEASUREMENTS

Table A 1.1 Previously published dextral displacement measurements (Quigley et al., 2012; Section 2) and fault perpendicular deformation zone width measurements (Section 6).

Site number	Easting[i]	Northing[i]	Trace	Marker / Preferred	Dataset	Displacement	Uncertainty	Type[ii]	Type 22[iii]	Quality[iv]	Width profile	Width 100%[v]	Width 50%	Comment
						(m)	(m)				Number[vi]	(m)	(m)	
1p	1527310.1	5172643.8	West	Preferred		1.2	0.2	p	pref			40	18	
1rtk	1527310.1	5172643.8	West	Wire fence	RTK	1.2	0.2	t	ind	H		40	18	
1tc	1527310.1	5172643.8	West	Wire fence	Tape and Compass	1.3	0.2	t	ind	H		91		
2	1526991.8	5172680.6	West	Wire fence	RTK	1	0.25	pt	pref	MH	5	106	35	
3	1526227.5	5172706.8	West	Wire fence	RTK	1	0.25	pt	pref	MH	4	70	40	
4	1524697.5	5172874.7	West	Wire fence	RTK	0.7	0.25	pt	pref	MH	3	35	18	
5	1524217.4	5173075.5	West	Wire fence	RTK									Fence not linear, cannot measure an offset
6	1523643	5173310.2	West	Wire fence	RTK	1.3	0.25	pt	pref	MH		78	44	
7a	1523252.3	5173428	West	Wire fence	RTK	1.1	0.2	t	ind	H	2			Eastern fence of double fence line
7b	1523249	5173428.9	West	Wire fence	RTK	1.7	0.5	t	ind	ML				Western fence of double fence line
7c	1523247.5	5173429.4	West	Power poles	RTK	0.75	0.25	min	min	MH				Minimum dextral value, only one power pole on south side of fault
7p	1523250	5173428.6	West	Preferred		1.1	0.2	p	pref	H		103	50	
8	1522915.2	5173610.6	West	Wire fence	RTK	0.75	0.3	min	min	M				Minimum dextral value, fence extends only 8 m NE of general fault location
9	1522846.3	5173672.5	West	Wire fence	RTK	0.85	0.3	min	min	M				Minimum dextral value, fence line does not extend very far on either side of fault
10p	1522166.5	5174432.5	West	Preferred		0.9	0.25	p	pref	MH		30		
10rtk1	1522166.5	5174432.5	West	Wire fence	RTK	0.9	0.25	t	ind	M				
10rtk2	1522166.5	5174432.5	West	Wire fence	RTK	2.6		max	max	M				Maximum based on an extreme, but possible, projection of fence
10tc	1522166.5	5174432.5	West	Wire fence	Tape and Compass	0.95	0.2	t	ind	M				
11	1521892.6	5174678.9	West	Wire fence	RTK	0.95	0.25	pt	pref	MH	1		140	
12	1527436.7	5172632.5	West	Crop row/plough line	RTK	1.95	0.4	max	max	ML				Maximum, feature is not co-linear across fault, projection from n side of fault based on northern-most two points on rtk line
13	1527526	5172614.3	West	Wire fence	RTK	1.65	0.2	pt	pref	MH	6	100	23	Slight possibility that this is a minimum. Fence does not extend on n side of fault for any great distance
14	1527566.8	5172609.4	West	Wire & wood fence	Orthophoto	0.3	0.3	min	min					Minimum dextral value, fence line does not extend very far on either side of fault
15	1527571.6	5172609	West	Concrete curbing, Greendale substation	Orthophoto	0.6	0.5	min	min	M				Minimum dextral value, curbing does not extend outside of fault deformation zone does not extend very far on either side of fault
16	1527608.2	5172606.1	West	Concrete curbing, Greendale substation	Orthophoto	0.9	0.5	min	min	M				Minimum dextral value, curbing does not extend outside of fault deformation zone does not extend very far on either side of fault
17	1527646.6	5172603	West	Power poles	Orthophoto	1.15	0.5	min	min	M				Possible minimum, only one pole controls n end of profile
18	1528109.3	5172545.2	West	Plough line NW of gorse fence line	Orthophoto	1.9	0.5	pt	pref	M		80	55	

Site number	Easting[i]	Northing[i]	Trace	Marker / Preferred	Dataset	Displacement	Uncertainty	Type[ii]	Type 22[iii]	Quality[iv]	Width profile	Width 100%[v]	Width 50%	Comment
						(m)	(m)				Number[vi]	(m)	(m)	
19	1528522.3	5172595.6	West	Gorse hedge/wire fence	RTK	1.7	0.3	pt	pref	MH	7	60	26	
20a	1529494.4	5172586.3	West	Wire fence, western side Hollands Road	RTK	3.2	0.5	t	ind	M / ML		(70)		
20b	1529502.7	5172586.4	West	Road edge, western side of Hollands Road	RTK	3.7	0.4	t	ind	M / ML				
20c	1529508.7	5172586.5	West	Road edge, eastern side of Hollands Road	RTK	3.7	0.4	t	ind	M / ML				
20d	1529515.3	5172586.5	West	Wire fence, eastern side Hollands Road	RTK	2.5	0.5	t	ind	M / ML	8			
20p	1529506.2	5172586.4	West	Preferred		3.1	0.6	p	pref	M / ML		130		Very approximate width. This site could benefit from being re-surveyed.
20tc	1529506.2	5172586.4	West		Tape and Compass	2.3	0.2	t	ind					
21	1530192	5172658.2	West	Wire fence between Hollands and Milton Rds	RTK	3.2	0.25	min	min	MH	9	165	49	Slight possibility that this is a minimum. Fence does not extend on s side of fault for any great distance
22	1531011.7	5172768	West	Wire fence between dairy shed and Milton Road	RTK	2.8	0.25	min	min	MH		85	26	Slight possibility that this is a minimum. Fence post profile does not extend on s side of fault for a great distance
23p	1531244.3	5172821.4	West	Preferred		2.85	0.3	p	pref	MH	10	145	74	
23rtk	1531244.3	5172821.4	West	Fence posts west side of Milton Rd	RTK	2.85	0.3	t	ind	MH		145	74	
23tc	1531244.3	5172821.4	West	Fence & power poles Milton Rd	Tape and Compass	3.5	0.5	t	ind	M				
24a	1532188.8	5172900.4	West	Wire fence, western fence of double fence line	RTK	3.1	0.25	min	min	MH	11			Minimum dextral value, fence line does not extend far enough south to cross entire deformation zone
24b	1532192	5172900	West	Wire fence, eastern fence of double fence line	RTK	2.6	0.5	t	ind	ML				
24p	1532190.6	5172900.2	West	Preferred		3.1	0.25	p	pref	MH		48	13	
25	1532636.5	5172916.3	West	Plough line NW of gorse fence line	Lidar 0.5 m HSNW	3.6	0.75	pt	pref	L				
26a	1532903.3	5172861.3	West	Wire fence, western most fence at site, Stranges Rd	RTK	4.9	1	min	min	L				Minimum dextral value, fence line does not extend far enough north to cross entire deformation zone
26b	1532905.7	5172860.8	West	Wire fence, Stranges Rd	RTK	4.1	0.3	min	min	M				Minimum dextral value, fence line does not extend far enough south to cross entire deformation zone
26c	1532908.2	5172860.3	West	Drain	RTK	3.8	0.5	t	ind	ML				

Site number	Easting[i]	Northing[i]	Trace	Marker / Preferred	Dataset	Displacement	Uncertainty	Type[ii]	Type 22[iii]	Quality[iv]	Width profile	Width 100%[v]	Width 50%	Comment
						(m)	(m)				Number[vi]	(m)	(m)	
26d	1532914.3	5172859	West	Tyre track in dirt road (western track)	RTK	3.5	0.75	min	min	L				Possibly a minimum, tracks not straight across fault deformation zone
26e	1532916.1	5172858.6	West	Tyre track in dirt road (eastern track)	RTK	3.3	0.75	min	min	L				Possibly a minimum, tracks not straight across fault deformation zone
26f	1532924.8	5172856.8	West	Hedge	Orthophoto	4.9	0.75	t	ind	L	12			
26p	1532911.2	5172859.5	West	Preferred		4.3	0.3	p	pref	MH		52		
26tc	1532911.2	5172859.5	West		Tape and Compass	4.3	0.2	t	ind	MH				
27	1533086.7	5172843.8	West	Wire fence between Stranges and Courtenay Rds	RTK	4.2	0.15	pt	pref	H	13	87	12	
28	1533130.3	5172833.6	West	Plough line	Orthophoto	3.6	1	pt	pref	L				Low quality offset, feature not parallel both sides of fault
29	1533179.6	5172822.1	West	Wire fence	RTK	4.2	0.4	pt	pref	MH	14	145	42	Uncertainty assessed by using two different, but equally fitting projections
30a	1533673.5	5172805	West	West side of Courtenay Rd	RTK	4.35	0.25	t	ind	MH	16			
30b	1533678.5	5172803	West	Eastern side of Courtenay Rd	RTK	3.7	0.5	t	ind	ML				Poor quality offset, road not parallel on both sides of fault
30c	1533685.5	5172800.2	West	Wire fence east side of Courtenay Rd	RTK	4.3	0.25	t	ind	MH				
30p	1533679.5	5172802.7	West	Preferred		4.3	0.25	p	pref	MH		57	18	
30tc	1533679.5	5172802.7	West		Tape and Compass	4.2	0.2	t	ind	H				
31a	1534075.8	5172766.3	West	Western side of farm race (dirt road)	RTK	4.5	0.5	max	max	ML				Maximum dextral offset, road not parallel on both sides of fault
31b	1534082.5	5172764.8	West	Eastern side of farm race (dirt road)	RTK	4.2	0.25	t	ind	MH	17			
31p	1534079.1	5172765.5	West	Preferred		4.2	0.25	p	pref	MH		53	10	
32	1534165.8	5172746.5	West	Old fence line	Lidar 0.5 m HSNW	4.2	0.5	pt	pref	ML		25	6	
33	1534262.8	5172765.7	West	Old fence line	Lidar 0.5 m HSNW	5	0.75	pt	pref	M	18	124	83	
34	1534339.5	5172742.5	West	Wire fence	RTK	4.15	0.5	min	min	M	19			Minimum dextral value, feature does not extend very far on N side of deformation zone, and is not parallel on both sides of fault
35	1534662.1	5172795.3	West	Wire fence west of road to Melrose	RTK	3.8	0.5	min	min	M				Possible minimum dextral value, feature does not extend very far across south side of deformation zone
36a	1534928.1	5172770	West	Wire fence on west side of drive to Melrose	RTK	4.85	0.4	t	ind	M	20			
36b	1534935	5172769.4	West	Wire fence on east side of drive to	RTK	4.9	0.25	t	ind	MH	21			

Site number	Easting[i]	Northing[i]	Trace	Marker / Preferred	Dataset	Displacement	Uncertainty	Type[ii]	Type 22[iii]	Quality[iv]	Width profile	Width 100%[v]	Width 50%	Comment
						(m)	(m)				Number[vi]	(m)	(m)	
				Melrose										
36p	1534932.2	5172769.6	West	Preferred		4.8	0.25	p	pref			92	37	
36tc	1534932.2	5172769.6	West		Tape and Compass	4.6	0.2	t	ind	H				
37	1535183.8	5172762.5	West	Wire fence east of road to Melrose	RTK	4.6	0.4	min	min	M	22	119	6	Possible minimum dextral displacement - wide deformation zone, fence does not extend very far south across low displacment southern side of deformation zone
38	1535368.4	5172737.2	West	Wire fence southwest of Clintons Rd and Telegraph Rd	RTK	4.6	0.3	max	max	MH	23			Maximum, have adopted projection that maximises displacement
39	1535555.1	5172711.7	West	Hedge	Orthophoto	3.3	0.5	min	min	M				Minimum dextral offset, hedge only extends across one side (southern side) of deformation zone
40	1535904.1	5172721.4	West	Wire fence east of Telegraph Rd	RTK	3.3	0.3	min	min	M				Minimum dextral offset, fence is short and does not extend across entire width of deformation zone
41	1536238	5172774	West	Crop / plough line east of Telegraph Rd	RTK	4.1	0.4	pt	pref	M	24	122	63	
42	1536270	5172772.2	West	Fence / crop line east of Telegraph Rd	Orthophoto	5.2	0.75	pt	pref	ML	25			
43	1536401.1	5172765.2	West	Crop / plough line east of Telegraph Rd	RTK	2.4	0.3	min	min	M				Minimum dextral offset, feature is short and does not north extend across entire width of deformation zone
44	1536432.5	5172763.6	West	Crop / plough line east of Telegraph Rd	RTK	2.9	0.3	min	min	M	26			Minimum dextral offset, feature is short and does not extend north across entire width of deformation zone
45	1536473.9	5172761.4	West	Fence line	RTK	4.7	0.25	pt	pref	H / MH	27	120	27	
46	1536706.6	5172847	West	Wire fence	RTK	4.65	0.3	min	min	MH	28			Minimum dextral offset, feature is short and does not extend south across entire width of deformation zone
47	1536759.7	5172854.8	West	Wire fence	RTK	4.4	0.3	min	min	MH	29			Minimum dextral offset, feature is short and does not extend south across entire width of deformation zone
48a	1536940.4	5172909.7	West	Western side of Highfield Rd (post repair)	RTK	4.4	1.3	t	ind	L				Long profile not parallel on both sides of deformation zone
48b	1536946.6	5172911.2	West	Eastern side of Highfield Rd (pre-repair)	RTK	4.8	0.9	t	ind	L				Profile is not parallel on both sides of deformation zone
48c	1536941.1	5172909.9	West	Western side of Highfield Rd (pre-repair)	RTK	4.2	0.4	min	min	ML				Minimum dextral offset, feature is short and does not extend south across entire width of deformation zone, and profiles are not parallel both sides of fault
48d	1536946.9	5172911.3	West	Eastern side of Highfield Rd (post repair)	RTK	5.1	0.5	t	ind	M				Profile not parallel on both sides of deformation zone

Site number	Easting[i]	Northing[i]	Trace	Marker / Preferred	Dataset	Displacement	Uncertainty	Type[ii]	Type 22[iii]	Quality[iv]	Width profile	Width 100%[v]	Width 50%	Comment
						(m)	(m)				Number[vi]	(m)	(m)	
48p	1536944	5172910.7	West	Preferred		4.8	0.8	p	pref	ML	30	170		Preferred value was assigned based on mean of the three non-minimum displacements. Uncertainty subjectively assigned a high value to acknowledge that no profile at this locality was parallel both sides of the fault and profiles had to be projected across a very wide deformation zone
48tc	1536944	5172910.7	West		Tape and Compass	4.15	0.3	min	min	M				Minimum dextral offset, profile is short and does not extend across entire width of deformation zone
49	1537235.4	5172991.5	West	Wire fence	RTK	1.35	0.2	min	min	MH	31			Minimum dextral offset, this short fence only crosses part of the deformation - does not extend across full width
50a	1537358.1	5172990.4	West	Wire fence, western fence line of double fence line	RTK	3.3	0.3	min	min	M	32	(25)		Minimum dextral offset, fence does not extend far enough north to cross entire deformation zone
50b	1537361.2	5172990.1	West	Wire fence, eastern fence line of double fence line	RTK	3.6	0.2	min	min	MH				Minimum dextral offset, fence does not extend far enough north to cross entire deformation zone. Fence is not parallel on both sides of fault - there is a large step-over to the north
50p	1537359.6	5172990.2	West	Preferred		3.6	0.2	minp	min	MH				Minimum dextral offset, fence does not extend far enough north to cross entire deformation zone. Fence is not parallel on both sides of fault - there is a large step-over to the north
50tc	1537359.6	5172990.2	West		Tape and Compass	3.6	0.2	min	min	H				Minimum dextral offset, fence does not extend far enough north to cross entire deformation zone. Fence is not parallel on both sides of fault - there is a large step-over to the north
51a	1537479.5	5172976.7	West	Hedge / fence line	Orthophoto	3.9	0.5	min	min	M	33			Minimum dextral offset. South side of step-over. Hedge does not extend far enough north to cross entire deformation zone. Feature is not parallel on both sides of fault - deformation is still accumulating north past north end of hedge
51b	1537600.7	5173169.3	West	Wire fence	RTK	1.1	0.3	min	min	M	34			Minimum dextral offset. North side of step-over. Fence does not extend far enough south to cross entire deformation zone. Feature is not parallel on both sides of fault.
51p	1537549.8	5173072.8	West			5	0.6	p	pref	ML		203		Combination of 51a & 51b across both sides of step-over
52p	1538098.9	5173115.3	West	Preferred		4.95	0.2	p	pref	H	35	120	15	
52rtk	1538098.9	5173115.3	West	Hedge / fence line	RTK	4.95	0.2	t	ind	H		120	15	Very good measurement - long profile that is parellel on both sides of deformation zone
52tc	1538098.9	5173115.3	West		T&C	4.1	0.3	t	ind					
53	1538220	5173137.8	West	Tyre tracks	RTK	4.6	1	pt	pref	L				Feature not parallel on both sides of deformation zone. Min and max projections used to assess uncertainty, and mean used to assign preferred value.
54	1538261.7	5173132.3	West	Tyre tracks	RTK	4.1	0.4	pt	pref	ML				Feature not parallel on both sides of deformation zone. Min and max projections used to assess uncertainty, and mean used to assign preferred value.
55ld	1538314.3	5173125.3	West	Hedge / fence line	Orthophoto / LiDAR	4.8	0.6	t	ind	M				
55p	1538314.3	5173125.3	West	Preferred		4.8	0.4	p	pref	M	36	29	3	
55tc	1538314.3	5173125.3	West		Tape and Compass	4.6	0.2	t	ind	H				
56	1538425.7	5173114.5	West	Tyre tracks	RTK	4.2	0.4	min	min	M				Minimum dextral offset. Profile line does not extend across entire deformation zone and feature is not parallel on both

Site number	Easting[i]	Northing[i]	Trace	Marker / Preferred	Dataset	Displacement	Uncertainty	Type[ii]	Type 22[iii]	Quality[iv]	Width profile	Width 100%[v]	Width 50%	Comment
						(m)	(m)				Number[vi]	(m)	(m)	
														sides of fault.
57	1538477.8	5173115.8	West	Tyre tracks	RTK	2.75	0.4	min	min	M	37			Minimum dextral offset. Profile line does not extend across entire deformation zone and feature is not parallel on both sides of fault.
58	1538608.4	5173189.5	West	Crop row	RTK	4.4	0.5	pt	pref	M	38	110		
59p	1538713.5	5173224.2	West	Preferred		3.9	0.3	p	pref	M / MH	39	23	6	
59rtk	1538713.5	5173224.2	West	Crop row	RTK	3.9	0.3	t	ind	M / MH		23	6	
59tc	1538713.5	5173224.2	West		Tape and Compass	3.8	0.5	t	ind	L				
60p	1538814.5	5173240.5	West	Preferred		4.1	0.6	minp	min	L				Minimum dextral offset. Profile line does not extend very far north and may not cross entire deformation zone; that said, may still be close to true
60rtk	1538814.5	5173240.5	West	Fence / hedge	RTK / Lidar 0.5 m HSNW / Orthophoto	4.1	0.5	min	min	ML				Minimum dextral offset. Profile line does not extend very far north and may not cross entire deformation zone
60tc	1538814.5	5173240.5	West		Tape and Compass	4.1	0.1	min	min	H				Minimum dextral offset. Profile line does not extend very far north and may not cross entire deformation zone
61	1539014.8	5173301.7	West	Fence	RTK	3.6	0.3	min	min	M				Minimum dextral offset. Profile line does not extend very far south and does not cross entire deformation zone
62	1539096.9	5173318.6	West	Crop row	RTK	4.95	0.4	min	min	M	40	71		Profile just crosses possible southern side of deformation zone, and is comprised of widely space points
63a	1539178.3	5173344.1	West	Fence	RTK	4.5	0.25	t	ind	H / MH		73	18	Very good measurement - long profile that is parellel on both sides of deformation zone
63b	1539178.5	5173344.2	West	Fence posts	RTK	4.5	0.2	t	ind	H	41			
63p	1539178.4	5173344.1	West	Preferred	RTK	4.5	0.2	p	pref	H				Very good measurement - long profile that is parellel on both sides of deformation zone
64	1539258.2	5173350.3	West	Crop row	RTK	3.9	0.3	min	min	M				Minimum dextral offset. Profile line does not extend very far south past deformation zone, and does not extend far enough north to cross northern side step-over
65a	1539681.6	5173388.2	West	Fence	RTK	2.5	0.3	min	min	M	42			Minimum dextral offset. Profile line crosses only southern side of step over zone
65b	1539741.3	5173589.4	West	Crop row	RTK	2.8	0.4	min	min	M	43	277		Minimum dextral offset. Profile line crosses only northern side of step over zone
65p	1539712.5	5173479.7	West	Preferred	RTK	5.3	0.5	p	pref	M / ML				Combination of 65a & 65b across both sides of step-over
66	1539757.1	5173588.8	West	Crop row	RTK	2.7	0.5	min	min	M				Minimum dextral offset. Profile line only partially crosses northern side of step over zone
67	1539781.8	5173587.8	West	Crop row	RTK	3.1	0.6	min	min	L				Minimum dextral offset. Profile line only partially crosses northern side of step over zone. Northern portion of profile line controlled by only 3-4 points (i.e. poorly constrained)
68	1539942.7	5173608.2	West	Crop row / fence line	Orthophoto	2.3	0.5	min	min	M				Minimum dextral offset. Profile line does not extend very far north across deformation zone, and is not parallel on both sides of deformation zone (i.e. displacement is still accumulating)
69a	1540262.2	5173639.6	West	East side of drain	RTK	3.4	0.4	t	ind	M	44			

Site number	Easting[i]	Northing[i]	Trace	Marker / Preferred	Dataset	Displacement	Uncertainty	Type[ii]	Type 22[iii]	Quality[iv]	Width profile	Width 100%[v]	Width 50%	Comment
						(m)	(m)				Number[vi]	(m)	(m)	
				in "Yeah Right" paddock										
69b	1540258	5173639.5	West	West side of drain in "Yeah Right" paddock	RTK	3.7	0.45	t	ind	M				
69p	1540260.3	5173639.6	West	Preferred	RTK	3.5	0.4	p	pref	M		61		
70a	1540529.5	5173645	West	Crop row	RTK	3.2	0.4	min	min	M				Minimum dextral offset (southern strand only). Profile line does not extend north across entire deformation zone
70b	1540560.1	5173752.3	West	Crop row	RTK	0.7	0.4	min	min	M				Minimum dextral offset (central strand only). Profile line does not extend north across entire deformation zone
70p	1540547.2	5173705.8	West	Combined local displacement		3.9	0.6	p	pref	M / ML				Minimum dextral offset. Profile line does not extend north across entire deformation zone.
71a	1541109.8	5173883.4	West	Crop row / track	RTK	1.9		min	min	L				Poor quality profile, uncertainty not assessed
71b	1541125.1	5173883.7	West	NW side of Kivers Road	RTK	3	0.4	t	ind	M				Uncertainty assessed based on two different but valid projections
71c	1541148.2	5173884.3	West	fence line to SE of Kivers Road	RTK	3.8	0.4	min	min	M	45			Possible minimum. Fence does not extend very far north across deformation zone, and is not parallel on both sides of deformation zone
71p	1541131.4	5173883.9	West	Preferred		3.4	0.5	p	pref	M / ML		88		
71tc	1541131.4	5173883.9	West		Tape and Compass	3.1	0.3	t	ind	M				
72	1541415.5	5173896.8	West	Hedge	Orthophoto	2.7	1.3	pt	pref	VL				Uncertainty assed based on two alternative projections, neither of which are parallel on both sides of deformation zone
73	1541713.7	5173902.5	West	Wire fence next to drain	RTK	2.6	0.3	pt	pref	M	46	44	5	
74	1541778.8	5173903.7	West	Wire fence	RTK	2.5	0.25	min	min	MH				Minimum, fence does not cross entire width of deformation zone
75	1542033.4	5173908.5	West	Wire fence	RTK	3	0.25	pt	pref	MH	47	123	27	
76a	1542389.6	5173871.8	West	Wire fence west of Aylesbury	RTK	1.9	0.3	min	min	M				Minimum, fence does not extend far on north side of deformation zone, and profiles are not parallel on both sides of fault
76b	1542411.3	5173868.4	West	Wire fence west of Aylesbury	RTK	2	0.25	t	ind	MH				
76p	1542400.8	5173870.2	West	Preferred	RTK	2	0.25	p	pref	MH		145	73	
77a	1543082.1	5173901.9	West	Wire fence next to Aylesbury Rd (southern)	RTK	1.1	0.25	t	ind					
77b	1543094.8	5173901.8	West	Centre line of Aylesbury Rd (southern)	RTK	1.2	0.25	t	ind	MH	49			
77c	1543102.3	5173901.8	West	Power poles east of Aylesbury Rd (southern)	RTK	0.7	0.2	t	ind	H				
77p	1543095.3	5173901.8	West	Preferred	RTK	1	0.25	p	pref	MH / H		138	92	

Site number	Easting[i]	Northing[i]	Trace	Marker / Preferred	Dataset	Displacement	Uncertainty	Type[ii]	Type 22[iii]	Quality[iv]	Width profile	Width 100%[v]	Width 50%	Comment
						(m)	(m)				Number[vi]	(m)	(m)	
77tc	1543095.3	5173901.8	West		T&C	0.8	0.3	t	ind	H				
78	1543421.5	5173899.8	West	Wire fence in paddock est of Aylesbury Rd	RTK	0.35	0.25	min	min	MH				Possible minimum, not sure if profile crosses entire southern strand of deformation zone
79	1544221.7	5173894.9	West	Wire fence	RTK	0		pt	pref					No evidence of right lateral deformation of this fence and fence to east.
80p	1542675.8	5174812.3	East	Preferred		0.6	0.4	p	pref	ML	48	162		
80rtk	1542675.8	5174812.3	East	Centre line of Aylesbury Rd	RTK	0.7	0.4	t	ind	ML				Uncertainty assessed based on anchoring southern projections at three different deformation widths (ranging between 50-150 m). Profiles are not parallel on both sides of fault. Northern projection was used as the reference trend.
80tc	1542675.8	5174812.3	East		Tape and Compass	0.45	0.3	t	ind	M				
81a	1543378.1	5174943.8	East	Fence line	RTK	1.5	0.3	max	max	M				Possible maximum due to projection that favours max
81b	1543379.4	5174943.5	East	Fence posts	RTK	0.9	0.2	min	min	MH				Minimum, fence does not extend south far enough to cross entire deformation zone. Profiles are not parallel on both sides of fault.
81p	1543378.7	5174943.7	East	Preferred		1.3	0.4	p	pref	M		206	82	Preferred value favour max because min value is definitely a min, but max value could be true
82	1543622.1	5174894.3	East	Wire fence	RTK	1.3	0.3	pt	pref	M		106	36	
83	1543829.6	5174855.9	East	Wire fence	RTK	1.1	0.25	min	min	MH				Minimum, fence does not extend north across entire deformation zone. Profile not parallel on both sides of deformation zone.
84	1544032.4	5174831.4	East	Wire fence	RTK	1.6	0.3	pt	pref	M		81	31	Profile relatively short and wobbly on north side of deformation zone
85	1544112.7	5174821.7	East	Wire fence / hedge	RTK	1.5	0.3	pt	pref	M	50	74	24	Profile relatively short and wobbly on north side of deformation zone
86	1544303.8	5174801.3	East	Wire fence	RTK	1.1	0.3	pt	pref	M		45	17	Profile relatively short and wobbly on north side of deformation zone
87	1545213.5	5174836.3	East	Wire fence	Orthophoto	0.8	0.5	min	min	ML				Minimum, fence does not extend south very far, and profile is not parallel on both sides of deformation zone.
88a	1545931.7	5174811.7	East	Fence immediately west of Tressillian Rd	RTK	1.4	0.5	t	ind	ML	51			Some question as to whether fence was linear across deformation zone prior to faulting. Gate in fence line right at location of deformation zone
88b	1545936.5	5174811.5	East	side of road	Orthophoto	1	0.5	t	ind	M				
88p	1545934.3	5174811.6	East	Preferred		1.1	0.4	p	pref	M		35	26	
88tc	1545934.3	5174811.6	East		Tape and Compass	0.9	0.2	t	ind	MH				
89	1546154.8	5174792.6	East	Crop row / wire	Orthophoto	0.7	0.5	min	min	M				Minimum, crop row does not extend south across entire deformation zone.
90	1546321	5174777.4	East	Wire fence line	RTK	1.2	0.3	min	min	M				Possible minimum, profile line is not parallel on both sides of fault, and southern end does not extend very far south
91	1546364.2	5174773.4	East	Wire fence line	RTK	1	0.25	pt	pref	MH	52	105	45	
92	1547147.2	5174848.7	East	Preferred		1.6	0.4	p	pref			79	57	

Site number	Easting[i]	Northing[i]	Trace	Marker / Preferred	Dataset	Displacement	Uncertainty	Type[ii]	Type 22[iii]	Quality[iv]	Width profile	Width 100%[v]	Width 50%	Comment
						(m)	(m)				Number[vi]	(m)	(m)	
92a	1547140.4	5174848.3	East		RTK	1.7	0.5	t	ind	L				Profile line is very oblique to trend of deformation zone (large projection uncertainties)
92b	1547153.1	5174848.6	East	Kerrs Rd centre line	RTK	1.6	0.4	t	ind	ML	53			Profile line is very oblique to trend of deformation zone (large projection uncertainties)
92tc	1547147.2	5174848.7	East		Tape and Compass	1.5	0.3	t	ind	M				
93a	1547532.7	5174865.9	East	Northeastern railway line	RTK	1.3	0.3	t	ind	MH	54			
93b	1547541	5174866.2	East	Power poles northeast of railway line	RTK	1.2	0.3	t	ind	MH				
93p	1547536.4	5174866	East	Preferred		1.2	0.3	p	pref	MH		128	112	
93tc	1547536.4	5174866	East		Tape and Compass	1.1	0.3	t	ind	M				
94	1548346.1	5174937.7	East	Deer fence	Tape and Compass	1.2	0.3	pt	pref	M				
95	1549479.2	5175260.7	East	Deer fence	Tape and Compass	0.2	0.2	pt	pref					Eastern-most identified deformation feature
96	1549712.4	5175269.8	East	Hoskyns Rd		0		pt	pref					No deformation observed across Hoskyns Rd
97	1542407.8	5174812.2	East	Fence line / drain west of Aylesbury Rd		0		pt	pref					No deformation observed along this fence line / drain
98	1521312.4	5175219.2	West	Paddock		0		pt	pref					No deformation observed in field in this paddock
99	1532655	5172911.6	West	Plough line NW of gorse fence line	Lidar 0.5 m HSNW	3	0.75	pt	pref	L				
100	1532974.4	5172846.6	West	Plough line	Lidar 0.5 m HSNW	2.2	1	min	min	VL				Minimum dextral value, feature not parallel across fault
101	1533644.9	5172816.1	West	Drain	Lidar 0.5 m HSNW	4.8	0.75	min	min	ML	15			Possible minimum dextral value, feature does not extend very far across north side of deformation zone

i New Zealand GD2000 New Zealand Transverse Mercator Projection.

ii min = minimum displacement, max = maximum displacement, p = preferred (2 or more measurements), pt = preferred total (1 measurement), t = total.

iii ind = individual measurement, min = minimum displacement, max = maximum displacement, pref = preferred.

iv H = high, L = low, M = medium, MH = medium to high, ML = medium to low, VL = very low.

vi Values in brackets are from Sharon Hornblow (unpublished data).

v Profiles of displacement perpendicular to fault strike in section 6.

Table A 1.2 Previously published vertical displacement measurements (Quigley et al., 2012). All are from Lidar 0.5 m DEM cross sections except site 94, which is from a tape and compass field measurement.

Site number	Easting[i]	Northing[i]	Trace	Displacement	Uncertainty	Type[ii]	Up side	Bulge Amplitude	Uncertainty	Comments
				(m)	(m)			(m)	(m)	
1	1527310.08	5172643.8	West	0.55	0.45	t	South	0.4	0.1	
2	1526991.76	5172680.57	West	0.05	0.05	min	South	0.05	0.05	Profile appears to show distinctly different gradients on either side of the fault - south side is flatter and may be Selwyn /river gradient, and north of fault is steeper gradient and may be Waimakariri fan
3	1526227.48	5172706.84	West	0.05	0.05	min	South	0.2	0.1	Profile does not extend very far north of fault
4	1524697.48	5172874.67	West	1.05	0.1	max	South			
6	1523643.03	5173310.15	West	0.55	0.2	t	South	0.45	0.1	
7	1523249.95	5173428.63	West	0.6	0.3	t	South	1.3	0.1	Bulge height is actually height of half-graben
9	1522846.32	5173672.45	West	1.65	0.2	max	South			
10	1522166.52	5174432.45	West	1.6	0.1	max	South			
11	1521892.58	5174678.88	West	1.05	0.1	max	South			
12	1527436.69	5172632.52	West	1.45	0.1	max	South	1	0.1	
13	1527525.99	5172614.34	West	1.6	0.1	max	South	0.75	0.1	
17	1527646.62	5172602.99	West	0.75	0.55	t	South	0.7	0.1	
18	1528109.26	5172545.21	West	0.4	0.2	t	South	0.35	0.1	
19	1528522.29	5172595.58	West	0.3	0.1	max	South	0.25	0.1	
20	1529506.19	5172586.38	West	0.25	0.2	t	South	0.15	0.1	
21	1530192.01	5172658.22	West	0.2	0.2	t	South	0.15	0.1	
22	1531011.69	5172767.97	West	0.3	0.2	t	South	0.4	0.1	
23	1531244.3	5172821.36	West	0.35	0.25	t	South	0.7	0.1	
24	1532190.62	5172900.16	West	0.15	0.15	t	South	0.6	0.1	
25	1532636.53	5172916.31	West	0.65	0.1	max	South	0.3	0.1	
26	1532911.2	5172859.51	West	0.3	0.15	t	South	0.2	0.1	Of the two profiles considered, 26a is much better, and it is this one that is used for the value chosen
27	1533086.74	5172843.75	West	0.6	0.25	t	South	0.2	0.1	
28	1533130.27	5172833.6	West	0.8	0.25	t	South	0.35	0.1	
29	1533179.64	5172822.08	West	0.3	0.2	t	South	0.4	0.1	
30	1533679.49	5172802.65	West	1.15	0.2	t	South	0.6	0.1	
31	1534079.13	5172765.54	West	0.4	0.2	t	South	0.35	0.1	Vertical throw based on average of two profiles approximately 30 m apart
32	1534165.76	5172746.48	West	0.4	0.2	t	South	0.3	0.1	
33	1534262.77	5172765.65	West	0.95	0.9	t	South	0.55	0.1	
34	1534339.52	5172742.53	West	0.6	0.2	t	South	0.5	0.1	
35	1534662.13	5172795.31	West	1.1	0.2	t	South	1.15	0.1	
36	1534932.18	5172769.59	West	0.65	0.65	t	South	0.85	0.1	Problematic flattening of gradient within 200 m either side of fault
37	1535183.8	5172762.45	West	0.2	0.15	t	North	0.25	0.1	

Site number	Easting[i]	Northing[i]	Trace	Displacement	Uncertainty	Type[ii]	Up side	Bulge Amplitude	Uncertainty	Comments
				(m)	(m)			(m)	(m)	
38	1535368.35	5172737.24	West	0.15	0.1	t	North	0.1	0.1	
39	1535555.11	5172711.74	West	0.6	0.35	t	South			
40	1535904.1	5172721.41	West	0.5	0.3	t	South	0.45	0.1	
41	1536238.02	5172773.96	West	0.6	0.3	t	South	0.3	0.1	
42	1536270	5172772.23	West	0.65	0.2	t	South	0.6	0.1	
43	1536401.12	5172765.24	West	0.9	0.2	t	South	0.65	0.1	
44	1536432.45	5172763.57	West	0.5	0.4	t	South	0.7	0.1	
45	1536473.88	5172761.36	West	0.45	0.25	t	South	0.45	0.15	
46	1536706.57	5172846.97	West	0.7	0.7	t	South	0.75	0.1	
47	1536759.7	5172854.79	West	0.9	0.35	t	South	0.75	0.1	
48	1536943.95	5172910.68	West	1.3	0.2	t	South	1.3	0.3	
49	1537235.4	5172991.48	West	1.2	0.2	t	South	0.8	0.1	
50	1537359.63	5172990.18	West	0.48	0.2	t	South	0.53	0.1	
51	1537549.8	5173072.83	West	0.65	0.25	t	South	0.85	0.65	
52	1538098.9	5173115.3	West	0.43	0.3	t	South	0.4	0.1	Difficult profiles, hard to find a projection that is parallel on both sides of fault.
53	1538219.95	5173137.76	West	0.65	0.6	t	South	0.45	0.15	Difficult profiles, hard to find a projection that is parallel on both sides of fault.
54	1538261.69	5173132.27	West	0.95	0.8	t	South	0.45	0.1	Difficult profiles, hard to find a projection that is parallel on both sides of fault.
55	1538314.27	5173125.34	West	1.2	0.1	max	South	0.4	0.1	
55	1538314.27	5173125.34	West				South			South side of fault is very flat compared to N side. Cannot find a workable projection using south side gradient.
56	1538425.65	5173114.5	West	0.35	0.2	t	South	0.35	0.1	
57	1538477.82	5173115.76	West	0.35	0.2	t	South	0.2	0.1	
58	1538608.35	5173189.5	West	0.3	0.3	t	South	1.3	0.3	
59	1538713.47	5173224.17	West	0.45	0.45	t	South			
60	1538814.53	5173240.52	West	0.3	0.3	t	South			
61	1539014.75	5173301.66	West	0.85	0.3	t	South	0.8	0.1	
62	1539096.89	5173318.61	West	1	0.2	t	South	0.55	0.1	
63	1539178.4	5173344.13	West	0.85	0.2	t	South	0.25	0.1	
64	1539258.23	5173350.26	West	0.2	0.2	t	South	0.5	0.1	
65	1539712.47	5173479.65	West	0.8	0.3	t	South			
66	1539757.11	5173588.78	West	0.35	0.35	t	South	0.25	0.1	
67	1539781.84	5173587.76	West	0.45	0.45	t	South	0.4	0.1	
68	1539942.71	5173608.16	West	0.05	0.6	t	North	0.8	0.1	
69	1540260.32	5173639.56	West	1	0.3	t	North			

Site number	Easting[i]	Northing[i]	Trace	Displacement	Uncertainty	Type[ii]	Up side	Bulge Amplitude	Uncertainty	Comments
				(m)	(m)			(m)	(m)	
70	1540547.16	5173705.77	West	0	1	t				Need to project across a 250 m wide side step - difficult to tell what side is up
71	1541131.4	5173883.87	West	0.2	0.2	t	North	0.95	0.1	
72	1541415.53	5173896.79	West	0.5	0.3	t	North	0.85	0.1	
73	1541713.72	5173902.46	West	0.55	0.25	t	North			
74	1541778.77	5173903.7	West	0.25	0.2	t	North	0.85	0.1	
75	1542033.43	5173908.52	West	0.55	0.2	t	South			
76	1542400.82	5173870.17	West	0	0.3	t		0.6	0.1	
77	1543095.31	5173901.84	West	0.25	0.2	t	South			
78	1543421.45	5173899.78	West	0.25	0.2	t	North			
79	1544221.66	5173894.85	West	0						
80	1542675.77	5174812.3	East	0.1	0.1	t	North			
81	1543378.65	5174943.66	East	0.25	0.25	t	South			
82	1543622.08	5174894.34	East	0.5	0.5	t	South			
83	1543829.58	5174855.88	East	0.55	0.25	t	South	0.25	0.1	
84	1544032.41	5174831.44	East	0.15	0.25	t	North			
85	1544112.74	5174821.65	East	0.25	0.1	min	South			
86	1544303.83	5174801.33	East	0.15	0.15	t	North			
87	1545213.52	5174836.26	East							Too channelized to measure a reliable vertical displacement
88	1545934.33	5174811.59	East	0.4	0.35	t	North			
89	1546154.75	5174792.64	East	0.45	0.25	t	North			
90	1546321.03	5174777.36	East	0.4	0.3	t	North			
91	1546364.22	5174773.39	East	0.5	0.3	t	North			
92	1547147.22	5174848.73	East	0.2	0.2	t	North			
93	1547536.44	5174866.04	East	0.7	0.2	t	North			
94	1548346.1	5174937.66	East	0.15	0.15	t	North			Tape and Compass measurement.
97	1542407.77	5174812.22	East	0		t				
99	1532654.96	5172911.59	West	0.5	0.2	t	South	0.35	0.1	
100	1532974.43	5172846.59	West	0.3	0.25	t	South	0.3	0.1	
101	1533644.91	5172816.07	West	0.85	0.2	t	South			
102	1533424.90	5172853.19	West	0.65	0.25	t	South	0.45	0.1	
103	1531939.71	5172876.61	West	0.3	0.3	t	South	0.2	0.1	
104	1531696.40	5172841.19	West	0.35	0.2	t	South	0.17	0.25	
105	1531492.99	5172861.26	West	0.6	0.2	t	South	0.5	0.1	
106	1530689.06	5172754.97	West	0.2	0.2	t	South			

Site number	Easting[i]	Northing[i]	Trace	Displacement	Uncertainty	Type[ii]	Up side	Bulge Amplitude	Uncertainty	Comments
				(m)	(m)			(m)	(m)	
107	1530546.33	5172711.33	West	0.15	0.15	t	South	0.15	0.1	
108	1530374.51	5172689.51	West	0.2	0.2	t	South	0.3	1	
109	1529899.95	5172604.96	West							
110	1529246.30	5172584.05	West	0.35	0.2	t	South	0.3	0.1	
111	1528319.91	5172579.51	West	0.85	0.1	max	South			Northern side of fault and profile appears to be on younger surface than southern side; therefore, vertical displacement measured is most likely a max
112	1527802.63	5172578.60	West	0.55	0.4	t	South	0.75	0.1	
113	1526777.05	5172729.65	West	0.15	0.15	min	South	0.1	0.1	Profile does not extend very far to N of fault (Lidar coverage stops)
114	1524958.13	5172696.67	West	0.7	0.4	t	South	0.75	0.1	Profile does not extend very far north of fault
115	1524874.49	5172753.65	West	0.8	0.4	t	South			
116	1524769.41	5172825.78	West	1.55	0.1	max	South			
117	1523758.08	5173323.66	West	0.15	0.1	min	South	0.5	0.5	
118	1523061.04	5173529.72	West	1.15	0.3	t	South	1.65	0.1	Bulge height is half-graben height. Profile does not extend very far to south of fault (if riser is not a riser, then vert displacement could be closer to 0.5 m)
119	1522733.32	5173791.43	West	1.45	0.2	t	South			
120	1522610.06	5173993.67	West	1.3	0.2	t	South			
121	1543620.35	5173901.49	West	0.15	0.15	t	North			
122	1544090.41	5173897.58	West	0						
123	1544650.93	5174856.56	East	0.75	0.2	max	South			Channel margin (riser) almost coincides with location of fault - cannot measure accurate vert displacement

i New Zealand GD2000 New Zealand Transverse Mercator Projection.

ii min = minimum displacement, max = maximum displacement, t = total.

APPENDIX 2: NEW DISPLACEMENT MEASUREMENTS

Table A 2.1 New dextral displacement measurements obtained (by one person – Nicola Litchfield) in this study (Section 4).

Dataset			RTK		Tape and Compass		Laser scan – all		Laser scan – selected		Orthophoto		Lidar 0.5 m HSNW		Lidar 0.5 m HSNE		Lidar 0.5 m Slope		Lidar 0.5 m Aspect		Lidar 0.25 m HSNW		Lidar 0.25 m HSNE		Lidar 0.25 m Slope		Lidar 0.25 m Aspect	
Site	Easting	Northing	Displ.	Unc.	Displ.	Unc.	Displ.	Unc.	Displ.	Unc.	Displ.	Unc.	Displ.	Unc.	Displ.	Unc.	Displ.	Unc.	Displ.	Unc.	Displ.	Unc.	Displ.	Unc.	Displ.	Unc.	Displ.	Unc.
No.			(m)	(m)	(m)	(m)	(m)	(m)	(m)	(m)	(m)	(m)	(m)	(m)	(m)	(m)	(m)	(m)	(m)	(m)	(m)	(m)	(m)	(m)	(m)	(m)	(m)	(m)
1	1527310.1	5172643.8	1.2	0.2	1.3	0.2					2.1	0.6	1.2	0.75			1.35	1			1.8	1	1.65	1.5	1.14	0.75	1.62	1
2	1526991.8	5172680.6	1	0.25							1.7	0.6	1	0.75					1.05	0.75	1.4	0.75			1.51	0.75	1.18	0.75
3	1526227.5	5172706.8	1	0.25							0.5	0.5	2.5	0.75													1.58	1
4	1524697.5	5172874.7	0.7	0.25																								
6	1523643	5173310.2	1.3	0.25																								
7a	1523252.3	5173428	1.1	0.2																								
7b	1523249	5173428.9	1.7	0.5																								
7c	1523247.5	5173429.4	0.75	0.25																								
8	1522915.2	5173610.6	0.75	0.3																								
9	1522846.3	5173672.5	0.85	0.3																								
10	1522166.5	5174432.5	0.9	0.25	0.95	0.2																						
11	1521892.6	5174678.9	0.95	0.25																								
12	1527436.7	5172632.5	1.95	0.4																								
13	1527526	5172614.3	1.65	0.2							1.6	0.5	2.1	1			1.8	1.25	1.7	1	1.47	1			1.38	1	1.32	1
14	1527566.8	5172609.4									0.3	0.3																
15	1527571.6	5172609									0.6	0.5																
16	1527608.2	5172606.1									0.9	0.5																
17	1527646.6	5172603									1.15	0.5	1.8	1														
18	1528109.3	5172545.2									1.9	0.5			1.6	0.75					4.98	0.75			1.25	1.25		
19	1528522.3	5172595.6	1.7	0.3									2.1	1	1.5	0.75					1.79	1	1.79	1	2.44	1	1.92	1
20a	1529494.4	5172586.3	3.2	0.5	2.3	0.2					2.1	0.5	2	0.75	2.1	0.75							2.44	1	1.18	1		
20b	1529502.7	5172586.4	3.7	0.4							2.1	0.5							5.4	1								
20c	1529508.7	5172586.5	3.7	0.4							1.85	0.5																
20d	1529515.3	5172586.5	2.5	0.5							1.35	0.5	3.2	1							2.27	0.75	2.48	0.75	1.82	0.75		
21	1530192	5172658.2	3.2	0.25							2.9	0.5	2.7	0.75	1.05	1			2.5	1	1.61	1.25	2.03	1.25	1.57	1	1.09	1
22	1531011.7	5172768	2.8	0.25																								
23	1531244.3	5172821.4	2.85	0.3	3.5	0.5					3.1	0.5	3.3	0.75	4	0.75	3.4	1.5			4.04	0.75	3.91	0.75	2.89	0.75	3.8	1
24a	1532188.8	5172900.4	3.1	0.25							3.8	0.5	3.7	0.75	3.1	0.75	1.5	1.5			2.42	0.75	2.71	1	2.76	0.75	2.21	1
24b	1532192	5172900	2.6	0.5															3.1	1.25								
25	1532636.5	5172916.3											3.6	0.75														
26a	1532903.3	5172861.3	4.9	1							6	0.75																
26b	1532905.7	5172860.8	4.1	0.3																								
26c	1532908.2	5172860.3	3.8	0.5	4.3	0.2					4	0.5	2.3	0.75	4.5	0.75	3.7	1.5	5.5	1.25	5	1.5	3.95	1	4.7	1		
26d	1532914.3	5172859	3.5	0.75																								
26e	1532916.1	5172858.6	3.3	0.75																								

Dataset			RTK		Tape and Compass		Laser scan – all		Laser scan – selected		Orthophoto		Lidar 0.5 m HSNW		Lidar 0.5 m HSNE		Lidar 0.5 m Slope		Lidar 0.5 m Aspect		Lidar 0.25 m HSNW		Lidar 0.25 m HSNE		Lidar 0.25 m Slope		Lidar 0.25 m Aspect	
Site	Easting	Northing	Displ.	Unc.	Displ.	Unc.	Displ.	Unc.	Displ.	Unc.	Displ.	Unc.	Displ.	Unc.	Displ.	Unc.	Displ.	Unc.	Displ.	Unc.	Displ.	Unc.	Displ.	Unc.	Displ.	Unc.	Displ.	Unc.
No.			(m)	(m)	(m)	(m)	(m)	(m)	(m)	(m)	(m)	(m)	(m)	(m)	(m)	(m)	(m)	(m)	(m)	(m)	(m)	(m)	(m)	(m)	(m)	(m)	(m)	(m)
26f	1532924.8	5172856.8									4.9	0.75			5.5	0.75			4.6	1								
27	1533086.7	5172843.8	4.2	0.15							4.2	0.5	4.05	1	5.1	1	5.3	1.5	4.25	1.25	4.1	1			5.09	1	4.45	1
28	1533130.3	5172833.6									3.6	1																
29	1533179.6	5172822.1	4.4	0.4							3.8	0.5	5.7	1	3.45	1					4.68	1	4.85	1				
30a	1533673.5	5172805	4.35	0.25	4.2	0.2					5.7	0.5	3.9	0.75					3.5	1								
30b	1533678.5	5172803	3.7	0.5							5.15	0.5	6.45	1											5.39	1		
30c	1533685.5	5172800.2	4.3	0.25																	5.25	1					4.29	1
31a	1534075.8	5172766.3	4.5	0.5							3.7	0.75	4.2	0.75	4.2	0.75	3.1	1.5	3.35	1	3.9	1	4.89	1	4.58	0.75	4.18	0.75
31b	1534082.5	5172764.8	4.2	0.25							4.9	0.5					3.65	1	4.9	1.25								
32	1534165.8	5172746.5									4.7	0.75	4.2	0.5			4.4	1	5.15	1	4.59	0.75	4.33	1	4.3	0.75	5.39	1
33	1534262.8	5172765.7									5.2	0.75	5	0.75														
34	1534339.5	5172742.5	4.15	0.5							4.2	0.75	4.05	0.75	3.4	1	3	1	3.35	1	4.11	0.75	3.4	1	3.6	0.75		
35	1534662.1	5172795.3	3.8	0.5							2	0.5			5.2	0.75					2.12	1			4.14	1		
36a	1534928.1	5172770	4.85	0.4	4.6	0.2	4.69	0.3	3.58	0.2	4.25	0.5	4.1	0.75			3.55	1			4.57	0.75	5.24	1.25	4.54	0.75	4	1
36b	1534935	5172769.4	4.9	0.25			4.62	0.3	4.29	0.2	5.6	0.5	4.85	0.75	4.7	0.75			4.45	1.25	4.49	0.75	3.93	1	3.95	0.75	5.45	1
37	1535183.8	5172762.5	4.6	0.4							3.8	0.5	4.4	0.75			3.4	1.25			4.52	0.75	3.84	1	3.81	1	4.24	0.75
38	1535368.4	5172737.2	4.6	0.3							4.95	0.5	4.95	0.75							4.75	0.75	3.83	1	4.83	0.75	4.81	1
39	1535555.1	5172711.7									3.3	0.5			1.75	0.75												
40	1535904.1	5172721.4	3.3	0.3							3.15	0.5																
41	1536238	5172774	4.1	0.4																								
42	1536270	5172772.2									5.2	0.75																
43	1536401.1	5172765.2	2.4	0.3																								
44	1536432.5	5172763.6	2.9	0.3																								
45	1536473.9	5172761.4	4.7	0.25							4.45	0.5	3.1	0.75	5	0.75	4.9	1	5.45	1	5.44	1	6.46	1	4.75	0.75	4.7	0.75
46	1536706.6	5172847	4.65	0.3							5.35	0.6	5.35	1					5.55	1.25	5.1	1					5.33	1
47	1536759.7	5172854.8	4.4	0.3																								
48a	1536940.4	5172909.7	4.4	1.3	4.15	0.3					5.5	0.6	5.6	0.75	1.75	1					4.87	1					6.15	1
48b	1536946.6	5172911.2	4.8	0.9							4	0.5																
48c	1536941.1	5172909.9	4.2	0.4																								
48d	1536946.9	5172911.3	5.1	0.5																								
48e	1536954.7	5172913.4					4.39	0.4	4.4	0.3																		
48f	1536958	5172913.9					5.16	0.4																				
48g	1536960.8	5172914.8					4.27	0.4																				
48h	1536962.5	5172915.2							4.125	0.25																		
48i	1536963.8	5172915.5					4.06	0.4	4	0.25																		
49	1537235.4	5172991.5	1.35	0.2																								
50a	1537358.1	5172990.4	3.3	0.3	3.6	0.2					3.9	0.5																

Dataset			RTK		Tape and Compass		Laser scan – all		Laser scan – selected		Orthophoto		Lidar 0.5 m HSNW		Lidar 0.5 m HSNE		Lidar 0.5 m Slope		Lidar 0.5 m Aspect		Lidar 0.25 m HSNW		Lidar 0.25 m HSNE		Lidar 0.25 m Slope		Lidar 0.25 m Aspect	
Site	Easting	Northing	Displ.	Unc.	Displ.	Unc.	Displ.	Unc.	Displ.	Unc.	Displ.	Unc.	Displ.	Unc.	Displ.	Unc.	Displ.	Unc.	Displ.	Unc.	Displ.	Unc.	Displ.	Unc.	Displ.	Unc.	Displ.	Unc.
No.			(m)	(m)	(m)	(m)	(m)	(m)	(m)	(m)	(m)	(m)	(m)	(m)	(m)	(m)	(m)	(m)	(m)	(m)	(m)	(m)	(m)	(m)	(m)	(m)	(m)	(m)
50b	1537361.2	5172990.1	3.6	0.2							3.4	0.75																
51a	1537479.5	5172976.7									3.9	0.5																
51b	1537600.7	5173169.3	1.1	0.3																								
52	1538098.9	5173115.3	4.95	0.2	4.1	0.3					5.2	0.5	4.15	0.75	5.9	1	4.65	1.25			3.48	1.5	2.79	1.5	3.69	1.5		
53	1538220	5173137.8	4.6	1																								
54	1538261.7	5173132.3	4.1	0.4																								
55	1538314.3	5173125.3	4.8	0.4	4.6	0.2					4.8	0.6	5.4	0.75	5.1	0.75			4.7	1.25	3.96	1	3.29	1.25			4.53	1
56	1538425.7	5173114.5	4.2	0.4																								
57	1538477.8	5173115.8	2.75	0.4																								
58	1538608.4	5173189.5	4.4	0.5							4	0.5			4.3	0.6												
59	1538713.5	5173224.2	3.9	0.3	3.8	0.5					4.9	0.5	3.55	0.75					3.6	1.25								
60	1538814.5	5173240.5	4.1	0.5	4.1	0.1					4.5	0.7	4.65	0.75	3	0.6			6.1	1.25	4.51	1					3.43	1
61	1539014.8	5173301.7	3.6	0.3							4.75	0.5																
62	1539096.9	5173318.6	4.95	0.4																								
63a	1539178.3	5173344.1	4.5	0.25							4.45	0.5	4.55	0.75	4.7	0.75					6.44	0.75	6.12	0.75	6.9	1		
64	1539258.2	5173350.3	3.9	0.3																								
65a	1539681.6	5173388.2	2.5	0.3																								
65b	1539741.3	5173589.4	2.8	0.4																								
66	1539757.1	5173588.8	2.7	0.5																								
67	1539781.8	5173587.8	3.1	0.6																								
68	1539942.7	5173608.2									2.3	0.5																
69a	1540262.2	5173639.6	3.4	0.4			3.57	0.5			3.4	0.7	3.3	0.75	4.8	1	4.1	1.25	2.7	0.75	2.9	1					4.08	1
69b	1540258	5173639.5	3.7	0.45			3.54	0.6			2.8	0.6	2.7	0.75			1.45	1.25										
70a	1540529.5	5173645	3.2	0.4							2.8	0.7	4.5	1														
70b	1540560.1	5173752.3	0.7	0.4							0.15	0.5																
71a	1541109.8	5173883.4	1.9	0.5							3.2	0.6	2.2	0.75	3.55	0.75	1.75	1.25	1.1	1	3.09	1	5.09	1.25	2.46	0.75	3.21	1
71b	1541125.1	5173883.7	3	0.4	3.1	0.3					2.9	0.7	3.1	1					6.45	1.25								
71c	1541148.2	5173884.3	3.8	0.4							4.14	0.6																
72	1541415.5	5173896.8									2.7	1.3			2.7	0.75			3.65	1								
73	1541713.7	5173902.5	2.6	0.3							2.75	0.75	2.3	0.75	2.8	1	2.35	1.25	2.6	1.25	1.88	1			2	0.75	3.12	1
74	1541778.8	5173903.7	2.5	0.25							2.45	0.6																
75	1542033.4	5173908.5	3	0.25							2.3	0.6	2.15	0.75	3.25	1	3.5	1.5	3.05	1	2.46	1			2.2	1	2.12	1
76a	1542389.6	5173871.8	1.9	0.3							1.95	0.5	4.85	0.75	1	0.75	2.9	1.5	4.99	1	2.84	0.75			3.38	0.75	3.45	1
76b	1542411.3	5173868.4	2	0.25																								
77a	1543082.1	5173901.9	1.1	0.25							0.8	0.5																
77b	1543094.8	5173901.8	1.2	0.25	0.8	0.3					0.4	0.5			0.6	0.75												
77c	1543102.3	5173901.8	0.7	0.2							0.2	0.5																

Dataset			RTK		Tape and Compass		Laser scan – all		Laser scan – selected		Orthophoto		Lidar 0.5 m HSNW		Lidar 0.5 m HSNE		Lidar 0.5 m Slope		Lidar 0.5 m Aspect		Lidar 0.25 m HSNW		Lidar 0.25 m HSNE		Lidar 0.25 m Slope		Lidar 0.25 m Aspect	
Site	Easting	Northing	Displ.	Unc.	Displ.	Unc.	Displ.	Unc.	Displ.	Unc.	Displ.	Unc.	Displ.	Unc.	Displ.	Unc.	Displ.	Unc.	Displ.	Unc.	Displ.	Unc.	Displ.	Unc.	Displ.	Unc.	Displ.	Unc.
No.			(m)	(m)	(m)	(m)	(m)	(m)	(m)	(m)	(m)	(m)	(m)	(m)	(m)	(m)	(m)	(m)	(m)	(m)	(m)	(m)	(m)	(m)	(m)	(m)	(m)	(m)
78	1543421.5	5173899.8	0.35	0.25							0.6	0.5	0.2	0.75			1.25	1.5			0.6	1.25	1.05	1.25	0.69	1	0.37	1
79	1544221.7	5173894.9	0								0.65	0.5																
80	1542675.8	5174812.3	0.7	0.4	0.45	0.3					0	0.5			0	1												
81a	1543378.1	5174943.8	1.5	0.3							1.7	0.6	0.95	0.75	1	1	0.3	1.5							0.68	1	0.63	1
81b	1543379.4	5174943.5	0.9	0.2																								
82	1543622.1	5174894.3	1.3	0.3							1	0.6	2.55	1			0.85	1.5			1.49	0.75	1.88	1	0.95	1		
83	1543829.6	5174855.9	1.1	0.25							1.6	0.75																
84	1544032.4	5174831.4	1.6	0.3							1.1	0.6																
85	1544112.7	5174821.7	1.5	0.3							1.5	0.5			0.8	0.75												
86	1544303.8	5174801.3	1.1	0.3							1.1	0.6	0.95	0.75	0.5	1	1.3	1.5			0.8	0.75	1.23	1	1.42	0.75	0.97	1
87	1545213.5	5174836.3									0.8	0.5																
88a	1545931.7	5174811.7	1.4	0.5	0.9	0.2					1.3	0.5	0								2.35	0.75	1.3	1	0.16	1		
88b	1545936.5	5174811.5									1	0.5																
89	1546154.8	5174792.6									0.7	0.5																
90	1546321	5174777.4	1.2	0.3							0.6	0.5																
91	1546364.2	5174773.4	1	0.25							0.4	0.6									1.06	1			1.03	0.75		
92a	1547140.4	5174848.3	1.7	0.5							0.5	0.7																
92b	1547153.1	5174848.6	1.6	0.4	1.5	0.3					1.2	0.7	0.6	1														
93a	1547532.7	5174865.9	1.3	0.3	1.1	0.3					1	0.6	2.7	1	1.9	0.75	1.6	1.25	1.2	1.25			0.55	1	0.94	0.75	0.1	1.25
93b	1547541	5174866.2	1.2	0.3											2.4	1												
94	1548346.1	5174937.7			1.2	0.3																						
95	1549479.2	5175260.7			0.2	0.2																						
96	1549712.4	5175269.8	0																									
97	1542407.8	5174812.2	0								0						0		0.4	1	0.55	1	0.16	1	0.95	0.75		
98	1521312.4	5175219.2	0																									
99	1532655	5172911.6											3	0.75														
100	1532974.4	5172846.6											2.2	1	3.9	1												
101	1533644.9	5172816.1									4.55	0.6	4.8	0.75			6.5	1.5			4.7	1	4.3	1	6	1	4	1

APPENDIX 3: COMPARISON BETWEEN TWO DATASETS: ALONG-STRIKE PLOTS

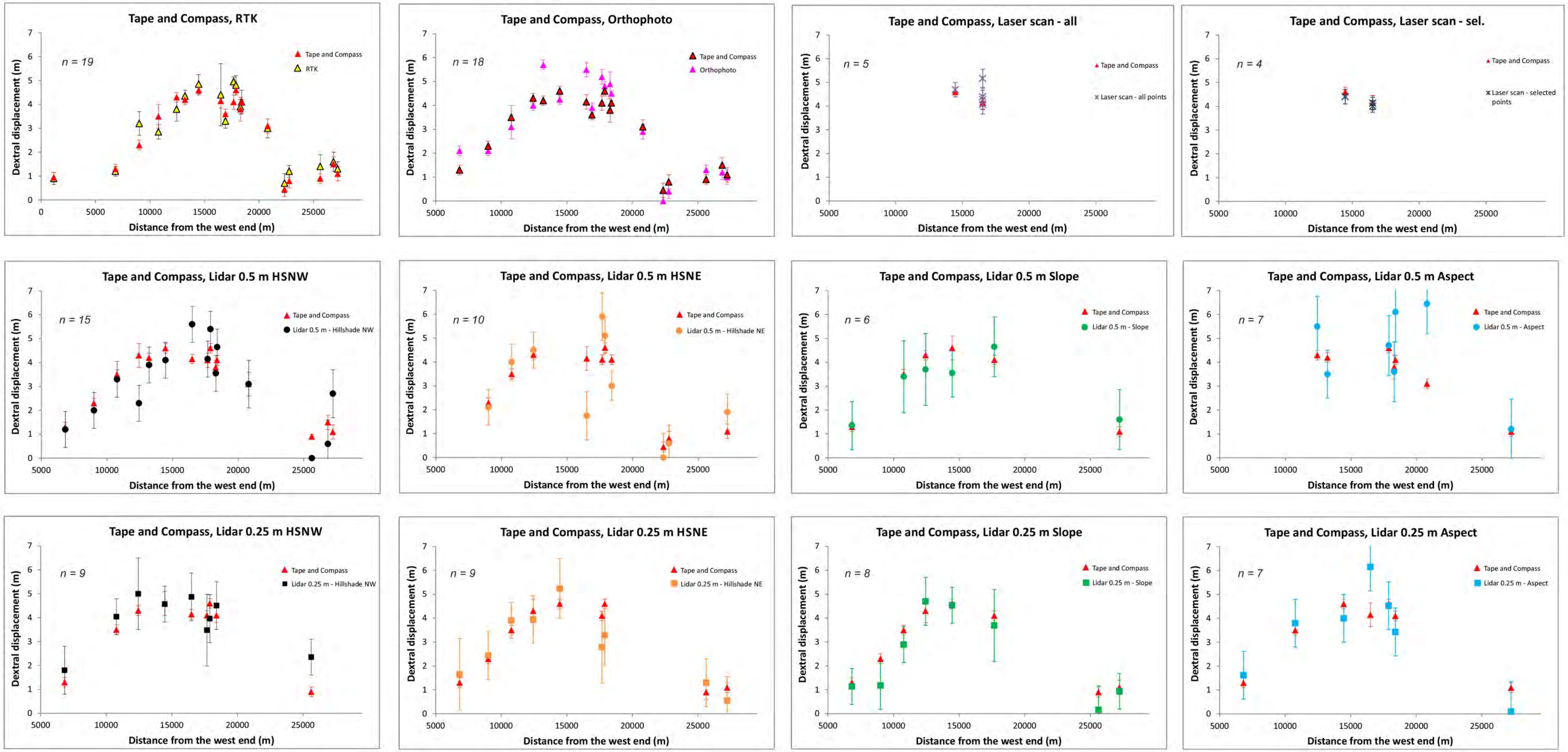

Figure A3.1

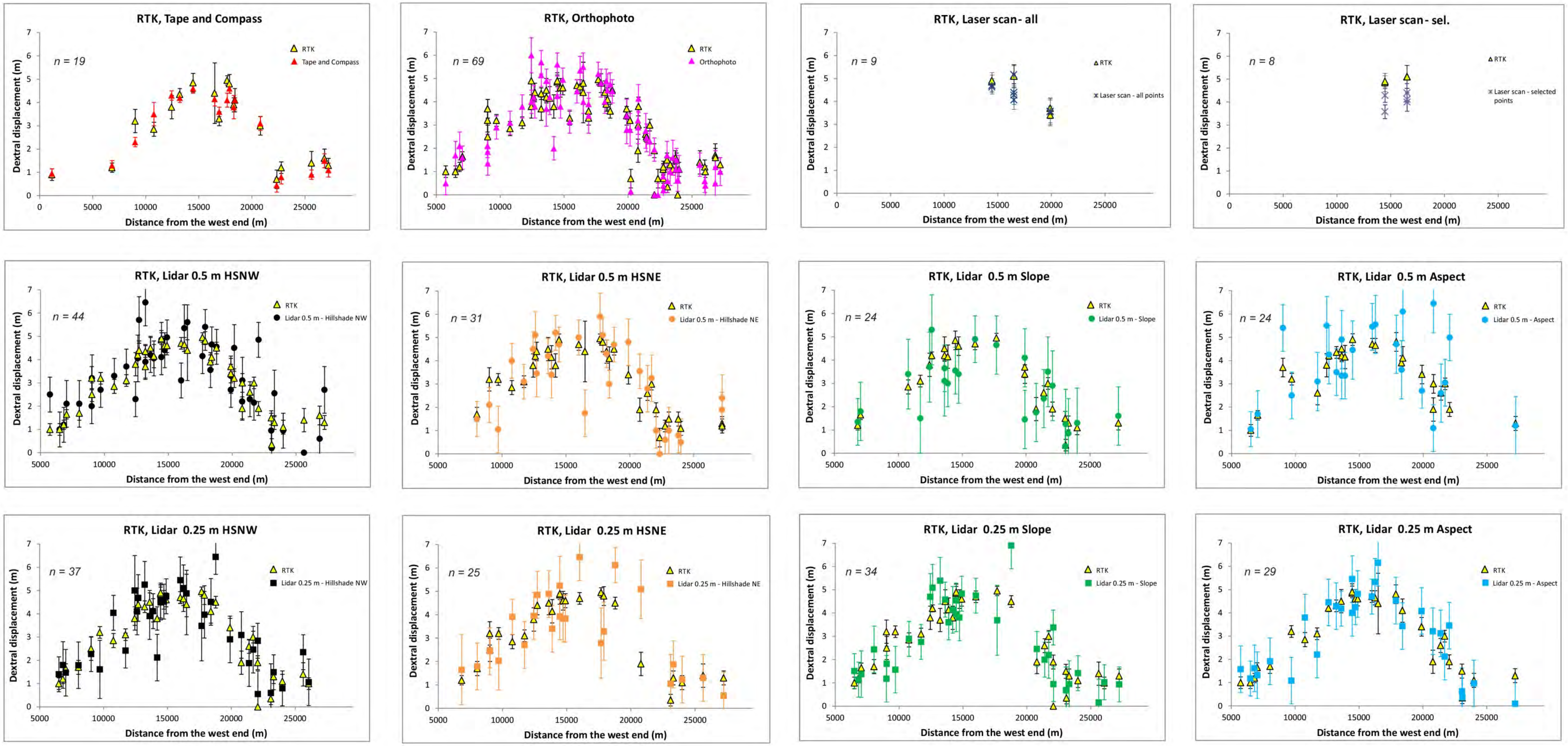
RTK, Tape and Compass
n = 19
RTK
Tape and Compass
RTK, Orthophoto
n = 69
RTK
Orthophoto
RTK, Laser scan- all
n = 9
RTK
Laser scan - all points
RTK, Laser scan- sel.
n = 8
RTK
Laser scan - selected points
RTK, Lidar 0.5 m HSNW
n = 44
RTK
Lidar 0.5 m - Hillshade NW
RTK, Lidar 0.5 m HSNE
n = 31
RTK
Lidar 0.5 m - Hillshade NE
RTK, Lidar 0.5 m Slope
n = 24
RTK
Lidar 0.5 m - Slope
RTK, Lidar 0.5 m Aspect
n = 24
RTK
Lidar 0.5 m - Aspect
RTK, Lidar 0.25 m HSNW
n = 37
RTK
Lidar 0.25 m - Hillshade NW
RTK, Lidar 0.25 m HSNE
n = 25
RTK
Lidar 0.25 m - Hillshade NE
RTK, Lidar 0.25 m Slope
n = 34
RTK
Lidar 0.25 m - Slope
RTK, Lidar 0.25 m Aspect
n = 29
RTK
Lidar 0.25 m - Aspect
Dextral displacement (m)
Distance from the west end (m)

Figure A3.2

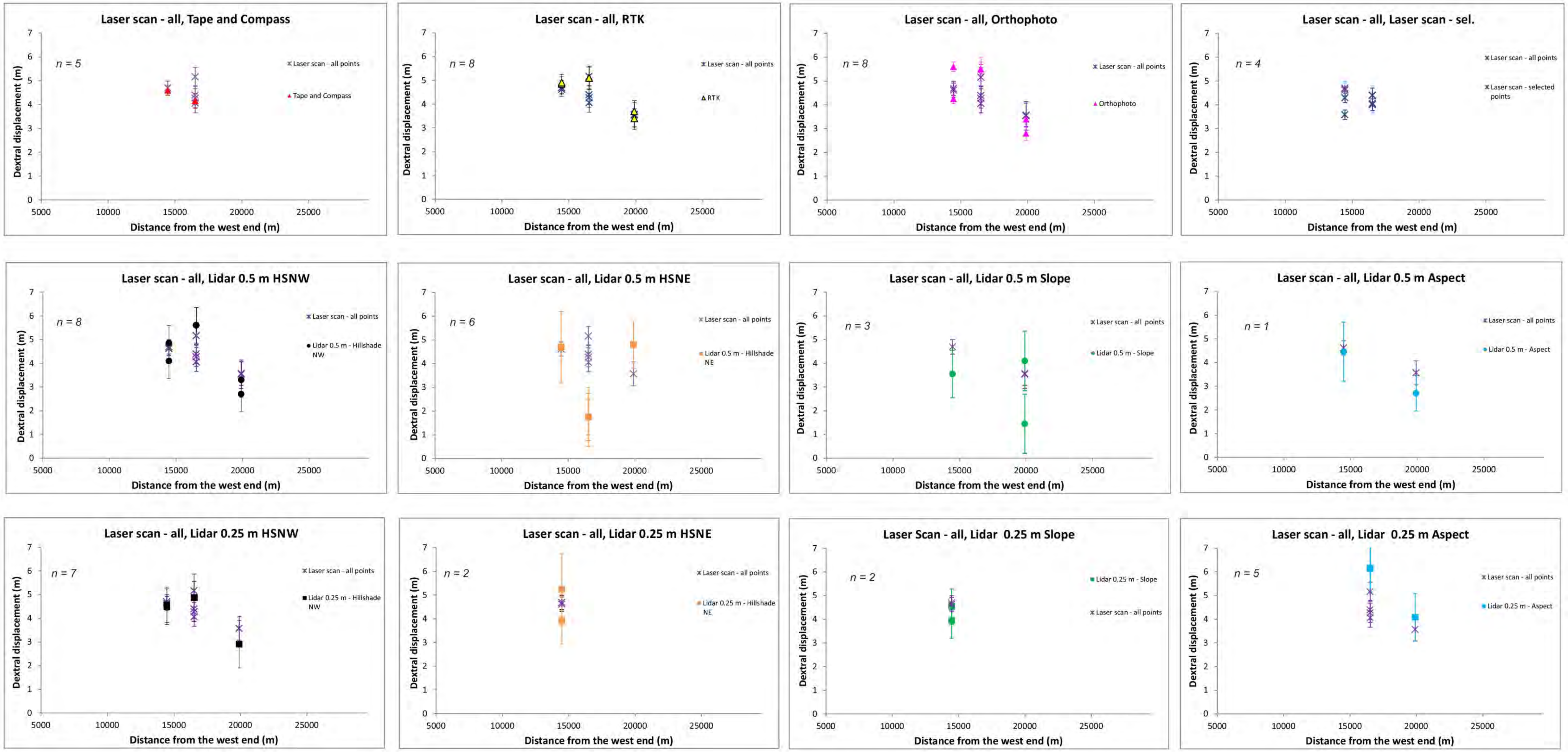
Laser scan - all, Tape and Compass
n = 5
Laser scan - all points
Tape and Compass
Laser scan - all, RTK
n = 8
Laser scan - all points
RTK
Laser scan - all, Orthophoto
n = 8
Laser scan - all points
Orthophoto
Laser scan - all, Laser scan - sel.
n = 4
Laser scan - all points
Laser scan - selected points
Laser scan - all, Lidar 0.5 m HSNW
n = 8
Laser scan - all points
Lidar 0.5 m - Hillshade NW
Laser scan - all, Lidar 0.5 m HSNE
n = 6
Laser scan - all points
Lidar 0.5 m - Hillshade NE
Laser scan - all, Lidar 0.5 m Slope
n = 3
Laser scan - all points
Lidar 0.5 m - Slope
Laser scan - all, Lidar 0.5 m Aspect
n = 1
Laser scan - all points
Lidar 0.5 m - Aspect
Laser scan - all, Lidar 0.25 m HSNW
n = 7
Laser scan - all points
Lidar 0.25 m - Hillshade NW
Laser scan - all, Lidar 0.25 m HSNE
n = 2
Laser scan - all points
Lidar 0.25 m - Hillshade NE
Laser Scan - all, Lidar 0.25 m Slope
n = 2
Lidar 0.25 m - Slope
Laser scan - all points
Laser scan - all, Lidar 0.25 m Aspect
n = 5
Laser scan - all points
Lidar 0.25 m - Aspect
Dextral displacement (m)
Distance from the west end (m)

Figure A3.3

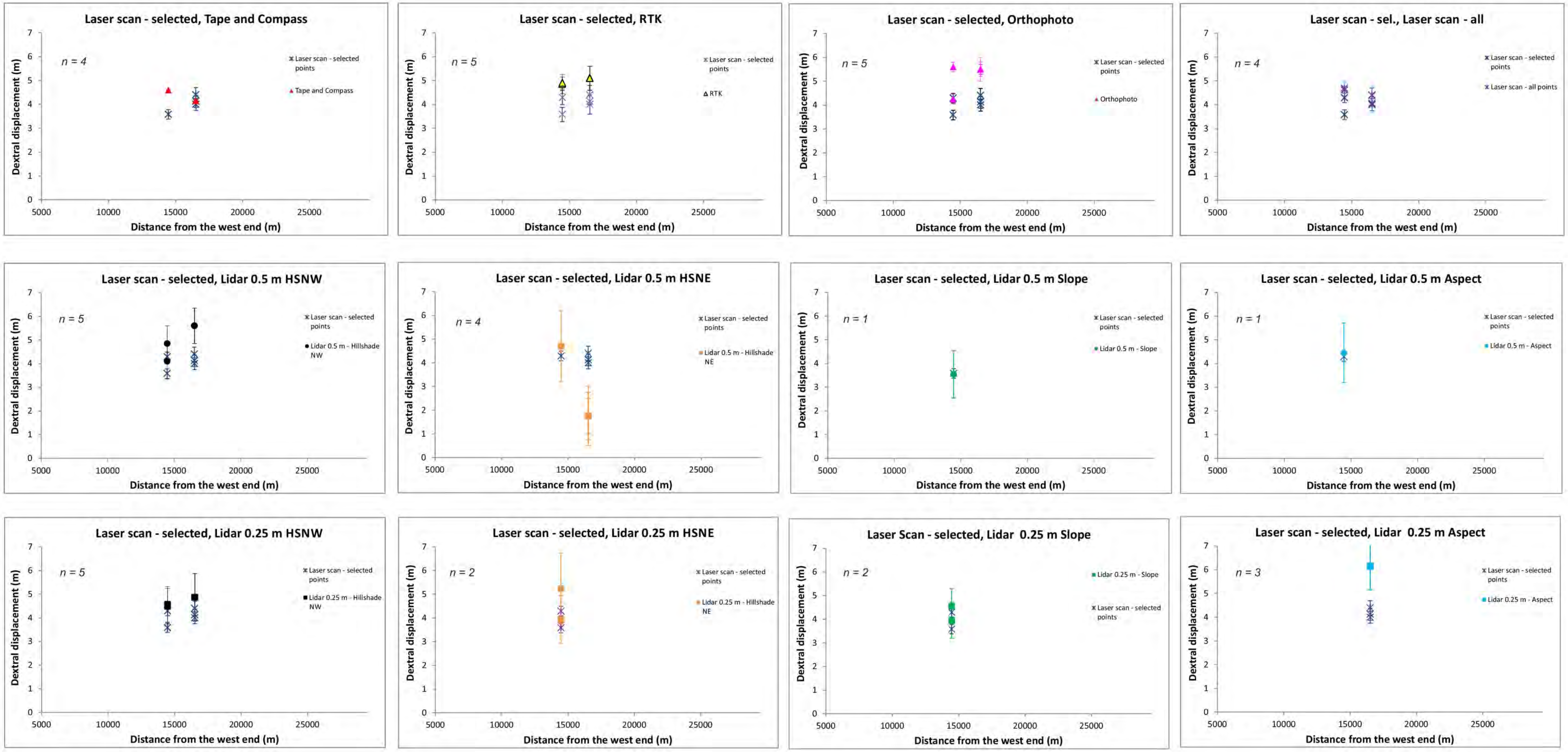
Laser scan - selected, Tape and Compass
n = 4
Laser scan - selected points
Tape and Compass
Laser scan - selected, RTK
n = 5
Laser scan - selected points
RTK
Laser scan - selected, Orthophoto
n = 5
Laser scan - selected points
Orthophoto
Laser scan - sel., Laser scan - all
n = 4
Laser scan - selected points
Laser scan - all points
Laser scan - selected, Lidar 0.5 m HSNW
n = 5
Laser scan - selected points
Lidar 0.5 m - Hillshade NW
Laser scan - selected, Lidar 0.5 m HSNE
n = 4
Laser scan - selected points
Lidar 0.5 m - Hillshade NE
Laser scan - selected, Lidar 0.5 m Slope
n = 1
Laser scan - selected points
Lidar 0.5 m - Slope
Laser scan - selected, Lidar 0.5 m Aspect
n = 1
Laser scan - selected points
Lidar 0.5 m - Aspect
Laser scan - selected, Lidar 0.25 m HSNW
n = 5
Laser scan - selected points
Lidar 0.25 m - Hillshade NW
Laser scan - selected, Lidar 0.25 m HSNE
n = 2
Laser scan - selected points
Lidar 0.25 m - Hillshade NE
Laser Scan - selected, Lidar 0.25 m Slope
n = 2
Lidar 0.25 m - Slope
Laser scan - selected points
Laser scan - selected, Lidar 0.25 m Aspect
n = 3
Laser scan - selected points
Lidar 0.25 m - Aspect
Dextral displacement (m)
Distance from the west end (m)
0
1
2
3
4
5
6
7
5000
10000
15000
20000
25000

Figure A3.4

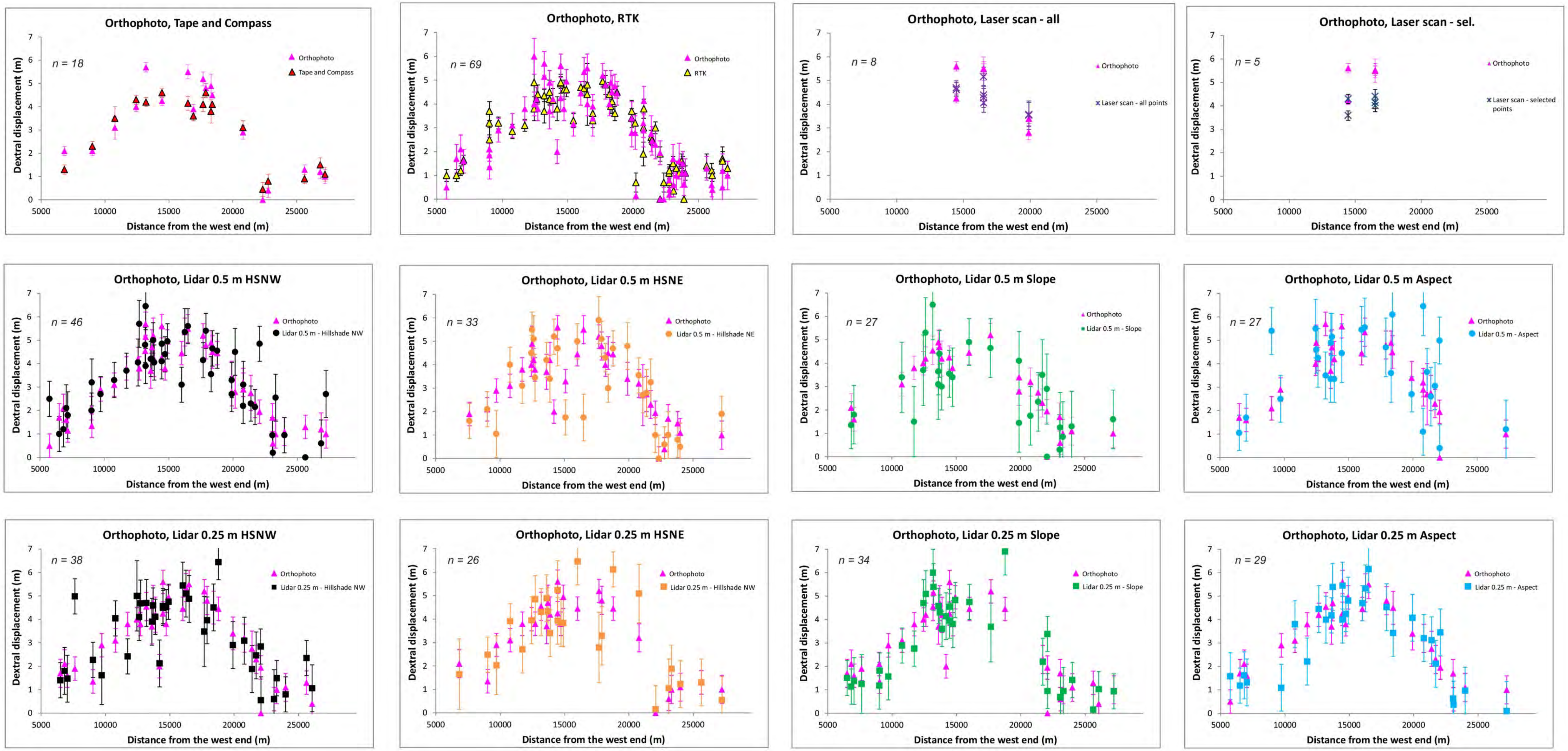
Orthophoto, Tape and Compass
n = 18
Orthophoto
Tape and Compass
Orthophoto, RTK
n = 69
Orthophoto
RTK
Orthophoto, Laser scan - all
n = 8
Orthophoto
Laser scan - all points
Orthophoto, Laser scan - sel.
n = 5
Orthophoto
Laser scan - selected points
Orthophoto, Lidar 0.5 m HSNW
n = 46
Orthophoto
Lidar 0.5 m - Hillshade NW
Orthophoto, Lidar 0.5 m HSNE
n = 33
Orthophoto
Lidar 0.5 m - Hillshade NE
Orthophoto, Lidar 0.5 m Slope
n = 27
Orthophoto
Lidar 0.5 m - Slope
Orthophoto, Lidar 0.5 m Aspect
n = 27
Orthophoto
Lidar 0.5 m - Aspect
Orthophoto, Lidar 0.25 m HSNW
n = 38
Orthophoto
Lidar 0.25 m - Hillshade NW
Orthophoto, Lidar 0.25 m HSNE
n = 26
Orthophoto
Lidar 0.25 m - Hillshade NW
Orthophoto, Lidar 0.25 m Slope
n = 34
Orthophoto
Lidar 0.25 m - Slope
Orthophoto, Lidar 0.25 m Aspect
n = 29
Orthophoto
Lidar 0.25 m - Aspect
Dextral displacement (m)
Distance from the west end (m)

Figure A3.5

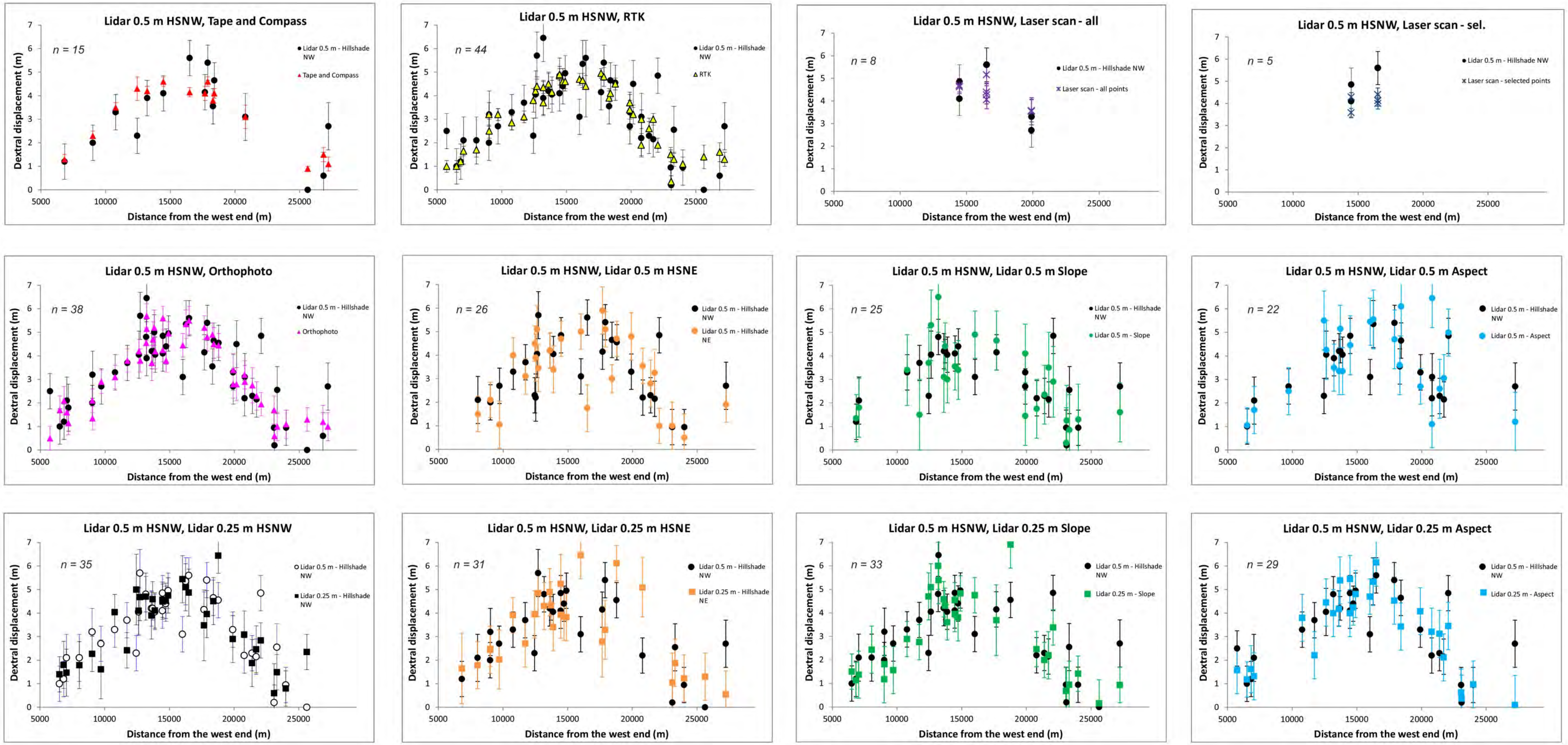
Lidar 0.5 m HSNW, Tape and Compass
n = 15
Lidar 0.5 m - Hillshade NW
Tape and Compass
Lidar 0.5 m HSNW, RTK
n = 44
Lidar 0.5 m - Hillshade NW
RTK
Lidar 0.5 m HSNW, Laser scan - all
n = 8
Lidar 0.5 m - Hillshade NW
Laser scan - all points
Lidar 0.5 m HSNW, Laser scan - sel.
n = 5
Lidar 0.5 m - Hillshade NW
Laser scan - selected points
Lidar 0.5 m HSNW, Orthophoto
n = 38
Lidar 0.5 m - Hillshade NW
Orthophoto
Lidar 0.5 m HSNW, Lidar 0.5 m HSNE
n = 26
Lidar 0.5 m - Hillshade NW
Lidar 0.5 m - Hillshade NE
Lidar 0.5 m HSNW, Lidar 0.5 m Slope
n = 25
Lidar 0.5 m - Hillshade NW
Lidar 0.5 m - Slope
Lidar 0.5 m HSNW, Lidar 0.5 m Aspect
n = 22
Lidar 0.5 m - Hillshade NW
Lidar 0.5 m - Aspect
Lidar 0.5 m HSNW, Lidar 0.25 m HSNW
n = 35
Lidar 0.5 m - Hillshade NW
Lidar 0.25 m - Hillshade NW
Lidar 0.5 m HSNW, Lidar 0.25 m HSNE
n = 31
Lidar 0.5 m - Hillshade NW
Lidar 0.25 m - Hillshade NE
Lidar 0.5 m HSNW, Lidar 0.25 m Slope
n = 33
Lidar 0.5 m - Hillshade NW
Lidar 0.25 m - Slope
Lidar 0.5 m HSNW, Lidar 0.25 m Aspect
n = 29
Lidar 0.5 m - Hillshade NW
Lidar 0.25 m - Aspect
Dextral displacement (m)
Distance from the west end (m)

Figure A3.6

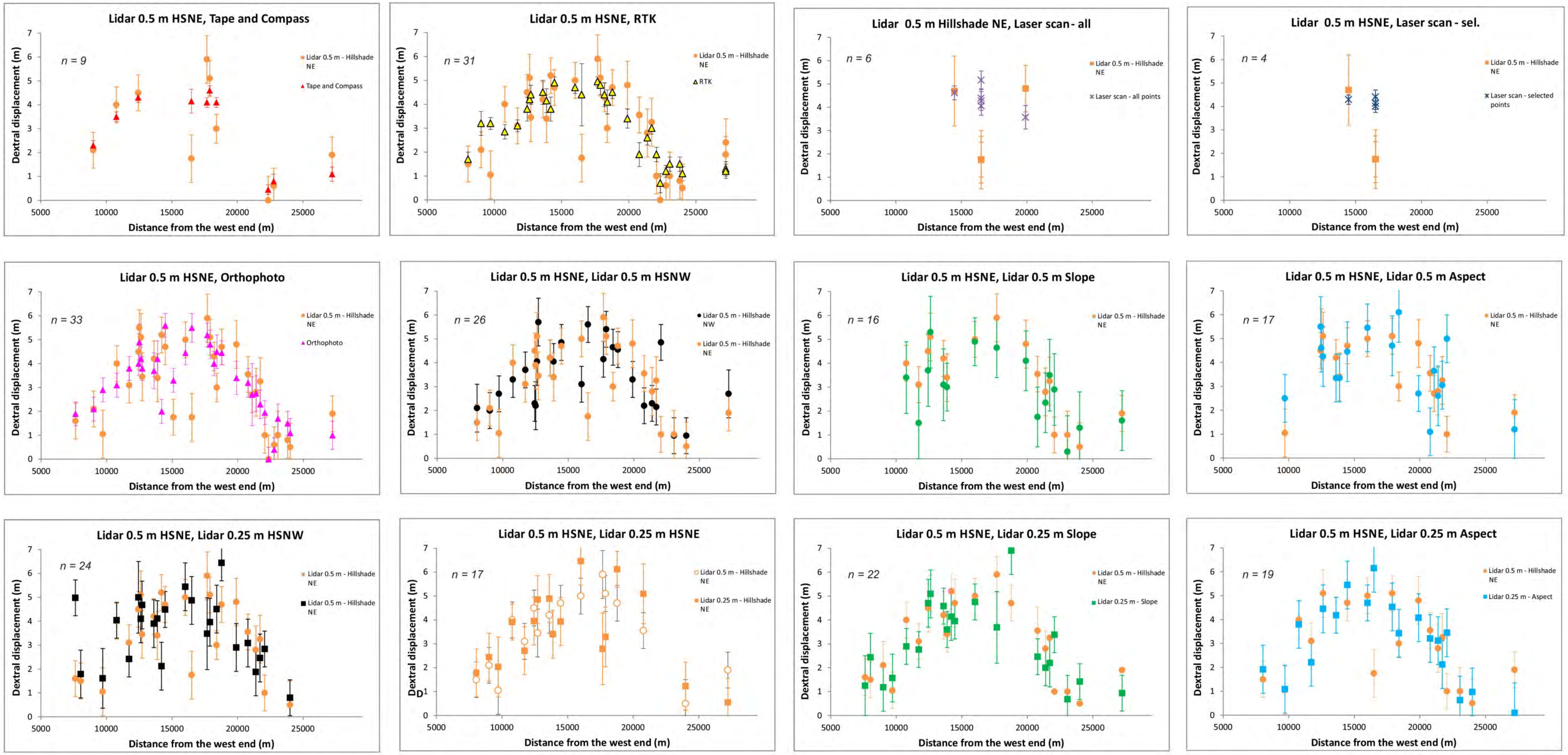

Lidar 0.5 m HSNE, Tape and Compass
n = 9
Lidar 0.5 m - Hillshade NE
Tape and Compass
Lidar 0.5 m HSNE, RTK
n = 31
Lidar 0.5 m - Hillshade NE
RTK
Lidar 0.5 m Hillshade NE, Laser scan - all
n = 6
Lidar 0.5 m - Hillshade NE
Laser scan - all points
Lidar 0.5 m HSNE, Laser scan - sel.
n = 4
Lidar 0.5 m - Hillshade NE
Laser scan - selected points
Lidar 0.5 m HSNE, Orthophoto
n = 33
Lidar 0.5 m - Hillshade NE
Orthophoto
Lidar 0.5 m HSNE, Lidar 0.5 m HSNW
n = 26
Lidar 0.5 m - Hillshade NW
Lidar 0.5 m - Hillshade NE
Lidar 0.5 m HSNE, Lidar 0.5 m Slope
n = 16
Lidar 0.5 m - Hillshade NE
Lidar 0.5 m HSNE, Lidar 0.5 m Aspect
n = 17
Lidar 0.5 m - Hillshade NE
Lidar 0.5 m HSNE, Lidar 0.25 m HSNW
n = 24
Lidar 0.5 m - Hillshade NE
Lidar 0.5 m - Hillshade NE
Lidar 0.5 m HSNE, Lidar 0.25 m HSNE
n = 17
Lidar 0.5 m - Hillshade NE
Lidar 0.25 m - Hillshade NE
Lidar 0.5 m HSNE, Lidar 0.25 m Slope
n = 22
Lidar 0.5 m - Hillshade NE
Lidar 0.25 m - Slope
Lidar 0.5 m HSNE, Lidar 0.25 m Aspect
n = 19
Lidar 0.5 m - Hillshade NE
Lidar 0.25 m - Aspect
Dextral displacement (m)
Distance from the west end (m)

Figure A3.7

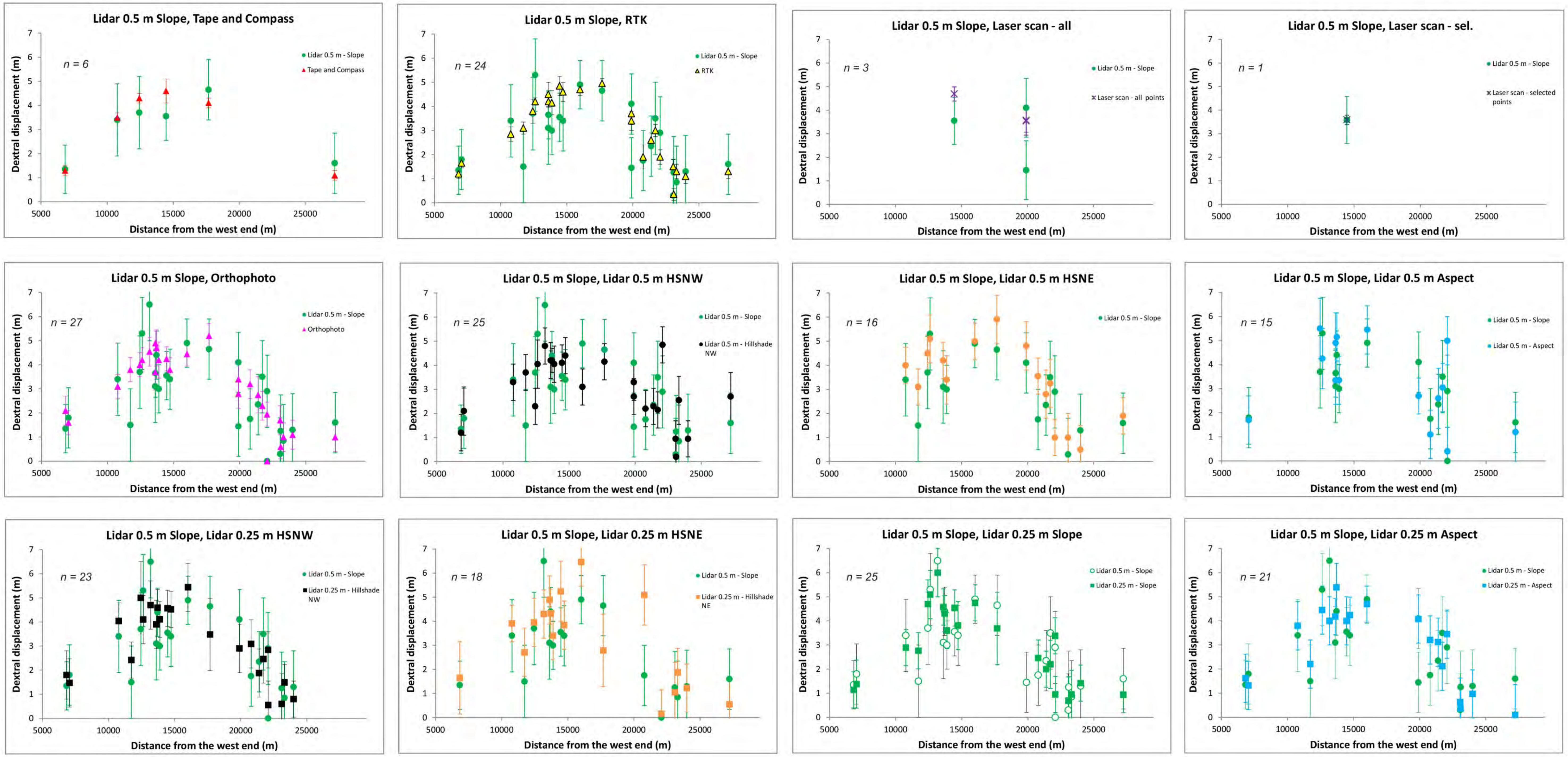
Lidar 0.5 m Slope, Tape and Compass
n = 6
Lidar 0.5 m - Slope
Tape and Compass
Lidar 0.5 m Slope, RTK
n = 24
Lidar 0.5 m - Slope
RTK
Lidar 0.5 m Slope, Laser scan - all
n = 3
Lidar 0.5 m - Slope
Laser scan - all points
Lidar 0.5 m Slope, Laser scan - sel.
n = 1
Lidar 0.5 m - Slope
Laser scan - selected points
Lidar 0.5 m Slope, Orthophoto
n = 27
Lidar 0.5 m - Slope
Orthophoto
Lidar 0.5 m Slope, Lidar 0.5 m HSNW
n = 25
Lidar 0.5 m - Slope
Lidar 0.5 m - Hillshade NW
Lidar 0.5 m Slope, Lidar 0.5 m HSNE
n = 16
Lidar 0.5 m - Slope
Lidar 0.5 m Slope, Lidar 0.5 m Aspect
n = 15
Lidar 0.5 m - Slope
Lidar 0.5 m - Aspect
Lidar 0.5 m Slope, Lidar 0.25 m HSNW
n = 23
Lidar 0.5 m - Slope
Lidar 0.25 m - Hillshade NW
Lidar 0.5 m Slope, Lidar 0.25 m HSNE
n = 18
Lidar 0.5 m - Slope
Lidar 0.25 m - Hillshade NE
Lidar 0.5 m Slope, Lidar 0.25 m Slope
n = 25
Lidar 0.5 m - Slope
Lidar 0.25 m - Slope
Lidar 0.5 m Slope, Lidar 0.25 m Aspect
n = 21
Lidar 0.5 m - Slope
Lidar 0.25 m - Aspect
Dextral displacement (m)
Distance from the west end (m)
0
1
2
3
4
5
6
7
5000
10000
15000
20000
25000

Figure A3.8

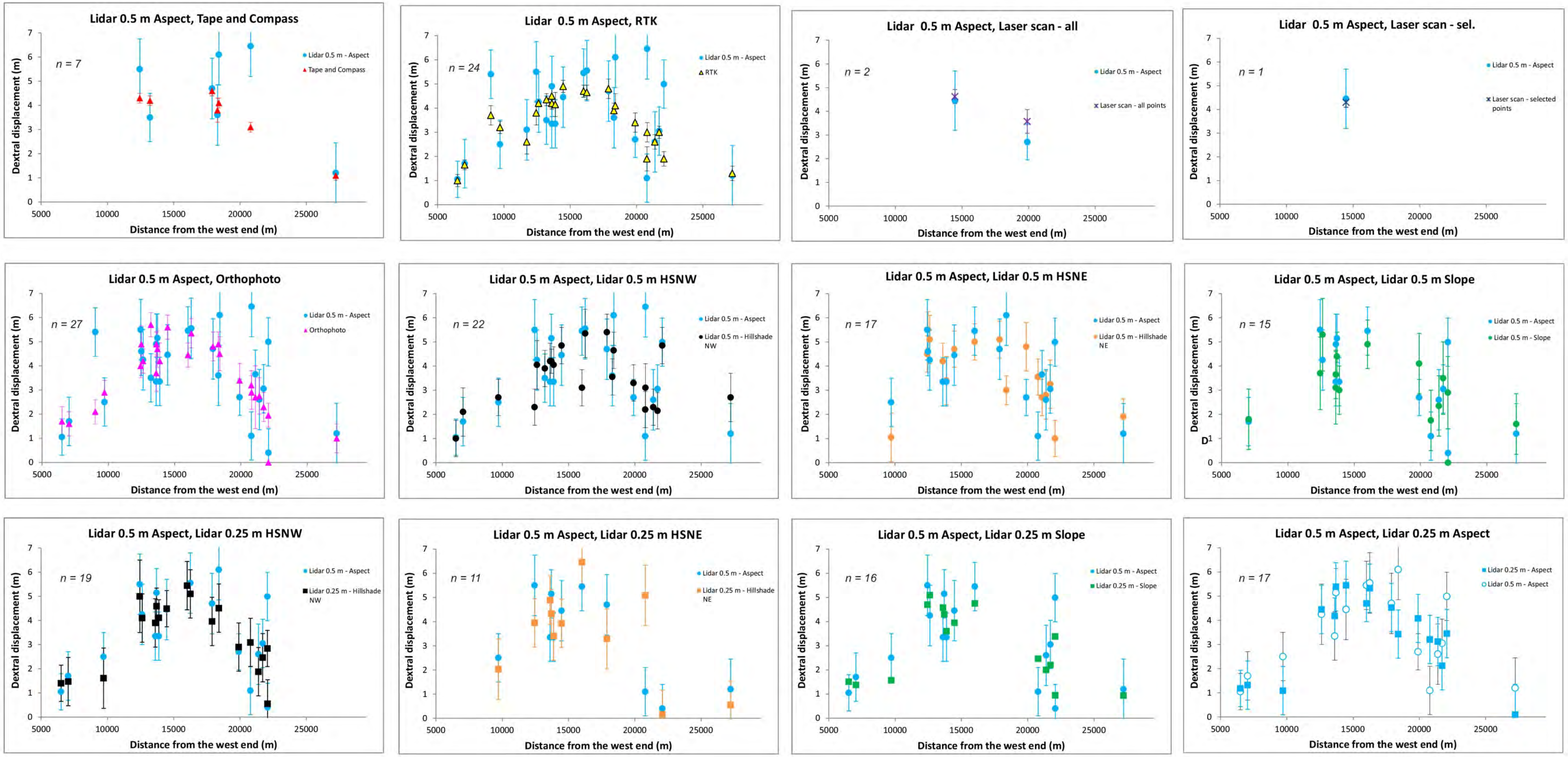
Lidar 0.5 m Aspect, Tape and Compass
n = 7
Lidar 0.5 m - Aspect
Tape and Compass
Lidar 0.5 m Aspect, RTK
n = 24
Lidar 0.5 m - Aspect
RTK
Lidar 0.5 m Aspect, Laser scan - all
n = 2
Lidar 0.5 m - Aspect
Laser scan - all points
Lidar 0.5 m Aspect, Laser scan - sel.
n = 1
Lidar 0.5 m - Aspect
Laser scan - selected points
Lidar 0.5 m Aspect, Orthophoto
n = 27
Lidar 0.5 m - Aspect
Orthophoto
Lidar 0.5 m Aspect, Lidar 0.5 m HSNW
n = 22
Lidar 0.5 m - Aspect
Lidar 0.5 m - Hillshade NW
Lidar 0.5 m Aspect, Lidar 0.5 m HSNE
n = 17
Lidar 0.5 m - Aspect
Lidar 0.5 m - Hillshade NE
Lidar 0.5 m Aspect, Lidar 0.5 m Slope
n = 15
Lidar 0.5 m - Aspect
Lidar 0.5 m - Slope
Lidar 0.5 m Aspect, Lidar 0.25 m HSNW
n = 19
Lidar 0.5 m - Aspect
Lidar 0.25 m - Hillshade NW
Lidar 0.5 m Aspect, Lidar 0.25 m HSNE
n = 11
Lidar 0.5 m - Aspect
Lidar 0.25 m - Hillshade NE
Lidar 0.5 m Aspect, Lidar 0.25 m Slope
n = 16
Lidar 0.5 m - Aspect
Lidar 0.25 m - Slope
Lidar 0.5 m Aspect, Lidar 0.25 m Aspect
n = 17
Lidar 0.25 m - Aspect
Lidar 0.5 m - Aspect
Dextral displacement (m)
Distance from the west end (m)
0
1
2
3
4
5
6
7
5000
10000
15000
20000
25000

Figure A3.9

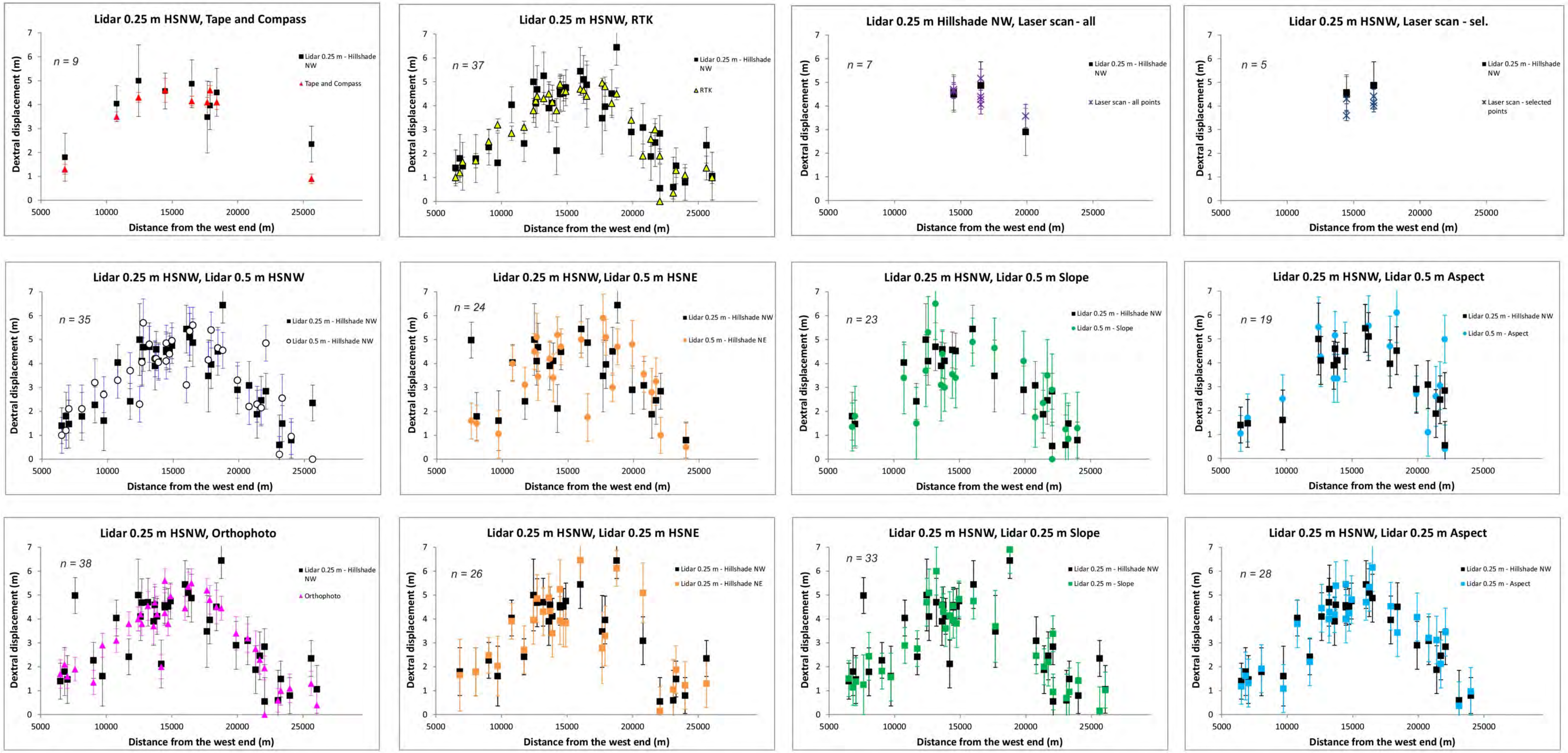
Lidar 0.25 m HSNW, Tape and Compass
n = 9
Lidar 0.25 m - Hillshade NW
Tape and Compass
Lidar 0.25 m HSNW, RTK
n = 37
Lidar 0.25 m - Hillshade NW
RTK
Lidar 0.25 m Hillshade NW, Laser scan - all
n = 7
Lidar 0.25 m - Hillshade NW
Laser scan - all points
Lidar 0.25 m HSNW, Laser scan - sel.
n = 5
Lidar 0.25 m - Hillshade NW
Laser scan - selected points
Lidar 0.25 m HSNW, Lidar 0.5 m HSNW
n = 35
Lidar 0.25 m - Hillshade NW
Lidar 0.5 m - Hillshade NW
Lidar 0.25 m HSNW, Lidar 0.5 m HSNE
n = 24
Lidar 0.25 m - Hillshade NW
Lidar 0.5 m - Hillshade NE
Lidar 0.25 m HSNW, Lidar 0.5 m Slope
n = 23
Lidar 0.25 m - Hillshade NW
Lidar 0.5 m - Slope
Lidar 0.25 m HSNW, Lidar 0.5 m Aspect
n = 19
Lidar 0.25 m - Hillshade NW
Lidar 0.5 m - Aspect
Lidar 0.25 m HSNW, Orthophoto
n = 38
Lidar 0.25 m - Hillshade NW
Orthophoto
Lidar 0.25 m HSNW, Lidar 0.25 m HSNE
n = 26
Lidar 0.25 m - Hillshade NW
Lidar 0.25 m - Hillshade NE
Lidar 0.25 m HSNW, Lidar 0.25 m Slope
n = 33
Lidar 0.25 m - Hillshade NW
Lidar 0.25 m - Slope
Lidar 0.25 m HSNW, Lidar 0.25 m Aspect
n = 28
Lidar 0.25 m - Hillshade NW
Lidar 0.25 m - Aspect
Dextral displacement (m)
Distance from the west end (m)

Figure A3.10

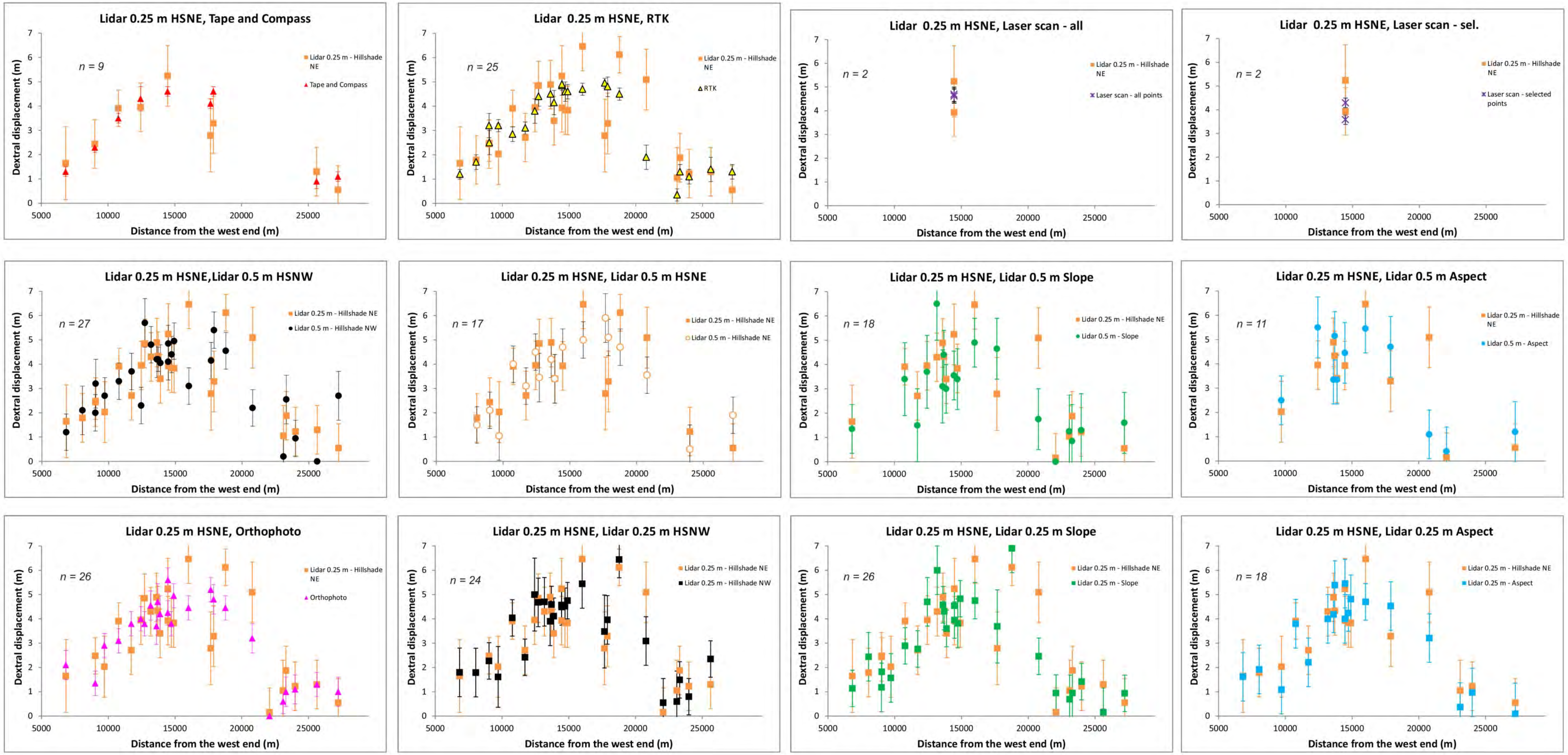
Lidar 0.25 m HSNE, Tape and Compass
Lidar 0.25 m HSNE, RTK
Lidar 0.25 m HSNE, Laser scan - all
Lidar 0.25 m HSNE, Laser scan - sel.
Lidar 0.25 m HSNE,Lidar 0.5 m HSNW
Lidar 0.25 m HSNE, Lidar 0.5 m HSNE
Lidar 0.25 m HSNE, Lidar 0.5 m Slope
Lidar 0.25 m HSNE, Lidar 0.5 m Aspect
Lidar 0.25 m HSNE, Orthophoto
Lidar 0.25 m HSNE, Lidar 0.25 m HSNW
Lidar 0.25 m HSNE, Lidar 0.25 m Slope
Lidar 0.25 m HSNE, Lidar 0.25 m Aspect
Dextral displacement (m)
Distance from the west end (m)
n = 9
n = 25
n = 2
n = 2
n = 27
n = 17
n = 18
n = 11
n = 26
n = 24
n = 26
n = 18
Lidar 0.25 m - Hillshade NE
Tape and Compass
RTK
Laser scan - all points
Laser scan - selected points
Lidar 0.5 m - Hillshade NW
Lidar 0.5 m - Hillshade NE
Lidar 0.5 m - Slope
Lidar 0.5 m - Aspect
Orthophoto
Lidar 0.25 m - Hillshade NW
Lidar 0.25 m - Slope
Lidar 0.25 m - Aspect

Figure A3.11

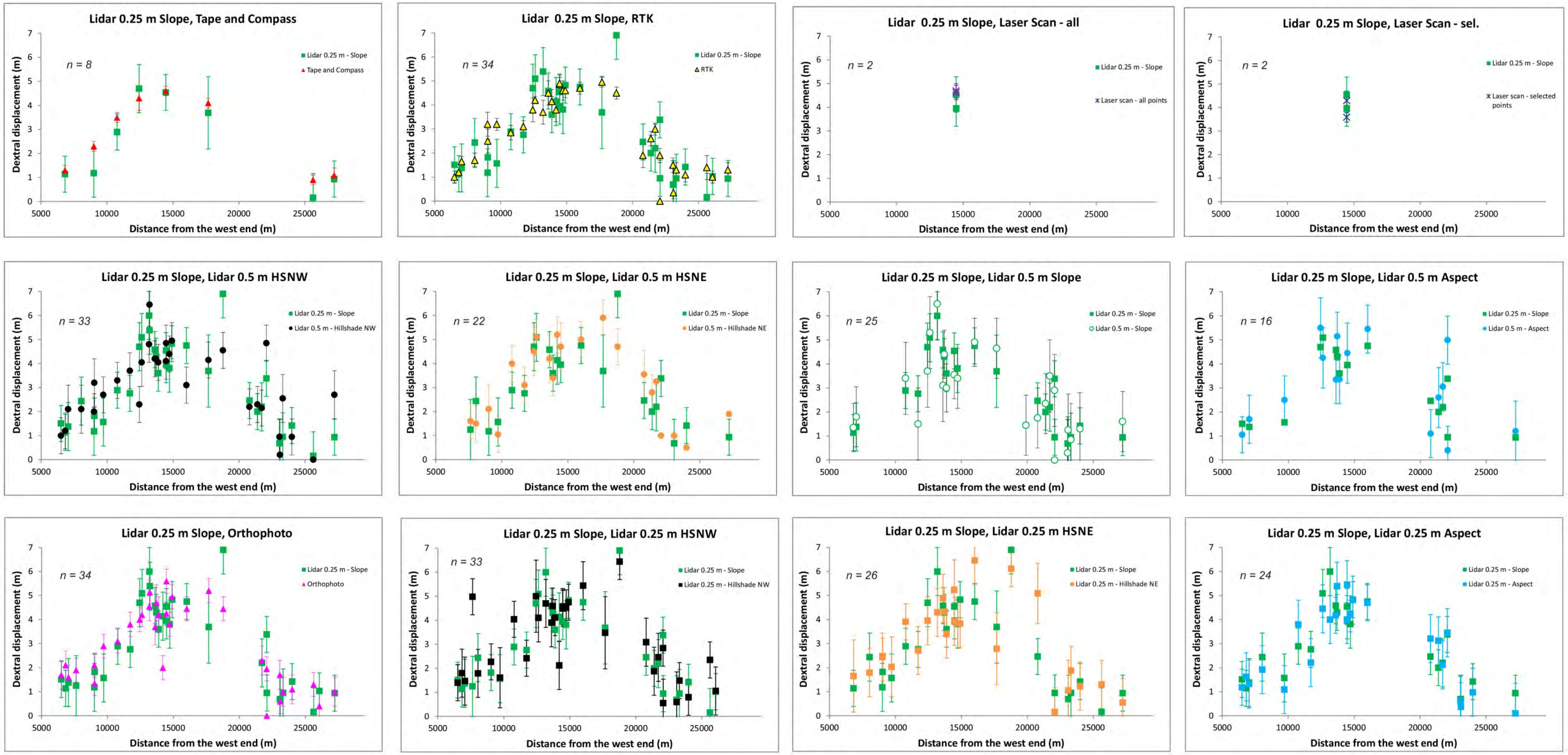
Lidar 0.25 m Slope, Tape and Compass
n = 8
Lidar 0.25 m - Slope
Tape and Compass
Lidar 0.25 m Slope, RTK
n = 34
Lidar 0.25 m - Slope
RTK
Lidar 0.25 m Slope, Laser Scan - all
n = 2
Lidar 0.25 m - Slope
Laser scan - all points
Lidar 0.25 m Slope, Laser Scan - sel.
n = 2
Lidar 0.25 m - Slope
Laser scan - selected points
Lidar 0.25 m Slope, Lidar 0.5 m HSNW
n = 33
Lidar 0.25 m - Slope
Lidar 0.5 m - Hillshade NW
Lidar 0.25 m Slope, Lidar 0.5 m HSNE
n = 22
Lidar 0.25 m - Slope
Lidar 0.5 m - Hillshade NE
Lidar 0.25 m Slope, Lidar 0.5 m Slope
n = 25
Lidar 0.25 m - Slope
Lidar 0.5 m - Slope
Lidar 0.25 m Slope, Lidar 0.5 m Aspect
n = 16
Lidar 0.25 m - Slope
Lidar 0.5 m - Aspect
Lidar 0.25 m Slope, Orthophoto
n = 34
Lidar 0.25 m - Slope
Orthophoto
Lidar 0.25 m Slope, Lidar 0.25 m HSNW
n = 33
Lidar 0.25 m - Slope
Lidar 0.25 m - Hillshade NW
Lidar 0.25 m Slope, Lidar 0.25 m HSNE
n = 26
Lidar 0.25 m - Slope
Lidar 0.25 m - Hillshade NE
Lidar 0.25 m Slope, Lidar 0.25 m Aspect
n = 24
Lidar 0.25 m - Slope
Lidar 0.25 m - Aspect
Dextral displacement (m)
Distance from the west end (m)
0
1
2
3
4
5
6
7
5000
10000
15000
20000
25000

Figure A3.12

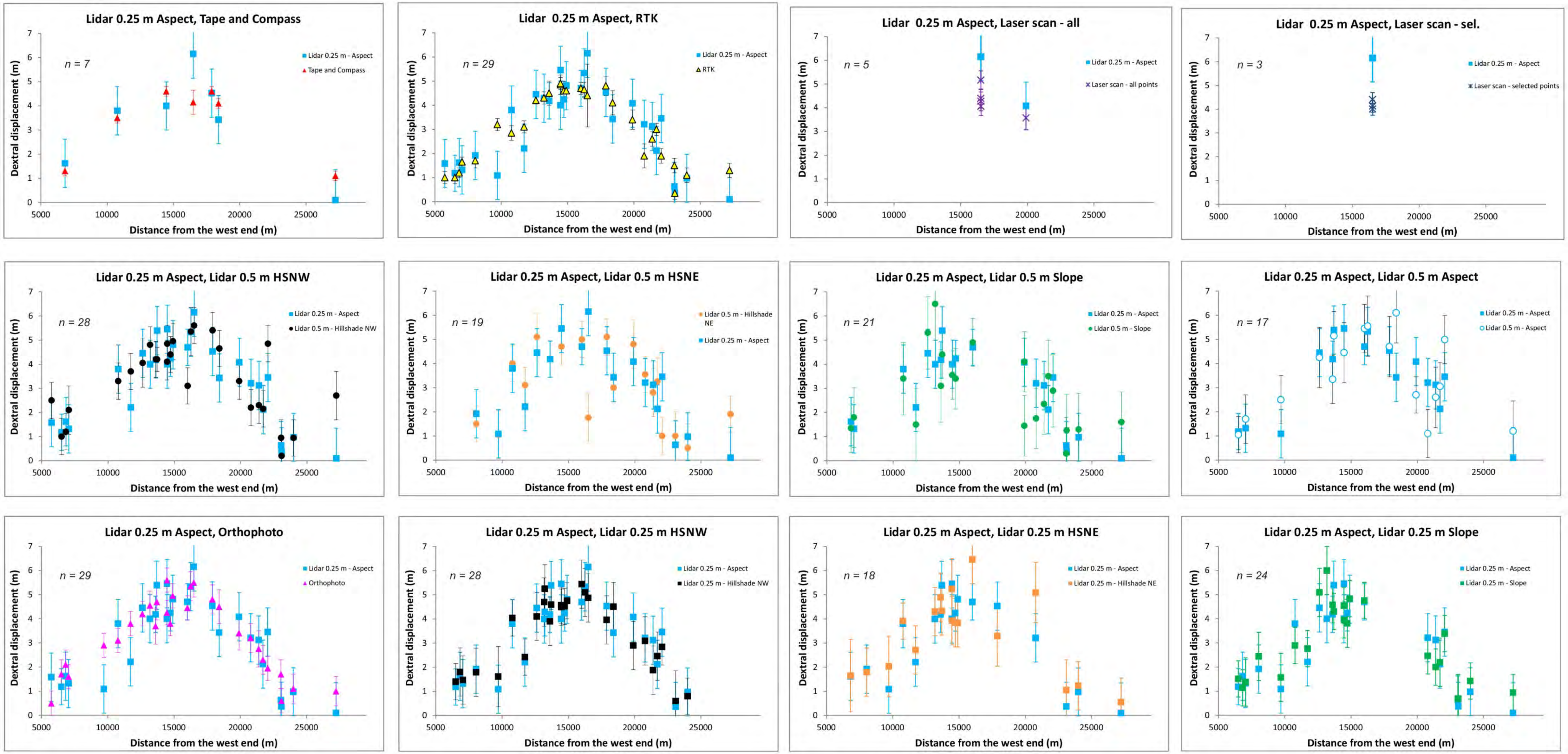

Lidar 0.25 m Aspect, Tape and Compass
n = 7
Lidar 0.25 m - Aspect
Tape and Compass
Lidar 0.25 m Aspect, RTK
n = 29
Lidar 0.25 m - Aspect
RTK
Lidar 0.25 m Aspect, Laser scan - all
n = 5
Lidar 0.25 m - Aspect
Laser scan - all points
Lidar 0.25 m Aspect, Laser scan - sel.
n = 3
Lidar 0.25 m - Aspect
Laser scan - selected points
Lidar 0.25 m Aspect, Lidar 0.5 m HSNW
n = 28
Lidar 0.25 m - Aspect
Lidar 0.5 m - Hillshade NW
Lidar 0.25 m Aspect, Lidar 0.5 m HSNE
n = 19
Lidar 0.5 m - Hillshade NE
Lidar 0.25 m - Aspect
Lidar 0.25 m Aspect, Lidar 0.5 m Slope
n = 21
Lidar 0.25 m - Aspect
Lidar 0.5 m - Slope
Lidar 0.25 m Aspect, Lidar 0.5 m Aspect
n = 17
Lidar 0.25 m - Aspect
Lidar 0.5 m - Aspect
Lidar 0.25 m Aspect, Orthophoto
n = 29
Lidar 0.25 m - Aspect
Orthophoto
Lidar 0.25 m Aspect, Lidar 0.25 m HSNW
n = 28
Lidar 0.25 m - Aspect
Lidar 0.25 m - Hillshade NW
Lidar 0.25 m Aspect, Lidar 0.25 m HSNE
n = 18
Lidar 0.25 m - Aspect
Lidar 0.25 m - Hillshade NE
Lidar 0.25 m Aspect, Lidar 0.25 m Slope
n = 24
Lidar 0.25 m - Aspect
Lidar 0.25 m - Slope
Dextral displacement (m)
Distance from the west end (m)

Figure A3.13

APPENDIX 4: COMPARISON BETWEEN TWO DATASETS: X–Y PLOTS

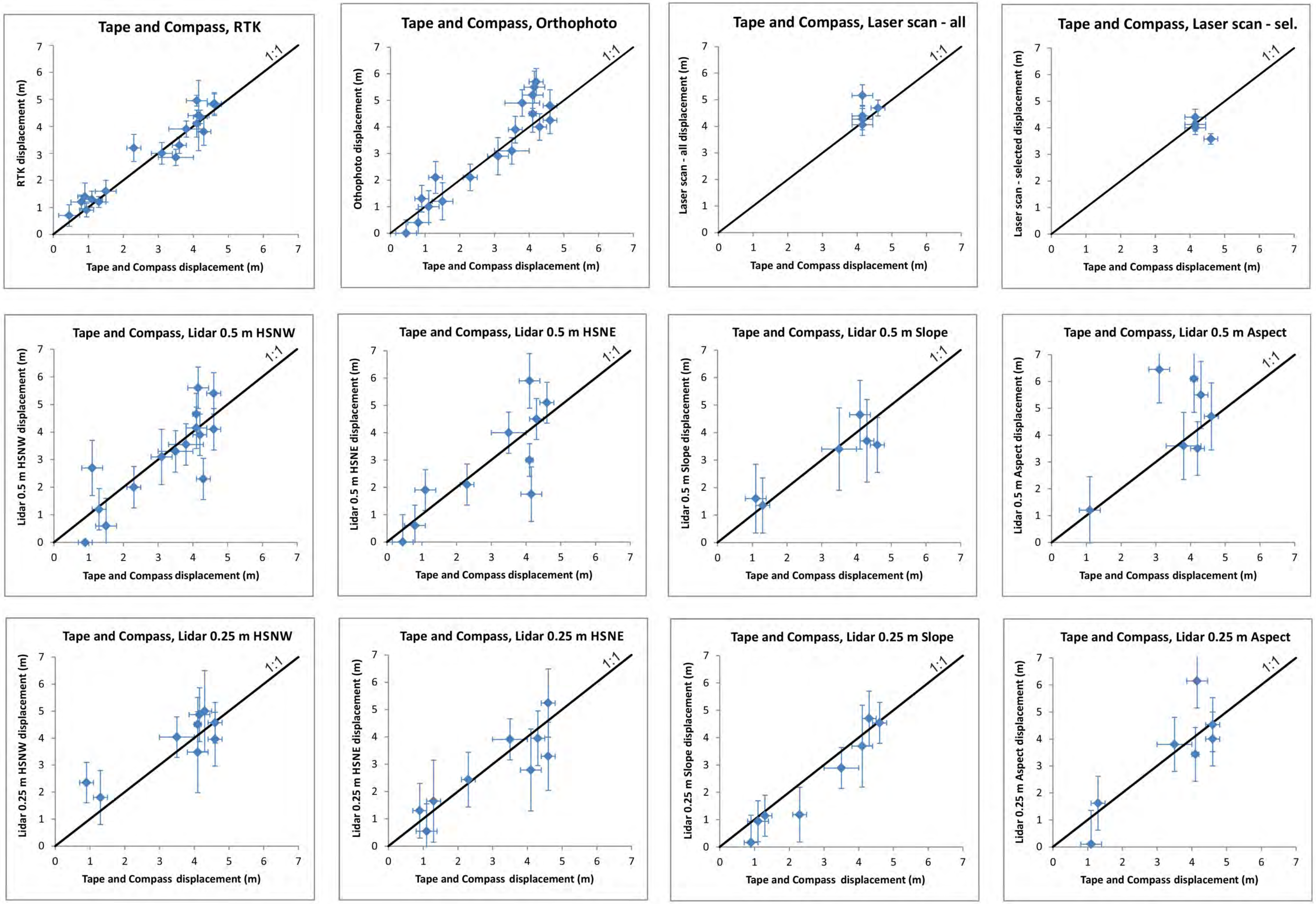

Figure A4.1

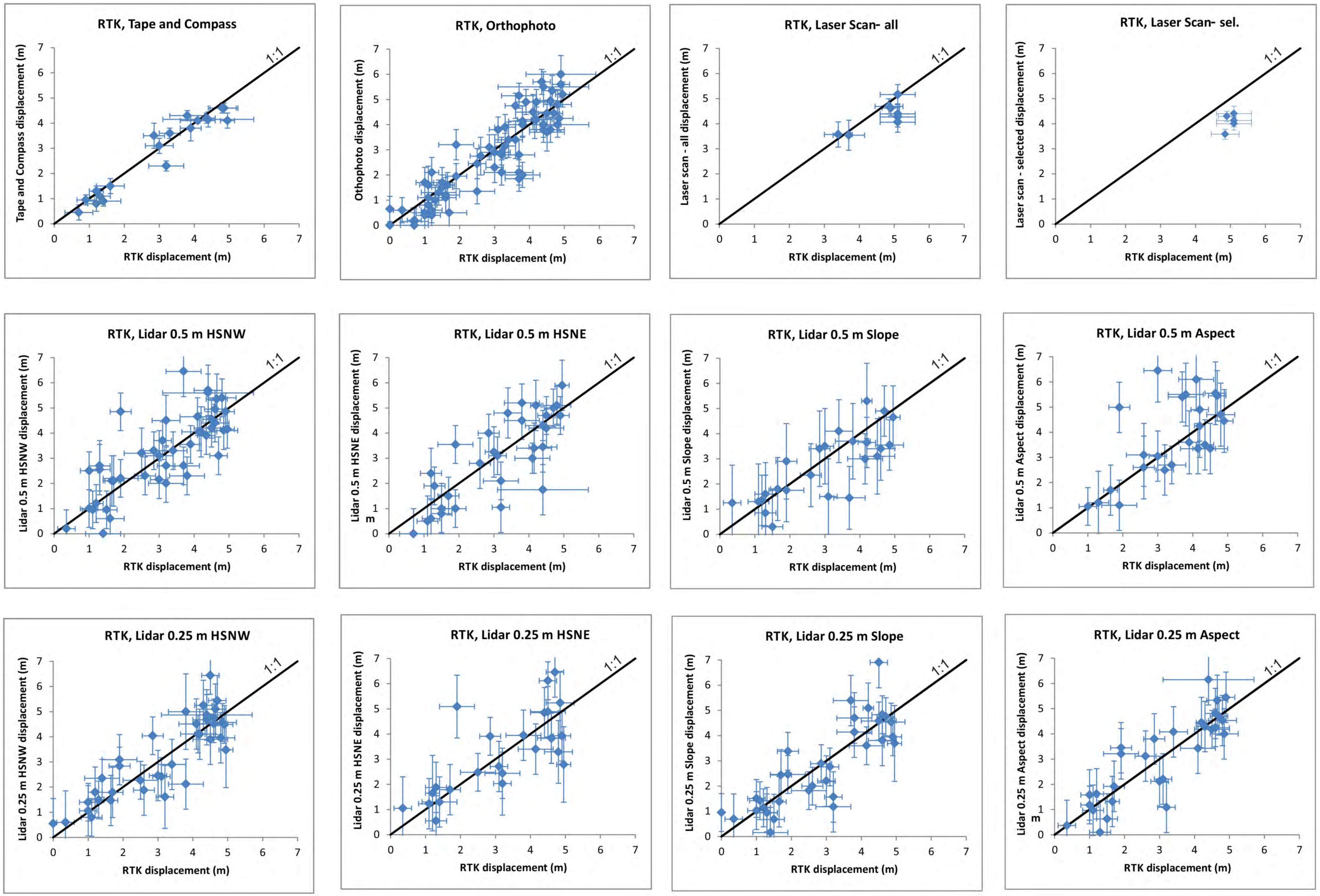
RTK, Tape and Compass
Tape and Compass displacement (m)
RTK displacement (m)
1:1
RTK, Orthophoto
Othophoto displacement (m)
RTK displacement (m)
1:1
RTK, Laser Scan- all
Laser scan - all displacement (m)
RTK displacement (m)
1:1
RTK, Laser Scan- sel.
Laser scan - selected displacement (m)
RTK displacement (m)
1:1
RTK, Lidar 0.5 m HSNW
Lidar 0.5 m HSNW displacement (m)
RTK displacement (m)
1:1
RTK, Lidar 0.5 m HSNE
Lidar 0.5 m HSNE displacement (m)
RTK displacement (m)
1:1
RTK, Lidar 0.5 m Slope
Lidar 0.5 m Slope displacement (m)
RTK displacement (m)
1:1
RTK, Lidar 0.5 m Aspect
Lidar 0.5 m Aspect displacement (m)
RTK displacement (m)
1:1
RTK, Lidar 0.25 m HSNW
Lidar 0.25 m HSNW displacement (m)
RTK displacement (m)
1:1
RTK, Lidar 0.25 m HSNE
Lidar 0.25 m HSNE displacement (m)
RTK displacement (m)
1:1
RTK, Lidar 0.25 m Slope
Lidar 0.25 m Slope displacement (m)
RTK displacement (m)
1:1
RTK, Lidar 0.25 m Aspect
Lidar 0.25 m Aspect displacement (m)
RTK displacement (m)
1:1

Figure A4.2

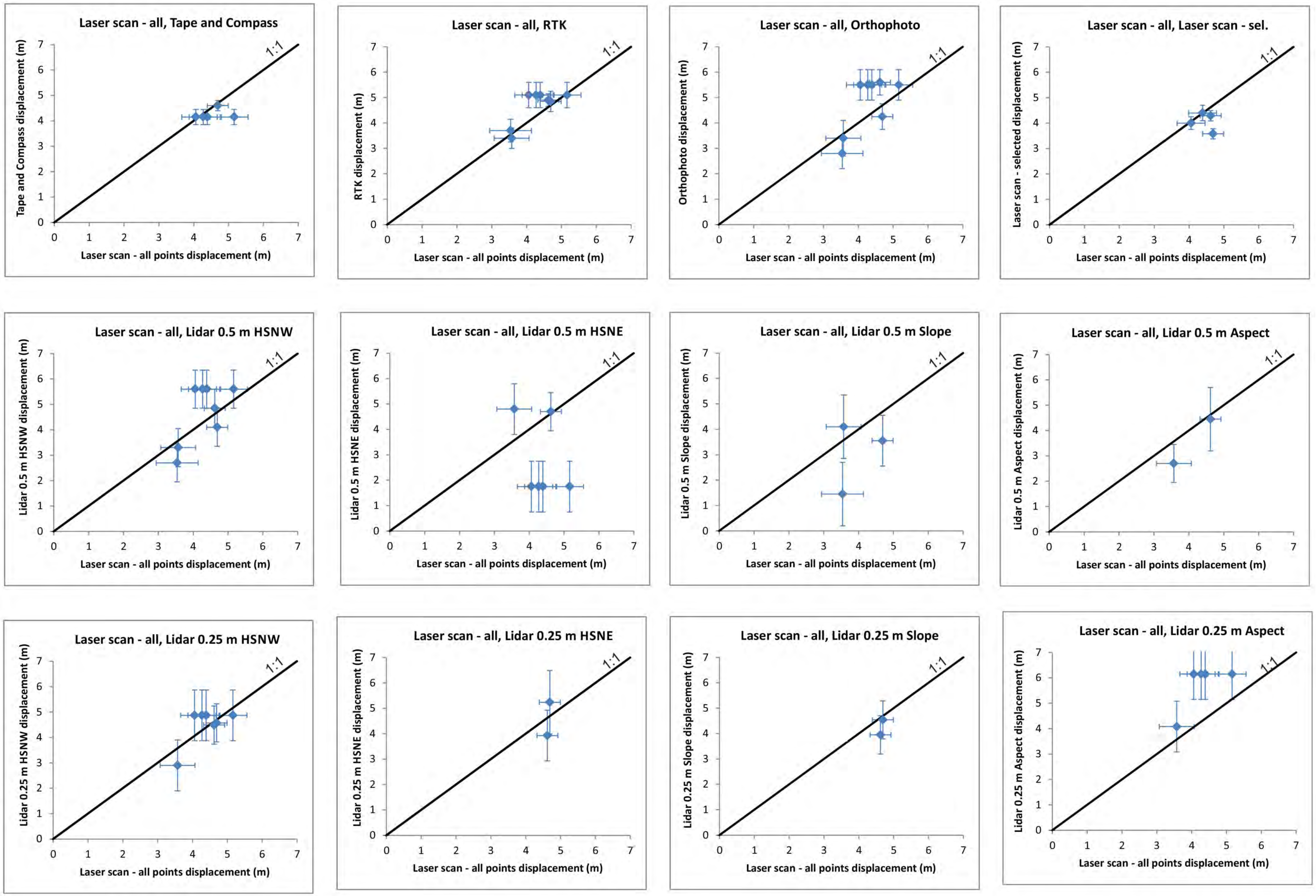
Laser scan - all, Tape and Compass
Tape and Compass displacement (m)
Laser scan - all points displacement (m)
1:1
Laser scan - all, RTK
RTK displacement (m)
Laser scan - all points displacement (m)
1:1
Laser scan - all, Orthophoto
Orthophoto displacement (m)
Laser scan - all points displacement (m)
1:1
Laser scan - all, Laser scan - sel.
Laser scan - selected displacement (m)
Laser scan - all points displacement (m)
1:1
Laser scan - all, Lidar 0.5 m HSNW
Lidar 0.5 m HSNW displacement (m)
Laser scan - all points displacement (m)
1:1
Laser scan - all, Lidar 0.5 m HSNE
Lidar 0.5 m HSNE displacement (m)
Laser scan - all points displacement (m)
1:1
Laser scan - all, Lidar 0.5 m Slope
Lidar 0.5 m Slope displacement (m)
Laser scan - all points displacement (m)
1:1
Laser scan - all, Lidar 0.5 m Aspect
Lidar 0.5 m Aspect displacement (m)
Laser scan - all points displacement (m)
1:1
Laser scan - all, Lidar 0.25 m HSNW
Lidar 0.25 m HSNW displacement (m)
Laser scan - all points displacement (m)
1:1
Laser scan - all, Lidar 0.25 m HSNE
Lidar 0.25 m HSNE displacement (m)
Laser scan - all points displacement (m)
1:1
Laser scan - all, Lidar 0.25 m Slope
Lidar 0.25 m Slope displacement (m)
Laser scan - all points displacement (m)
1:1
Laser scan - all, Lidar 0.25 m Aspect
Lidar 0.25 m Aspect displacement (m)
Laser scan - all points displacement (m)
1:1

Figure A4.3

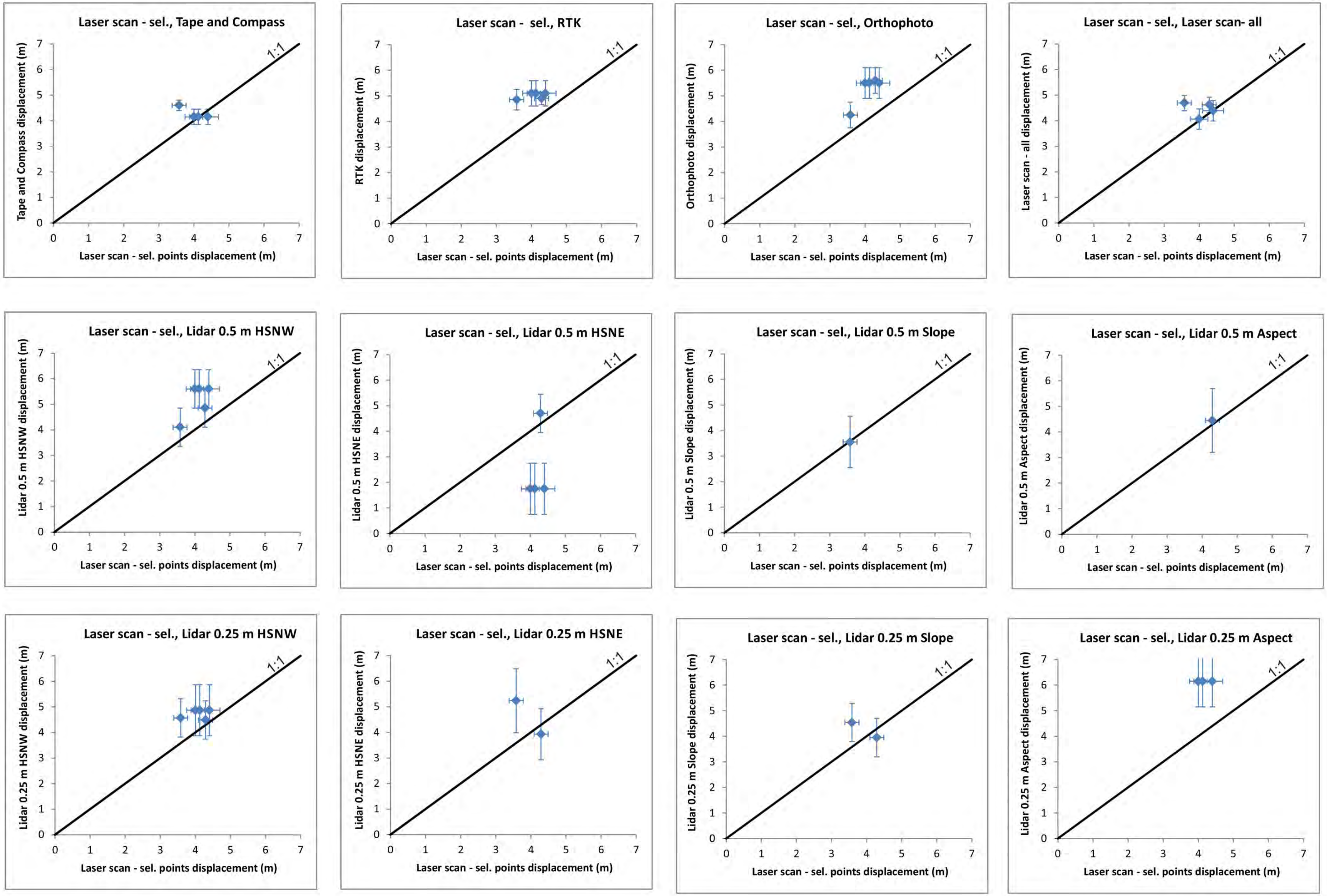

Laser scan - sel., Tape and Compass
Tape and Compass displacement (m)
Laser scan - sel., RTK
RTK displacement (m)
Laser scan - sel., Orthophoto
Orthophoto displacement (m)
Laser scan - sel., Laser scan- all
Laser scan - all displacement (m)
Laser scan - sel., Lidar 0.5 m HSNW
Lidar 0.5 m HSNW displacement (m)
Laser scan - sel., Lidar 0.5 m HSNE
Lidar 0.5 m HSNE displacement (m)
Laser scan - sel., Lidar 0.5 m Slope
Lidar 0.5 m Slope displacement (m)
Laser scan - sel., Lidar 0.5 m Aspect
Lidar 0.5 m Aspect displacement (m)
Laser scan - sel., Lidar 0.25 m HSNW
Lidar 0.25 m HSNW displacement (m)
Laser scan - sel., Lidar 0.25 m HSNE
Lidar 0.25 m HSNE displacement (m)
Laser scan - sel., Lidar 0.25 m Slope
Lidar 0.25 m Slope displacement (m)
Laser scan - sel., Lidar 0.25 m Aspect
Lidar 0.25 m Aspect displacement (m)
Laser scan - sel. points displacement (m)
1:1

Figure A4.4

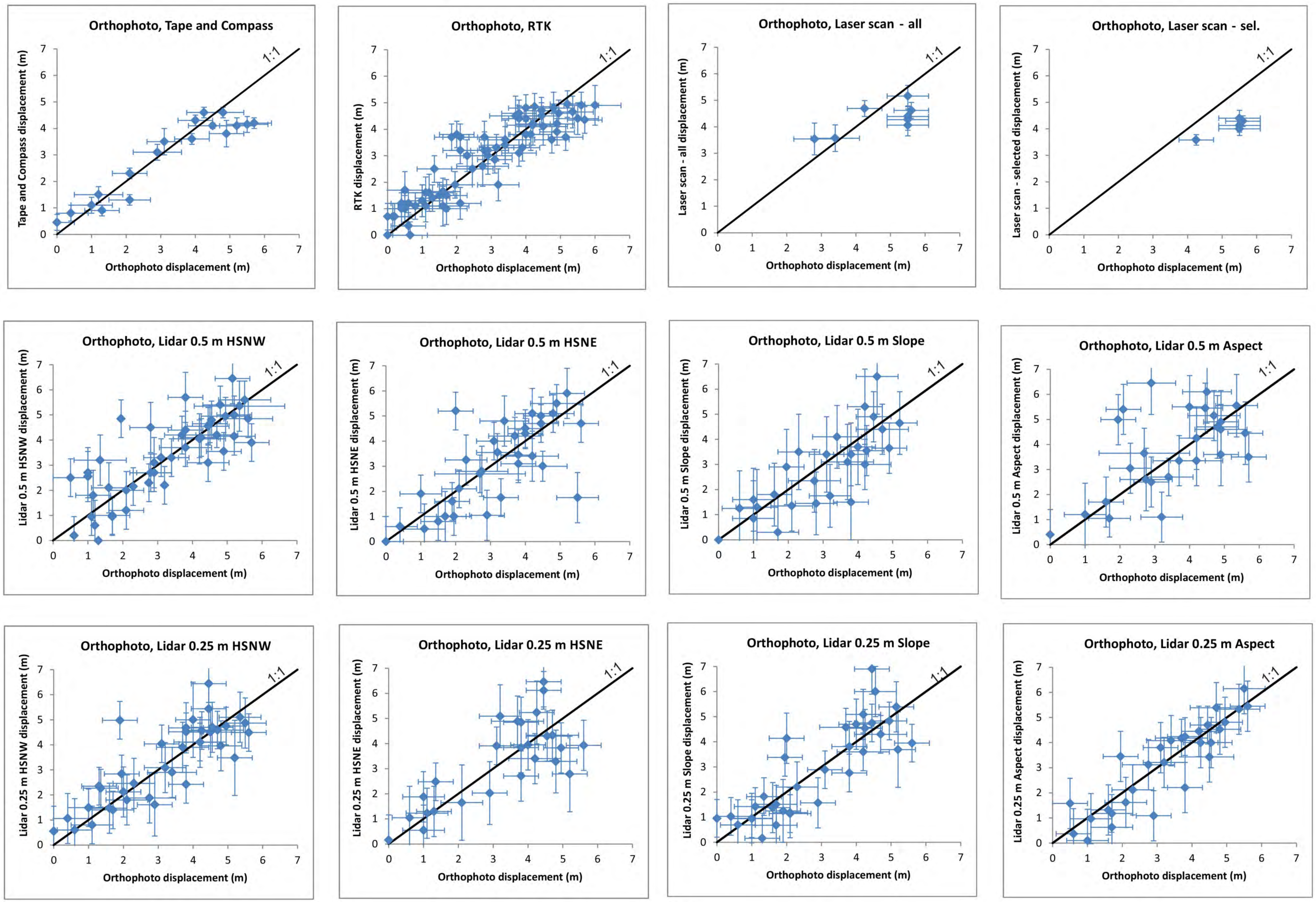

Orthophoto, Tape and Compass
Tape and Compass displacement (m)
Orthophoto displacement (m)
1:1
Orthophoto, RTK
RTK displacement (m)
Orthophoto displacement (m)
1:1
Orthophoto, Laser scan - all
Laser scan - all displacement (m)
Orthophoto displacement (m)
1:1
Orthophoto, Laser scan - sel.
Laser scan - selected displacement (m)
Orthophoto displacement (m)
1:1
Orthophoto, Lidar 0.5 m HSNW
Lidar 0.5 m HSNW displacement (m)
Orthophoto displacement (m)
1:1
Orthophoto, Lidar 0.5 m HSNE
Lidar 0.5 m HSNE displacement (m)
Orthophoto displacement (m)
1:1
Orthophoto, Lidar 0.5 m Slope
Lidar 0.5 m Slope displacement (m)
Orthophoto displacement (m)
1:1
Orthophoto, Lidar 0.5 m Aspect
Lidar 0.5 m Aspect displacement (m)
Orthophoto displacement (m)
1:1
Orthophoto, Lidar 0.25 m HSNW
Lidar 0.25 m HSNW displacement (m)
Orthophoto displacement (m)
1:1
Orthophoto, Lidar 0.25 m HSNE
Lidar 0.25 m HSNE displacement (m)
Orthophoto displacement (m)
1:1
Orthophoto, Lidar 0.25 m Slope
Lidar 0.25 m Slope displacement (m)
Orthophoto displacement (m)
1:1
Orthophoto, Lidar 0.25 m Aspect
Lidar 0.25 m Aspect displacement (m)
Orthophoto displacement (m)
1:1

Figure A4.5

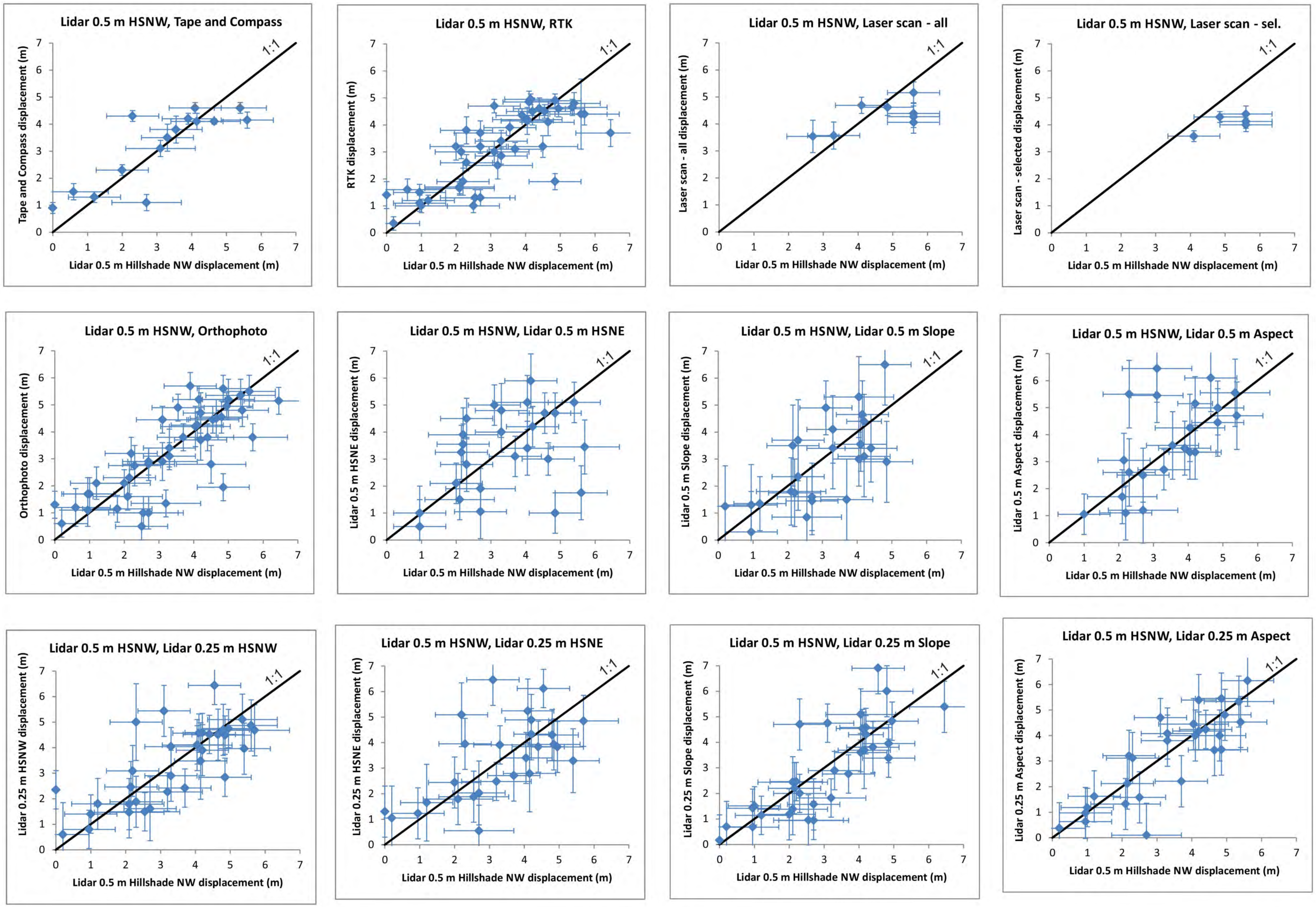
Lidar 0.5 m HSNW, Tape and Compass
Tape and Compass displacement (m)
Lidar 0.5 m HSNW, RTK
RTK displacement (m)
Lidar 0.5 m HSNW, Laser scan - all
Laser scan - all displacement (m)
Lidar 0.5 m HSNW, Laser scan - sel.
Laser scan - selected displacement (m)
Lidar 0.5 m HSNW, Orthophoto
Orthophoto displacement (m)
Lidar 0.5 m HSNW, Lidar 0.5 m HSNE
Lidar 0.5 m HSNE displacement (m)
Lidar 0.5 m HSNW, Lidar 0.5 m Slope
Lidar 0.5 m Slope displacement (m)
Lidar 0.5 m HSNW, Lidar 0.5 m Aspect
Lidar 0.5 m Aspect displacement (m)
Lidar 0.5 m HSNW, Lidar 0.25 m HSNW
Lidar 0.25 m HSNW displacement (m)
Lidar 0.5 m HSNW, Lidar 0.25 m HSNE
Lidar 0.25 m HSNE displacement (m)
Lidar 0.5 m HSNW, Lidar 0.25 m Slope
Lidar 0.25 m Slope displacement (m)
Lidar 0.5 m HSNW, Lidar 0.25 m Aspect
Lidar 0.25 m Aspect displacement (m)
Lidar 0.5 m Hillshade NW displacement (m)
1:1
0
1
2
3
4
5
6
7

Figure A4.6

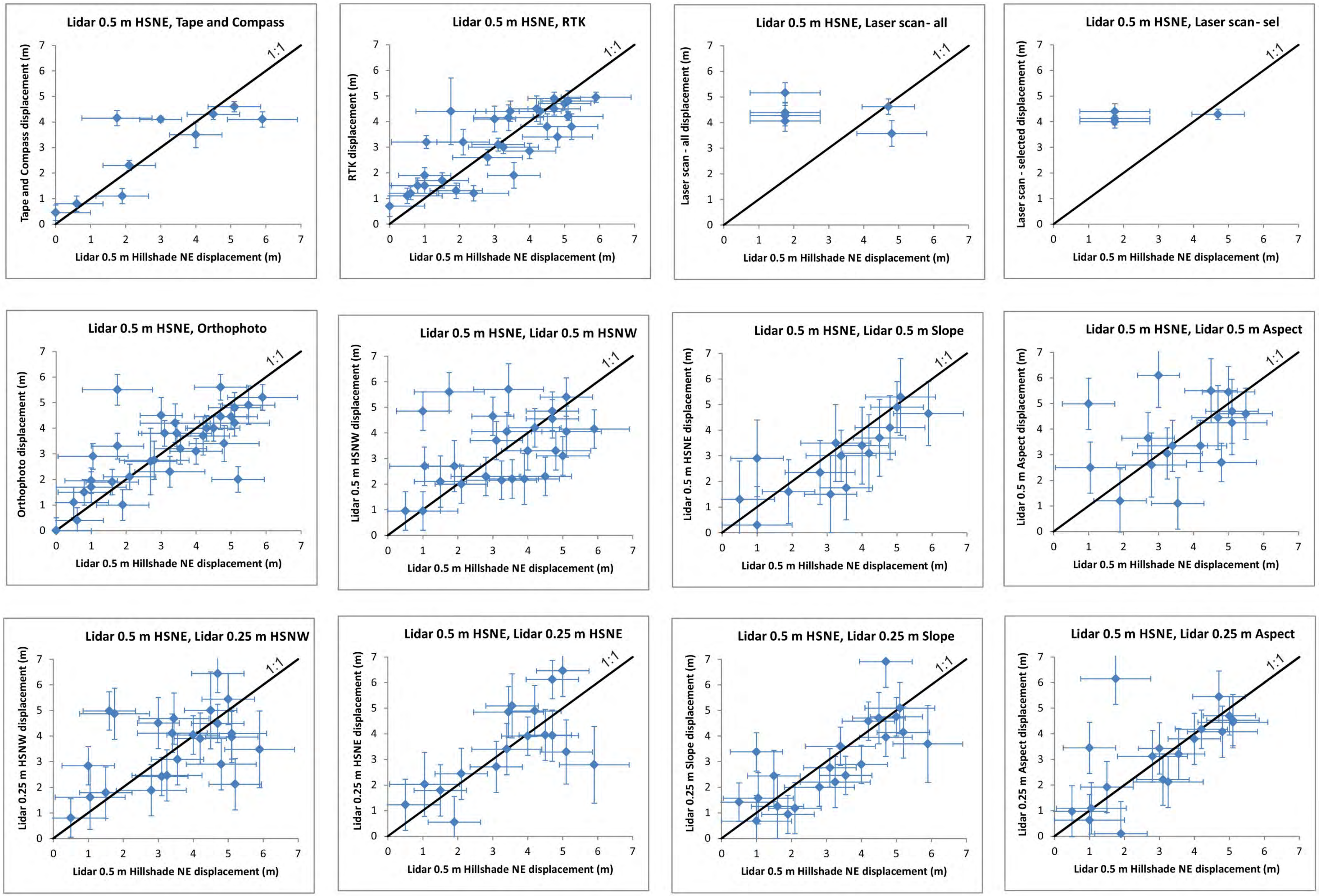
Lidar 0.5 m HSNE, Tape and Compass
Tape and Compass displacement (m)
Lidar 0.5 m HSNE, RTK
RTK displacement (m)
Lidar 0.5 m HSNE, Laser scan- all
Laser scan - all displacement (m)
Lidar 0.5 m HSNE, Laser scan- sel
Laser scan - selected displacement (m)
Lidar 0.5 m HSNE, Orthophoto
Orthophoto displacement (m)
Lidar 0.5 m HSNE, Lidar 0.5 m HSNW
Lidar 0.5 m HSNW displacement (m)
Lidar 0.5 m HSNE, Lidar 0.5 m Slope
Lidar 0.5 m HSNE displacement (m)
Lidar 0.5 m HSNE, Lidar 0.5 m Aspect
Lidar 0.5 m Aspect displacement (m)
Lidar 0.5 m HSNE, Lidar 0.25 m HSNW
Lidar 0.25 m HSNW displacement (m)
Lidar 0.5 m HSNE, Lidar 0.25 m HSNE
Lidar 0.25 m HSNE displacement (m)
Lidar 0.5 m HSNE, Lidar 0.25 m Slope
Lidar 0.25 m Slope displacement (m)
Lidar 0.5 m HSNE, Lidar 0.25 m Aspect
Lidar 0.25 m Aspect displacement (m)
Lidar 0.5 m Hillshade NE displacement (m)
1:1

Figure A4.7

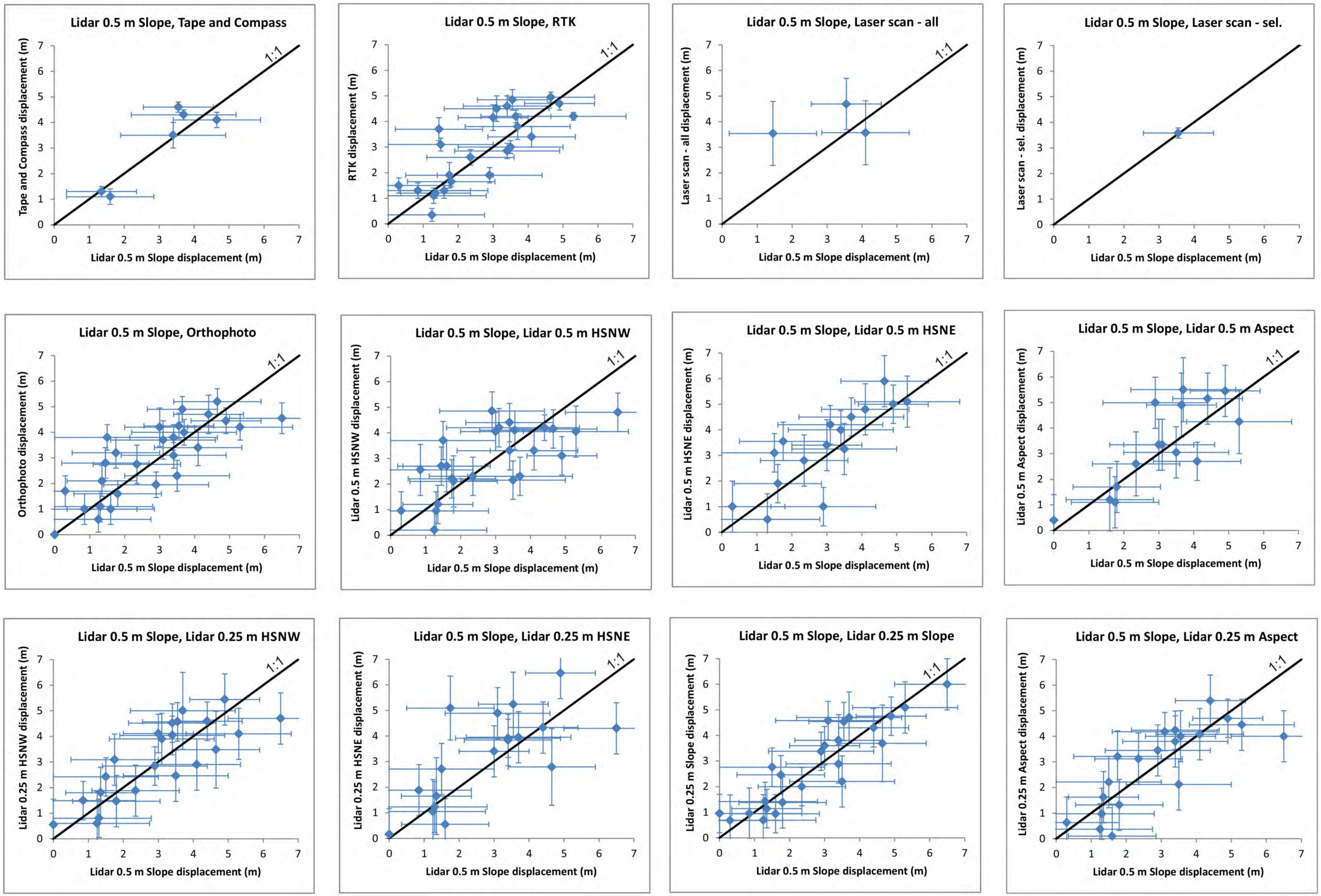
Lidar 0.5 m Slope, Tape and Compass
Tape and Compass displacement (m)
Lidar 0.5 m Slope displacement (m)
1:1
Lidar 0.5 m Slope, RTK
RTK displacement (m)
Lidar 0.5 m Slope displacement (m)
1:1
Lidar 0.5 m Slope, Laser scan - all
Laser scan - all displacement (m)
Lidar 0.5 m Slope displacement (m)
1:1
Lidar 0.5 m Slope, Laser scan - sel.
Laser scan - sel. displacement (m)
Lidar 0.5 m Slope displacement (m)
Lidar 0.5 m Slope, Orthophoto
Orthophoto displacement (m)
Lidar 0.5 m Slope displacement (m)
1:1
Lidar 0.5 m Slope, Lidar 0.5 m HSNW
Lidar 0.5 m HSNW displacement (m)
Lidar 0.5 m Slope displacement (m)
1:1
Lidar 0.5 m Slope, Lidar 0.5 m HSNE
Lidar 0.5 m HSNE displacement (m)
Lidar 0.5 m Slope displacement (m)
1:1
Lidar 0.5 m Slope, Lidar 0.5 m Aspect
Lidar 0.5 m Aspect displacement (m)
Lidar 0.5 m Slope displacement (m)
1:1
Lidar 0.5 m Slope, Lidar 0.25 m HSNW
Lidar 0.25 m HSNW displacement (m)
Lidar 0.5 m Slope displacement (m)
1:1
Lidar 0.5 m Slope, Lidar 0.25 m HSNE
Lidar 0.25 m HSNE displacement (m)
Lidar 0.5 m Slope displacement (m)
1:1
Lidar 0.5 m Slope, Lidar 0.25 m Slope
Lidar 0.25 m Slope displacement (m)
Lidar 0.5 m Slope displacement (m)
1:1
Lidar 0.5 m Slope, Lidar 0.25 m Aspect
Lidar 0.25 m Aspect displacement (m)
Lidar 0.5 m Slope displacement (m)
1:1

Figure A4.8

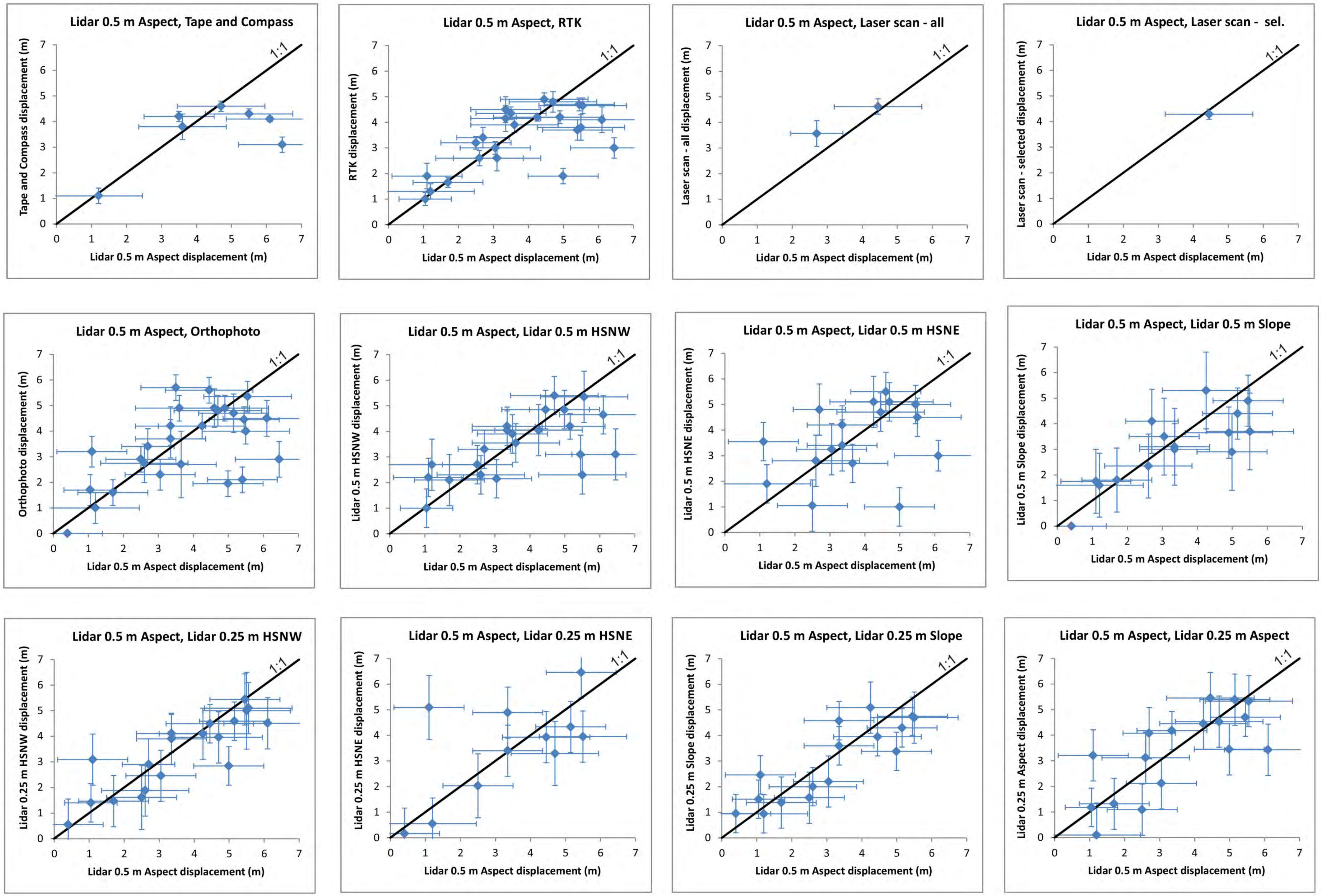
Lidar 0.5 m Aspect, Tape and Compass
Tape and Compass displacement (m)
Lidar 0.5 m Aspect, RTK
RTK displacement (m)
Lidar 0.5 m Aspect, Laser scan - all
Laser scan - all displacement (m)
Lidar 0.5 m Aspect, Laser scan - sel.
Laser scan - selected displacement (m)
Lidar 0.5 m Aspect, Orthophoto
Orthophoto displacement (m)
Lidar 0.5 m Aspect, Lidar 0.5 m HSNW
Lidar 0.5 m HSNW displacement (m)
Lidar 0.5 m Aspect, Lidar 0.5 m HSNE
Lidar 0.5 m HSNE displacement (m)
Lidar 0.5 m Aspect, Lidar 0.5 m Slope
Lidar 0.5 m Slope displacement (m)
Lidar 0.5 m Aspect, Lidar 0.25 m HSNW
Lidar 0.25 m HSNW displacement (m)
Lidar 0.5 m Aspect, Lidar 0.25 m HSNE
Lidar 0.25 m HSNE displacement (m)
Lidar 0.5 m Aspect, Lidar 0.25 m Slope
Lidar 0.25 m Slope displacement (m)
Lidar 0.5 m Aspect, Lidar 0.25 m Aspect
Lidar 0.25 m Aspect displacement (m)
Lidar 0.5 m Aspect displacement (m)
1:1

Figure A4.9

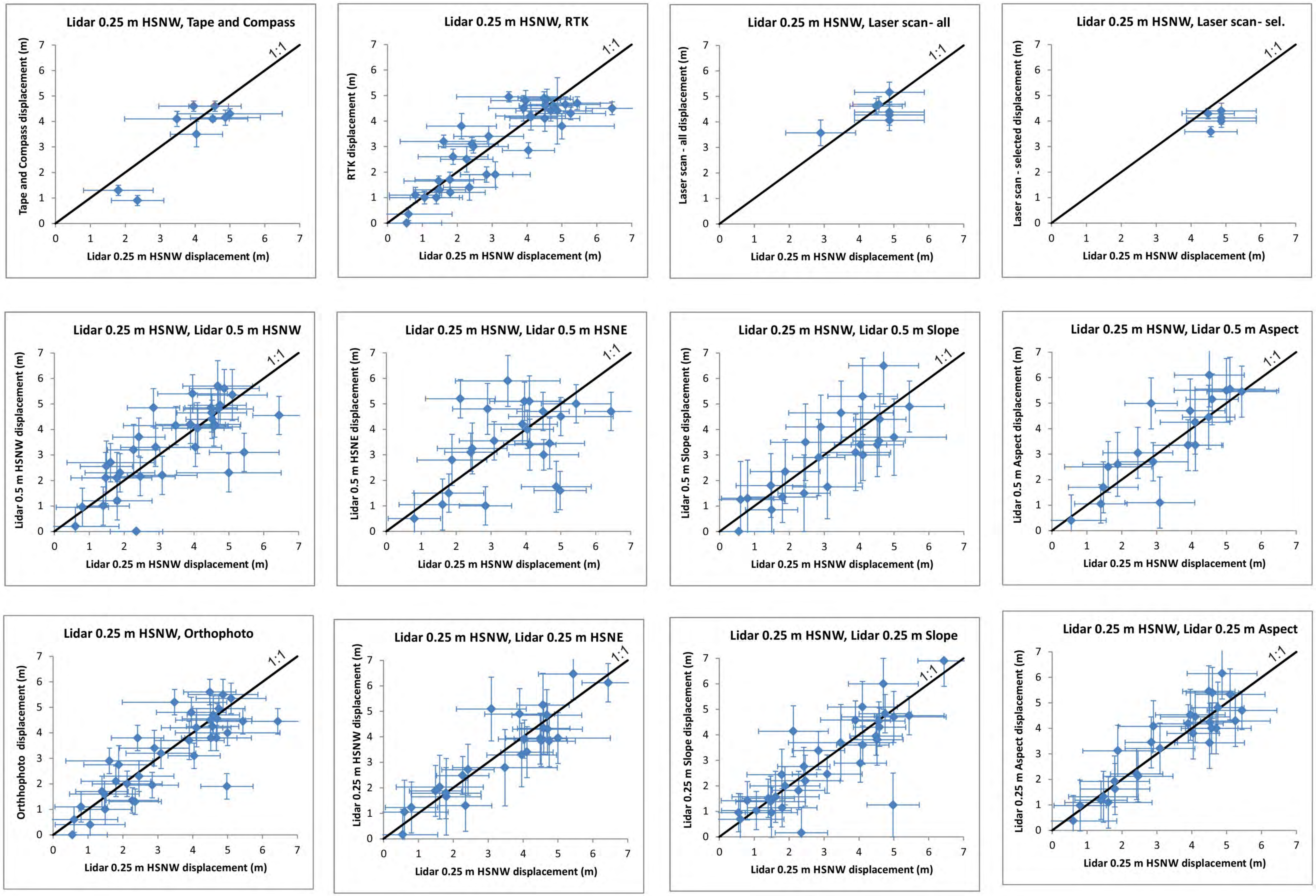
Lidar 0.25 m HSNW, Tape and Compass
Tape and Compass displacement (m)
Lidar 0.25 m HSNW, RTK
RTK displacement (m)
Lidar 0.25 m HSNW, Laser scan- all
Laser scan - all displacement (m)
Lidar 0.25 m HSNW, Laser scan- sel.
Laser scan - selected displacement (m)
Lidar 0.25 m HSNW, Lidar 0.5 m HSNW
Lidar 0.5 m HSNW displacement (m)
Lidar 0.25 m HSNW, Lidar 0.5 m HSNE
Lidar 0.5 m HSNE displacement (m)
Lidar 0.25 m HSNW, Lidar 0.5 m Slope
Lidar 0.5 m Slope displacement (m)
Lidar 0.25 m HSNW, Lidar 0.5 m Aspect
Lidar 0.5 m Aspect displacement (m)
Lidar 0.25 m HSNW, Orthophoto
Orthophoto displacement (m)
Lidar 0.25 m HSNW, Lidar 0.25 m HSNE
Lidar 0.25 m HSNW displacement (m)
Lidar 0.25 m HSNW, Lidar 0.25 m Slope
Lidar 0.25 m Slope displacement (m)
Lidar 0.25 m HSNW, Lidar 0.25 m Aspect
Lidar 0.25 m Aspect displacement (m)
Lidar 0.25 m HSNW displacement (m)
1:1

Figure A4.10

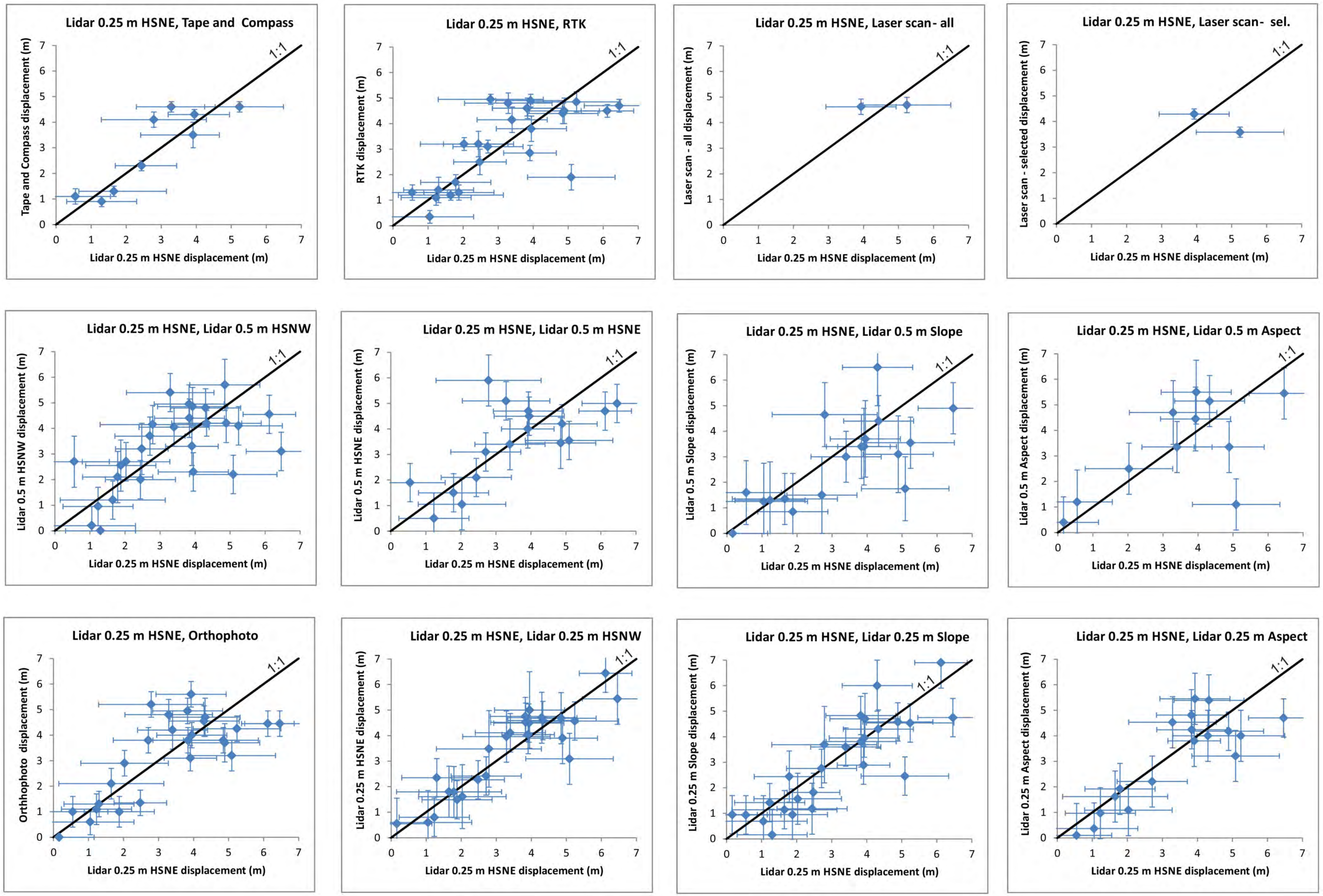
Lidar 0.25 m HSNE, Tape and Compass
Tape and Compass displacement (m)
Lidar 0.25 m HSNE, RTK
RTK displacement (m)
Lidar 0.25 m HSNE, Laser scan- all
Laser scan - all displacement (m)
Lidar 0.25 m HSNE, Laser scan- sel.
Laser scan - selected displacement (m)
Lidar 0.25 m HSNE, Lidar 0.5 m HSNW
Lidar 0.5 m HSNW displacement (m)
Lidar 0.25 m HSNE, Lidar 0.5 m HSNE
Lidar 0.5 m HSNE displacement (m)
Lidar 0.25 m HSNE, Lidar 0.5 m Slope
Lidar 0.5 m Slope displacement (m)
Lidar 0.25 m HSNE, Lidar 0.5 m Aspect
Lidar 0.5 m Aspect displacement (m)
Lidar 0.25 m HSNE, Orthophoto
Orthophoto displacement (m)
Lidar 0.25 m HSNE, Lidar 0.25 m HSNW
Lidar 0.25 m HSNE displacement (m)
Lidar 0.25 m HSNE, Lidar 0.25 m Slope
Lidar 0.25 m Slope displacement (m)
Lidar 0.25 m HSNE, Lidar 0.25 m Aspect
Lidar 0.25 m Aspect displacement (m)
Lidar 0.25 m HSNE displacement (m)
1:1

Figure A4.11

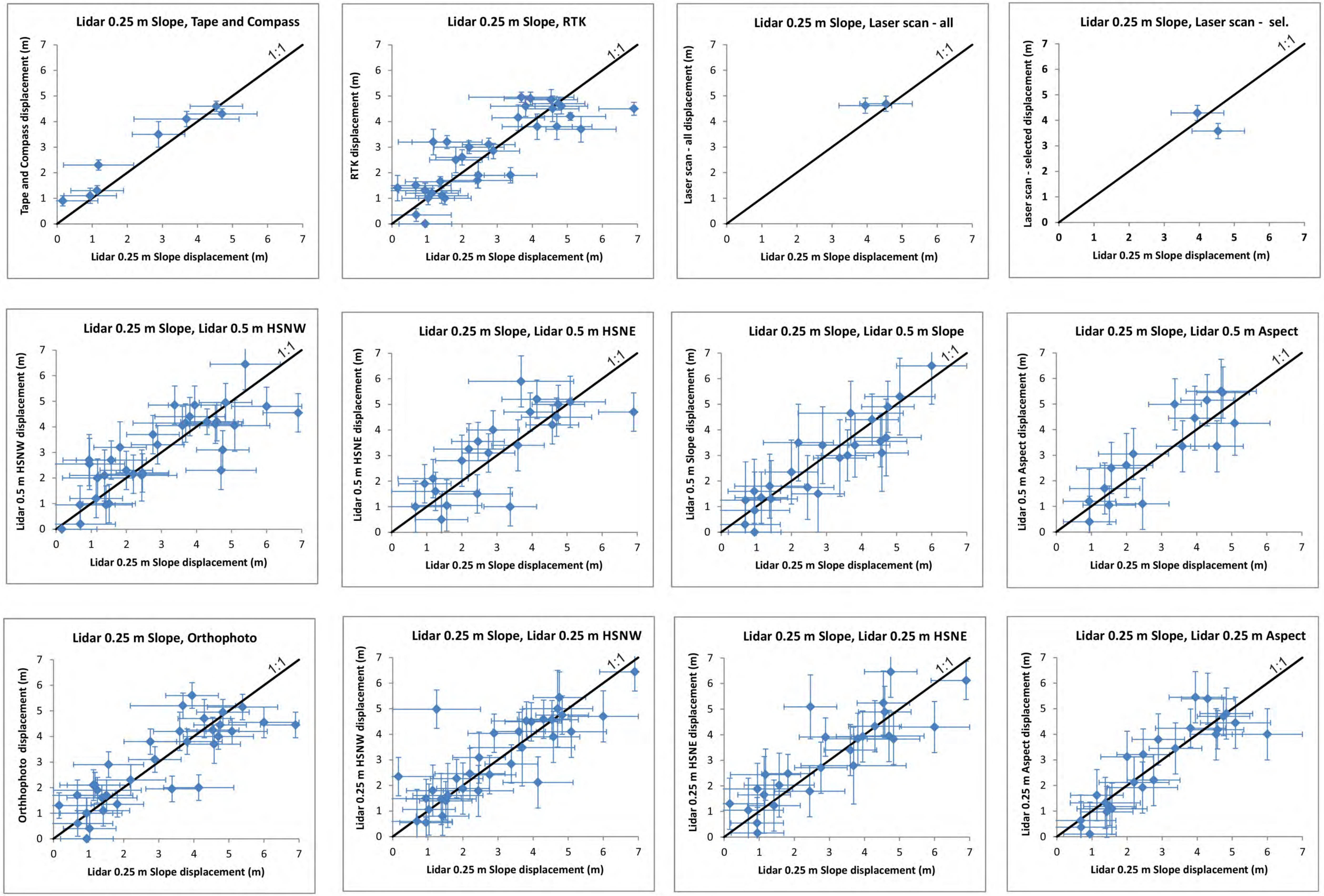
Lidar 0.25 m Slope, Tape and Compass
Tape and Compass displacement (m)
Lidar 0.25 m Slope displacement (m)
Lidar 0.25 m Slope, RTK
RTK displacement (m)
Lidar 0.25 m Slope displacement (m)
Lidar 0.25 m Slope, Laser scan - all
Laser scan - all displacement (m)
Lidar 0.25 m Slope displacement (m)
Lidar 0.25 m Slope, Laser scan - sel.
Laser scan - selected displacement (m)
Lidar 0.25 m Slope displacement (m)
Lidar 0.25 m Slope, Lidar 0.5 m HSNW
Lidar 0.5 m HSNW displacement (m)
Lidar 0.25 m Slope displacement (m)
Lidar 0.25 m Slope, Lidar 0.5 m HSNE
Lidar 0.5 m HSNE displacement (m)
Lidar 0.25 m Slope displacement (m)
Lidar 0.25 m Slope, Lidar 0.5 m Slope
Lidar 0.5 m Slope displacement (m)
Lidar 0.25 m Slope displacement (m)
Lidar 0.25 m Slope, Lidar 0.5 m Aspect
Lidar 0.5 m Aspect displacement (m)
Lidar 0.25 m Slope displacement (m)
Lidar 0.25 m Slope, Orthophoto
Orthophoto displacement (m)
Lidar 0.25 m Slope displacement (m)
Lidar 0.25 m Slope, Lidar 0.25 m HSNW
Lidar 0.25 m HSNW displacement (m)
Lidar 0.25 m Slope displacement (m)
Lidar 0.25 m Slope, Lidar 0.25 m HSNE
Lidar 0.25 m HSNE displacement (m)
Lidar 0.25 m Slope displacement (m)
Lidar 0.25 m Slope, Lidar 0.25 m Aspect
Lidar 0.25 m Aspect displacement (m)
Lidar 0.25 m Slope displacement (m)
1:1

Figure A4.12

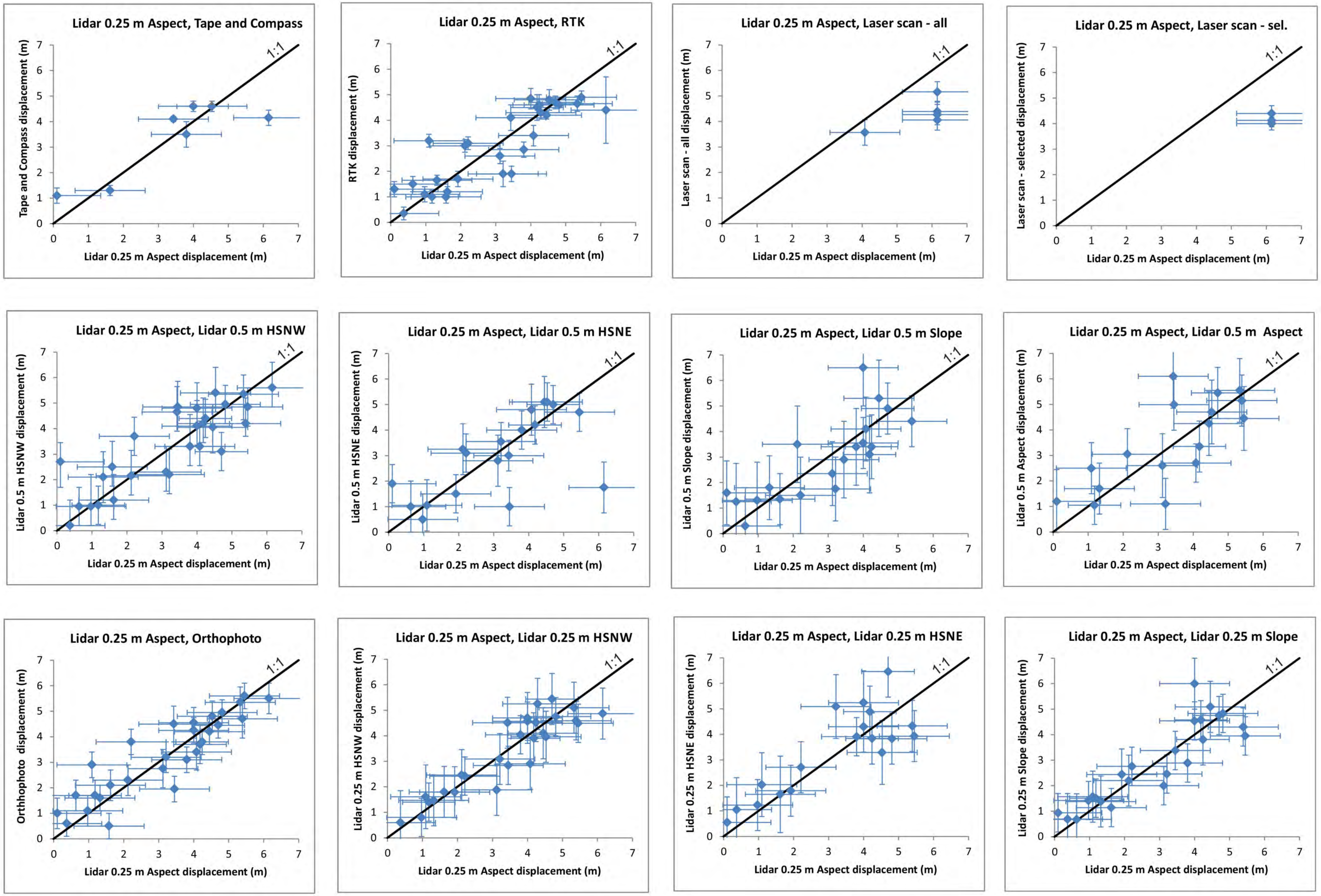

Lidar 0.25 m Aspect, Tape and Compass
Lidar 0.25 m Aspect, RTK
Lidar 0.25 m Aspect, Laser scan - all
Lidar 0.25 m Aspect, Laser scan - sel.
Lidar 0.25 m Aspect, Lidar 0.5 m HSNW
Lidar 0.25 m Aspect, Lidar 0.5 m HSNE
Lidar 0.25 m Aspect, Lidar 0.5 m Slope
Lidar 0.25 m Aspect, Lidar 0.5 m Aspect
Lidar 0.25 m Aspect, Orthophoto
Lidar 0.25 m Aspect, Lidar 0.25 m HSNW
Lidar 0.25 m Aspect, Lidar 0.25 m HSNE
Lidar 0.25 m Aspect, Lidar 0.25 m Slope
Lidar 0.25 m Aspect displacement (m)
Tape and Compass displacement (m)
RTK displacement (m)
Laser scan - all displacement (m)
Laser scan - selected displacement (m)
Lidar 0.5 m HSNW displacement (m)
Lidar 0.5 m HSNE displacement (m)
Lidar 0.5 m Slope displacement (m)
Lidar 0.5 m Aspect displacement (m)
Orthophoto displacement (m)
Lidar 0.25 m HSNW displacement (m)
Lidar 0.25 m HSNE displacement (m)
Lidar 0.25 m Slope displacement (m)
1:1

Figure A4.13

APPENDIX 5: COMPARISON BETWEEN TWO DATASETS: HISTOGRAMS

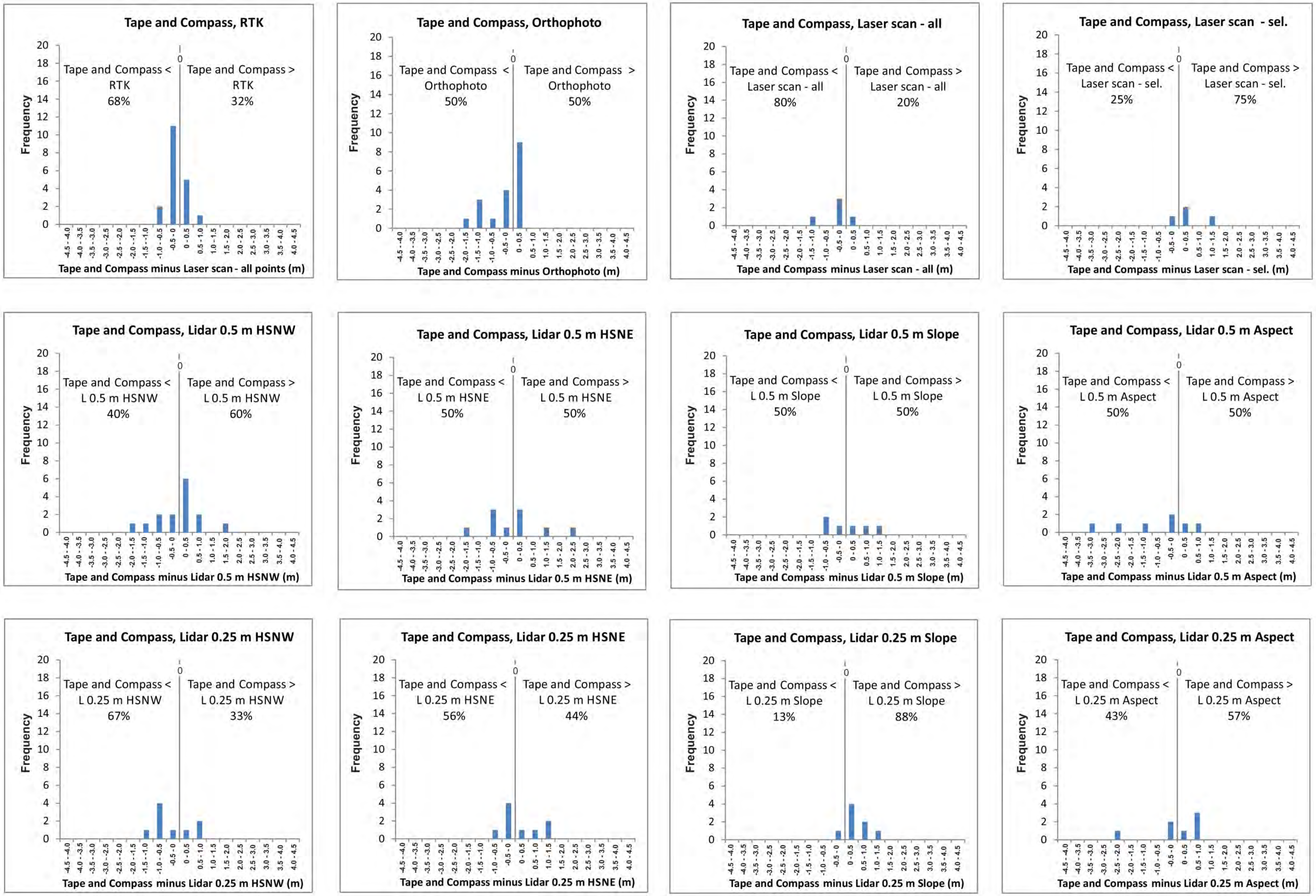

Figure A5.1

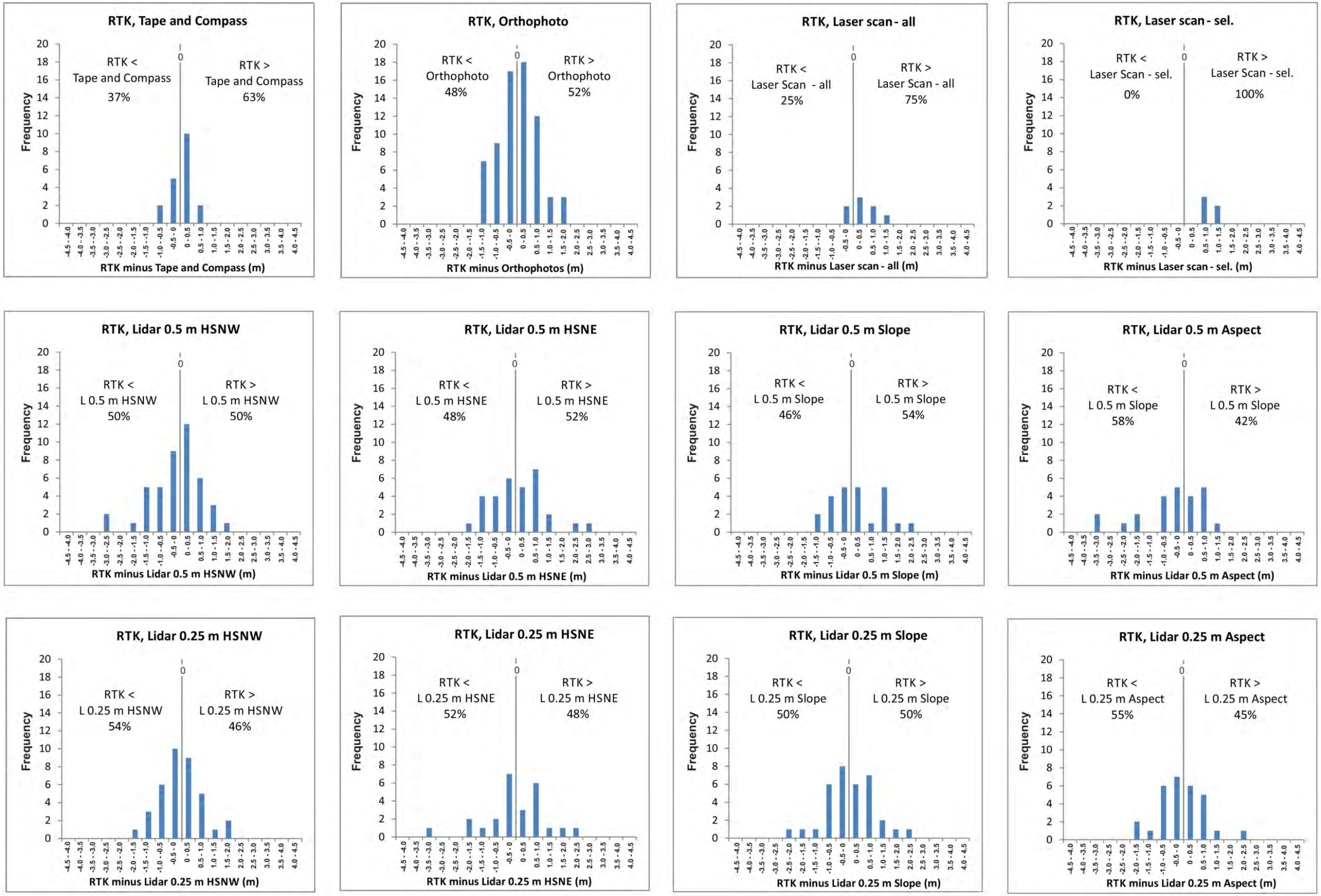
RTK, Tape and Compass
RTK < Tape and Compass 37%
RTK > Tape and Compass 63%
Frequency
RTK minus Tape and Compass (m)
RTK, Orthophoto
RTK < Orthophoto 48%
RTK > Orthophoto 52%
RTK minus Orthophotos (m)
RTK, Laser scan - all
RTK < Laser Scan - all 25%
RTK > Laser Scan - all 75%
RTK minus Laser scan - all (m)
RTK, Laser scan - sel.
RTK < Laser Scan - sel. 0%
RTK > Laser Scan - sel. 100%
RTK minus Laser scan - sel. (m)
RTK, Lidar 0.5 m HSNW
RTK < L 0.5 m HSNW 50%
RTK > L 0.5 m HSNW 50%
RTK minus Lidar 0.5 m HSNW (m)
RTK, Lidar 0.5 m HSNE
RTK < L 0.5 m HSNE 48%
RTK > L 0.5 m HSNE 52%
RTK minus Lidar 0.5 m HSNE (m)
RTK, Lidar 0.5 m Slope
RTK < L 0.5 m Slope 46%
RTK > L 0.5 m Slope 54%
RTK minus Lidar 0.5 m Slope (m)
RTK, Lidar 0.5 m Aspect
RTK < L 0.5 m Slope 58%
RTK > L 0.5 m Slope 42%
RTK minus Lidar 0.5 m Aspect (m)
RTK, Lidar 0.25 m HSNW
RTK < L 0.25 m HSNW 54%
RTK > L 0.25 m HSNW 46%
RTK minus Lidar 0.25 m HSNW (m)
RTK, Lidar 0.25 m HSNE
RTK < L 0.25 m HSNE 52%
RTK > L 0.25 m HSNE 48%
RTK minus Lidar 0.25 m HSNE (m)
RTK, Lidar 0.25 m Slope
RTK < L 0.25 m Slope 50%
RTK > L 0.25 m Slope 50%
RTK minus Lidar 0.25 m Slope (m)
RTK, Lidar 0.25 m Aspect
RTK < L 0.25 m Aspect 55%
RTK > L 0.25 m Aspect 45%
RTK minus Lidar 0.25 m Aspect (m)

Figure A5.2

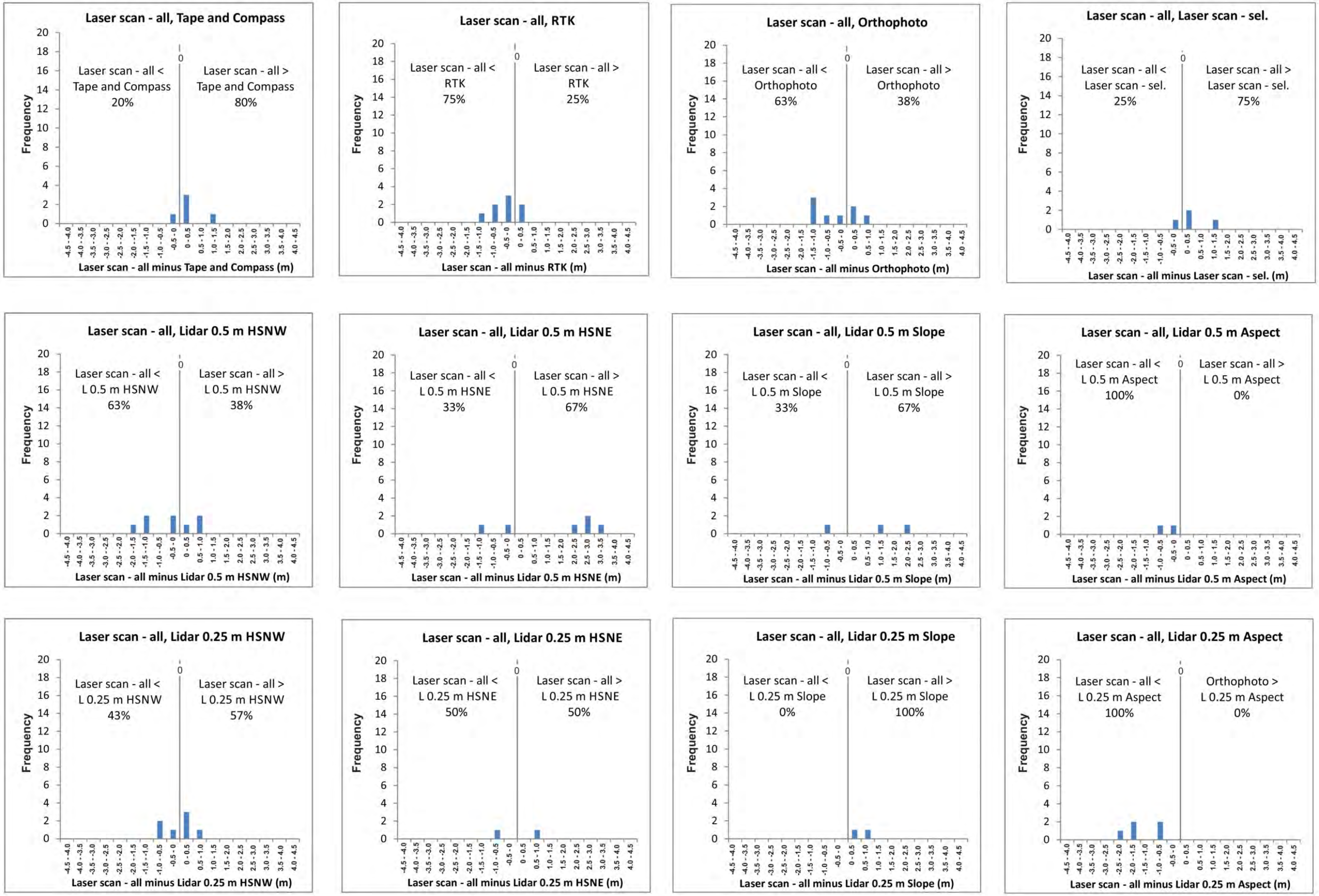
Laser scan - all, Tape and Compass
Laser scan - all < Tape and Compass 20%
Laser scan - all > Tape and Compass 80%
Frequency
Laser scan - all minus Tape and Compass (m)
Laser scan - all, RTK
Laser scan - all < RTK 75%
Laser scan - all > RTK 25%
Laser scan - all minus RTK (m)
Laser scan - all, Orthophoto
Laser scan - all < Orthophoto 63%
Laser scan - all > Orthophoto 38%
Laser scan - all minus Orthophoto (m)
Laser scan - all, Laser scan - sel.
Laser scan - all < Laser scan - sel. 25%
Laser scan - all > Laser scan - sel. 75%
Laser scan - all minus Laser scan - sel. (m)
Laser scan - all, Lidar 0.5 m HSNW
Laser scan - all < L 0.5 m HSNW 63%
Laser scan - all > L 0.5 m HSNW 38%
Laser scan - all minus Lidar 0.5 m HSNW (m)
Laser scan - all, Lidar 0.5 m HSNE
Laser scan - all < L 0.5 m HSNE 33%
Laser scan - all > L 0.5 m HSNE 67%
Laser scan - all minus Lidar 0.5 m HSNE (m)
Laser scan - all, Lidar 0.5 m Slope
Laser scan - all < L 0.5 m Slope 33%
Laser scan - all > L 0.5 m Slope 67%
Laser scan - all minus Lidar 0.5 m Slope (m)
Laser scan - all, Lidar 0.5 m Aspect
Laser scan - all < L 0.5 m Aspect 100%
Laser scan - all > L 0.5 m Aspect 0%
Laser scan - all minus Lidar 0.5 m Aspect (m)
Laser scan - all, Lidar 0.25 m HSNW
Laser scan - all < L 0.25 m HSNW 43%
Laser scan - all > L 0.25 m HSNW 57%
Laser scan - all minus Lidar 0.25 m HSNW (m)
Laser scan - all, Lidar 0.25 m HSNE
Laser scan - all < L 0.25 m HSNE 50%
Laser scan - all > L 0.25 m HSNE 50%
Laser scan - all minus Lidar 0.25 m HSNE (m)
Laser scan - all, Lidar 0.25 m Slope
Laser scan - all < L 0.25 m Slope 0%
Laser scan - all > L 0.25 m Slope 100%
Laser scan - all minus Lidar 0.25 m Slope (m)
Laser scan - all, Lidar 0.25 m Aspect
Laser scan - all < L 0.25 m Aspect 100%
Orthophoto > L 0.25 m Aspect 0%
Laser scan - all minus Lidar 0.25 m Aspect (m)

Figure A5.3

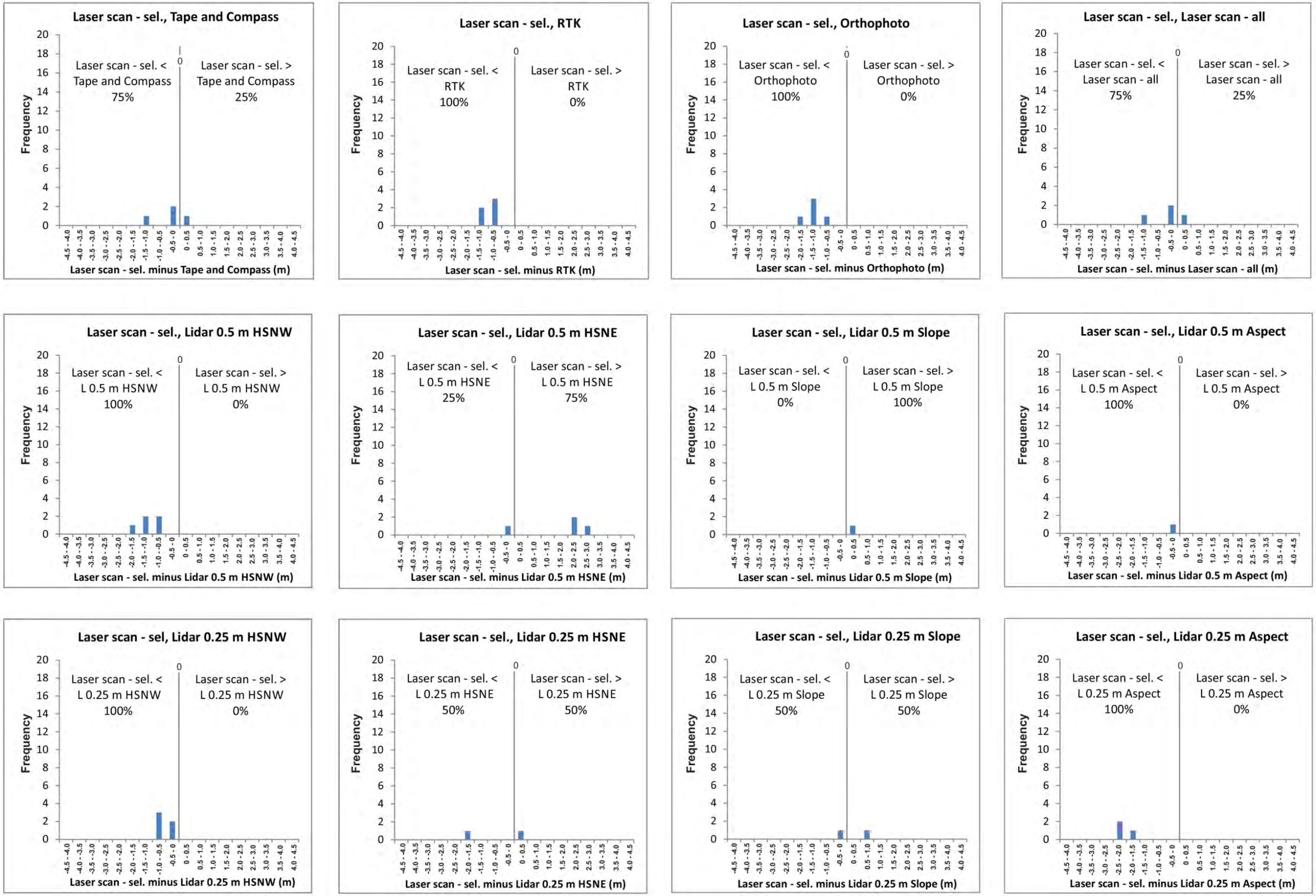

Laser scan - sel., Tape and Compass
Laser scan - sel. < Tape and Compass 75%
Laser scan - sel. > Tape and Compass 25%
Frequency
Laser scan - sel. minus Tape and Compass (m)
Laser scan - sel., RTK
Laser scan - sel. < RTK 100%
Laser scan - sel. > RTK 0%
Laser scan - sel. minus RTK (m)
Laser scan - sel., Orthophoto
Laser scan - sel. < Orthophoto 100%
Laser scan - sel. > Orthophoto 0%
Laser scan - sel. minus Orthophoto (m)
Laser scan - sel., Laser scan - all
Laser scan - sel. < Laser scan - all 75%
Laser scan - sel. > Laser scan - all 25%
Laser scan - sel. minus Laser scan - all (m)
Laser scan - sel., Lidar 0.5 m HSNW
Laser scan - sel. < L 0.5 m HSNW 100%
Laser scan - sel. > L 0.5 m HSNW 0%
Laser scan - sel. minus Lidar 0.5 m HSNW (m)
Laser scan - sel., Lidar 0.5 m HSNE
Laser scan - sel. < L 0.5 m HSNE 25%
Laser scan - sel. > L 0.5 m HSNE 75%
Laser scan - sel. minus Lidar 0.5 m HSNE (m)
Laser scan - sel., Lidar 0.5 m Slope
Laser scan - sel. < L 0.5 m Slope 0%
Laser scan - sel. > L 0.5 m Slope 100%
Laser scan - sel. minus Lidar 0.5 m Slope (m)
Laser scan - sel., Lidar 0.5 m Aspect
Laser scan - sel. < L 0.5 m Aspect 100%
Laser scan - sel. > L 0.5 m Aspect 0%
Laser scan - sel. minus Lidar 0.5 m Aspect (m)
Laser scan - sel, Lidar 0.25 m HSNW
Laser scan - sel. < L 0.25 m HSNW 100%
Laser scan - sel. > L 0.25 m HSNW 0%
Laser scan - sel. minus Lidar 0.25 m HSNW (m)
Laser scan - sel., Lidar 0.25 m HSNE
Laser scan - sel. < L 0.25 m HSNE 50%
Laser scan - sel. > L 0.25 m HSNE 50%
Laser scan - sel. minus Lidar 0.25 m HSNE (m)
Laser scan - sel., Lidar 0.25 m Slope
Laser scan - sel. < L 0.25 m Slope 50%
Laser scan - sel. > L 0.25 m Slope 50%
Laser scan - sel. minus Lidar 0.25 m Slope (m)
Laser scan - sel., Lidar 0.25 m Aspect
Laser scan - sel. < L 0.25 m Aspect 100%
Laser scan - sel. > L 0.25 m Aspect 0%
Laser scan - sel. minus Lidar 0.25 m Aspect (m)

Figure A5.4

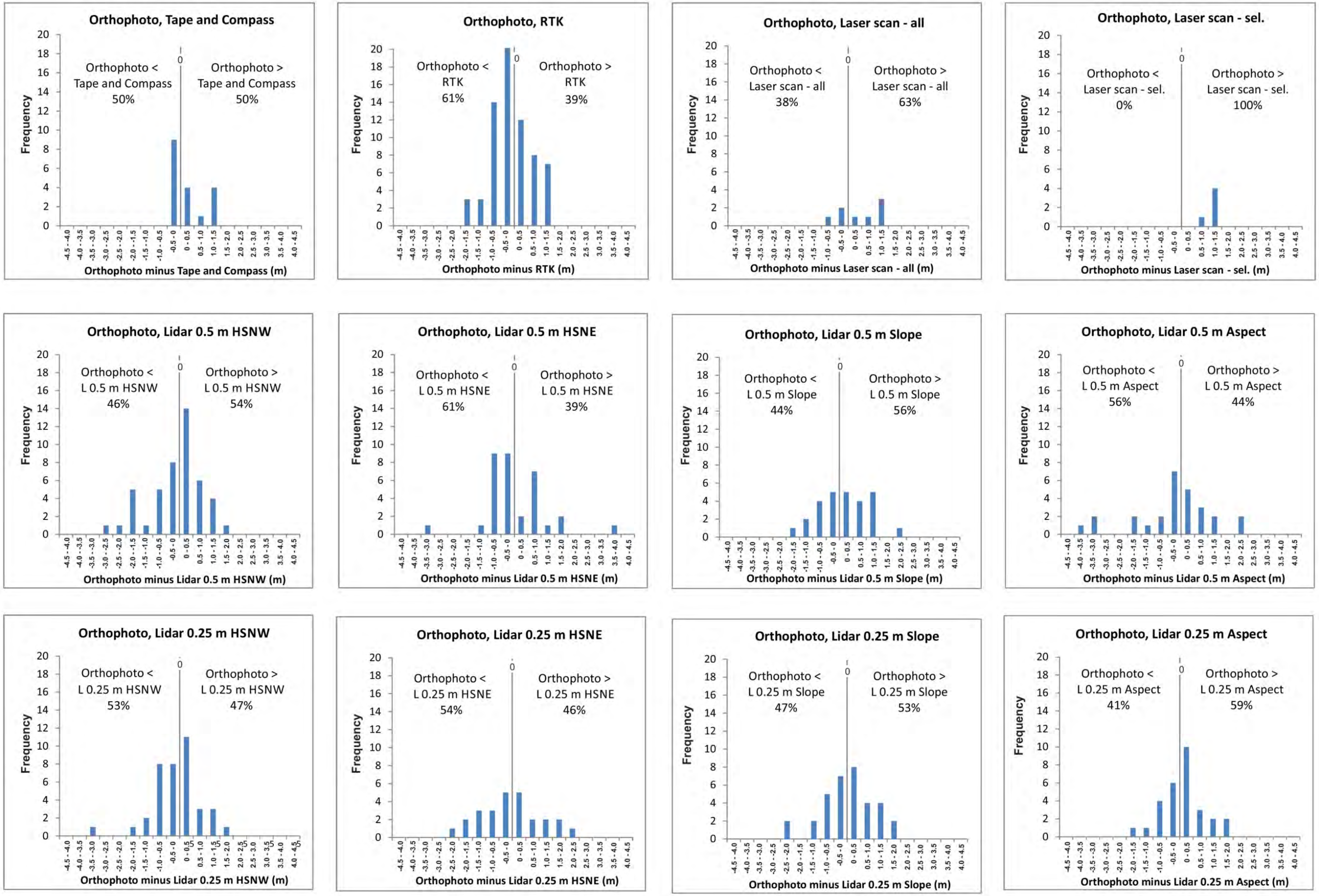
Orthophoto, Tape and Compass
Orthophoto < Tape and Compass 50%
Orthophoto > Tape and Compass 50%
Orthophoto minus Tape and Compass (m)
Orthophoto, RTK
Orthophoto < RTK 61%
Orthophoto > RTK 39%
Orthophoto minus RTK (m)
Orthophoto, Laser scan - all
Orthophoto < Laser scan - all 38%
Orthophoto > Laser scan - all 63%
Orthophoto minus Laser scan - all (m)
Orthophoto, Laser scan - sel.
Orthophoto < Laser scan - sel. 0%
Orthophoto > Laser scan - sel. 100%
Orthophoto minus Laser scan - sel. (m)
Orthophoto, Lidar 0.5 m HSNW
Orthophoto < L 0.5 m HSNW 46%
Orthophoto > L 0.5 m HSNW 54%
Orthophoto minus Lidar 0.5 m HSNW (m)
Orthophoto, Lidar 0.5 m HSNE
Orthophoto < L 0.5 m HSNE 61%
Orthophoto > L 0.5 m HSNE 39%
Orthophoto minus Lidar 0.5 m HSNE (m)
Orthophoto, Lidar 0.5 m Slope
Orthophoto < L 0.5 m Slope 44%
Orthophoto > L 0.5 m Slope 56%
Orthophoto minus Lidar 0.5 m Slope (m)
Orthophoto, Lidar 0.5 m Aspect
Orthophoto < L 0.5 m Aspect 56%
Orthophoto > L 0.5 m Aspect 44%
Orthophoto minus Lidar 0.5 m Aspect (m)
Orthophoto, Lidar 0.25 m HSNW
Orthophoto < L 0.25 m HSNW 53%
Orthophoto > L 0.25 m HSNW 47%
Orthophoto minus Lidar 0.25 m HSNW (m)
Orthophoto, Lidar 0.25 m HSNE
Orthophoto < L 0.25 m HSNE 54%
Orthophoto > L 0.25 m HSNE 46%
Orthophoto minus Lidar 0.25 m HSNE (m)
Orthophoto, Lidar 0.25 m Slope
Orthophoto < L 0.25 m Slope 47%
Orthophoto > L 0.25 m Slope 53%
Orthophoto minus Lidar 0.25 m Slope (m)
Orthophoto, Lidar 0.25 m Aspect
Orthophoto < L 0.25 m Aspect 41%
Orthophoto > L 0.25 m Aspect 59%
Orthophoto minus Lidar 0.25 m Aspect (m)
Frequency

Figure A5.5

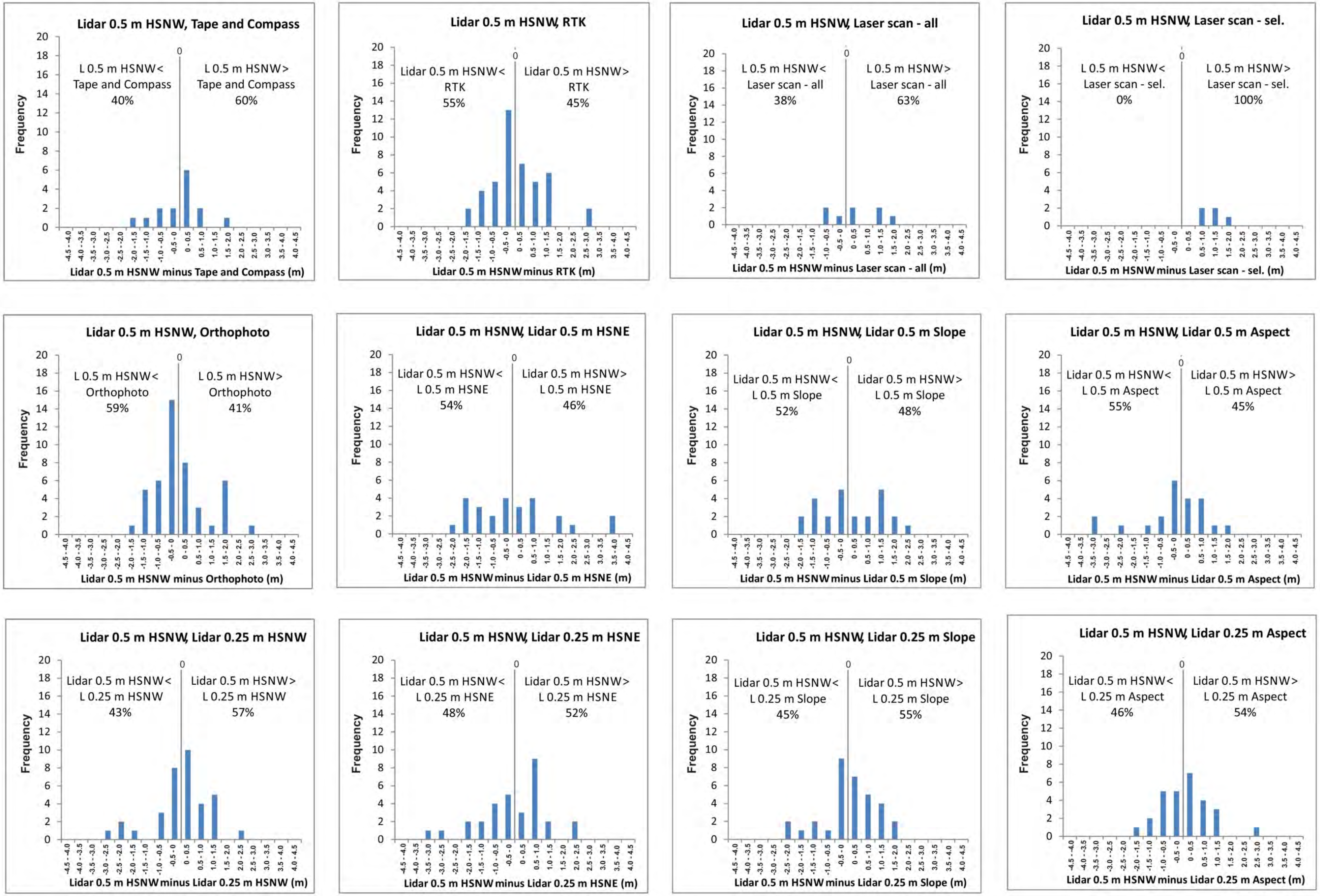
Lidar 0.5 m HSNW, Tape and Compass
L 0.5 m HSNW< Tape and Compass 40%
L 0.5 m HSNW> Tape and Compass 60%
Frequency
Lidar 0.5 m HSNW minus Tape and Compass (m)
Lidar 0.5 m HSNW, RTK
Lidar 0.5 m HSNW< RTK 55%
Lidar 0.5 m HSNW> RTK 45%
Frequency
Lidar 0.5 m HSNW minus RTK (m)
Lidar 0.5 m HSNW, Laser scan - all
L 0.5 m HSNW< Laser scan - all 38%
L 0.5 m HSNW> Laser scan - all 63%
Frequency
Lidar 0.5 m HSNW minus Laser scan - all (m)
Lidar 0.5 m HSNW, Laser scan - sel.
L 0.5 m HSNW< Laser scan - sel. 0%
L 0.5 m HSNW> Laser scan - sel. 100%
Frequency
Lidar 0.5 m HSNW minus Laser scan - sel. (m)
Lidar 0.5 m HSNW, Orthophoto
L 0.5 m HSNW< Orthophoto 59%
L 0.5 m HSNW> Orthophoto 41%
Frequency
Lidar 0.5 m HSNW minus Orthophoto (m)
Lidar 0.5 m HSNW, Lidar 0.5 m HSNE
Lidar 0.5 m HSNW< L 0.5 m HSNE 54%
Lidar 0.5 m HSNW> L 0.5 m HSNE 46%
Frequency
Lidar 0.5 m HSNW minus Lidar 0.5 m HSNE (m)
Lidar 0.5 m HSNW, Lidar 0.5 m Slope
Lidar 0.5 m HSNW< L 0.5 m Slope 52%
Lidar 0.5 m HSNW> L 0.5 m Slope 48%
Frequency
Lidar 0.5 m HSNW minus Lidar 0.5 m Slope (m)
Lidar 0.5 m HSNW, Lidar 0.5 m Aspect
Lidar 0.5 m HSNW< L 0.5 m Aspect 55%
Lidar 0.5 m HSNW> L 0.5 m Aspect 45%
Frequency
Lidar 0.5 m HSNW minus Lidar 0.5 m Aspect (m)
Lidar 0.5 m HSNW, Lidar 0.25 m HSNW
Lidar 0.5 m HSNW< L 0.25 m HSNW 43%
Lidar 0.5 m HSNW> L 0.25 m HSNW 57%
Frequency
Lidar 0.5 m HSNW minus Lidar 0.25 m HSNW (m)
Lidar 0.5 m HSNW, Lidar 0.25 m HSNE
Lidar 0.5 m HSNW< L 0.25 m HSNE 48%
Lidar 0.5 m HSNW> L 0.25 m HSNE 52%
Frequency
Lidar 0.5 m HSNW minus Lidar 0.25 m HSNE (m)
Lidar 0.5 m HSNW, Lidar 0.25 m Slope
Lidar 0.5 m HSNW< L 0.25 m Slope 45%
Lidar 0.5 m HSNW> L 0.25 m Slope 55%
Frequency
Lidar 0.5 m HSNW minus Lidar 0.25 m Slope (m)
Lidar 0.5 m HSNW, Lidar 0.25 m Aspect
Lidar 0.5 m HSNW< L 0.25 m Aspect 46%
Lidar 0.5 m HSNW> L 0.25 m Aspect 54%
Frequency
Lidar 0.5 m HSNW minus Lidar 0.25 m Aspect (m)

Figure A5.6

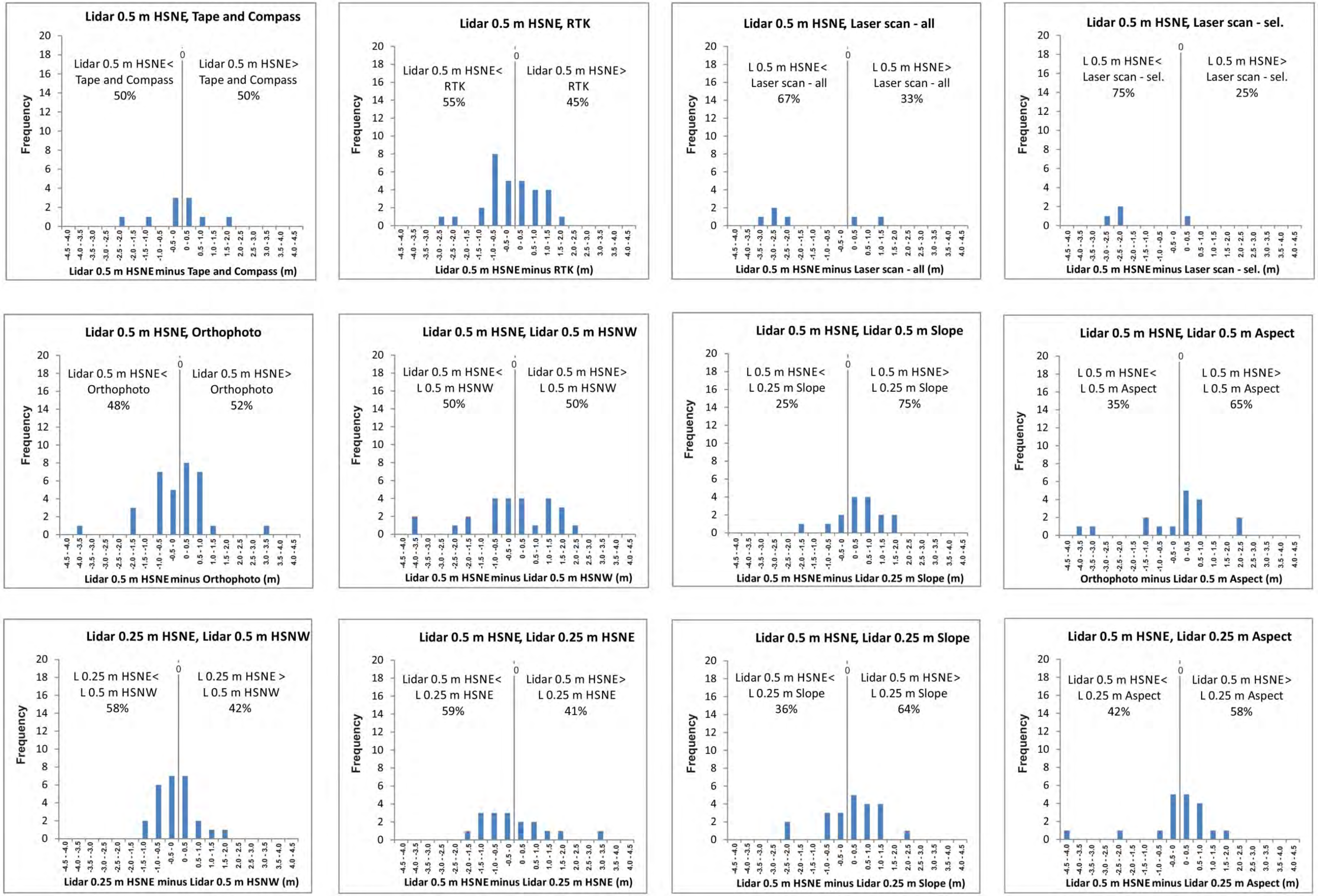
Lidar 0.5 m HSNE, Tape and Compass
Lidar 0.5 m HSNE< Tape and Compass 50%
Lidar 0.5 m HSNE> Tape and Compass 50%
Frequency
Lidar 0.5 m HSNE minus Tape and Compass (m)
Lidar 0.5 m HSNE, RTK
Lidar 0.5 m HSNE< RTK 55%
Lidar 0.5 m HSNE> RTK 45%
Lidar 0.5 m HSNE minus RTK (m)
Lidar 0.5 m HSNE, Laser scan - all
L 0.5 m HSNE< Laser scan - all 67%
L 0.5 m HSNE> Laser scan - all 33%
Lidar 0.5 m HSNE minus Laser scan - all (m)
Lidar 0.5 m HSNE, Laser scan - sel.
L 0.5 m HSNE< Laser scan - sel. 75%
L 0.5 m HSNE> Laser scan - sel. 25%
Lidar 0.5 m HSNE minus Laser scan - sel. (m)
Lidar 0.5 m HSNE, Orthophoto
Lidar 0.5 m HSNE< Orthophoto 48%
Lidar 0.5 m HSNE> Orthophoto 52%
Lidar 0.5 m HSNE minus Orthophoto (m)
Lidar 0.5 m HSNE, Lidar 0.5 m HSNW
Lidar 0.5 m HSNE< L 0.5 m HSNW 50%
Lidar 0.5 m HSNE> L 0.5 m HSNW 50%
Lidar 0.5 m HSNE minus Lidar 0.5 m HSNW (m)
Lidar 0.5 m HSNE, Lidar 0.5 m Slope
L 0.5 m HSNE< L 0.25 m Slope 25%
L 0.5 m HSNE> L 0.25 m Slope 75%
Lidar 0.5 m HSNE minus Lidar 0.25 m Slope (m)
Lidar 0.5 m HSNE, Lidar 0.5 m Aspect
L 0.5 m HSNE< L 0.5 m Aspect 35%
L 0.5 m HSNE> L 0.5 m Aspect 65%
Orthophoto minus Lidar 0.5 m Aspect (m)
Lidar 0.25 m HSNE, Lidar 0.5 m HSNW
L 0.25 m HSNE< L 0.5 m HSNW 58%
L 0.25 m HSNE > L 0.5 m HSNW 42%
Lidar 0.25 m HSNE minus Lidar 0.5 m HSNW (m)
Lidar 0.5 m HSNE, Lidar 0.25 m HSNE
Lidar 0.5 m HSNE< L 0.25 m HSNE 59%
Lidar 0.5 m HSNE> L 0.25 m HSNE 41%
Lidar 0.5 m HSNE minus Lidar 0.25 m HSNE (m)
Lidar 0.5 m HSNE, Lidar 0.25 m Slope
Lidar 0.5 m HSNE< L 0.25 m Slope 36%
Lidar 0.5 m HSNE> L 0.25 m Slope 64%
Lidar 0.5 m HSNE minus Lidar 0.25 m Slope (m)
Lidar 0.5 m HSNE, Lidar 0.25 m Aspect
Lidar 0.5 m HSNE< L 0.25 m Aspect 42%
Lidar 0.5 m HSNE> L 0.25 m Aspect 58%
Lidar 0.5 m HSNE minus Lidar 0.25 m Aspect (m)

Figure A5.7

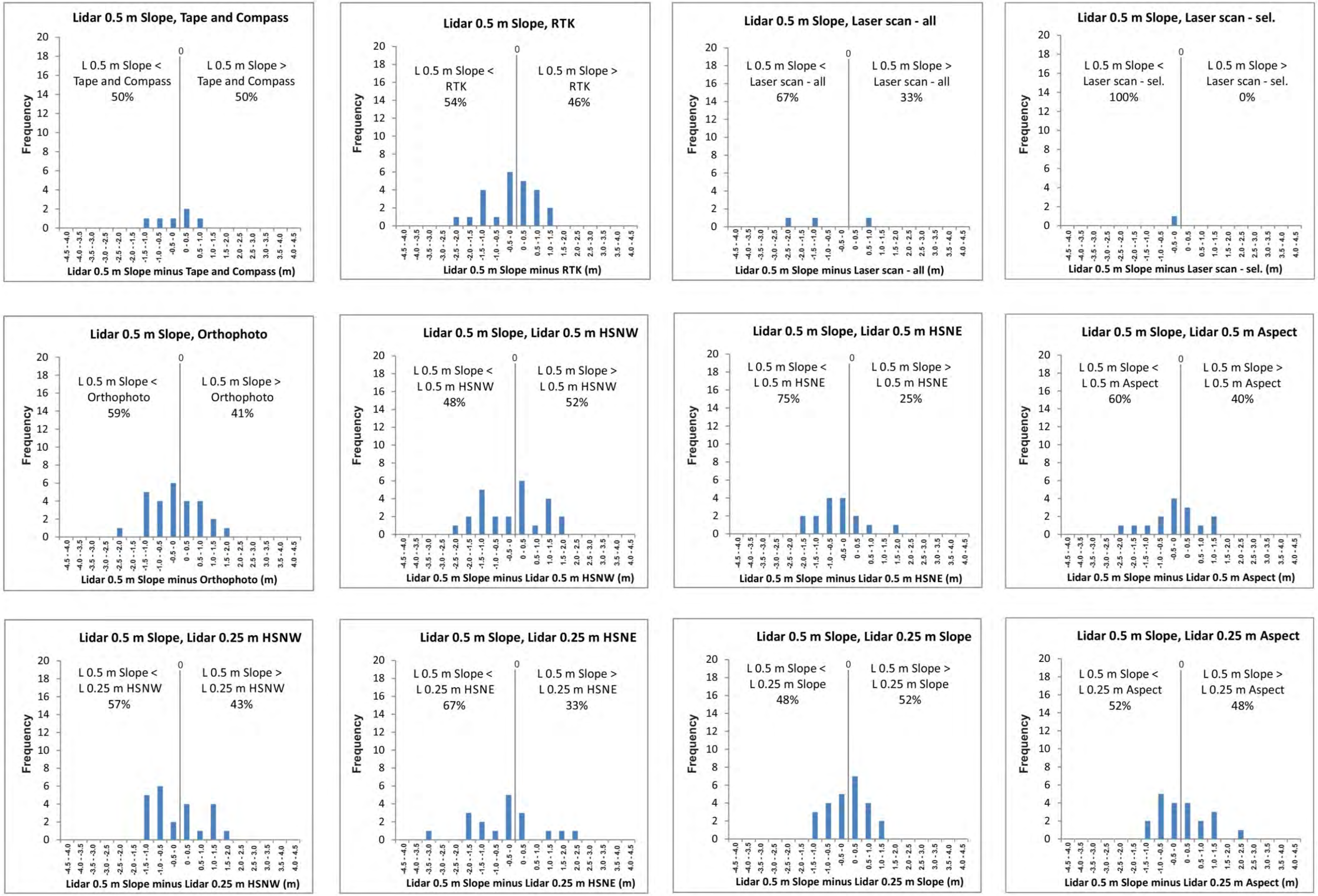
Lidar 0.5 m Slope, Tape and Compass
L 0.5 m Slope < Tape and Compass 50%
L 0.5 m Slope > Tape and Compass 50%
Frequency
Lidar 0.5 m Slope minus Tape and Compass (m)
Lidar 0.5 m Slope, RTK
L 0.5 m Slope < RTK 54%
L 0.5 m Slope > RTK 46%
Lidar 0.5 m Slope minus RTK (m)
Lidar 0.5 m Slope, Laser scan - all
L 0.5 m Slope < Laser scan - all 67%
L 0.5 m Slope > Laser scan - all 33%
Lidar 0.5 m Slope minus Laser scan - all (m)
Lidar 0.5 m Slope, Laser scan - sel.
L 0.5 m Slope < Laser scan - sel. 100%
L 0.5 m Slope > Laser scan - sel. 0%
Lidar 0.5 m Slope minus Laser scan - sel. (m)
Lidar 0.5 m Slope, Orthophoto
L 0.5 m Slope < Orthophoto 59%
L 0.5 m Slope > Orthophoto 41%
Lidar 0.5 m Slope minus Orthophoto (m)
Lidar 0.5 m Slope, Lidar 0.5 m HSNW
L 0.5 m Slope < L 0.5 m HSNW 48%
L 0.5 m Slope > L 0.5 m HSNW 52%
Lidar 0.5 m Slope minus Lidar 0.5 m HSNW (m)
Lidar 0.5 m Slope, Lidar 0.5 m HSNE
L 0.5 m Slope < L 0.5 m HSNE 75%
L 0.5 m Slope > L 0.5 m HSNE 25%
Lidar 0.5 m Slope minus Lidar 0.5 m HSNE (m)
Lidar 0.5 m Slope, Lidar 0.5 m Aspect
L 0.5 m Slope < L 0.5 m Aspect 60%
L 0.5 m Slope > L 0.5 m Aspect 40%
Lidar 0.5 m Slope minus Lidar 0.5 m Aspect (m)
Lidar 0.5 m Slope, Lidar 0.25 m HSNW
L 0.5 m Slope < L 0.25 m HSNW 57%
L 0.5 m Slope > L 0.25 m HSNW 43%
Lidar 0.5 m Slope minus Lidar 0.25 m HSNW (m)
Lidar 0.5 m Slope, Lidar 0.25 m HSNE
L 0.5 m Slope < L 0.25 m HSNE 67%
L 0.5 m Slope > L 0.25 m HSNE 33%
Lidar 0.5 m Slope minus Lidar 0.25 m HSNE (m)
Lidar 0.5 m Slope, Lidar 0.25 m Slope
L 0.5 m Slope < L 0.25 m Slope 48%
L 0.5 m Slope > L 0.25 m Slope 52%
Lidar 0.5 m Slope minus Lidar 0.25 m Slope (m)
Lidar 0.5 m Slope, Lidar 0.25 m Aspect
L 0.5 m Slope < L 0.25 m Aspect 52%
L 0.5 m Slope > L 0.25 m Aspect 48%
Lidar 0.5 m Slope minus Lidar 0.25 m Aspect (m)

Figure A5.8

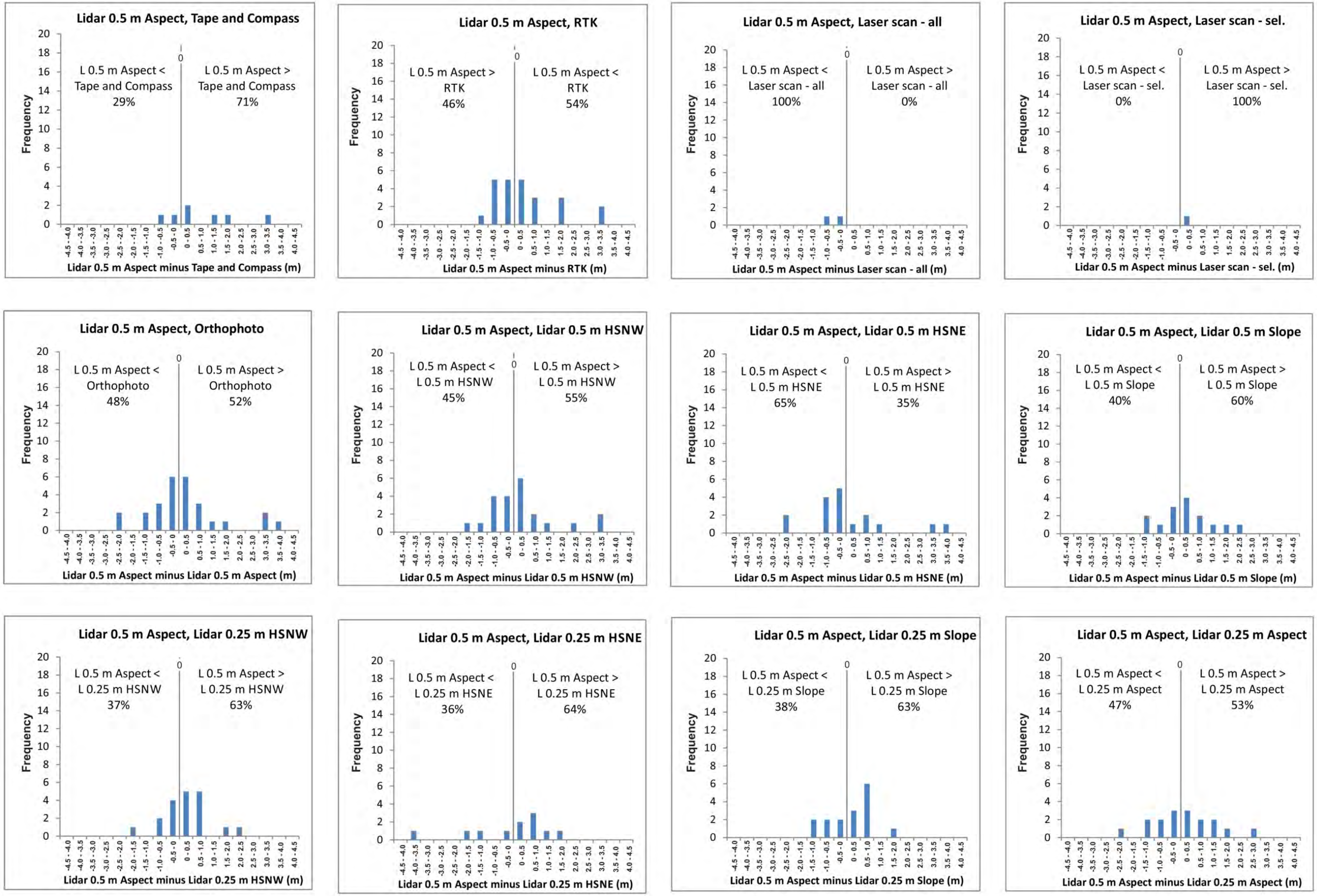

Lidar 0.5 m Aspect, Tape and Compass
L 0.5 m Aspect < Tape and Compass 29%
L 0.5 m Aspect > Tape and Compass 71%
Frequency
Lidar 0.5 m Aspect minus Tape and Compass (m)
Lidar 0.5 m Aspect, RTK
L 0.5 m Aspect > RTK 46%
L 0.5 m Aspect < RTK 54%
Lidar 0.5 m Aspect minus RTK (m)
Lidar 0.5 m Aspect, Laser scan - all
L 0.5 m Aspect < Laser scan - all 100%
L 0.5 m Aspect > Laser scan - all 0%
Lidar 0.5 m Aspect minus Laser scan - all (m)
Lidar 0.5 m Aspect, Laser scan - sel.
L 0.5 m Aspect < Laser scan - sel. 0%
L 0.5 m Aspect > Laser scan - sel. 100%
Lidar 0.5 m Aspect minus Laser scan - sel. (m)
Lidar 0.5 m Aspect, Orthophoto
L 0.5 m Aspect < Orthophoto 48%
L 0.5 m Aspect > Orthophoto 52%
Lidar 0.5 m Aspect minus Lidar 0.5 m Aspect (m)
Lidar 0.5 m Aspect, Lidar 0.5 m HSNW
L 0.5 m Aspect < L 0.5 m HSNW 45%
L 0.5 m Aspect > L 0.5 m HSNW 55%
Lidar 0.5 m Aspect minus Lidar 0.5 m HSNW (m)
Lidar 0.5 m Aspect, Lidar 0.5 m HSNE
L 0.5 m Aspect < L 0.5 m HSNE 65%
L 0.5 m Aspect > L 0.5 m HSNE 35%
Lidar 0.5 m Aspect minus Lidar 0.5 m HSNE (m)
Lidar 0.5 m Aspect, Lidar 0.5 m Slope
L 0.5 m Aspect < L 0.5 m Slope 40%
L 0.5 m Aspect > L 0.5 m Slope 60%
Lidar 0.5 m Aspect minus Lidar 0.5 m Slope (m)
Lidar 0.5 m Aspect, Lidar 0.25 m HSNW
L 0.5 m Aspect < L 0.25 m HSNW 37%
L 0.5 m Aspect > L 0.25 m HSNW 63%
Lidar 0.5 m Aspect minus Lidar 0.25 m HSNW (m)
Lidar 0.5 m Aspect, Lidar 0.25 m HSNE
L 0.5 m Aspect < L 0.25 m HSNE 36%
L 0.5 m Aspect > L 0.25 m HSNE 64%
Lidar 0.5 m Aspect minus Lidar 0.25 m HSNE (m)
Lidar 0.5 m Aspect, Lidar 0.25 m Slope
L 0.5 m Aspect < L 0.25 m Slope 38%
L 0.5 m Aspect > L 0.25 m Slope 63%
Lidar 0.5 m Aspect minus Lidar 0.25 m Slope (m)
Lidar 0.5 m Aspect, Lidar 0.25 m Aspect
L 0.5 m Aspect < L 0.25 m Aspect 47%
L 0.5 m Aspect > L 0.25 m Aspect 53%
Lidar 0.5 m Aspect minus Lidar 0.25 m Aspect (m)

Figure A5.9

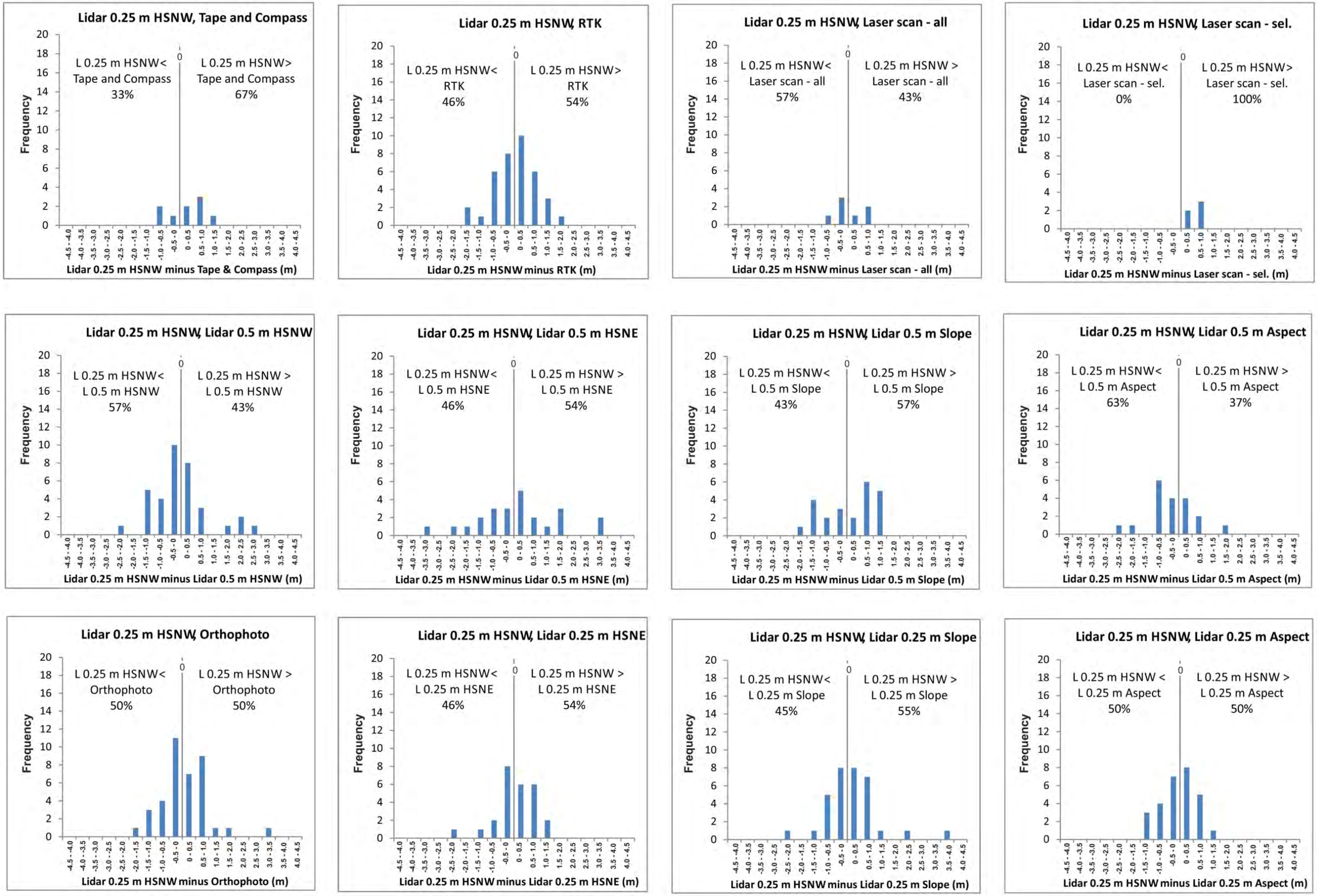
Lidar 0.25 m HSNW, Tape and Compass
L 0.25 m HSNW< Tape and Compass 33%
L 0.25 m HSNW> Tape and Compass 67%
Frequency
Lidar 0.25 m HSNW minus Tape & Compass (m)
Lidar 0.25 m HSNW, RTK
L 0.25 m HSNW< RTK 46%
L 0.25 m HSNW> RTK 54%
Lidar 0.25 m HSNW minus RTK (m)
Lidar 0.25 m HSNW, Laser scan - all
L 0.25 m HSNW< Laser scan - all 57%
L 0.25 m HSNW > Laser scan - all 43%
Lidar 0.25 m HSNW minus Laser scan - all (m)
Lidar 0.25 m HSNW, Laser scan - sel.
L 0.25 m HSNW< Laser scan - sel. 0%
L 0.25 m HSNW> Laser scan - sel. 100%
Lidar 0.25 m HSNW minus Laser scan - sel. (m)
Lidar 0.25 m HSNW, Lidar 0.5 m HSNW
L 0.25 m HSNW< L 0.5 m HSNW 57%
L 0.25 m HSNW > L 0.5 m HSNW 43%
Lidar 0.25 m HSNW minus Lidar 0.5 m HSNW (m)
Lidar 0.25 m HSNW, Lidar 0.5 m HSNE
L 0.25 m HSNW< L 0.5 m HSNE 46%
L 0.25 m HSNW > L 0.5 m HSNE 54%
Lidar 0.25 m HSNW minus Lidar 0.5 m HSNE (m)
Lidar 0.25 m HSNW, Lidar 0.5 m Slope
L 0.25 m HSNW< L 0.5 m Slope 43%
L 0.25 m HSNW > L 0.5 m Slope 57%
Lidar 0.25 m HSNW minus Lidar 0.5 m Slope (m)
Lidar 0.25 m HSNW, Lidar 0.5 m Aspect
L 0.25 m HSNW< L 0.5 m Aspect 63%
L 0.25 m HSNW > L 0.5 m Aspect 37%
Lidar 0.25 m HSNW minus Lidar 0.5 m Aspect (m)
Lidar 0.25 m HSNW, Orthophoto
L 0.25 m HSNW< Orthophoto 50%
L 0.25 m HSNW > Orthophoto 50%
Lidar 0.25 m HSNW minus Orthophoto (m)
Lidar 0.25 m HSNW, Lidar 0.25 m HSNE
L 0.25 m HSNW< L 0.25 m HSNE 46%
L 0.25 m HSNW > L 0.25 m HSNE 54%
Lidar 0.25 m HSNW minus Lidar 0.25 m HSNE (m)
Lidar 0.25 m HSNW, Lidar 0.25 m Slope
L 0.25 m HSNW< L 0.25 m Slope 45%
L 0.25 m HSNW > L 0.25 m Slope 55%
Lidar 0.25 m HSNW minus Lidar 0.25 m Slope (m)
Lidar 0.25 m HSNW, Lidar 0.25 m Aspect
L 0.25 m HSNW < L 0.25 m Aspect 50%
L 0.25 m HSNW > L 0.25 m Aspect 50%
Lidar 0.25 m HSNW minus Lidar 0.25 m Aspect (m)

Figure A5.10

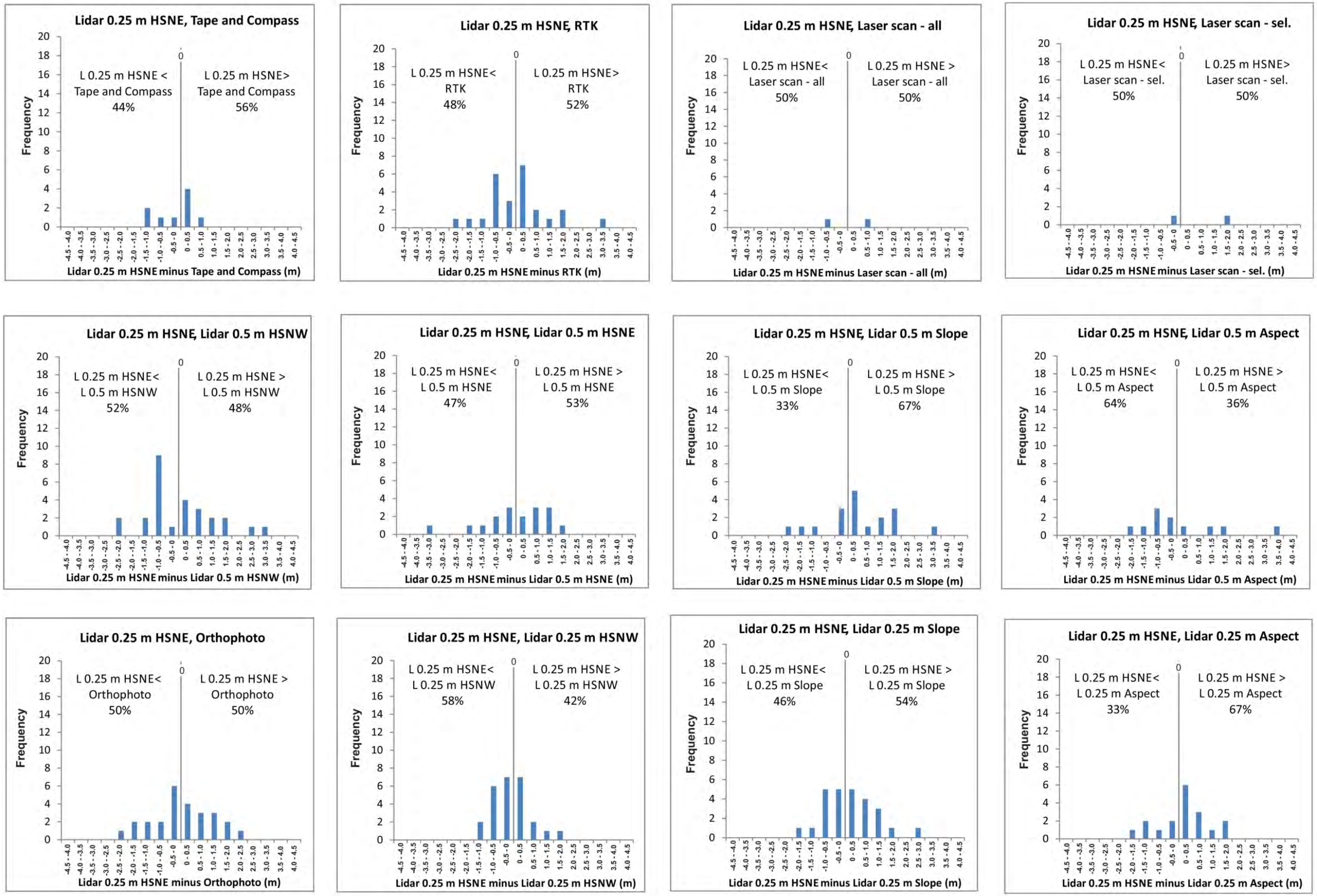

Lidar 0.25 m HSNE, Tape and Compass
L 0.25 m HSNE < Tape and Compass 44%
L 0.25 m HSNE> Tape and Compass 56%
Frequency
Lidar 0.25 m HSNE minus Tape and Compass (m)
Lidar 0.25 m HSNE, RTK
L 0.25 m HSNE< RTK 48%
L 0.25 m HSNE> RTK 52%
Lidar 0.25 m HSNE minus RTK (m)
Lidar 0.25 m HSNE, Laser scan - all
L 0.25 m HSNE< Laser scan - all 50%
L 0.25 m HSNE > Laser scan - all 50%
Lidar 0.25 m HSNE minus Laser scan - all (m)
Lidar 0.25 m HSNE, Laser scan - sel.
L 0.25 m HSNE< Laser scan - sel. 50%
L 0.25 m HSNE> Laser scan - sel. 50%
Lidar 0.25 m HSNE minus Laser scan - sel. (m)
Lidar 0.25 m HSNE, Lidar 0.5 m HSNW
L 0.25 m HSNE< L 0.5 m HSNW 52%
L 0.25 m HSNE > L 0.5 m HSNW 48%
Lidar 0.25 m HSNE minus Lidar 0.5 m HSNW (m)
Lidar 0.25 m HSNE, Lidar 0.5 m HSNE
L 0.25 m HSNE< L 0.5 m HSNE 47%
L 0.25 m HSNE > L 0.5 m HSNE 53%
Lidar 0.25 m HSNE minus Lidar 0.5 m HSNE (m)
Lidar 0.25 m HSNE, Lidar 0.5 m Slope
L 0.25 m HSNE< L 0.5 m Slope 33%
L 0.25 m HSNE > L 0.5 m Slope 67%
Lidar 0.25 m HSNE minus Lidar 0.5 m Slope (m)
Lidar 0.25 m HSNE, Lidar 0.5 m Aspect
L 0.25 m HSNE< L 0.5 m Aspect 64%
L 0.25 m HSNE > L 0.5 m Aspect 36%
Lidar 0.25 m HSNE minus Lidar 0.5 m Aspect (m)
Lidar 0.25 m HSNE, Orthophoto
L 0.25 m HSNE< Orthophoto 50%
L 0.25 m HSNE > Orthophoto 50%
Lidar 0.25 m HSNE minus Orthophoto (m)
Lidar 0.25 m HSNE, Lidar 0.25 m HSNW
L 0.25 m HSNE< L 0.25 m HSNW 58%
L 0.25 m HSNE > L 0.25 m HSNW 42%
Lidar 0.25 m HSNE minus Lidar 0.25 m HSNW (m)
Lidar 0.25 m HSNE, Lidar 0.25 m Slope
L 0.25 m HSNE< L 0.25 m Slope 46%
L 0.25 m HSNE > L 0.25 m Slope 54%
Lidar 0.25 m HSNE minus Lidar 0.25 m Slope (m)
Lidar 0.25 m HSNE, Lidar 0.25 m Aspect
L 0.25 m HSNE< L 0.25 m Aspect 33%
L 0.25 m HSNE > L 0.25 m Aspect 67%
Lidar 0.25 m HSNE minus Lidar 0.25 m Aspect (m)

Figure A5.11

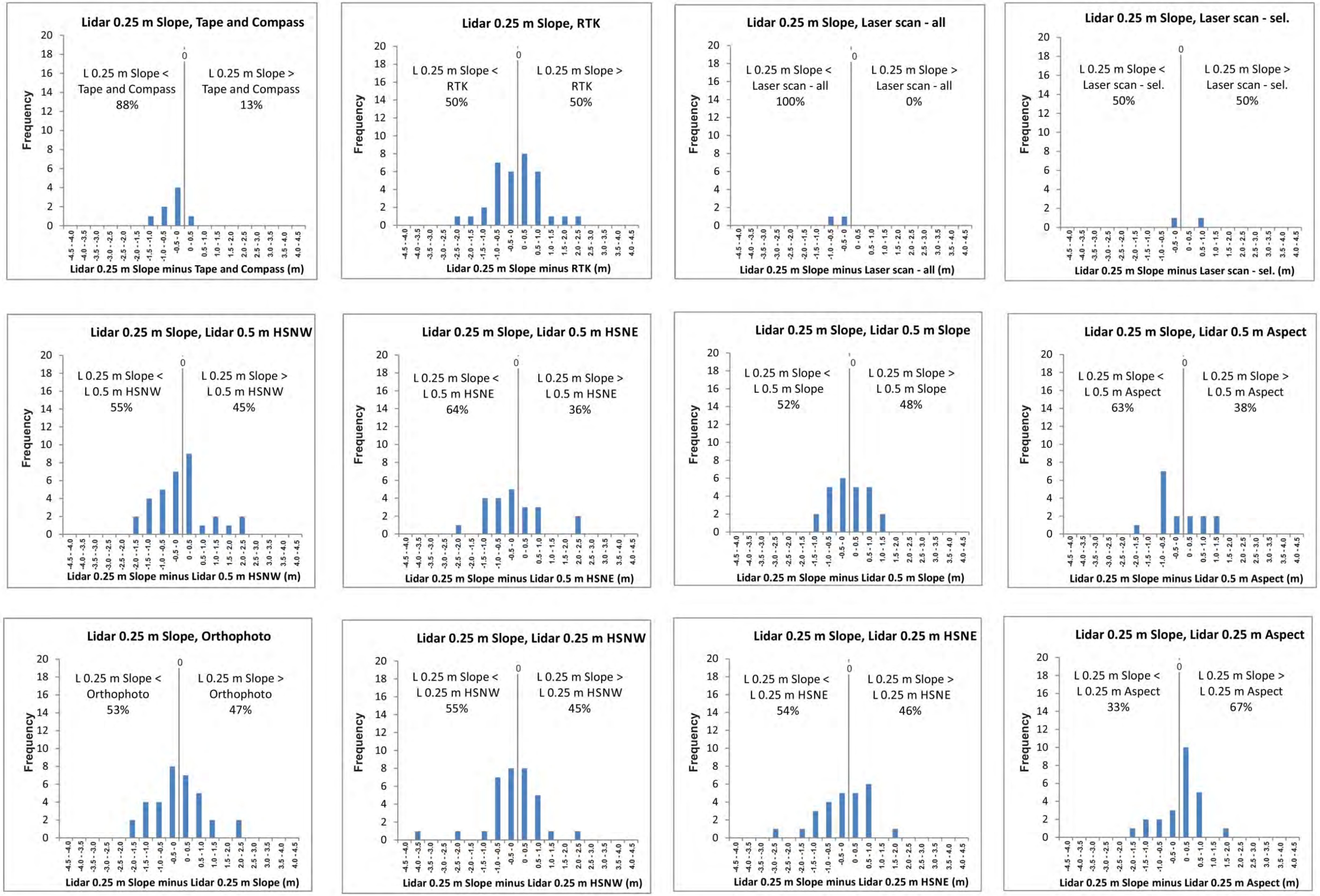
Lidar 0.25 m Slope, Tape and Compass
L 0.25 m Slope < Tape and Compass 88%
L 0.25 m Slope > Tape and Compass 13%
Frequency
Lidar 0.25 m Slope minus Tape and Compass (m)
Lidar 0.25 m Slope, RTK
L 0.25 m Slope < RTK 50%
L 0.25 m Slope > RTK 50%
Lidar 0.25 m Slope minus RTK (m)
Lidar 0.25 m Slope, Laser scan - all
L 0.25 m Slope < Laser scan - all 100%
L 0.25 m Slope > Laser scan - all 0%
Lidar 0.25 m Slope minus Laser scan - all (m)
Lidar 0.25 m Slope, Laser scan - sel.
L 0.25 m Slope < Laser scan - sel. 50%
L 0.25 m Slope > Laser scan - sel. 50%
Lidar 0.25 m Slope minus Laser scan - sel. (m)
Lidar 0.25 m Slope, Lidar 0.5 m HSNW
L 0.25 m Slope < L 0.5 m HSNW 55%
L 0.25 m Slope > L 0.5 m HSNW 45%
Lidar 0.25 m Slope minus Lidar 0.5 m HSNW (m)
Lidar 0.25 m Slope, Lidar 0.5 m HSNE
L 0.25 m Slope < L 0.5 m HSNE 64%
L 0.25 m Slope > L 0.5 m HSNE 36%
Lidar 0.25 m Slope minus Lidar 0.5 m HSNE (m)
Lidar 0.25 m Slope, Lidar 0.5 m Slope
L 0.25 m Slope < L 0.5 m Slope 52%
L 0.25 m Slope > L 0.5 m Slope 48%
Lidar 0.25 m Slope minus Lidar 0.5 m Slope (m)
Lidar 0.25 m Slope, Lidar 0.5 m Aspect
L 0.25 m Slope < L 0.5 m Aspect 63%
L 0.25 m Slope > L 0.5 m Aspect 38%
Lidar 0.25 m Slope minus Lidar 0.5 m Aspect (m)
Lidar 0.25 m Slope, Orthophoto
L 0.25 m Slope < Orthophoto 53%
L 0.25 m Slope > Orthophoto 47%
Lidar 0.25 m Slope minus Lidar 0.25 m Slope (m)
Lidar 0.25 m Slope, Lidar 0.25 m HSNW
L 0.25 m Slope < L 0.25 m HSNW 55%
L 0.25 m Slope > L 0.25 m HSNW 45%
Lidar 0.25 m Slope minus Lidar 0.25 m HSNW (m)
Lidar 0.25 m Slope, Lidar 0.25 m HSNE
L 0.25 m Slope < L 0.25 m HSNE 54%
L 0.25 m Slope > L 0.25 m HSNE 46%
Lidar 0.25 m Slope minus Lidar 0.25 m HSNE (m)
Lidar 0.25 m Slope, Lidar 0.25 m Aspect
L 0.25 m Slope < L 0.25 m Aspect 33%
L 0.25 m Slope > L 0.25 m Aspect 67%
Lidar 0.25 m Slope minus Lidar 0.25 m Aspect (m)

Figure A5.12

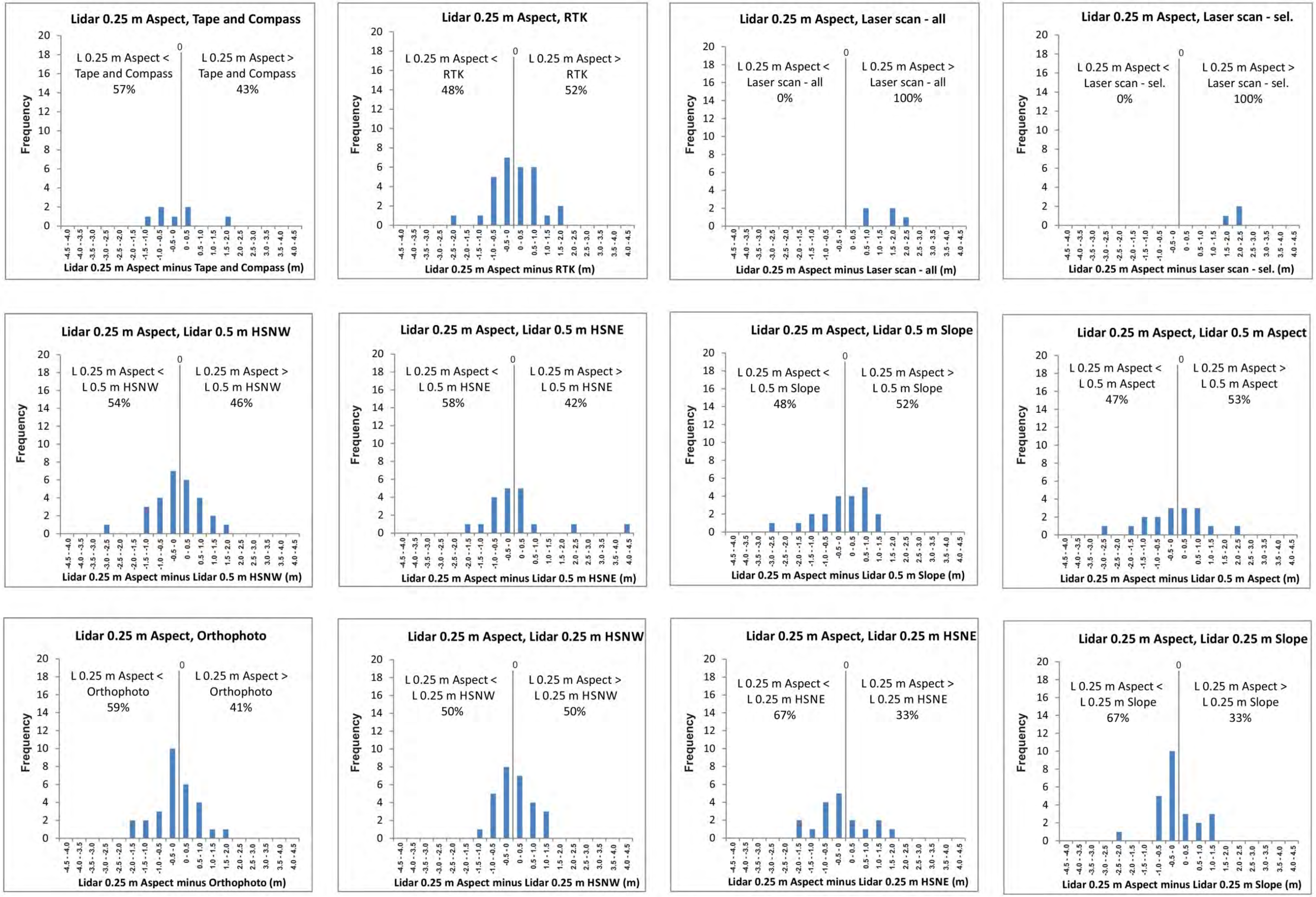

Figure A5.13

S

APPENDIX 6: MULTIPLE GEOLOGIST MEASUREMENTS

Table A 6.1 Information supplied at the start of the multiple geologist measurement workshops.

Locality Number	X	Y	Locality description	Tape and Compass Displacement	Tape and Compass Uncertainty
1	1527310.1	5172643.8	Fence by Greendale substation	1.3	0.2
20a	1529494.4	5172586.25	Fence on W side of Hollands Road	2.3	0.2
23	1531244.3	5172821.36	Fence on W side of Milton Road	3.5	0.5
26c	1532908.2	5172860.29	Drain beside Stranges Road	4.3	0.2
30a	1533673.5	5172804.96	W edge of Courtney Road	4.2	0.2
36a	1534928.1	5172770	Fence on W side of drive to Melrose	4.6	0.2
48a	1536940.4	5172909.69	W edge of Highfield Road	4.15	0.3
50a	1537358.1	5172990.43	Small trees beside fence ~270 m east of Highfield Road	3.6	0.2
52	1538098.9	5173115.3	Hedge ~1.1 km east of Highfield Road	4.1	0.3
55	1538314.3	5173125.34	Hedge ~1.3 km east of Highfield Road	4.6	0.2
59	1538713.5	5173224.17	Crop row ~1.67 km east of Highfield Road	3.8	0.5
60	1538814.5	5173240.52	Hedge ~1.77 km east of Highfield Road	4.1	0.1
71b	1541125.1	5173883.73	NW edge of Kivers Road	3.1	0.3
77b	1543094.8	5173901.79	Centreline of Aylesbury Road	0.8	0.3
80	1542675.8	5174812.3	Centreline of Aylesbury Road	0.45	0.3
88a	1545931.7	5174811.65	Fence on W side of Tressillian Drive	0.9	0.2
92b	1547153.1	5174848.56	Centreline of Kerrs Road	1.5	0.3
93a	1547532.7	5174865.89	Fence northeast of railway tracks	1.1	0.3

Table A 6.2 Greendale Fault dextral displacement measurements from multiple geologists at workshop 1. Orth = Orthophoto, HSNW = Lidar 0.5 m HSNW, HSNE = Lidar 0.5 m HSNE, Slope = Lidar 0.5 m Slope, Aspect = Lidar 0.5 m Aspect.

Locality	Geologist 1 – Displacements (m)						Geologist 2 – Displacements (m)						Geologist 3 – Displacements (m)						Geologist 4 – Displacements (m)						Geologist 5 – Displacements (m)					
Number	RTK	Orth	HSNW	HSNE	Slope	Aspect	RTK	Orth	HSNW	HSNE	Slope	Aspect	RTK	Orth	HSNW	HSNE	Slope	Aspect	RTK	Orth	HSNW	HSNE	Slope	Aspect	RTK	Orth	HSNW	HSNE	Slope	Aspect
1	2.7	4.68	2.94				3.53	3.89	1.74				2.45	4.13	3.08				1.86	3.5			1.77		1.42	1.99			1.66	
20a	4.79	2.89	0.45				2.3	3.04	2.66				3.22	1.71	1.42				2.53	3.26		2.1			2.47	2.31		1.92		
23	1.33	2.92	4.77				1.65	2.45	3.29				2.62	2.8	6.06				1.13	3.5		2.3			2.18	3.48		3.22		
26c	4.4	3.63	4.2				4.21	5.01	4.67				3.69	4.79	3.64				4.28	2.69				3.27	3.92	4.2			4.62	
30a	3.69	6.1	5.6				4.23	4.1	3.1				3.25	4.49	9.57				4.78	3.83				4.56	4.04	4.28		4.4		
36a	3.79	4.7	4.04				4.65	4.42	3.8				3.83	3.71	3.26				3.7	3.84			7.4		3.92	5.72			3.43	
48a	3.44	5.82				6.77	4.95	4.07	1.95				3.81	5.03	5.44				3.51	5.29				4.51	5.78	5.75	4.29			
50a	3.26	4.7		3.26			3.61	2.56		4.1			5.2	3.75		2.66			3.18	3.65		4.67			3.71	3.59		1.7		
52	4.5	5.9		4.2			4.9	5.56		3.74			4.78	7.98			4.92		4.81	5.08			6.18		4.83	4.91		3.9		
55	4.95	4.78		3.65			4.96	5.21		5.53			5.5	7.27	5.33				5.52	4.74	5.79				5.16	5.2		5.23		
59	4.74	4.74				4.62	3.56	4.52			3.31		3.71	4.38	5.37				4.52	4.98		5.84			4.41	5.01				2.83
60	3.67	4.12		4.71			3.85	4.63		3.37			3.7	6.26	5.89				3.26	4.53				4.06	3.77	4.3		4.01		
71b	3.55	4.79				2.85	3.51	3.01			3.97		3.1	1.94	-0.35				3.21	2.58				1.83	3.87	3.73	2.91			
77b	2.1	2.85		3.75			1.87	2.88		2.08			2.1	1.35	1.42				0.34	1.04				0.11	0.44	0.98				
80	1.01	0.51				1.02	1.12	2.22		1.17			1.61	-0.94					2.42	0.43				-0.13						
88a	0.97	0.86		1.8			0.71	1.2		1.44									1.04	2.7	1.49									
92b	1.64	2.15				3.5	1.45	3.7			0.47								0.3	2.6				-0.25						
93a	1.16	3.41		3.15			0.59	2.52		0.31									0.19	1.93			1.2							

Table A 6.3 Greendale Fault dextral displacement measurements from multiple geologists at workshop 2 (geologists 6-8) and prior to the workshop, for section 4 (geologist 9). Orth = Orthophoto, HSNW = Lidar 0.5 m HSNW, HSNE = Lidar 0.5 m HSNE, Slope = Lidar 0.5 m Slope, Aspect = Lidar 0.5 m Aspect.

Locality	Geologist 6 – Displacements (m)						Geologist 7 – Displacements (m)						Geologist 8 – Displacements (m)						Geologist 9 – Displacements (m)					
Number	RTK	Orth	HSNW	HSNE	Slope	Aspect	RTK	Orth	HSNW	HSNE	Slope	Aspect	RTK	Orth	HSNW	HSNE	Slope	Aspect	RTK	Orth	HSNW	HSNE	Slope	Aspect
1		3.02	2.54	2.15	1.08	2.33	0.72	3.2	3.27	2.44	1.14		2.2	2.12	2.67		1.4	0.74	1.2	2.1	1.2		1.35	
20a		2.87	3.75	3.15	2.75	2.73	3.11	2.46	1.69	0.92	2.69		2.29	2.52	2.06	2.72		1.5	3.2	2.1	2	2.1		
23		2.35	6.42	3.01	4.18		0.48	6.44	1.63	4.26	1.24	8.1	2.15	3.67	3.27	1.82	2.11	2.15	2.85	3.1	3.3	4	3.4	
26c		4.28	4.7	4.33	4.57		4.18	2.35	5.35	5.37	2.43	3.35	4.27	3.84	4.04	4.26	5.4	4.74	3.8	4	2.3	4.5	3.7	5.5
30a		4.27	4.18	4.16	4		4.02	6.06	2.46	2.79	5.84	6.94	4.34	4.61	4.6	5.14	5.02	4.88	4.35	5.7	3.9			3.5
36a	3.61	4.03	4.5	5.84	3.64		4.56	3.29	5.64	7.1	3.47	3.44	4.09	3.89	4.1	4.51	5.45	4.57	4.85	4.25	4.1		3.55	
48a	6.6	3.39	6.56	5.05	3.57		2.91	2.76	3.67	5.33	1.59	4.81	4.07	4.18	5.13	3.56	5.31	4.73	4.4	5.5	5.6	1.75		
50a	3.25	3.9		2.47			3.51	3.83		2.95			3.21	3.84		2.73			3.3	3.9				
52	4.7	6.86	4.85	6.77			4.67	6.07	3.96	6.81	5.58	8.17	4.41	4.33	4.34	4.24	5.4		4.95	5.2	4.15	5.9	4.65	
55	5.2	5.24	4.83	4.89				5.18	5.58				4.96	4.58	5.11				4.8	4.8	5.4	5.1		4.7
59	3.93	4.22	4.55	4.29				5.62	4.3				4.09	4.27	4.84				3.9	4.9	3.55			3.6
60	3.86	6.18	5.24	3.48				5.86	4.03				3.27	4.66	4.5				4.1	4.5	4.65	3		6.1
71b	2.91	2.86	3.83	3.32				4.47	3.9				3.24	3	3.85				3	2.9	3.1			6.45
77b		-0.08	-0.7	2.78				0.79	0.29				0.14		0.45				1.2	0.4		0.6		
80		-0.15	2.02	1.1				0.28	0.74				0.04						0.7	0		0		
88a	1.7	1.92	1.28	1.43				1.39	0.37				0.44	0.49					1.4	1.3	0			
92b	1.65	1.29	1.67	1.93				1.22	1.47				0.9	1.24	1.5				1.6	1.2	0.6			
93a	0.85	1.03	1.35	0.98				1.06	5.45				1.29	1.31	1.1				1.3	1	2.7	1.9	1.6	1.2

APPENDIX 7: COMPARISON BETWEEN A GEOLOGISTS MEASUREMENTS AND MEDIAN DISPLACEMENT MEASUREMENTS: HISTOGRAMS

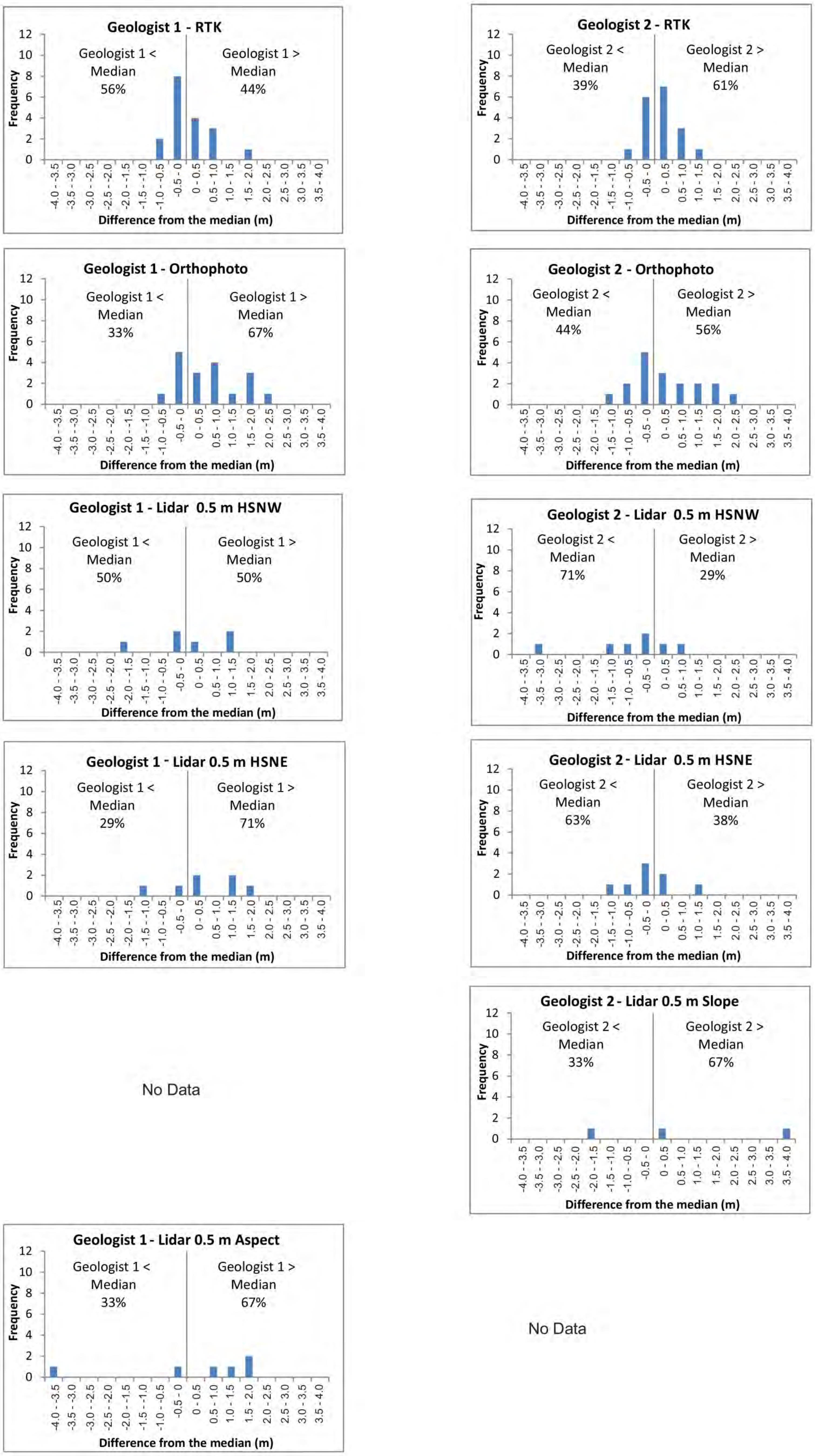

Figure A7.1

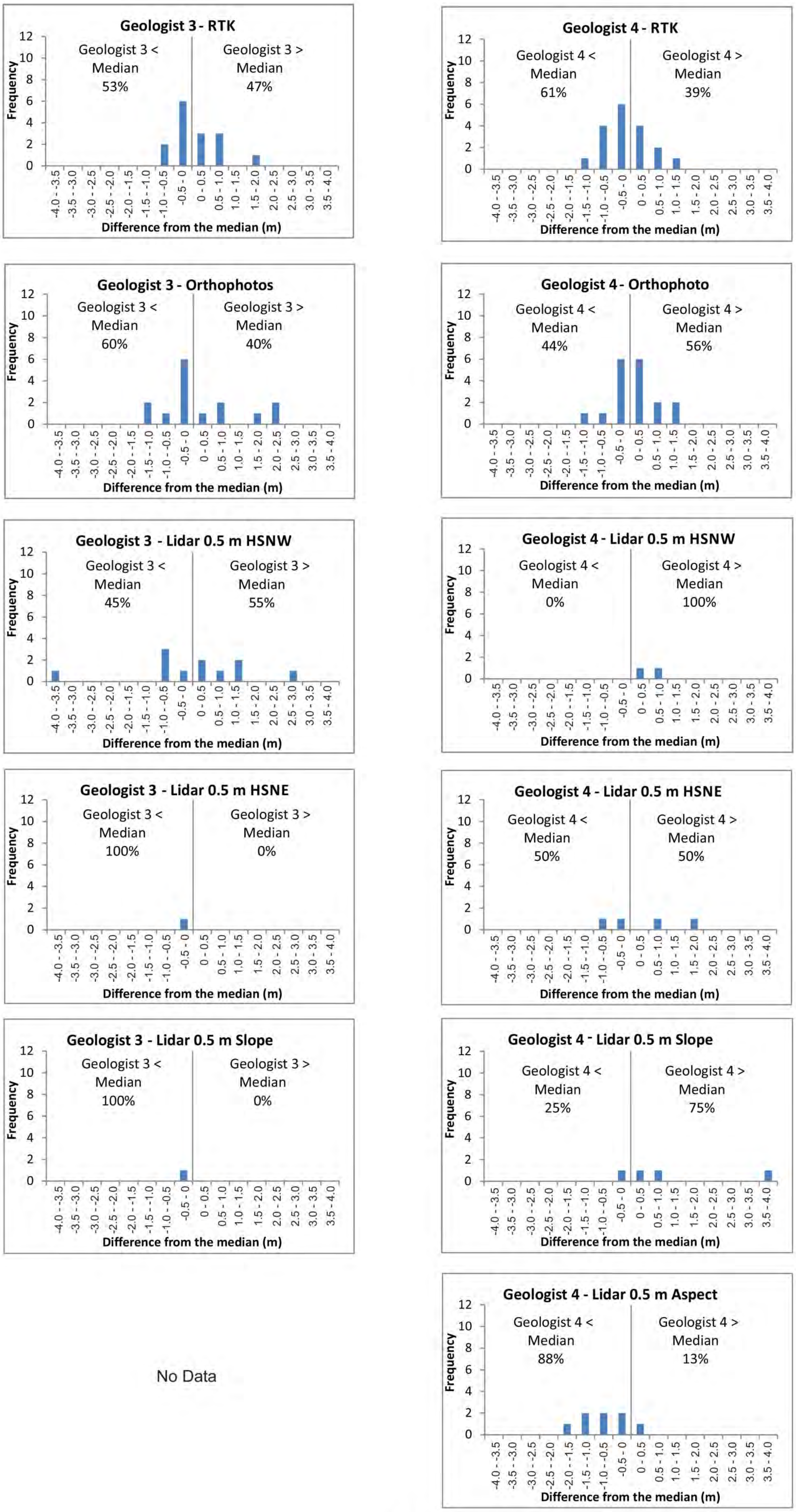

Geologist 3 - RTK
Geologist 3 < Median 53%
Geologist 3 > Median 47%
Geologist 4 - RTK
Geologist 4 < Median 61%
Geologist 4 > Median 39%
Geologist 3 - Orthophotos
Geologist 3 < Median 60%
Geologist 3 > Median 40%
Geologist 4 - Orthophoto
Geologist 4 < Median 44%
Geologist 4 > Median 56%
Geologist 3 - Lidar 0.5 m HSNW
Geologist 3 < Median 45%
Geologist 3 > Median 55%
Geologist 4 - Lidar 0.5 m HSNW
Geologist 4 < Median 0%
Geologist 4 > Median 100%
Geologist 3 - Lidar 0.5 m HSNE
Geologist 3 < Median 100%
Geologist 3 > Median 0%
Geologist 4 - Lidar 0.5 m HSNE
Geologist 4 < Median 50%
Geologist 4 > Median 50%
Geologist 3 - Lidar 0.5 m Slope
Geologist 3 < Median 100%
Geologist 3 > Median 0%
Geologist 4 - Lidar 0.5 m Slope
Geologist 4 < Median 25%
Geologist 4 > Median 75%
No Data
Geologist 4 - Lidar 0.5 m Aspect
Geologist 4 < Median 88%
Geologist 4 > Median 13%
Frequency
Difference from the median (m)

Figure A7.2

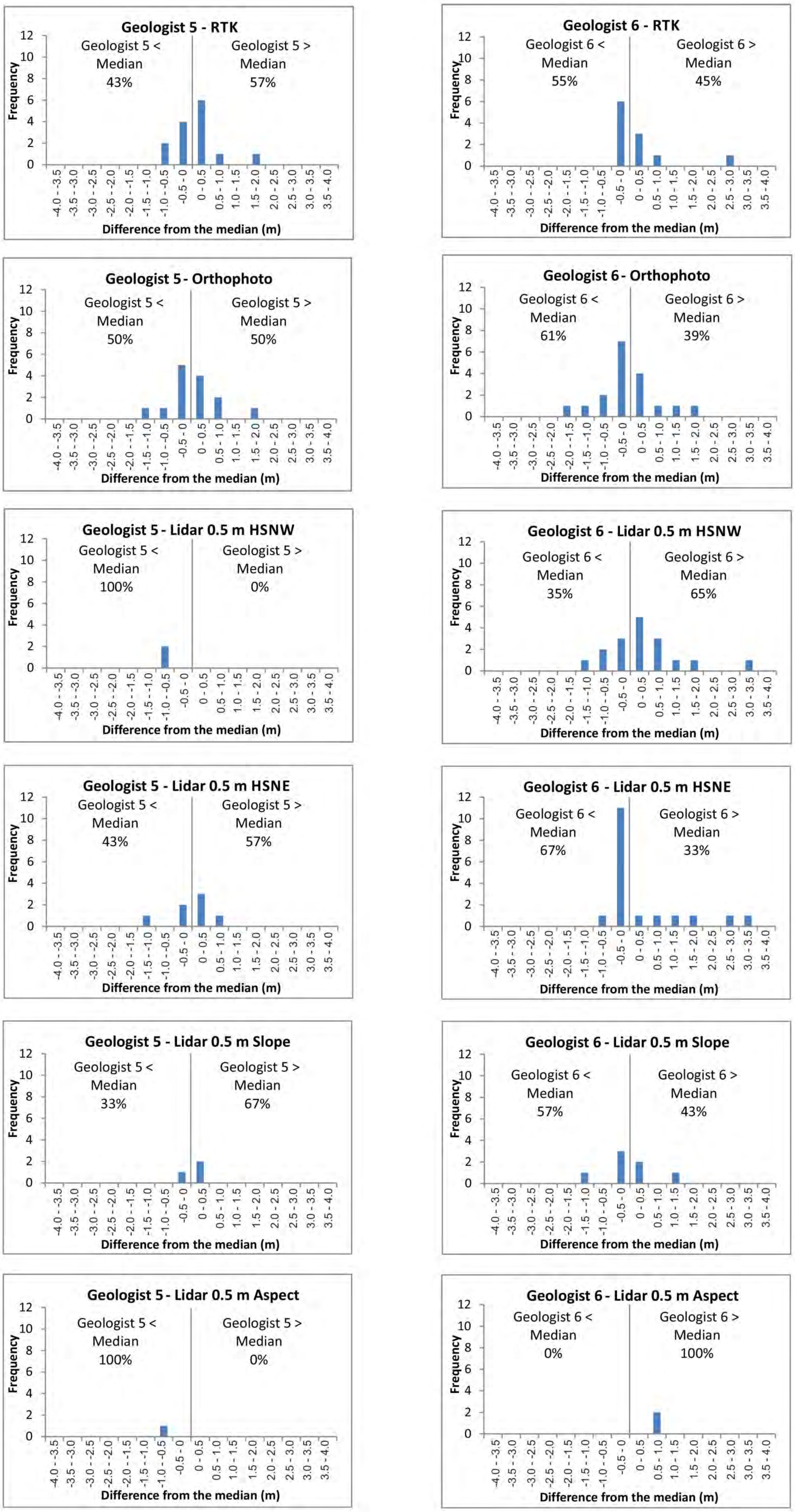

Geologist 5 - RTK
Geologist 5 < Median 43%
Geologist 5 > Median 57%
Geologist 6 - RTK
Geologist 6 < Median 55%
Geologist 6 > Median 45%
Geologist 5 - Orthophoto
Geologist 5 < Median 50%
Geologist 5 > Median 50%
Geologist 6 - Orthophoto
Geologist 6 < Median 61%
Geologist 6 > Median 39%
Geologist 5 - Lidar 0.5 m HSNW
Geologist 5 < Median 100%
Geologist 5 > Median 0%
Geologist 6 - Lidar 0.5 m HSNW
Geologist 6 < Median 35%
Geologist 6 > Median 65%
Geologist 5 - Lidar 0.5 m HSNE
Geologist 5 < Median 43%
Geologist 5 > Median 57%
Geologist 6 - Lidar 0.5 m HSNE
Geologist 6 < Median 67%
Geologist 6 > Median 33%
Geologist 5 - Lidar 0.5 m Slope
Geologist 5 < Median 33%
Geologist 5 > Median 67%
Geologist 6 - Lidar 0.5 m Slope
Geologist 6 < Median 57%
Geologist 6 > Median 43%
Geologist 5 - Lidar 0.5 m Aspect
Geologist 5 < Median 100%
Geologist 5 > Median 0%
Geologist 6 - Lidar 0.5 m Aspect
Geologist 6 < Median 0%
Geologist 6 > Median 100%
Frequency
Difference from the median (m)

Figure A7.3

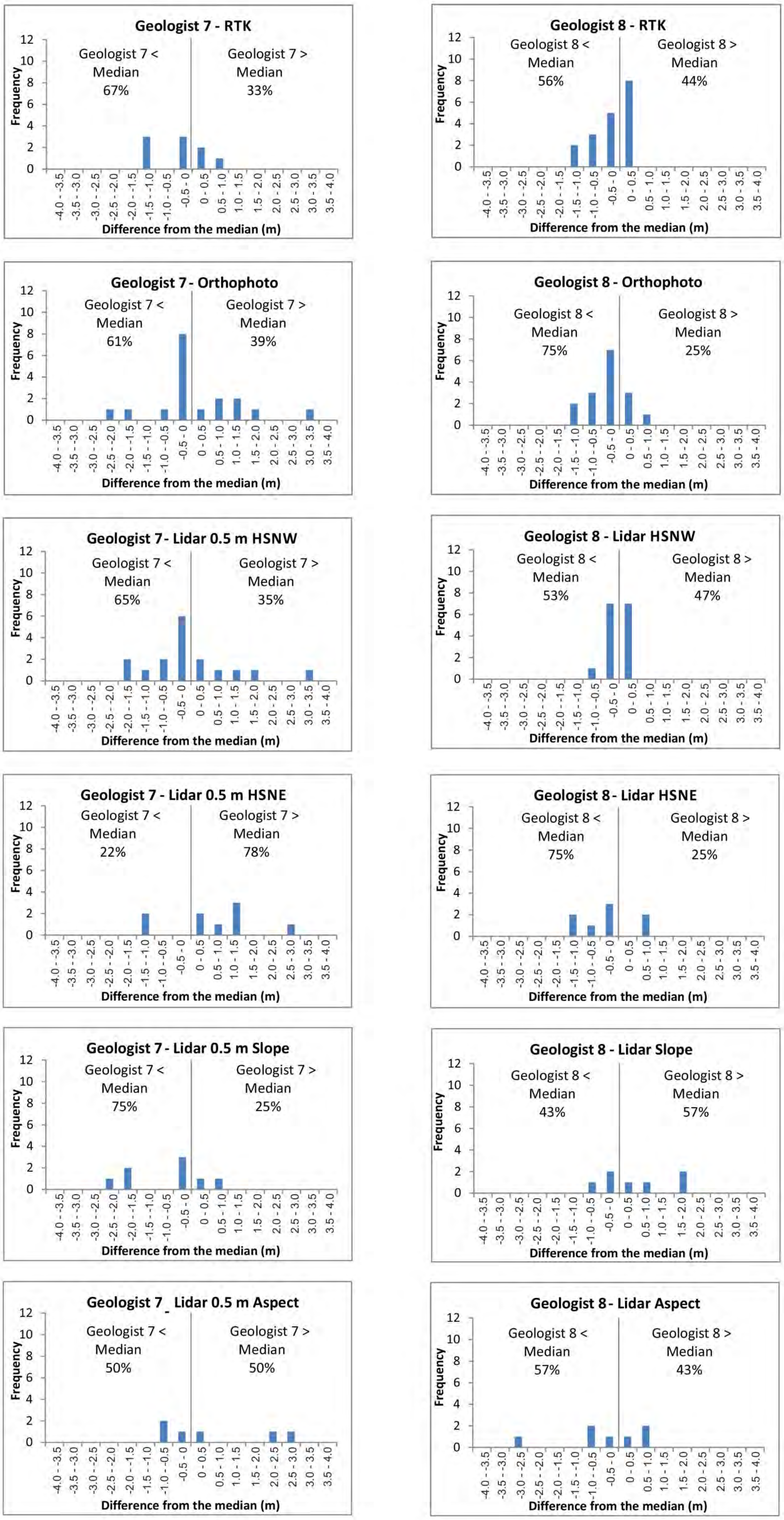
Geologist 7 - RTK
Geologist 7 < Median 67%
Geologist 7 > Median 33%
Geologist 8 - RTK
Geologist 8 < Median 56%
Geologist 8 > Median 44%
Geologist 7 - Orthophoto
Geologist 7 < Median 61%
Geologist 7 > Median 39%
Geologist 8 - Orthophoto
Geologist 8 < Median 75%
Geologist 8 > Median 25%
Geologist 7 - Lidar 0.5 m HSNW
Geologist 7 < Median 65%
Geologist 7 > Median 35%
Geologist 8 - Lidar HSNW
Geologist 8 < Median 53%
Geologist 8 > Median 47%
Geologist 7 - Lidar 0.5 m HSNE
Geologist 7 < Median 22%
Geologist 7 > Median 78%
Geologist 8 - Lidar HSNE
Geologist 8 < Median 75%
Geologist 8 > Median 25%
Geologist 7 - Lidar 0.5 m Slope
Geologist 7 < Median 75%
Geologist 7 > Median 25%
Geologist 8 - Lidar Slope
Geologist 8 < Median 43%
Geologist 8 > Median 57%
Geologist 7 _ Lidar 0.5 m Aspect
Geologist 7 < Median 50%
Geologist 7 > Median 50%
Geologist 8 - Lidar Aspect
Geologist 8 < Median 57%
Geologist 8 > Median 43%
Frequency
0
2
4
6
8
10
12
-4.0 - -3.5
-3.5 - -3.0
-3.0 - -2.5
-2.5 - -2.0
-2.0 - -1.5
-1.5 - -1.0
-1.0 - -0.5
-0.5 - 0
0 - 0.5
0.5 - 1.0
1.0 - 1.5
1.5 - 2.0
2.0 - 2.5
2.5 - 3.0
3.0 - 3.5
3.5 - 4.0
Difference from the median (m)

Figure A7.4

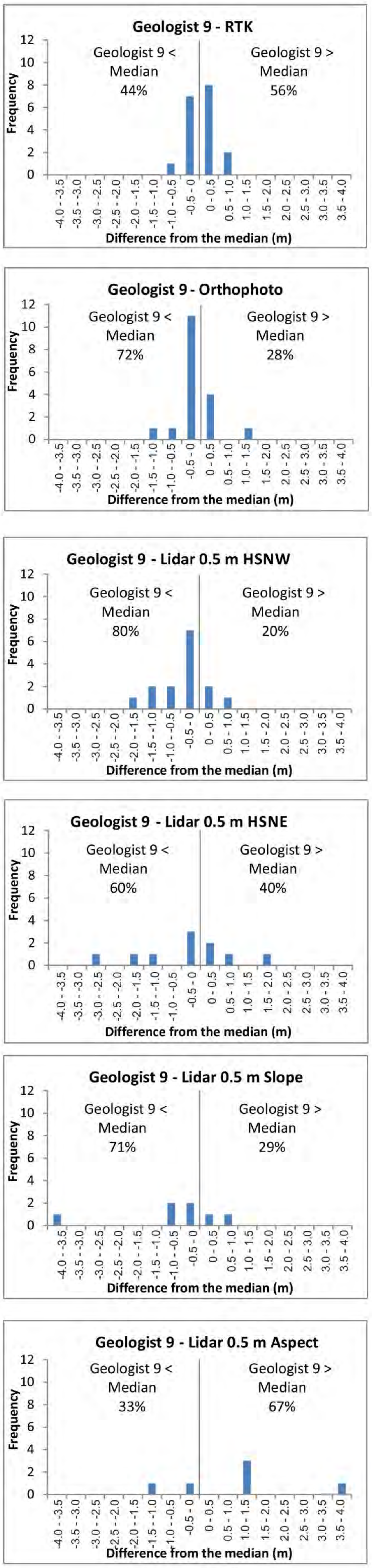
Geologist 9 - RTK
Geologist 9 < Median 44%
Geologist 9 > Median 56%
Geologist 9 - Orthophoto
Geologist 9 < Median 72%
Geologist 9 > Median 28%
Geologist 9 - Lidar 0.5 m HSNW
Geologist 9 < Median 80%
Geologist 9 > Median 20%
Geologist 9 - Lidar 0.5 m HSNE
Geologist 9 < Median 60%
Geologist 9 > Median 40%
Geologist 9 - Lidar 0.5 m Slope
Geologist 9 < Median 71%
Geologist 9 > Median 29%
Geologist 9 - Lidar 0.5 m Aspect
Geologist 9 < Median 33%
Geologist 9 > Median 67%
Frequency
0
2
4
6
8
10
12
-4.0 - -3.5
-3.5 - -3.0
-3.0 - -2.5
-2.5 - -2.0
-2.0 - -1.5
-1.5 - -1.0
-1.0 - -0.5
-0.5 - 0
0 - 0.5
0.5 - 1.0
1.0 - 1.5
1.5 - 2.0
2.0 - 2.5
2.5 - 3.0
3.0 - 3.5
3.5 - 4.0
Difference from the median (m)

Figure A7.5

GNS SCIENCE
TE PŪ AO

www.gns.cri.nz

Principal Location

1 Fairway Drive
Avalon
Lower Hutt 5010
PO Box 30368
Lower Hutt 5040
New Zealand
T +64-4-570 1444
F +64-4-570 4600

Other Locations

Dunedin Research Centre
764 Cumberland Street
Dunedin 9016
Private Bag 1930
Dunedin 9054
New Zealand
T +64-3-477 4050
F +64-3-477 5232

Wairakei Research Centre
114 Karetoto Road, Wairakei
Taupo 3377
Private Bag 2000
Taupo 3352
New Zealand
T +64-7-374 8211
F +64-7-374 8199

National Isotope Centre
30 Gracefield Road, Gracefield
Lower Hutt 5010
PO Box 31312
Lower Hutt 5040
New Zealand
T +64-4-570 1444
F +64-4-570 4657